UNIVERSIDADE DA BEIRA INTERIOR
Ciências

Production and characterization of electrospun membranes for wound dressing applications

Sónia Alexandra Pereira Miguel

Tese para obtenção do Grau de Doutor em
Bioquímica
(3º ciclo de estudos)

Orientador: Professor Doutor Ilídio Joaquim Sobreira Correia

Covilhã, dezembro de 2019

Everything is theoretically impossible, until it is done"
Robert A. Heinlein

Dedicatória

Aos meus pais, à minha irmã e ao meu noivo.

Agradecimentos

Estes últimos 4 anos foram sem dúvida uma incrível viagem recheada de experiências, crescimento profissional e pessoal. Deste capítulo da minha vida que está prestes a terminar, fizeram parte pessoas fantásticas, bons amigos, muitas lições aprendidas, incontáveis fracassos e alguns sucessos. Por isso, está na altura de agradecer aqueles que contribuíram para tornar esta viagem inesquecível.

Em primeiro lugar, quero expressar a minha mais profunda gratidão ao meu orientador Professor Ilídio Correia, por tudo o que fez por mim. Ele deu-me a oportunidade de trabalhar no seu grupo desde 2012, e a sua ambição e paixão pela ciência foi algo que realmente me inspirou. A sua orientação e apoio incondicional contribuíram para a pessoa e profissional que sou hoje. Acima de tudo, ele acreditou em mim e me encorajou, mesmo quando eu pensei que não poderia ir mais longe.

Quero também manifestar os meus sinceros agradecimentos ao Maximiano Ribeiro, pela sua amizade e apoio constante desde que cheguei ao laboratório de Biomateriais e Engenharia de Tecidos. Ele ensinou-me que devemos de acreditar em nós próprios, mesmo nos momentos mais difíceis. "Nós temos os substitutos de pele no sangue"

Quero expressar a minha gratidão aos meus colegas de doutoramento (André, Bete e Duarte) pelo apoio, troca de ideias, força e encorajamento nos momentos menos positivos, mas também por todos os momentos de diversão e felicidade que passamos juntos. Eu sinto-me uma sortuda por vos ter na minha vida.

Aos meus "meninos" (Kevin, Daniela, João, Déborah, Cátia e Rosa), quero agradecer pela amizade, companheirismo e confiança. Pude com vocês compartilhar o meu conhecimento e a minha experiência, mas também tive a oportunidade de aprender coisas novas com vocês. A co-supervisão dos vossos trabalhos de mestrado foi sem dúvida uma experiência única e enriquecedora. Desejo o melhor do mundo para vocês.

Quero também agradecer às minhas amigas de sempre e para sempre (Ana, Raquel e Catarina), vocês fizeram e fazem parte da minha vida. "A amizade verdadeira é aquela que o tempo não apaga, a distância não separa e a maldade não destrói".

Quero ainda agradecer profundamente à minha família pelo amor e apoio incondicional, não apenas durante estes anos, mas ao longo de toda a minha vida. Telma, és a melhor irmã que alguém pode ter. Cumplicidade, alegria contagiante, amor de irmãs, e apoio incondicional são apenas algumas das palavras que descrevem tudo aquilo que és para mim. Obrigada também ao mais recente membro da família, o meu cunhado João, pela sua hospitalidade e

compreensão. Quero agradecer aos meus pais António e Helena. O vosso amor, apoio e constante presença são a força que me inspira e me faz continuar sempre em frente. Tudo o que sou hoje devo a vocês e à excelente educação e valores que sempre me incutiram. Espero estar à altura das vossas expectativas e fazer-vos muito orgulhosos. Vocês são os pilares que me mantêm forte. Obrigada por tudo!

Quero ainda mostrar o meu profundo apreço e amor ao Roberto, o meu namorado, o meu companheiro, o meu melhor amigo, o meu noivo. Tu entraste na minha vida no meio deste capítulo como uma brisa agradável de ar fresco, e presenteaste-me com uma infinita paciência, apoio incondicional e amor nos momentos mais difíceis e exigentes deste doutoramento. Juntos somos mais fortes e vamos mais longe!

Além disso, gostaria também de agradecer à Universidade da Beira Interior (UBI), em particular ao Centro de Investigação em Ciências da Saúde da UBI (CICS-UBI) por me providenciar as instalações, os equipamentos e os recursos necessários à realização desta tese de doutoramento.

Por último, gostaria de expressar a minha gratidão à Fundação para a Ciência e a Tecnologia (FCT) pelo apoio financeiro através da bolsa individual de doutoramento (SFRH/BD/109563/2015). E também agradecer o financiamento proveniente dos projetos POCI-01-0145-FEDER-007491, UID/Multi/00709/2013, CENTRO-01-0145-FEDER-028989 e POCI-01-0145-FEDER-031462.

List of publications

Articles published in peer-reviewed international journals included in this Doctoral thesis

I. Electrospun Polycaprolactone/Aloe Vera_Chitosan Nanofibrous Asymmetric Membranes Aimed for Wound Healing Applications
Sónia P. Miguel, Maximiano P. Ribeiro, Paula Coutinho, Ilídio J. Correia
Polymers, 2017, 9(5):183
DOI: 10.3390/polym9050183
I.F. = 3.164; Q1 Polymer Science (17/87)
Citations - ISI Web of Knowledge: 25, Google Scholar: 32, Scopus: 32

II. Electrospun polymeric nanofibers as wound dressings: a review
Sónia P. Miguel, Daniela R. Figueira, Déborah Simões, Maximiano P. Ribeiro, Paula Coutinho, Paula Ferreira, Ilídio J. Correia
Colloids and Surfaces B: Biointerfaces, 2018, 169(5):60-71
DOI: 10.1016/j.colsurfb.2018.05.011
I.F. = 3.973; Q1 Biophysics (15/72)
Citations - ISI Web of Knowledge: 22, Google Scholar: 31, Scopus: 25

III. Production and characterization of electrospun Silk Fibroin based asymmetric membranes for wound dressing applications
Sónia P. Miguel, Déborah Simões, André F. Moreira, Rosa S. Sequeira, Ilídio J. Correia
International Journal of Biological Macromolecules, 2019, 121: 524-535
DOI: 10.1016/j.ijbiomac.2018.10.041
I.F.= 4.784; Q1 and TOP10 Chemistry Applied (9/71), Polymer Science (8/87)
Citations - ISI Web of Knowledge: 4, Google Scholar: 8, Scopus: 8

IV. Chitosan based-asymmetric membranes for wound healing: a review
Sónia P. Miguel, André F. Moreira, Ilídio J. Correia
International Journal of Biological Macromolecules, 2019, 127: 460-475
DOI: 10.1016/j.ijbiomac.2019.01.072
I.F.= 4.784; Q1 and TOP10 Chemistry Applied (9/71), Polymer Science (8/87)
Citations - ISI Web of Knowledge: 3, Google Scholar: 9, Scopus: 8

V. An overview of electrospun membranes loaded with bioactive molecules for improving the wound healing process

Sónia P. Miguel*, Rosa S. Sequeira*, André F. Moreira, Cátia S. D. Cabral, António G. Mendonça, Paula Ferreira, Ilídio J. Correia

*Authors contributed equally to this work

European Journal of Pharmaceutics and Biopharmaceutics, 2019, 139: 1-22

DOI: 10.1016/j.ejpb.2019.03.010

I.F.= 4.708; Q1 Pharmacology & Pharmacy (28/267)

Citations - ISI Web of Knowledge: 0, Google Scholar: 3, Scopus: 3

VI. Production and characterization of a novel asymmetric 3D printed construct aimed for skin tissue regeneration

Sónia P. Miguel, Cátia S. D. Cabral, André F. Moreira, Ilídio J. Correia

Colloids and Surfaces B: Biointerfaces, 2019, 181:994-1003

DOI: 10.1016/j.colsurfb.2019.06.063

I.F. = 3.973; Q1 Biophysics (15/72)

Citations - ISI Web of Knowledge: 0, Google Scholar: 0, Scopus: 0

Articles published in peer-reviewed international journals not included in this Doctoral thesis

I. Dextran based-hydrogel containing chitosan microparticles loaded with growth factors to be used in wound healing
Maximiano P. Ribeiro, Patrícia I. Morgado, Sónia P. Miguel, Paula Coutinho, Ilídio J. Correia
Materials Science & Engineering C, 2013, 33(5): 2958-2966
DOI: 10.1016/j.msec.2013.03.025
IF= 4.959; Q1 and TOP10 Materials Science, Biomaterials (7/32)
Citations - ISI Web of Knowledge: 67, Google Scholar: 100, Scopus: 70

II. *In vivo* high-content evaluation of three-dimensional scaffolds biocompatibility
Mariana B. Oliveira, Maximiano P. Ribeiro, Sónia P. Miguel, Ana I. Neto, Paula Coutinho, Ilídio J. Correia, João F. Mano
Tissue Engineering Part C: Methods, 2014, 20(11): 851-864
DOI: 10.1089/ten.tec.2013.0738
IF= 2.638; Q2 Biotechnology & Applied Microbiology (71/162)
Citations - ISI Web of Knowledge: 15, Google Scholar: 21, Scopus: 18

III. Thermoresponsive chitosan-agarose hydrogel for skin regeneration
Sónia P. Miguel, Maximiano P. Ribeiro, Hugo Brancal, Paula Coutinho, Ilídio J. Correia
Carbohydrate Polymers, 2014, 111: 366-373
DOI: 10.1016/j.carbpol.2014.04.093
IF= 6.044; Q1 and TOP5 Chemistry applied (2/71)
Citations - ISI Web of Knowledge: 98, Google Scholar: 134, Scopus: 100

IV. PVP-coated silver nanoparticles showing antifungal improved activity against dermatophytes
Edgar Silva, Sofia Saraiva, Sónia P. Miguel, Ilídio J. Correia
Journal of Nanoparticle Research, 2014, 16:2726
DOI: 10.1007/s11051-014-2726-2
IF= 2.009; Q3 Materials Science, Multidisciplinary (162/293)
Citations - ISI Web of Knowledge: 10, Google Scholar: 16, Scopus: 10

V. Poly(vinyl alcohol)/chitosan asymmetric membranes: highly controlled morphology toward the ideal wound dressing
Patrícia I. Morgado, Pedro F. Lisboa, Maximiano P. Ribeiro, Sónia P. Miguel, Pedro C. Simões, Ilídio J. Correia, Ana Aguiar-Ricardo
Journal of Membrane Science, 2014, 469: 262-271
DOI: 10.1016/j.memsci.2014.06.035

IF= 7.015; Q1 and TOP5 Polymer Science (2/87)
Citations - ISI Web of Knowledge: 39, Google Scholar: 62, Scopus: 49

VI. Production and characterization of Chitosan/Gelatin/β-TCP scaffolds for improved bone tissue regeneration
Inês R. Serra, Ricardo G. Fradique, Mariana C. Vallejo, Tiago R. Correia, Sónia P. Miguel, Ilídio J. Correia
Materials Science & Engineering C, 2015, 55: 592-604
DOI: 10.1016/j.msec.2015.05.072
IF= 4.959; Q1 and TOP10 Materials Science, Biomaterials (7/32)
Citations - ISI Web of Knowledge: 45, Google Scholar: 62, Scopus: 51

VII. Synthesis and characterization of a photocrosslinkable chitosan-gelatin hydrogel aimed for tissue regeneration
Sofia Saraiva, Sónia P. Miguel, Maximiano P. Ribeiro, Paula Coutinho, Ilídio J. Correia
RSC Advances, 2015, 5: 63478-63488
DOI: 10.1039/C5RA10638A
IF= 3.049; Q2 Chemistry Multidisciplinary (69/172)
Citations - ISI Web of Knowledge: 20, Google Scholar: 31, Scopus: 22

VIII. Production of new 3D scaffolds for bone tissue regeneration by rapid prototyping
Ricardo Fradique, Tiago R. Correia, Sónia P. Miguel, Kevin D. de Sá, Daniela R. Figueira, António G. Mendonça, Ilídio J. Correia
Journal of Materials Science: Materials in Medicine, 2016, 27(69)
DOI: 10.1007/s10856-016-5681-x
IF= 2.467; Q2 Engineering, Biomedical (34/80)
Citations - ISI Web of Knowledge: 13, Google Scholar: 19, Scopus: 12

IX. Nanogold Poxylation: towards always-on fluorescent lung cancer targeting
Ana Sofia Silva, Marta C. Silva, Sónia P. Miguel, Vasco D. B. Bonifácio, Ilídio J. Correia, Ana Aguiar-Ricardo
RSC Advances, 2016, 6 (40): 33631-33635
DOI: 10.1039/C6RA00532B
IF= 3.049; Q2 Chemistry Multidisciplinary (69/172)
Citations - ISI Web of Knowledge: 8, Google Scholar: 9, Scopus: 8

X. Tumor spheroid assembly on hyaluronic acid-based structures: A review
Marco P. Carvalho, Elisabete C. Costa, Sónia P. Miguel, Ilídio J. Correia
Carbohydrate Polymers, 2016, 150: 139-148
DOI: 10.1080/00914037.2015.1129962
IF= 6.044; Q1 and TOP5 Chemistry applied (2/71)
Citations - ISI Web of Knowledge: 18, Google Scholar: 22, Scopus: 18

XI. 3D printed scaffolds with bactericidal activity aimed for bone tissue regeneration
Tiago R. Correia, Daniela R. Figueira, Kevin D. de Sá, Sónia P. Miguel, Ricardo G. Fradique, Ilídio J. Correia
International Journal of Biological Macromolecules, 2016, 93 (Part B): 1432-1445
DOI: 10.1016/j.ijbiomac.2016.06.004
I.F.= 4.784; Q1 and TOP10 Chemistry Applied (9/71), Polymer Science (8/87)
Citations - ISI Web of Knowledge: 8, Google Scholar: 15, Scopus: 9

XII. Production and characterization of polycaprolactone-hyaluronic acid/chitosan-zein electrospun bilayer nanofibrous membrane for tissue regeneration
Daniela R. Figueira, Sónia P. Miguel, Kevin D. de Sá, Ilídio J. Correia
International Journal of Biological Macromolecules, 2016, 93 (Part A): 1100-1110
DOI: 10.1016/j.ijbiomac.2016.09.080
I.F.= 4.784; Q1 and TOP10 Chemistry Applied (9/71), Polymer Science (8/87)
Citations - ISI Web of Knowledge: 25, Google Scholar: 35, Scopus: 29

XIII. 3D Scaffolds Coated with Nanofibers Displaying Bactericidal Activity for Bone Tissue Applications
Kevin D. de Sá, Daniela R. Figueira, Sónia P. Miguel, Tiago R. Correia, Abílio P. Silva, Ilídio J. Correia
International Journal of Polymeric Materials and Polymeric Biomaterials, 2017, 66(9): 432-442
DOI: 10.1080/00914037.2016.1236338
I.F.= 2.263; Q2 Polymer Science (34/87)
Citations - ISI Web of Knowledge: 2, Google Scholar: 4, Scopus: 3

XIV. Aerosolizable gold nano-in-micro dry powder formulations for theragnosis and lung delivery
Sofia Silva, Ana M. Sousa, Renato P. Cabral, Marta C. Silva, Clarinda Costa, Sónia P. Miguel, Vasco D. B. Bonifácio, Teresa Casimiro, Ilídio J. Correia, Ana Aguiar-Ricardo
International Journal of Pharmaceutics, 2017, 519(1-2): 240-249
DOI: 10.1016/j.ijpharm.2017.01.032
I.F.= 4.213; Q1 Pharmacology & Pharmacy (44/267)
Citations - ISI Web of Knowledge: 10, Google Scholar: 12, Scopus: 10

XV. Ibuprofen loaded PVA/Chitosan membranes: a highly efficient strategy towards an improved skin wound healing
Patrícia I. Morgado, Sónia P. Miguel, Ilídio J. Correia, Ana Aguiar-Ricardo
Carbohydrate Polymers, 2017, 159: 136-145
DOI: 10.1016/j.carbpol.2016.12.029
IF= 6.044; Q1 and TOP5 Chemistry applied (2/71)

Citations - ISI Web of Knowledge: 24, Google Scholar: 37, Scopus: 28

XVI. Coaxial electrospun PCL/Gelatin-MA fibers as scaffolds for vascular tissue engineering
Patrícia Coimbra, Patrícia Santos, Patrícia Alves, Sónia P. Miguel, Marco P. Carvalho, Kevin D. de Sá, Ilídio J. Correia, Paula Ferreira
Colloids and Surfaces B: Biointerfaces, 2017, 159: 7-15
DOI: 10.1016/j.colsurfb.2017.07.065
I.F. = 3.973; Q1 Biophysics (15/72)
Citations - ISI Web of Knowledge: 15, Google Scholar: 17, Scopus: 16

XVII. Photocrosslinkable electrospun fiber meshes for tissue engineering applications
Paula Ferreira, Patrícia Santos, Patrícia Alves, Marco P. Carvalho, Kevin D. de Sá, Sónia P. Miguel, Ilídio J. Correia, Patrícia Coimbra
European Polymer Journal, 2017, 97: 210-219
DOI: 10.1016/j.eurpolymj.2017.10.018
I.F. = 3.621; Q1 Polymer Science (14/87)
Citations - ISI Web of Knowledge: 7, Google Scholar: 9, Scopus: 8

XVIII. Recent advances on antimicrobial wound dressing: a review
Déborah Simões, Sónia P. Miguel, Maximiano P. Ribeiro, Paula Coutinho, António G. Mendonça, Ilídio J. Correia
European Journal of Pharmaceutics and Biopharmaceutics, 2018, 127: 130-141
DOI: 10.1016/j.ejpb.2018.02.022
I.F.= 4.708; Q1 Pharmacology & Pharmacy (28/267)
Citations - ISI Web of Knowledge: 44, Google Scholar: 61, Scopus: 52

XIX. *In vitro* characterization of 3D printed scaffolds aimed at bone tissue regeneration
João C. Boga, Sónia P. Miguel, Duarte de Melo-Diogo, António G. Mendonça, Ricardo O. Louro, Ilídio J. Correia
Colloids and Surfaces B: Biointerfaces, 2018, 165: 207-218
DOI: 10.1016/j.colsurfb.2018.02.038
I.F. = 3.973; Q1 Biophysics (15/72)
Citations - ISI Web of Knowledge: 8, Google Scholar: 13, Scopus: 11

XX. Engineering star-shaped lactic acid oligomers to develop novel functional adhesives
João M. C. Santos, Diana R. S. Travassos, Paula Ferreira, Dina S. Marques, Maria H. Gil, Sónia P. Miguel, Maximiano P. Ribeiro, Ilídio J. Correia, Cristina M. S. G. Baptista
Journal of Materials Research, 2018, 33(10): 1463-1474
DOI: 10.1557/jmr.2018.73
I.F. = 1.982; Q3 Materials Science, Multidisciplinary (165/293)
Citations - ISI Web of Knowledge: 1, Google Scholar: 1, Scopus: 1

XXI. Bioinspired multilayer membranes as potential adhesive patch for skin wound healing
Maria P. Sousa, Ana I. Neto, Tiago R. Correia, Sónia P. Miguel, Michiya Matsusaki, Ilídio J. Correia, João F. Mano
Biomaterials Science, 2018, 6(7): 1962-1975
DOI: 10.1039/c8bm00319j
I.F. = 5.251; Q1 and TOP5 Materials Science, Biomaterials (5/32)
Citations - ISI Web of Knowledge: 6, Google Scholar: 8, Scopus: 8

XXII. Biofunctionalization of electrospun Poly(caprolactone) fibers with Maillard Reaction Products for wound dressing applications
Déborah Simões, Sónia P. Miguel, Ilídio J. Correia
Reactive and Functional Polymers, 2018, 131: 191-202
DOI: 10.1016/j.reactfunctpolym.2018.07.021
I.F. = 3.074; Q1 Chemistry, Applied (16/72)
Citations - ISI Web of Knowledge: 2, Google Scholar: 5, Scopus: 5

XXIII. Microstructural, mechanical and biological properties of hydroxyapatite- CaZrO3 biocomposites
Mariana F. Vassal, J. Nunes-Pereira, Sónia P. Miguel, Ilídio J. Correia, Abílio P. Silva
Ceramics International, 2019, 45(7-Part A): 8195-8203
DOI: 10.1016/j.ceramint.2019.01.122
I.F. = 3.450; Q1 and TOP5 Materials Science, Ceramics (2/28)
Citations - ISI Web of Knowledge: 0, Google Scholar: 1, Scopus: 1

XXIV. Functionalization of AuMSS nanorods towards more effective cancer therapies
Carolina F. Rodrigues, Telma A. Jacinto, André F. Moreira, Elisabete C. Costa, Sónia P. Miguel, Ilídio J. Correia
Nano Research, 2019, 12(4): 719–732
DOI: 10.1007/s12274-019-2286-y
I.F. = 8.515; Q1 Chemistry, Physical (23/148)
Citations - ISI Web of Knowledge: 0, Google Scholar: 2, Scopus: 0

XXV. Green reduced graphene oxide functionalized 3D printed scaffolds for bone tissue regeneration
Cátia S. D. Cabral, Sónia P. Miguel, Duarte de Melo-Diogo, Ricardo O. Louro, Ilídio J. Correia
Carbon, 2019, 146: 513-523
DOI: 10.1016/j.carbon.2019.01.100
I.F. = 7.466; Q1 Chemistry, Physical (27/148)
Citations - ISI Web of Knowledge: 0, Google Scholar: 3, Scopus: 2

XXVI. Photocrosslinkable Nanofibrous Asymmetric Membrane Designed for Wound Dressing
Patrícia Alves, Marta Santos, Sabrina Mendes, Sónia P. Miguel, Kevin D. de Sá, Cátia S. D. Cabral, Ilídio J. Correia, Paula Ferreira
Polymers, 2019, 11(4): 653
DOI: 10.3390/polym11040653
I.F. = 3.164; Q1 Polymer Science (17/87)
Citations - ISI Web of Knowledge: 0, Google Scholar: 0, Scopus: 0

XXVII. Preparation of biodegradable functionalized polyesters aimed to be used as surgical adhesives
T. M. Cernadas, F. A. M. M. Gonçalves, Patrícia Alves, Sónia P. Miguel, Cátia S. D. Cabral, Ilídio J. Correia, Paula Ferreira
European Polymer Journal, 2019, 117: 442-454
DOI: 10.1016/j.eurpolymj.2019.05.019
I.F. = 3.621; Q1 Polymer Science (14/87)
Citations - ISI Web of Knowledge: 0, Google Scholar: 1, Scopus: 0

XXVIII. Development of a Poly(vinyl alcohol)/Lysine electrospun membrane-based drug delivery system for improved skin regeneration
Rosa S. Sequeira, Sónia P. Miguel, Cátia S. D. Cabral, André F. Moreira, Ilídio J. Correia
International Journal of Pharmaceutics, 2019, 22: 118640
DOI: 10.1016/j.ijpharm.2019.118640
I.F.= 4.213; Q1 Pharmacology & Pharmacy (44/267)
Citations - ISI Web of Knowledge: 0, Google Scholar: 0, Scopus: 0

XXIX. Microneedle-based delivery devices for cancer therapy: a review
André F. Moreira, Carolina F. Rodrigues, Telma A. Jacinto, Sónia P. Miguel, Elisabete C. Costa, Ilídio J. Correia
Pharmacological Research, 2019, *In press*
DOI: 10.1016/j.phrs.2019.104438
I.F.= 5.574; Q1 Pharmacology & Pharmacy (18/267)
Citations - ISI Web of Knowledge: 0, Google Scholar: 0, Scopus: 0

Manuscripts submitted for publication in peer-reviewed international journals not included in this Doctoral thesis

I. Xanthan Gum-Konjac Glucomannan blend in situ hydrogel for wound dressing
Andreia Alves, Sónia P. Miguel, Andre R. T. S. Araujo, Ilídio J. Correia, Maximiano P. Ribeiro, Paula Coutinho
Submitted for publication.

II. Hyaluronic acid and Vitamin E polyethylene glycol succinate functionalized gold core silica shell nanorods for cancer targeted photothermal therapy
Telma A. Jacinto, Carolina F. Rodrigues, André F. Moreira, Sónia P. Miguel, Elisabete C. Costa, Paula Ferreira, Ilídio J. Correia
Submitted for publication

III. Layer-by-Layer Microneedles for Cancer Chemo-Photothermal Therapy
André F. Moreira, Carolina F. Rodrigues, Telma A. Jacinto, Sónia P. Miguel, Elisabete C. Costa, Ilídio J. Correia
Submitted for publication

Book chapters submitted for publication in international publishers not included in this Doctoral thesis

I. Sónia P. Miguel*, André F. Moreira*, Déborah Simões, Ilídio J. Correia, António G. Mendonça. "3D Printed scaffolds with antibacterial properties for bone tissue regeneration". *Under revision*
* Authors contributed equally to this work

List of Scientific Communications

Oral scientific communications related to this Doctoral thesis

I. Sónia P. Miguel, Ilídio J. Correia, *Development of a bioactive nanofibrous membrane loaded with bioactive molecules for wound healing*, 3 minutes, 1 slide Your thesis!, Universidade da Beira Interior, November 24th, 2015, Covilhã, Portugal.

II. Sónia P. Miguel, Maximiano P. Ribeiro, Paula Coutinho, Ilídio J. Correia, *Electrospun Polycaprolactone/ Aloe Vera_Chitosan nanofibrous asymmetric membranes aimed for wound healing applications*, II International Congress in Health Sciences Research Towards innovation and entrepeneurship: Trends in Biotechnology for Biomedical Applications, Universidade da Beira Interior, May 17th to 20th, 2017, Covilhã, Portugal.

III. Maximiano P. Ribeiro, Sónia P. Miguel, Déborah Simões, Andreia Alves, Paula Coutinho, Ilídio J. Correia, *Development and characterization of Skin substitutes*, XVI Portuguese Conference on Fracture, April 23rd to 24th, 2018, Covilhã, Portugal.

IV. Sónia P. Miguel, Maximiano P. Ribeiro, Paula Coutinho, Ilídio J. Correia, *Electrospun Polycaprolactone/ Aloe Vera_Chitosan nanofibrous asymmetric membranes aimed for wound healing applications*, VI Jornadas de Bioengenharia, Universidade da Beira Interior, May 2nd to 3rd, 2018, Covilhã, Portugal (invited speaker).

Oral scientific communications not related to this Doctoral thesis

I. Maximiano P. Ribeiro, Patrícia I. Morgado, Sónia P. Miguel, Paula Coutinho, Ilídio J. Correia, *Dextran-based hydrogel containing chitosan microparticles loaded with growth factors to be used in wound healing*, VI Jornadas sobre Tecnologia e Saúde, Instituto Politécnico da Guarda, May 3rd, 2013, Guarda, Portugal.

II. Maximiano P. Ribeiro, Sónia P. Miguel, Paula Coutinho, Ilídio J. Correia, *Biomateriais na regeneração da pele*, I Ciclo de Conferências "Biomédicas à tarde", Universidade da Beira Interior, May 7th, 2013, Covilhã, Portugal.

III. Maximiano P. Ribeiro, Sónia P. Miguel, Paula Coutinho, Ilídio J. Correia, *Biomateriais na regeneração da pele*, II Jornadas de Bioengenharia, Universidade da Beira Interior, May 16th, 2013, Covilhã, Portugal.

IV. Maximiano P. Ribeiro, Sónia P. Miguel, Paula Coutinho, Ilídio J. Correia, *Biomateriais na regeneração da pele*, I Encontro Nacional de Estudantes de Biotecnologia, Universidade da Beira Interior, May 25th, 2013, Covilhã, Portugal.

V. Sónia P. Miguel, Maximiano P. Ribeiro, Paula Coutinho, Ilídio J. Correia, *Thermoresponsive chitosan-agarose hydrogel for skin regeneration*, IX CICS Symposium, Universidade da Beira Interior, June 30th to July 1st, 2014, Covilhã, Portugal.

VI. Ana Sofia Silva, Ana M. Sousa, Renato P. Cabral, Marta C. Silva, Sónia P. Miguel, Vasco D. B. Bonifácio, Teresa Casimiro, Ilídio J. Correia, Ana Aguiar-Ricardo, *Aerosolizable gold nano-in-micro dry poder formulations: new prospects for theragnosis and lung cancer delivery*, XX Encontro Luso-Galego de Química, Universidade do Porto, November 26th to 28th, 2014, Porto, Portugal.

VII. Ana Sofia Silva, Sónia P. Miguel, Vasco D. B. Bonifácio, Ilídio J. Correia, Ana Aguiar-Ricardo, *Synthesis, characterization and cellular internalization of gold nanoevices for future microencapsulation for lung delivery*, 1st International Symposium on Nanoparticles/Nanomaterials and Applications, January 20th to 22th, 2014, Caparica, Lisboa, Portugal.

VIII. Kevin D. de Sá, Daniela R. Figueira, Sónia P. Miguel, Tiago R. Correia, Abílio Silva, Ilídio J. Correia, *New antimicrobial hybrid scaffolds based on silver nanoparticles and antimicrobial drug aimed for improved bone regeneration*, XI CICS Symposium, Universidade da Beira Interior, June 30th to July 1st, 2016, Covilhã, Portugal.

IX. Daniela R. Figueira, Sónia P. Miguel, Kevin D. de Sá, Ilídio J. Correia, *"Production and characterization of a new electrospun nanofibrous membrane aimed for skin tissue engineering*, XI CICS Symposium, Universidade da Beira Interior, June 30th to July 1st, 2016, Covilhã, Portugal.

X. Sónia P. Miguel, Kevin D. De Sá, João C. Boga, Daniela R. Figueira, Duarte de Melo-Diogo, Tiago R. Correia, Abílio P. Silva, António G. Mendonça, Ricardo O. Louro, Ilídio J. Correia, *Functionalization of 3D printed scaffolds for bone tissue regeneration*, XVI Portuguese Conference on Fracture, April 23rd to 24th, 2018, Covilhã, Portugal.

Poster presentations within the scope of this Doctoral thesis

I. Sónia P. Miguel, Ilídio J. Correia, *Development of a bioactive nanofibrous membrane loaded with bioactive molecules for wound healing*, Semana da Ciência e Tecnologia, Universidade da Beira Interior, November 23rd to 29th, 2015, Covilhã, Portugal.

II. Sónia P. Miguel, Maximiano P. Ribeiro, Paula Coutinho, Ilídio J. Correia, *Electrospun Polycaprolactone/Aloe Vera_Chitosan Nanofibrous Asymmetric Membranes Aimed for Wound Healing Applications*, Encontro com a Ciência e Tecnologia 2017, Centro de Congressos de Lisboa, July 3rd to 5th, 2017, Lisboa, Portugal.

III. Sónia P. Miguel, Cátia S. D. Cabral, André F. Moreira, Ilídio J. Correia, *Novel asymmetric 3d printed construct for skin regeneration*, XIV CICS Symposium, Universidade da Beira Interior, July 4th to 5th, 2019, Covilhã, Portugal.

Poster presentations not related to this Doctoral thesis

I. Patrícia I. Morgado, Maximiano P. Ribeiro, Sónia P. Miguel, Ilídio J. Correia Ana Aguiar-Ricardo, *Development of poly(vinyl alcohol) and chitosan wound dressings using supercritical fluids technology* , 11º Encontro Nacional de Química-Física, Universidade do Porto, May 9th to 10th, 2013, Porto, Portugal.

II. Sónia P. Miguel, Maximiano P. Ribeiro, Hugo Brancal, Paula Coutinho, Ilídio J. Correia, *Thermoresponsive chitosan-agarose hydrogel for skin regeneration*, Encontro Bienal das Divisões Técnicas da Sociedade Portuguesa de Materiais (SPM), Universidade da Beira Interior, May 4th, 2014, Covilhã, Portugal.

III. Anita Lourenço, Pedro F. Lisboa, Alexandre Paiva, António Ornelas-Soares, Marco Miranda, Sónia P. Miguel, Ilídio J. Correia, Rosário Mato, Ilda Santos-Sanches, Ana Aguiar-Ricardo, Pedro Simões, Teresa Casimiro, *Extraction and impregnation of lavender essential oil in HDPE using supercritical carbon dioxide*, 14th European Meeting on Supercritical Fluids, Palais du Pharo, Marcelh, May 18th to 21th, 2014, Marcelha, France.

IV. Patrícia I. Morgado, Pedro F. Lisboa, Maximiano P. Ribeiro, Sónia P. Miguel, Pedro C. Simões, Ilídio J. Correia, Ana Aguiar-Ricardo, *ScCO_2-phase inversion technique: a sustainable method to produce asymmetric membranes with highly controlled morphology toward the ideal wound dressing*, Gordon Research Conference / Seminar on Green Chemistry, The Chinese University of Hong Kong, July 26th to 27th, 2014, Hong Kong, China.

V. Mariana B. Oliveira, Maximiano P. Ribeiro, Sónia P. Miguel, Ana I. Neto, Paula Coutinho, Ilídio J. Correia, João F. Mano, *Biomimetic superhydrophobic surfaces patterned with wettable spots as implantable chips for in vivo high-content 3D biomaterials response assessment*, 4th TERMIS World Congress - Past, Present Future: The Evolution of Regenerative Medicine, September 8th to 11th, 2015, Boston, United States of America.

VI. Ana Sofia Silva, Renato P. Cabral, Ana M. Sousa, Marta C. Silva, Vanessa Almeida, Sónia P. Miguel, Vasco D. B. Bonifácio, Teresa Casimiro, Ilídio J. Correia, Ana Aguiar-Ricardo, *Innovative development of nano-in-micro dry powder formulations for lung cancer treatment*, 2nd EuChems on Green and Sustainable Chemistry, Faculdade de Ciências e Tecnologia, Universidade NOVA de Lisboa, October 4th to 7th, 2015, Lisboa, Portugal.

VII. Patrícia Morgado, Sónia P. Miguel, Ilídio J. Correia, Ana Aguiar-Ricardo, *Designing ibuprofen carriers to modify the release behavior from hydrogel dressings: A highly efficient strategy towards faster skin wound healing*, 2nd EuCheMS Congress on Green and Sustainable Chemistry, Faculdade de Ciências e Tecnologia, Universidade NOVA de Lisboa, October 4 to 7th, 2015, Lisboa, Portugal.

VIII. Kevin D. de Sá, Daniela R. Figueira, Sónia P. Miguel, Tiago R. Correia, Abílio Silva, Ilídio J. Correia, *3D scaffolds coated with nanofibers displaying bactericidal activity for bone tissue applications*, V Encontro de Estudantes de Materiais (ENEM), Universidade da Beira Interior, September 29th to 30th, 2016, Covilhã, Portugal.

IX. João C. Boga, Sónia P. Miguel, António G. Mendonça, Ilídio J. Correia, *"New 3D printed structures for bone tissue regeneration*, V Encontro de Estudantes de Materiais (ENEM), Universidade da Beira Interior, September 29th to 30th, 2016, Covilhã, Portugal.

X. Kevin D. de Sá, Daniela R. Figueira, Sónia P. Miguel, Tiago R. Correia, Abílio Silva, Ilídio J. Correia, *3D scaffolds coated with nanofibers displaying bactericidal activity for bone tissue applications*, V Ciclo de Conferências da Faculdade de Ciências, Universidade da Beira Interior, January 21st, 2017, Covilhã, Portugal.

XI. João C. Boga, Sónia P. Miguel, António G. Mendonça, Ilídio J. Correia, *New 3D printed structures for bone tissue regeneration*, V Ciclo de Conferências da Faculdade de Ciências, Universidade da Beira Interior, January 21st, 2017, Covilhã, Portugal.

XII. Daniela R. Figueira, Kevin D. de Sá, Sónia P. Miguel, Ilídio J. Correia, *Production and characterization of polycaprolactone-hyaluronic acid/chitosan-zein electrospun bilayer nanofibrous membrane for tissue regeneration*, II International Congress in Health Sciences Research Towards innovation and entrepeneurship: Trends in Biotechnology for Biomedical Applications, Universidade da Beira Interior, May 17th to 20th , 2017, Covilhã, Portugal.

XIII. Daniela R. Figueira, Kevin D. de Sá, Sónia P. Miguel, Ilídio J. Correia, *Production and characterization of polycaprolactone-hyaluronic acid/chitosan-zein electrospun bilayer nanofibrous membrane for tissue regeneration,* Encontro com a Ciência e Tecnologia 2018, Centro de Congressos de Lisboa, July 2nd to 4th, 2018, Lisboa, Portugal.

XIV. Cátia S. D. Cabral, Sónia P. Miguel, Duarte de Melo-Diogo, Ilídio J. Correia, *3D printed scaffolds functionalized with Graphene Oxide: a new strategy to improve bone tissue regeneration*, XIII CICS Symposium, Universidade da Beira Interior, July 5th to 6th, 2018, Covilhã, Portugal.

XV. Déborah Simões, Sónia P. Miguel, Ilídio J. Correia, *Biofunctionalization of electrospun Polycaprolactone fibers with Maillard Reaction Products for Wound Dressing Applications*, XIII CICS Symposium, Universidade da Beira Interior, July 5th to 6th, 2018, Covilhã, Portugal.

XVI. Teresa Cernadas, Filipa Gonçalves, Sónia P. Miguel, Ilídio J. Correia, Paula Ferreira, *Synthesis and functionalization of unsatured polyesters to be applied as tissue adhesives*, XVI Latin-American Polymer Symposium (SLAP 2018) and XIV Iberoamerican Polymer Congress (CIP 2018), November 6th to 9th, 2018, Mar del Plata, Argentina.

XVII. Patrícia Alves, Patrícia Coimbra, Sónia P. Miguel, Marco P. Carvalho, Kevin D. de Sá, Ilídio J. Correia, Paula Ferreira, *Photocrosslinkable coaxial electrospun fibers as scaffolds for vascular tissue engineering*, XVI Latin-American Polymer Symposium (SLAP 2018) and XIV Iberoamerican Polymer Congress (CIP 2018), November 6th to 9th, 2018, Mar del Plata, Argentina.

XVIII. Cátia S. D. Cabral, Sónia P. Miguel, Duarte de Melo-Diogo, Ricardo O. Louro, Ilídio J. Correia, *Bioactive 3D printed scaffolds functionalized with reduced graphene oxide for bone tissue regeneration*, 6th IEEE Portuguese Meeting on Bioengineering (ENBENG 2019), Instituto Superior de Engenharia de Lisboa, February 22nd to 23rd, 2019, Lisboa, Portugal.

XIX. Rosa S. Sequeira, Sónia P. Miguel, Cátia S. D. Cabral, André Moreira, Ilídio J. Correia, *Production of new electrospun membrane-based drug delivery system for wound dressing applications*, XIV CICS Symposium, Universidade da Beira Interior, July 4th to 5th, 2019, Covilhã, Portugal.

XX. Cátia S. D. Cabral, Sónia P. Miguel, Duarte de Melo-Diogo, Ricardo O. Louro, Ilídio J. Correia, *3D printed scaffolds functionalized with in situ reduced graphene oxide for bone tissue regeneration*, Encontro com a Ciência e Tecnologia 2019, Centro de Congressos de Lisboa, July 8th to 10th, 2019, Lisboa, Portugal.

Awards not related to this Doctoral thesis

I. Poster presentation of the work entitled "Thermoresponsive chitosan-agarose hydrogel for skin regeneration" presented in Encontro Bienal das Divisões Técnicas da Sociedade Portuguesa de Materiais (SPM), Universidade da Beira Interior, May 4th, 2014, Covilhã, Portugal.

II. Winner in SCIENT Competition- Entrepreneurship Academy and Business Competition, performed in Universidade da Beira Interior, Covilhã, Portugal, October 28th, 2016.

III. Winner in SCIENT Competition- Entrepreneurship Academy and Business Competition, performed in University of Cyprus, Nicósia, Chyprus, September 11th to 14th, 2017.

Conference Organizing Committees

Member of the organizing committee of scientific conferences

I. XVI Portuguese Conference on Fracture, TRYP Dona Maria, April 23rd to 24th, 2018, Covilhã, Portugal.

Resumo alargado

A Organização Mundial de Saúde estima que, anualmente, 180 000 mortes ocorrem como consequência de queimaduras. Só nos Estados Unidos, as feridas crónicas (por exemplo úlceras diabéticas e de pressão) afetam 6,5 milhões de pessoas. Desta forma, as lesões cutâneas constituem uma das maiores preocupações de saúde a nível mundial.

Com o objetivo de minimizar os efeitos das lesões cutâneas, é crucial proteger a lesão de forma a reduzir o risco de infeção e, por outro lado, promover/acelerar o processo de cicatrização. Neste contexto, os investigadores têm desenvolvido diferentes tipos de biomateriais (hidrocolóides, esponjas, hidrogéis, membranas, etc.), que sejam capazes de estabelecer uma barreira mecânica contra os microrganismos, prevenir a desidratação e, ainda, acelerar o processo de cicatrização. Nos últimos anos, as membranas produzidas através da técnica de electrofiação têm sido intensamente investigadas para aplicação no tratamento de feridas. Esta técnica permite a produção de redes de nanofibras com diâmetros entre 50-500 nm, que reproduzem a estrutura das fibras de colagénio presentes na matriz extracelular da pele nativa. Por outro lado, a elevada porosidade e o tamanho de poro exibido pela rede de nanofibras permitem as trocas gasosas, a absorção do exsudado das feridas, e conferem proteção ao local da ferida contra a invasão por microrganismos e a desidratação. Além disso, as membranas eletrofiadas têm sido funcionalizadas com moléculas com atividade antimicrobiana (por exemplo antibióticos, nanopartículas de prata e extratos naturais), ou com atividade biológica (fatores de crescimento, vitaminas e anti-inflamatórios), com o objetivo de melhorar o processo de cicatrização de feridas. Entre os diversos tipos de moléculas utilizados até ao momento, os extratos de origem natural, como sejam os de Aloe Vera e os óleos essenciais têm sido incorporados nos revestimentos cutâneos, devido às suas excelentes propriedades biológicas e aos efeitos benéficos que estes apresentam para o processo de cicatrização.

Por outro lado, os investigadores começaram, recentemente, a explorar a produção de membranas assimétricas para aplicação como revestimentos cutâneos. Estas membranas são compostas por duas camadas, que mimetizam a morfologia da pele nativa, *i.e.* reproduzem a estrutura da epiderme e da derme. Até ao momento, as membranas assimétricas foram principalmente produzidas através da técnica de inversão de fase seca/húmida e da técnica de inversão de fases por dióxido de carbono supercrítico ($scCO_2$). Tendo isto em conta, o plano de trabalhos desenvolvido durante o meu doutoramento teve como principal objetivo explorar a técnica de electrofiação para a produção de membranas assimétricas que possam ser usadas para melhorar o processo de cicatrização de feridas. Para tal, foram exploradas diferentes estratégias: i) produção de membranas assimétricas combinando diferentes tipos de polímeros naturais (fibroína de seda (SF), ácido hialurónico (HA), sericina de seda (SS)), e/ou sintéticos; ii) incorporação de biomoléculas no interior das nanofibras com o objetivo de melhorar as

propriedades biológicas das membranas (Aloe Vera e timol (THY)); iii) combinação das membranas nanofibrosas com hidrogéis produzidos por impressão tridimensional (3D), de forma a obter um substituto de pele com geometria assimétrica.

No primeiro estudo apresentado nesta tese, foi produzida e caracterizada uma membrana assimétrica composta por uma camada superior de Policaprolactona (PCL) e uma camada inferior de Quitosano (CS)/Aloe Vera. A escolha do polímero sintético e hidrofóbico (PCL) para produzir a camada superior permitiu obter uma membrana densa capaz de fornecer suporte mecânico ao local da lesão. Os resultados obtidos neste estudo demonstraram que a baixa porosidade e caracter hidrofóbico apresentado pela camada superior foi essencial para evitar a infiltração de microrganismos (*Staphylococcus aureus* (*S. aureus*) e *Escherichia coli* (*E. coli*)). Por outro lado, a incorporação de Aloe Vera nas nanofibras de CS permitiu a produção de uma camada inferior capaz de providenciar um ambiente húmido ao local da lesão, e ainda promover uma melhor e mais rápida adesão/proliferação dos fibroblastos. Além disso, o crescimento de microrganismos na parte inferior da membrana foi inibido devido às propriedades antimicrobianas do CS e do Aloe Vera.

No segundo estudo realizado, foram exploradas as propriedades da SF na produção de membranas assimétricas à base de nanofibras, nas quais foi incorporada uma biomolécula (THY), com vista a melhorar o processo de cicatrização de feridas. A SF foi selecionada para este estudo tendo em conta que é uma proteína fibrosa, a qual apresenta excelente biocompatibilidade, biodegradabilidade e força mecânica. A camada superior da membrana foi produzida com uma mistura de PCL/SF com o intuito de obter uma camada com propriedades mecânicas semelhantes à epiderme. Por outro lado, para obter uma camada inferior que reproduza a derme, a SF foi combinada com o HA. A combinação destes compostos permitiu obter uma camada capaz de absorver o exsudado, bem como promover a adesão e proliferação celular. Adicionalmente, o THY foi incorporado nas nanofibras da camada inferior, para lhe conferir propriedades antibacterianas e antioxidantes. Os resultados obtidos mostraram que a camada superior da membrana assimétrica possui uma baixa porosidade, o que lhe permitiu evitar a infiltração dos microrganismos. Por outro lado, a elevada porosidade da camada inferior é essencial para providenciar um ambiente hidratado ao local da lesão, bem como promover a migração/infiltração das células. Além disso, os ensaios mecânicos evidenciaram que as membranas assimétricas possuem propriedades mecânicas semelhantes às exibidas pela pele nativa. Os ensaios *in vitro* demonstraram ainda que os fibroblastos humanos aderiram e proliferaram na superfície das membranas. A incorporação do THY na camada inferior conferiu propriedades antioxidantes e antibacterianas à membrana produzida.

No terceiro estudo apresentado nesta tese foi produzido, através da combinação da técnica de electrofiação com a impressão 3D, um substituto de pele assimétrico. Neste trabalho além de ter sido usada uma nova combinação de polímeros, foram também utilizadas técnicas diferentes

para reproduzir as propriedades/estrutura da epiderme e da derme. Desta forma, a técnica de electrofiação foi utilizada com o intuito de obter uma camada superior composta por uma malha de nanofibras, com excelentes propriedades mecânicas e capacidade de efetuar trocas gasosas. Por outro lado, a camada inferior foi produzida através da impressão 3D de um hidrogel, permitindo assim obter uma estrutura 3D capaz de absorver grandes quantidades de exsudado, bem como promover a migração celular. Os resultados obtidos demonstraram que a camada superior composta por PCL e SS evitou a infiltração de microrganismos (*S. aureus* e *Pseudomonas aeruginosa* (*P. aeruginosa*)), e apresentou excelentes propriedades mecânicas semelhantes às exibidas pela epiderme da pele nativa. Em contrapartida, a camada inferior constituída por um hidrogel impresso de CS e alginato de sódio apresentou uma porosidade adequada, hidrofilicidade e as propriedades biológicas necessárias para suportar a adesão, migração e proliferação dos fibroblastos. Além disso, as propriedades antimicrobianas do CS foram demonstradas pela capacidade da camada inferior inibir o crescimento de *S. aureus* e *P. aeruginosa*.

Em suma, os resultados obtidos nos estudos realizados demonstram a versatilidade da técnica de electrofiação para a produção de membranas assimétricas. Esta técnica permite combinar diferentes polímeros naturais/sintéticos, incorporar biomoléculas no interior das nanofibras e, ainda reproduzir as propriedades da epiderme e da derme. No futuro, a performance destas membranas no tratamento de lesões cutâneas poderá ser incrementada através da incorporação de biomoléculas/células. O uso de outras técnicas poderá também ser considerado, com o objetivo de produzir estruturas com forma/tamanho adequados à lesão do paciente. Além disso, os ensaios *in vivo* poderão ainda revelar resultados promissores, que contribuirão para a translação destes substitutos de pele para os ensaios clínicos.

Palavras-chave

Electrofiação; membranas assimétricas; nanofibras; polímeros; regeneração da pele; substitutos de pele.

Abstract

According to the World Health Organization, it is estimated that 180 000 deaths occur, every year, as consequence of burns. In United States, it is expected that chronic wounds (*e.g.* diabetic and pressure ulcers) affect 6.5 million people. Thus, skin lesions are a public health problem.

To minimize the effects of skin injuries, it is crucial to protect the wound site for decreasing the risk of infection, as well as promote/accelerate the wound healing process. In this context, researchers have been developing different types of biomaterials (*e.g.* hydrocolloids, sponges, hydrogels, membranes) to provide a barrier against microorganisms, avoid the dehydration, and enhance the healing process. Among them, the membranes obtained through the electrospinning technique have been investigated for wound dressing applications. This technique allows the production of fibers networks with diameters between 50-500 nm, that mimic the dimensions of the collagen fibers found in the skin' extracellular matrix. Furthermore, the membranes' high porosity and small pore size allow gaseous exchanges and exudates absorption, as well as provide protection at the wound site from microorganisms' invasion and dehydration. Moreover, the electrospun membranes have been functionalized with antibacterial molecules (*e.g.* antibiotics, silver nanoparticles, and natural extracts) or molecules with biological activity (growth factors, vitamins, and anti-inflammatory) to improve the skin regeneration process. Among the different types of molecules, the natural extracts, like Aloe Vera (AV) and essential oils, have triggered the attention of the researchers to produce wound dressings, due to their excellent biological properties and beneficial effects for the healing process.

More recently, researchers started to explore the production of the membranes with asymmetric structure to be applied as wound dressings. These membranes are composed of two layers, that mimic the morphology of native skin, thereby reproducing the properties of the epidermis and dermis. Heretofore, the asymmetric membranes were mainly produced by using dry/wet phase and supercritical carbon dioxide ($scCO_2$)- assisted phase inversion techniques. Taking this into consideration, the work plan developed during my PhD had as main goal to explore the electrospinning technique to produce asymmetric membranes, aimed to improve healing process. To accomplish that, different strategies were explored: i) production of asymmetric electrospun membranes by combining different types of polymers (naturals (silk fibroin (SF), hyaluronic acid (HA), silk sericin (SS) and/or synthetic); ii) incorporation of biomolecules within nanofibers to improve the biological properties of membranes (AV and thymol (THY)); iii) combination of the electrospun nanofibrous membranes with three-dimensional (3D) printed hydrogels, to obtain an asymmetric skin substitute.

In the first study presented in thesis, an asymmetric electrospun membrane with a top layer composed of Polycaprolactone (PCL) and a bottom layer of CS/AV was produced and characterized. The results obtained in this study demonstrated that the low porosity and hydrophobic character exhibited by top layer was crucial to avoid the microorganism infiltration (*S. aureus*) and *Escherichia coli* (*E. coli*)). On the other side, the AV incorporation into CS nanofibers allowed the production of a bottom layer that was able to provide a moist environment at the wound site, as well as promote an improved fibroblasts' adhesion and proliferation. Further, the microorganism growth at bottom layer' surface was inhibited due to the antimicrobial properties of CS and AV.

In the second study presented herein, SF was used to produce an asymmetric electrospun nanofibrous membranes, in which a bioactive compound (THY) was incorporated to improve the wound healing process. SF is a fibrous protein, that presents excellent biocompatibility, good water vapor permeability, biodegradability, mechanical strength, and minimal inflammatory reaction. In this way, the SF was combined with PCL to produce the top layer, that mimic the epidermis layer. On the other hand, SF was also mixed with HA to produce a bottom layer that mimic the dermis layer. This polymeric combination allowed the production of a structure able to absorb the wound exudates and promote the cell's adhesion and proliferation. In addition, THY was incorporated into the bottom nanofibrous membrane to provide antibacterial and antioxidant properties. The results obtained showed that the top layer of the asymmetric membrane displays a low porosity was able to avoid microorganisms' infiltration, whereas the high porosity of the bottom layer is crucial to assure a moist environment at the wound site as well as promote the cellular migration/infiltration. Further, the mechanical assays demonstrated that the asymmetric membranes displayed mechanical parameters that are similar to those exhibited by native skin. On the other side, the *in vitro* assays demonstrated that the human fibroblasts adhered and proliferated at the membranes' surface, and the THY incorporation into bottom layer conferred antioxidant and antibacterial properties to the membrane.

In the third study presented in this thesis, a 3D skin asymmetric construct (SAC) was produced, by combining the electrospinning and the 3D printing techniques. In this work, the asymmetric skin construct was obtained through the combination of materials (that was performed for the first time) and by using different production techniques to reproduce the properties/structure of epidermis and dermis. In this way, the electrospinning technique was used to obtain a top layer composed of a nanofibrous mesh presenting excellent mechanical properties and gaseous exchange capacity. On the other side, the dermis-like layer was produced by using the 3D printing of hydrogel, allowing to achieve a 3D structure able to absorb high amounts of exudate, as well as to promote the cell migration. The obtained results demonstrate that the epidermis-like top layer composed of PCL and SS electrospun nanofibers avoided the microorganisms' infiltration (*S. aureus* and *Pseudomonas aeruginosa* (*P. aeruginosa*)) and displayed excellent

mechanical properties quite similar to those of the native skin. In contrast, the bottom layer produced, by performing the 3D printing of CS and sodium alginate (SA) hydrogel, presented suitable porosity, wettability, and biological properties that supported fibroblasts' adhesion, migration and proliferation. Further, the antimicrobial properties of CS enabled the inhibition of the *S. aureus and P. aeruginosa* growth at the bottom layer's surface.

Overall, the results obtained in these experimental works demonstrate the versality of the electrospinning technique, which allows to combine different natural/synthetic polymers, incorporate biomolecules within nanofibers, and produce two distinct layers that mimic the epidermis and dermis features. On the other side, membranes' performance on the treatment of skin injuries can be improved by the incorporation of biomolecules or cells. The use of the other techniques can also be hypothesized to produce structures with a personalized shape/size that fulfil the patient needs. Further, the realization of *in vivo* assays may reveal promising results that will speed up the evaluation of these skin substitutes in clinical assays.

Keywords

Asymmetric membranes; electrospinning; nanofibers; polymers; skin regeneration; wound dressing.

Thesis overview

This Doctoral thesis is organized in 6 chapters.

The first chapter comprises the overall objectives established for the development of the work plan defined for the PhD thesis.

The second chapter enclose the Introductory section, which gives an overview of the properties and functionalization strategies used so far to produce the electrospun membranes aimed to be used as wound dressings; the state-of-the-art of the bioactive molecules that have been incorporated into electrospun membranes aimed to avoid skin infections and/or to improve the healing process; the production techniques used to obtain asymmetric membranes aimed for wound dressing applications.

The third, fourth, and fifth chapter present three research works:

- Research Work 1: Electrospun Polycaprolactone/Aloe Vera_Chitosan Nanofibrous Asymmetric Membranes Aimed for Wound Healing Applications (Chapter 3)

- Research Work 2: Production and characterization of electrospun Silk Fibroin based asymmetric membranes for wound dressing applications (Chapter 4)

- Research Work 3: Production and characterization of a novel asymmetric 3D printed construct aimed for skin tissue regeneration (Chapter 5)

Finally, the sixth chapter includes the concluding remarks, where the main results obtained during my PhD are highlighted and discussed. Furthermore, future perspectives regarding this research topic are also addressed in this chapter.

Table of Contents

Chapter III- Research Work 1

Chapter IV- Research Work 2

Chapter V- Research Work 3

Chapter VI- Concluding Remarks and Future Perspectives

List of Figures

Chapter II

Chapter III

Chapter IV

Chapter V

Chapter VI

List of Tables

Chapter II

Chapter III

Chapter IV

Chapter VI

List of Acronyms

3D_SAC	Three-dimensional skin asymmetric construct
AA	Acetic acid
AgNPs	Silver nanoparticles
ANOVA	One-way analysis of variance
ATR-FTIR	Attenuated Total Reflectance–Fourier Transform Infrared Spectroscopy Analysis
AV	Aloe Vera
bFGF	Basic fibroblast growth factor
BSA	Bovine serum albumin
CA	Cellulose acetate
CAD	Computer aided design
CFU	Colony forming units
Chr	Chrysin
CIF	Ciprofloxacin
CLSM	Confocal laser scanning microscopy
CMCS	Carboxymethyl chitosan
CN	Cinnamon
COX	Cyclooxygenase
CS	Chitosan
CS-NPs	Chitosan nanoparticles
DCM	Dichloromethane
DD	Degree of deacetylation
DEX	Dexamethasone
DLF	Diclofenac
DMEM-F12	Dulbecco's modified Eagle's medium
dsDNA	Double-stranded deoxyribonucleic acid
E. coli	*Escherichia coli*
EAM	Electrospun asymmetric membrane
ECM	Extracellular matrix
EDTA	Ethylenediaminetetraacetic acid
EE	Encapsulation efficiency
EGF	Epidermal growth factor
EIF	Epidermal induction factors
EOs	Essential oils
FA	Formic acid
FBS	Fetal bovine serum
FGF	Fibroblast growth factor
GA	Glutaraldehyde
GAGs	Glycosaminoglycans
GFs	Growth factors
HA	Hyaluronic acid
HaCaT	Human keratinocyte cell line
IBP	Ibuprofen

IL-1	Interleukin 1
IL-6	Interleukin 6
IL-10	Interleukin 10
K^-	Negative control
K^+	Positive control
L929	Mouse fibroblast cells
LbL	Layer-by-layer
LG	Lemongrass
LPS	Lipopolysaccharide
MBC	Minimum bactericidal concentration
MIC	Minimal inhibitory concentration
MMPs	Metalloproteinases
MRSA	Methicillin-resistant *Staphylococcus aureus*
MTS	3-(4,5-Dimethylthiazol-2-yl)-5-(3-carboxymethoxyphenyl)-2 (4-sulfophenyl)-2H-tetrazolium
NAP	Naproxen
NHDF	Normal human dermal fibroblasts
NO	Nitric oxide
OREC	Organic rectorite
P(LLA-CL)	Poly(L-lactic acid-*co*-ε-caprolactone)
P. aeruginosa	*Pseudomonas aeruginosa*
PAN	Polyacrylonitrile
PBS	Phosphate-buffered saline solution
PCL	Polycaprolactone
PDEGMA	Poly(di(ethylene glycol) methyl ether methacrylate)
PDGF	Platelet-derived growth factor
PDMAEMA	Poly((2-dimethylamino)ethyl methacrylate)
PEG	Polyethylene glycol
PEO	Polyethylene oxide
PFA	Paraformaldehyde
PGA	Poly(glycolic acid)
PHT-Na	Phenytoin sodium
PI	Propidium iodide
PIECs	Porcine hip artery endothelial cells
PLA	Polylactic acid
PLGA	Poly(lactide-*co*-glycolide)
PLLCL	Poly(L-lactic acid)-*co*-poly-(ε-caprolactone)
PM	Peppermint
PMS	Phenazine methosulfate
PMVEMA	Poly(methyl vinyl etherco-maleic acid)
POCA	Phosphino carboxylic acid polymer
PPF	Polypropylene fumarate
PU	Polyurethane
PVA	Polyvinyl alcohol
PVP	Polyvinylpyrrolidone
ROS	Reactive oxygen species

RPM	Rotation per minute
RT	Room temperature
S. aureus	*Staphylococcus aureus*
$scCO_2$	Supercritical carbon dioxide
SA	Sodium alginate
S. epidermis	*Staphylococcus epidermis*
SEM	Scanning electron microscopy
SF	Silk fibroin
SS	Silk sericin
SSD	Silver sulfadiazine
TCH	Tetracycline hydrochloride
TFA	Trifluoroacetic acid
TFE	Trifluoroethanol
TGF-β	Transforming growth factor-β
THY	Thymol
TNF-α	Tumor necrosis factor-α
TPGS	PEGylated derivative of Vitamin E
TPP	Sodium Tripolyphosphate
UV	Ultraviolet radiation
VEGF	Vascular endothelial growth factor
VE-SNPs	Starch nanoparticles loaded with Vitamin E
Vit-A	Vitamin A
Vit-C	Vitamin C
Vit-E	Vitamin E
WCA	Water contact angle
WVTR	Water vapor transmission rate
ZN	Zein
ZnO	Zinc oxide

Chapter I

Global Aims

1. Global Aims

The electrospun membranes display auspicious properties for assisting the healing process. On the other side, recently the asymmetric membranes have arisen as a promising approach for developing more effective wound dressings. However, the production of asymmetric membranes through the electrospinning technique has been poorly explored in the literature.

So, the main objective of this PhD thesis was to explore the application of the electrospinning technique for the production of asymmetric membranes aimed to be applied in the treatment of skin injuries. Thus, the specific aims of this thesis were:

1. Produce electrospun asymmetric wound dressings by combining natural/synthetic polymers and incorporating a natural extract (AV);

2. Produce a SF-based electrospun asymmetric membrane (EAM) that can act as drug delivery system, incorporating an essential oil (THY);

3. Produce a new asymmetric skin construct using electrospinning and 3D printing techniques;

4. Characterize the morphology, asymmetric geometry and mechanical properties of the wound dressings produced;

5. Characterize the porosity, wettability, swelling and biodegradation profile of the produced membranes;

6. Evaluate the biological properties (cytocompatibility, antioxidant, cell adhesion and migration) of the asymmetric wound dressings' layers;

7. Evaluate the antimicrobial properties of the produced membranes.

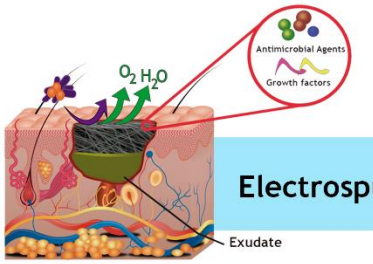

Electrospun membranes as wound dressing

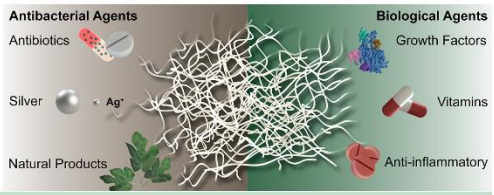

Bioactive molecules

Chapter II

Introduction

Asymmetric membranes

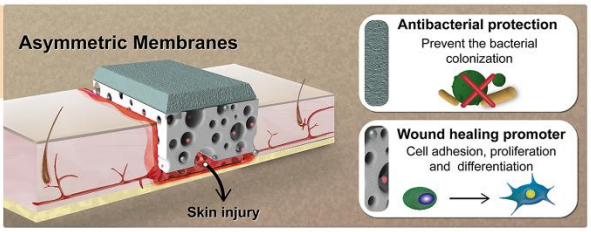

This chapter is based on the following publications:

- Sónia P. Miguel, Daniela R. Figueira, Déborah Simões, Maximiano P. Ribeiro, Paula Coutinho, Paula Ferreira, Ilídio J. Correia; Electrospun polymeric nanofibers as wound dressings: a review, *Colloids and Surfaces B: Biointerfaces*, 2018, 169(5):60-71.
(DOI: 10.1016/j.colsurfb.2018.05.011).
- Sónia P. Miguel, Rosa S. Sequeira, André F. Moreira, Cátia S. D. Cabral, António G. Mendonça, Paula Ferreira, Ilídio J. Correia; An overview of electrospun membranes loaded with bioactive molecules for improving the wound healing process, *European Journal of Pharmaceutics and Biopharmaceutics*, 2019, 139: 1-22.
(DOI: 10.1016/j.ejpb.2019.03.010).
- Sónia P. Miguel, André F. Moreira, Ilídio J. Correia; Chitosan based-asymmetric membranes for wound healing: a review, *International Journal of Biological Macromolecules*, 2019, 127: 460-475.
(DOI: 10.1016/j.ijbiomac.2019.01.072).

2.1 Skin structure and functions

Skin is the largest organ of the human body, acting as a protective barrier against the external environment [1]. Moreover, the skin is also involved in sensation, thermoregulation, biochemical, metabolic and immune functions [2]. Skin is composed of three connected layers: epidermis, dermis, and hypodermis (as illustrated in Figure 2.1) [3].

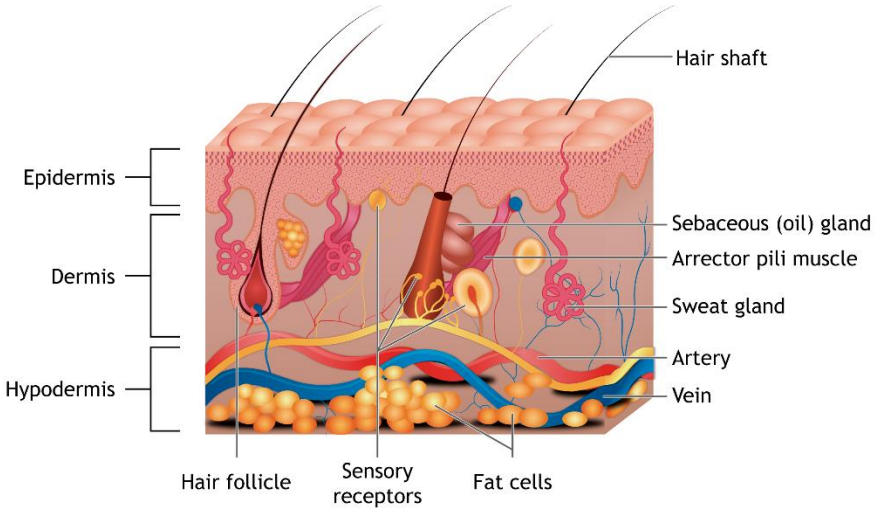

Figure 2.1. Representation of the skin structure.

The epidermis is the outermost layer, displaying a stratified structure and an high impermeability that provide a physical, chemical/biochemical and an adaptive immunological barrier to the human body [4]. This layer consists mainly of a stratified squamous epithelium where the predominant cells are keratinocytes (90-95%). These cells are involved in the formation of cytoskeleton filaments that maintain the structural cohesion. Other types of cells that can also be found in epidermis, like antigen-processing Langerhans cells, pigment-containing melanocytes and Merkel cells for pressure sensing [5].

In turn, the dermis is composed by a collagen-rich extracellular matrix (ECM) and others structural proteins (hyaluronic acid (HA), elastin and glycosaminoglycans (GAGs)), that confer the physical strength as well as flexibility to the skin. Fibroblasts are the most abundant cells in the dermis, and they are responsible for the synthesis of ECM components. In turn, the basement membrane separates the dermis from the epidermis and supports its extensive vasculature, lymphatic system and nerve bundles [6]. The hypodermis, the bottom layer, is essentially composed by adipose tissue and it is determinant for the thermoregulatory and mechanical properties of the skin [7].

Therefore, the skin is a multifunctional organ that provides protection to muscles, bones, ligaments and internal organs against external biological, chemical, mechanical and physical agents [2]. Further, skin is also involved in sensation, temperature regulation, immunological

surveillance, prevention of water loss (dehydration) and synthesis of vitamin D3 [8]. These skin functions would be impaired by any defect or damage caused by physical or thermal factors (fire-related burns, chemical or mechanical trauma and surgical procedures) or by infectious disease [9, 10].

2.2 Wounds classification

The Wound Healing Society defines "wound" as being the result of the disruption of the normal anatomic structure and functions of the skin [11]. Based on the nature and duration of the healing process, wounds can be classified as acute or chronic (as represented in Figure 2.2) [12, 13]. An acute wound is an injury that occurs suddenly due to mechanical damage induced by sheer, blunting, and/or stabling action of hard objects. Furthermore, this type of wounds may also occur as consequence of extreme heat exposure, irradiation, electrical shock, and/or contact with corrosive chemicals. The healing process of these wounds lasts between 8-12 weeks depending on the size, depth and the extent of damage [12, 14].

Contrariwise, chronic wounds are characterized by presenting a slow healing rate and severe scars. The healing process of these type of wounds may span for more than 12 weeks, and usually occur in patients who have co-morbidities, like obesity, diabetes, tumors, and severe bacterial contamination [12, 15].

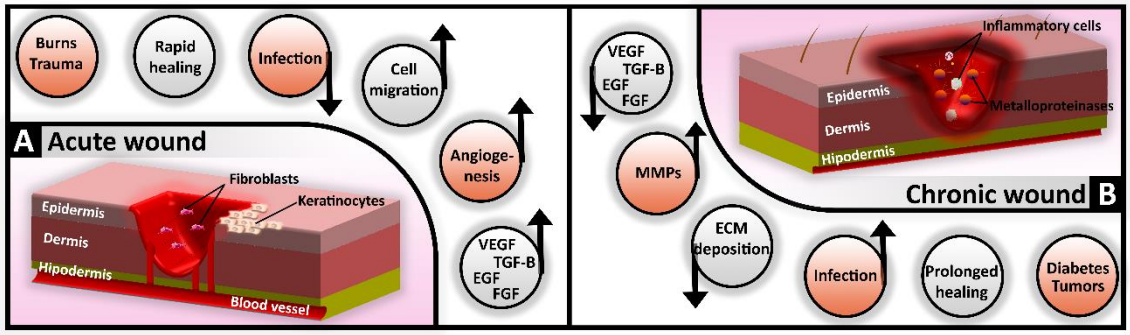

Figure 2.2. Illustrative representation of the healing process that occurs in acute and chronic wounds. Acute wound healing (A) is associated to the cell migration, proliferation and the secretion of high levels of growth factors, which are involved in the stimulation of the synthesis of new ECM; In turn, the chronic wound healing (B) is characterized by an exuberant inflammation, increased matrix metalloproteinases production that impairs cell proliferation and hence delays the formation of the new skin tissue.

2.3 Wound healing process

The healing process starts immediately after an injury occurs and it involves complex interactions between ECM molecules, soluble mediators and various resident cells (fibroblasts and keratinocytes) that act together for the re-establishment of the integrity of a damaged tissue [12, 16]. Skin wound healing comprises five overlapping phases: wounding, haemostasis, inflammation, proliferation and remodelling, as depicted in Figure 2.3 [17-20].

Wounding is represented in Figure 2.3A and it involves the filling of the wound site with blood and fluid from the lymphatic vessels. Although, the wound remains open and highly susceptible to bacterial contamination. Therefore, to avoid the entrance of pathogenic organisms into the human body, the **haemostasis phase** begins (Figure 2.3B). In this phase, vascular constriction occurs, and a fibrin clot is formed in order to act as a provisional matrix that supports the migration of inflammatory cells into the wound site. After, the inflammatory cells release pro-inflammatory cytokines and growth factors (GFs), like platelet-derived growth factor (PDGF), that stimulate mesenchymal cells proliferation [14, 16, 21, 22].

In the **inflammatory phase** (Figure 2.3C), neutrophils are attracted to the clot area through various chemotactic agents such as N-formyl peptides, which are released by bacteria. The presence of these cells is crucial, since they perform phagocytosis and secrete proteases that kill bacteria and help in necrotic tissue removal. Simultaneously, monocytes also migrate into the wound site, where they become differentiated into macrophages and perform engulfment of microorganisms and foreign material via phagocytosis [23]. Once activated, macrophages produce numerous enzymes like collagenases (involved in wound debridement), cytokines (interleukin 1 (IL-1) and interleukin 6 (IL-6) that stimulate the re-epithelialization), and secrete essential GFs (epidermal growth factor (EGF), transforming growth factor (TGF-β) and fibroblast growth factor (FGF)), that are required for the enhancement of cell proliferation, synthesis of ECM components as well as angiogenesis and granulation tissue formation [9]. In chronic wounds, inflammatory cells display an up-regulated gene expression (such as TNF, CD163 and Interleukin 10 (IL-10)) as a consequence of pressure, bacterial overgrowth, leukocyte trapping or ischemic injury, impairing the occurrence of the normal wound healing process [24].

The re-epithelization of the epidermis, dermis repair and neovascularization occur during the **proliferative phase** (Figure 2.3D). In this phase, keratinocyte cells play a key role in epidermis re-establishment, since these cells migrate from the surrounding tissue to the wound, where they become stratified in layers, leading to the closure of the epithelial gap and the restoration of the epithelium. On the other hand, dermis regeneration is performed by migrating fibroblasts, that perform collagen synthesis, having a direct impact on the strength of the regenerated skin. At the end of this phase, some fibroblasts become differentiated into myofibroblasts and these cells bring together the edges of the wound and interact with fibroblasts to produce new ECM components (*e.g.* collagen, fibronectin), which ultimately form the bulk of the mature scar. Concurrently, the angiogenesis process starts with the proliferation and migration of endothelial cells into the wound site for building sprouts that originate the temporary vessels. These events are fundamental for the reconnection of the wound bed to the nutritive perfusion system [17, 22, 25].

Lastly, in the **remodelling phase** (Figure 2.3E), all the processes that were activated after injury, wind down and cease. Endothelial cells, macrophages and myofibroblasts undergo apoptosis or exit from the wound [22]. In addition, over 6 to 12 months, the acellular matrix is

actively remodelled, where the immature collagen type III is replaced by mature collagen type I. Such process is mediated by metalloproteinases (MMPs) that are secreted by fibroblasts, macrophages and endothelial cells. Likewise, fibronectin gradually disappears, whereas HA and GAGs are replaced by proteoglycans, that confer an enhanced strength to the repaired tissue [16, 22, 25].

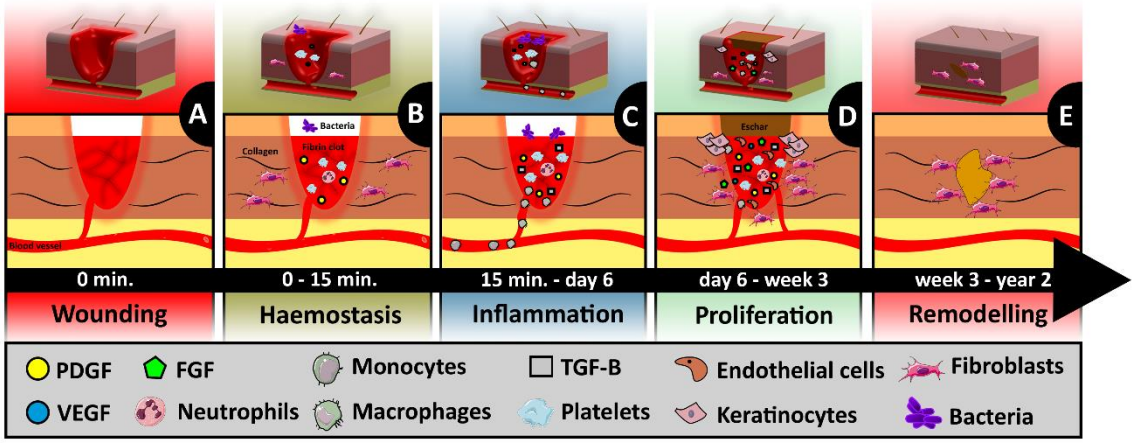

Figure 2.3. Representation of the different phases of the wound healing process. Wounding phase: start after injury (**A**); Haemostasis phase: platelets migrate into the wound site and a fibrin clot is formed (**B**); Inflammatory phase: immune cells migrate into the wound bed for removing any necrotic tissue and bacteria. These cells also release growth factors that trigger the proliferation of cells involved in the tissue reconstruction (**C**); Proliferative phase: endothelial cells and fibroblasts secrete essential growth factors and produced new extracellular matrix components (**D**); Remodelling phase: comprises the reorganization and maturation of the connective tissue (**E**).

2.4 Skin substitutes

In the late years of the 20th century, new devices were developed to confer protection to the wound against potentially harmful agents [26-28]. However, depending on skin injuries causes (*e.g.* burns, trauma or chronic ulcers), effective and interactive dressings, that not only cover the wound but also have the ability to promote healing, are demanded [11, 29]. Foams, hydrocolloids, hydrogels and transparent films emerged as therapeutic approaches for skin regeneration that provide a moist environment to the wound, absorb wound exudates, improve the cosmetic appearance and reduce pain and infection, leading to an increased healing rate (by enhancing the re-epithelialization, collagen synthesis, and angiogenesis) [29].

Nowadays, skin substitutes are produced with different materials, namely with polymeric materials (acellular matrices), that can be loaded with cells (like keratinocytes and/or fibroblasts) within their matrix or with bioactive molecules (EGF and basic fibroblast growth factor (bFGF)) [30, 31]. This new generation of dressings is known for their biocompatibility and biodegradability [32]. According to the skin layer they are aimed to replace, they are classified into epidermal (Epicel®, Myskin®, CellSpray®), dermal (AlloDerm®, Matriderm®,

Integra®, Biobrane®) and epidermal/dermal substitutes (KaroSkin®, Apligraf®, Orcel®) (further details can be seen in Table 2.1).

Epicel® was the first skin substitute available on the market. Epicel grafts are composed by sheets of skin cells that grown on own healthy skin and are cultured with murine fibroblasts [32]. They are used on patients that suffered burns and do not have appropriate donor sites for autografting [32, 33]. However, Epicel® has some disadvantages like mechanical fragility, hyperkeratosis, contracture and scarring [32]. Alloderm® is an acellular dermis substitute that can be loaded with skin cells (keratinocytes, fibroblasts, or both). Despite the immediate barrier protection conferred by this substitute, poor ingrowth of dermal fibroblasts has been observed, making it an unsatisfactory skin graft [34]. When the replacement of both epidermal and dermal layers is required, a full-skin substitute must be used. Apligraf® is the most used epidermal/dermal substitute. This dressing comprises cells from healthy human skin (keratinocytes and fibroblasts) that play a pivotal role during the healing process [35, 36]. Nevertheless, Apligraf® may be involved in virus transmission, which is highlighted as its main disadvantage [36].

Besides these individual shortcomings, all of them have high production cost associated. For example, the cost of covering 1% of the body surface area with Epicel® is over $13,000. Moreover, the commercially available skin substitutes have a poor tissue integration due to an inappropriate vascularization, inefficient adhesion to the wound bed, scarring at graft margins, and inability to restore skin appendages [37, 38]. Up to now, none of the developed wound dressings is suitable for treating all types of wounds, and often, one type is not enough for the healing of a single wound.

Table 2.1. Examples of the commercially available skin substitutes.

	Commercial product	Description	Duration of the cover	Ref.
Epidermal Substitutes	Epicel®	Sheets of skin cells (autologous keratinocytes) are grown on support composed by own healthy skin, in the presence of murine fibroblasts.	Permanent	[39, 40]
	Myskin®	Autologous keratinocytes are cultured on a silicone support layer.	Permanent	[41]
	CellSpray®	Pre-confluent autologous keratinocytes are delivered as a spray.	Permanent	[42]
	Epidex®	Culture of autologous keratinocytes obtained from the outer root sheet of hair follicle.	Permanent	[43]
	Laserskin®	Culture of autologous keratinocytes in a HA membrane.	Permanent	[44]
	Bioseed-S®	Culture of autologous keratinocytes in a fibrin sealant.	Permanent	[45]
Dermal Substitutes	AlloDerm®	Acellular allograft human dermis.	Permanent	[46]
	Matriderm®	Acellular xenograft bovine dermal containing collagen types I, III, V and elastin.	Permanent	[47]
	EZ Derm®	Aldehyde-crosslinked porcine dermal collagen.	Temporary	[48]
	Integra®	Acellular dermis composed of polysiloxane, bovine tendon collagen, and GAGs.	Semi-permanent	[49]
	Biobrane®	Acellular dermis composed of a silicon film, nylon fabric and porcine collagen.	Temporary	[50]
	Transcyte®	Skin substitute composed of a silicon film, nylon mesh, porcine dermal collagen and neonatal fibroblasts.	Temporary	[51]
	Dermagraft®	Bioabsorbable polyglactin mesh containing human allogeneic neonatal fibroblasts.	Temporary	[52]
	Hyalograft 3D®	Esterified HA matrix containing autologous fibroblasts.	Permanent	[53]
Epidermal/dermal Substitutes	KaroSkin®	Native human decellularized cadaveric skin loaded with dermal and epidermal cells.	Temporary	[54]
	Apligraf ®	Culture of human allogeneic keratinocytes and fibroblasts in a matrix composed of bovine collagen.	Temporary	[55]
	Orcel®	Bilayered cellular matrix in which normal human allogeneic skin cells (epidermal keratinocytes and dermal fibroblasts) are cultured in two separate layers into a bovine collagen sponge.	Temporary	[56]
	TissueTech®	Combination of Hyalograft 3D® and Laserskin®.	Permanent	[57]

2.5 Electrospun membranes

Different techniques, including self-assembly, phase separation and electrospinning have been used to produce micro to nano scale meshes aimed to be used as wound dressings [58]. Among them, electrospinning has captured the attention of researchers due to its simplicity, cost-effectiveness and versatility to produce nanofibrous membranes capable of mimicking the morphological characteristics of the skin´s ECM. Moreover, these nanofibrous meshes are also able to support cell adhesion, migration, growth and differentiation as well as angiogenesis, which are vital events for the occurrence of an effective wound healing process [6, 59-62]. In addition, bioactive molecules have also been incorporated into the electrospun nanofibers to improve the biologic performance of these membranes [63].
In the following sections of this chapter, it is provided an overview of the recent studies concerning the production, surface functionalization and evaluation of electrospun polymeric nanofibrous membranes performance in skin regeneration.

2.5.1 Electrospun membranes aimed to be used in skin regeneration

To overcome the handicaps displayed by the skin substitutes available in the market, different tissue engineering labs around the world are focused on the development of new wound dressings that mimic the architecture of native skin [64]. Nanofibrous meshes, which are able to reproduce the features of the ECM of skin, display a microporous structure and their nanofibers exhibit a high surface area to volume ratio that encourages cell adhesion, proliferation, migration and differentiation [65, 66]. In fact, the researchers have been producing electrospun membranes with specific characteristics that allow them to confer protection to the wound against external contaminants and also display a 3D fibre mesh architecture that mimics skin ECM (as represented in Figure 2.4). Furthermore, the high surface-to-volume ratio promotes cell attachment and the microscale interconnected pores are compatible with gas exchange, nutrient supply and control of fluid loss [67-69]. Such properties are vital for assuring the maintenance of a moist environment at the wound site to prevent wound dehydration and enhance angiogenesis and collagen synthesis [70]. Moreover, dressings composed of nanofibers can reduce scar formation, since the biodegradation of fibers provides a suitable roadmap for tissue healing [71, 72].

2.5.1.1 Electrospinning set-up used to produce electrospun nanofibrous membranes for the regeneration of skin

An electrospinning apparatus usually is comprised of a syringe pump, a capillary needle (the spinneret), a high-voltage power supply and a metal collector (see Figure 2.5 for further details) [37]. During the electrospinning process, a high voltage is generated to produce an electrically charged jet of the polymeric solution that is directed to a collector by the electrostatic forces, resulting in the production of an interconnected fibrous membrane [37, 73].

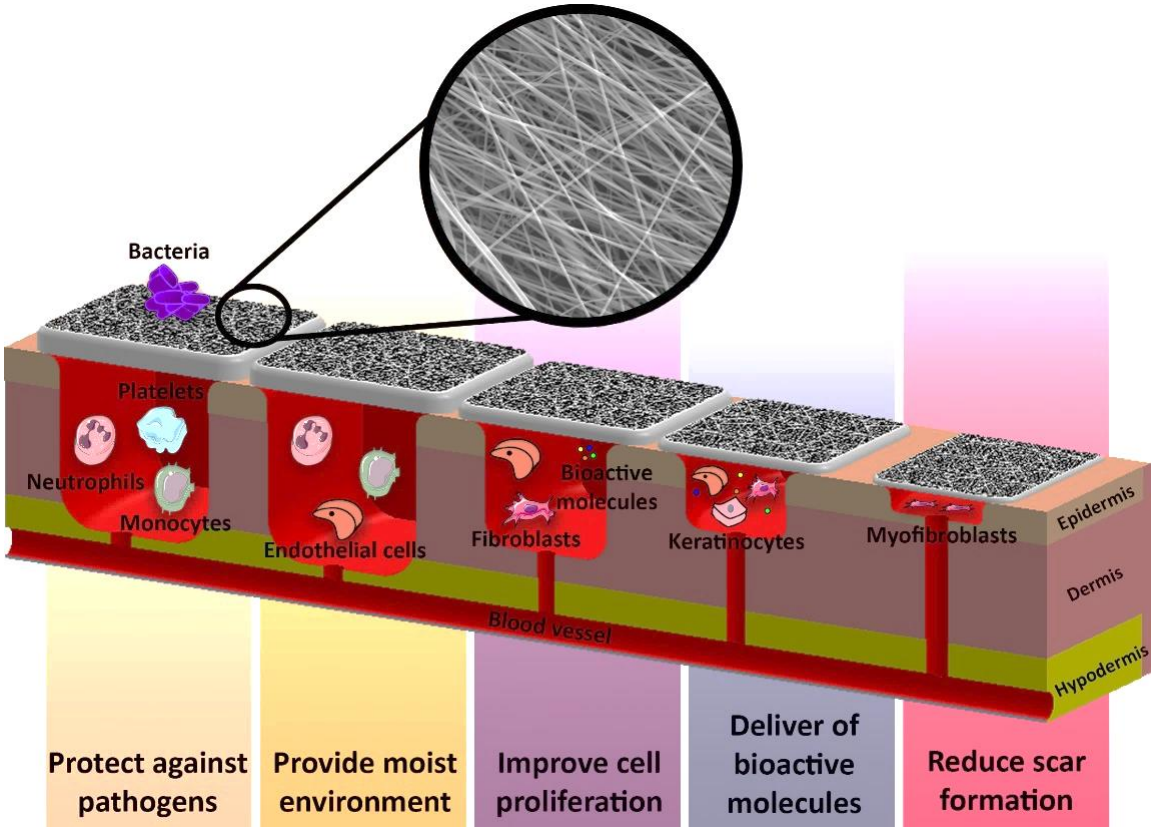

Figure 2.4. Representation of the properties that electrospun membranes must display to be used as wound dressings.

The features of the electrospun membranes are dependent on the properties of the precursor solution (*e.g.* conductivity, surface tension, viscosity and solvent selection), processing variables (*e.g.* flow rate, voltage, and the distance between the capillary and the collector) and environmental conditions (*e.g.* temperature and humidity) [59]. The control of these particular parameters has a direct impact on the mean diameter and arrangement of the produced nanofibers [74]. Moreover, the type of collector used has an impact on the arrangement and packing of the produced fibers, thus determining the morphological and mechanical properties of the electrospun fibers [75]. When the nanofibers are collected in a stationary collector, the membranes produced show a highly porous and randomly-orientated structure that mimics the 3D architecture of collagen fibers found within the ECM of normal skin [66, 76]. To the contrary, nanofibrous membranes to be used for muscle and nervous tissue regeneration must display a specific orientation. To obtain meshes with these structural features, researchers are using rotating collectors, where the rotation speed of the collector has a direct effect on the diameter and the alignment of the produced fibers [75, 77].

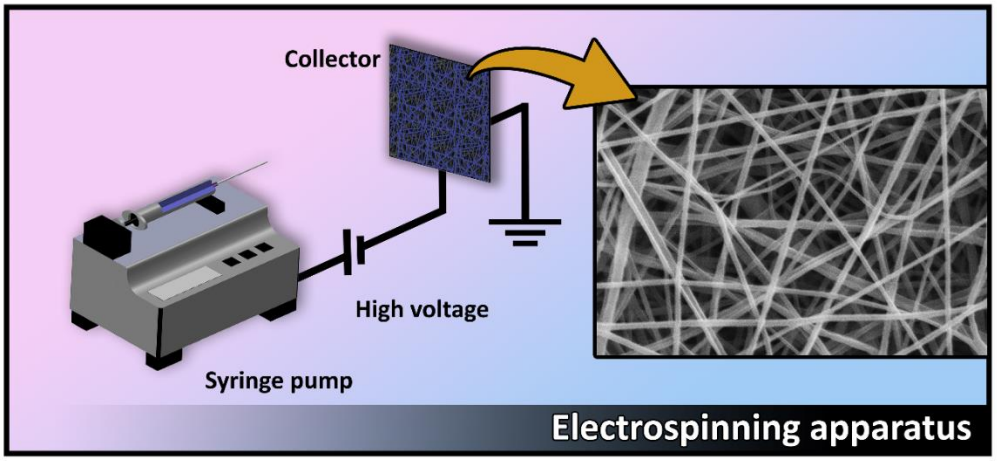

Figure 2.5. Representation of the electrospinning setup usually applied to produce nanofibrous meshes.

2.5.2 Polymers used to produce electrospun nanofibers membranes

2.5.2.1 Synthetic Polymers

Synthetic polymers have been used to produce electrospun nanofibers membranes. This type of polymers can be tailored to exhibit excellent mechanical properties, thermal stability and an appropriated degradation profile. In 2003, for the first time, Khil *et al*. used Polyurethane (PU) to produce nanofibrous membranes to be applied as skin substitutes [78]. Their results revealed that the PU membranes were able to control the water vapor transmission rate (WVTR), displayed an excellent oxygen permeability, and presented fluid drainage ability. The assessment of the biologic performance of the membranes demonstrated their biocompatibility as well as their capacity to avoid exogenous microorganisms penetration into the wound. Moreover, *in vivo* data showed that, after 15 days of treatment, animals treated with PU-electrospun membranes displayed a well-organized dermis and granulation tissue [78]. Kumbar *et al*. produced Poly(lactide-*co*-glycolide) (PLGA) nanofibers that were then seeded on the surface with human skin fibroblasts [79]. The results obtained showed that cells were able to spread, adhere and form multiple layers, after 28 days in culture. However, in other studies, the hydrophobic character of the synthetic polymers used (*e.g*. Polycaprolactone (PCL) and Poly(glycolic acid) (PGA)), and the absence of peptide sequences on the materials' surface impaired cell adhesion and/or proliferation [80].

2.5.2.2 Natural Polymers

To circumvent some of the limitations presented by synthetic materials, natural polymers became a viable option because of the availability of peptide sequences at their surfaces that can be recognized by cell surface receptors and, subsequently, trigger cell adhesion and proliferation [63, 81]. In 2006, Rho *et al*. produced a Collagen nanofibrous matrix to be used as wound dressing, for the first time. Their results showed that this matrix exhibited a good tensile strength (≈ 7 MPa), high porosity and high surface area-to-volume ratio as well as features

required for cell adhesion, growth and proliferation. Moreover, *in vivo* assays also demonstrated that collagen nanofibrous membranes were able to improve the healing process [10]. Hyung *et al*. used Silk Fibroin (SF) to produce nanofibrous membranes and evaluated their biologic performance in *in vivo* assays. The acquired data revealed that the produced SF nanomatrices were able to induce a higher rate of epithelialization and collagen production than commercially available dressings (*e.g.* Mediofoam® and medical gauze). Furthermore, the SF membranes produced were also able to modulate the concentration of inflammatory cytokines involved in wound healing (IL-10 and TGF-β1). This emphasizes the suitability of SF nanomatrices for the treatment of injured skin, *i.e.* they were able to decrease injury inflammation and reduce the wound healing period as well as scar formation [82]. Lin *et al*. produced a biocompatible nanofibrous membrane using Zein (ZN) and Collagen and then evaluated its capacity to be used in the treatment of full-thickness skin wounds induced in mice [83]. Nevertheless, the biodegradation rate and mechanical properties displayed by these natural materials was found to be restrictive, so their application may be avoided in the biomedical field [84].

2.5.2.3 Synthetic/Natural Polymeric Blends

The blending of synthetic and natural polymers was also seen as a promising strategy to overcome the limitations of both synthetic and natural polymers. This approach combines the strength and durability of a synthetic polymer with the biocompatibility and bioactivity of natural polymers [85-87].

In 2004, Venugopal *et al*. evaluated the performance of electrospun matrices prepared with PCL and Collagen blends. These membranes were able to promote cell adhesion and proliferation where their PCL nanofibers counterparts could not. This result can be explained by the excellent intrinsic biological properties displayed by collagen [88]. Nonetheless, the collagen used in tissue engineering applications is usually obtained from animal sources, which is associated to the risk of disease transmission. Therefore, alternative materials have been considered, like gelatin which, despite being a cheaper collagen derivative (obtained through collagen denaturation), exhibits all the required biological properties. Duan *et al*. investigated the suitability of PCL/gelatin electrospun membranes to be used as engineered epidermal skin grafts. Their results showed that HaCaT cells (a human keratinocyte cell line) were able to adhere and spread on the membranes' surface for at least 7 days. Furthermore, the *in vivo* assays demonstrated that the groups treated with PCL/gelatin membranes exhibited an improved healing process, since the wound closure occurred in a shorter period of time [89]. In order to overcome the drawbacks associated with PCL (*e.g.* its hydrophobic character as wells as its low degradation profile), other researchers tested alternative materials to produce nanofibrous meshes, like Polyethylene oxide (PEO), Polyvinyl alcohol (PVA), Polylactic acid (PLA) and PLGA.

Zhou *et al*. produced a water-soluble carboxyethyl Chitosan (CS)/PVA blend to improve chitosan electro-spinnability. Subsequently, mouse fibroblast cells were seeded at the surface of the membranes produced and, after 48 h in culture cells, these were able to adhere and proliferate [90]. Gu *et al*. used a mixture of PLA and gelatin to produce electrospun meshes. These membranes were able to reduce water loss in wounds, which is essential for avoiding dehydration. Moreover, dermal fibroblasts remained viable, for at least 4 days, after seeded on the top of those membranes [91]. In another study, PLGA was combined with collagen to produce nanofibrous wound dressings that reproduce the native structure and biological function of the ECM of skin. Both *in vitro* and *in vivo* assays showed that PLGA/collagen membranes improve the healing process [92]. Suganya *et al*. combined poly(L-lactic acid)-*co*-poly(ϵ -caprolactone) (PLLCL) with AV and SF to produce electrospun meshes that promote dermal regeneration. Their results showed that the SF provides a favorable environment for cell adhesion and migration, while the AV components, mannose 6-phosphate and acemannan are known to promote epithelialization and the synthesis of collagen, processes that are essential for an effective healing process [93].

Besides the data available in the above published articles, there are also some patents focused on the application of electrospun membranes as wound dressings. Kataphinan *et al*. patented their production of a skin mask through the direct deposit of electrospun fibers onto the skin surface [94]. Smith *et al*. patented their production of electrospun fibers containing a pH-adjusting compound that prevents wound contamination and promotes the healing process [95]. Yarin *et al*. patented the use of the electrospinning technique for the production of a biodegradable plant-based wound dressing (composed of a biopolymers extracted from plants and synthetic polymers) [96]. Table 2.2 presents further examples of different electrospun membranes produced with natural, synthetic and blends of natural and synthetic polymers to be applied as skin substitutes.

2.6 Modification of the surface of electrospun polymeric nanofibers

The modification of a material's surface can be done by changing the topography or the functional groups available [108]. In order to improve the performance of electrospun polymeric nanofibers performance in skin regeneration, the surfaces have been chemically and physically modified with bioactive molecules and cell-recognizable ligands [109]. In the following sections, the most common surface modification techniques used for this purpose are presented.

Table 2.2. Nanofibrous meshes produced through the electrospinning that are aimed to be used as wound dressings.

Polymers	Solvent	Cell line used in biocompatibility assays	Main findings	Ref.
Carboxyethyl chitosan/ PVA	Deionized water	Mouse fibroblasts (L929)	Biocompatible nanofibers were prepared using water soluble CS. *In vitro assays* showed that fibrous mats promote cell adhesion and proliferation.	[90]
CS/ arginine-chitosan	Trifluoroacetic acid (TFA): Dichloromethane (DCM)	Human dermal fibroblasts	The modification of CS with L-arginine allowed the production of nanofibrous meshes able to improve the healing process and increased bactericidal activity.	[97]
CS/SF	HFIP:TFA	L929	Blended CS and SF nanofibrous membranes promoted cell attachment and proliferation.	[98]
CS/PVA	Deionized water for PVA; Hydroxybenzotriazole, Sodium Tripolyphosphate and EDTA for CS	Human foreskin fibroblast	CS/PVA membranes induce a reduction in wound size, during the first week after tissue damage.	[99]
Collagen	HFIP	Normal human oral keratinocytes	The electrospun collagen nanofibrous membranes were produced and characterized, for the first time, aimed to be used as wound dressings.	[10]
Collagen/ZN	AA	L9229	The ZN improved the electrospinnability of the blend and fiber tensile strength, while the collagen enhanced cell adhesion.	[83]
Gelatin/PU	HFIP	NIH3T3 fibroblast	The gelatin improved cell adhesion and proliferation, whereas PU allowed the production of elastic nanofibers.	[100]
Gelatin/ PLLA	Acetic acid; DCM	WI-38 fibroblast	The electrospun gelatin/PLLA membranes showed controlled water loss, displayed fluid drainage ability, and an excellent biocompatibility.	[91]
Gelatin/PCL	TFE: acetic acid	HaCaT keratinocytes	Membranes exhibited good mechanical properties and did not elicit any toxic effect on cells.	[89]
PCL/SF/HA	Hexafluoro-2-propanol; Formic acid (FA)	FEK4 derived from a newborn foreskin explants	The incorporation of HA into nanofibrous scaffolds enhanced cell infiltration both *in vitro* and *in vivo*.	[101]
PCL/SF	THF and DMF	NIH3T3 fibroblasts	PCL/SF nanofibrous matrix provided favourable spatial cues, surface topography and chemistry for cell infiltration.	[102]

PCL/collagen	TFE	Human dermal fibroblast	Core-shell composite nanofibers improved cell-scaffold interactions.	[103]
PCL/Zinc oxide (ZnO)	Acetone	Human dermal fibroblast	PCL/ZnO membranes showed excellent fibroblast cell attachment and good antimicrobial activity.	[104]
PLGA/ collagen	HFIP	Human dermal fibroblasts	PLGA/collagen nanofibrous meshes improve the wound-healing process in an early stage.	[92]
PLGA/gelatin	Chloroform: acetone	Postnatal human fibroblasts	Hybrid scaffolds presented the desired bioactivity, haemostasis, and are also capable of encapsulate and perform a controlled release of EGF. Such properties highlight their potential to be applied in skin tissue engineering.	[63]
PCL_HA/ CS_ZN	TFE; DMF; AA and ethanol	Human dermal fibroblasts	The produced bilayered electrospun membrane protect the wound as well as enhanced the wound healing process.	[105]
PLLCL/SF/ AV	DCM: DMF	Human dermal fibroblasts	The synergistic effect of AV and SF resulted in the production of the nanofibrous scaffolds with excellent properties to be used in skin tissue regeneration.	[93]
PCL/AV_CS	TFE; AA and water	Human dermal fibroblasts	The asymmetric membrane containing AV showed enhanced biological properties.	[106]
PLA/MWCNTs/REC	DCM:DMF	L9229 fibroblast cells	The incorporation of inorganic materials improved the thermal stability of the composite nanofibrous membranes. Moreover, these membranes exhibited a biocompatible profile.	[107]
SF	FA	Oral keratinocytes, epidermal keratinocytes	SF nanofibers exhibited a pore size distribution, porosity and surface area-to-volume ratio favourable for cell attachment, growth and proliferation.	[67]

2.6.1 Techniques used to functionalize a material's surface

As previously described, the use of synthetic polymers presents some limitations, due to their hydrophobic character and inability to encourage cell adhesion and proliferation [80]. As a possible solution, surface functionalization techniques, which are represented in Figure 2.6, like the wet chemical method, plasma treatment and graft polymerization are usually applied [109]. The wet chemical method is based on the reaction under acidic or basic conditions, between the mesh and liquid reagents in order to add new chemical groups to the polymeric backbone [110]. Khorsand-Ghayeni *et al*. produced electrospun PLGA nanofibrous matrices and modified them by adding carboxyl and hydroxyl groups on their surface through alkaline hydrolysis, followed by a collagen coating. Their results demonstrated that the surface functionalization decreased the PLGA hydrophobicity, which is essential for this material to exhibit a wettability suitable for cell adhesion [111].

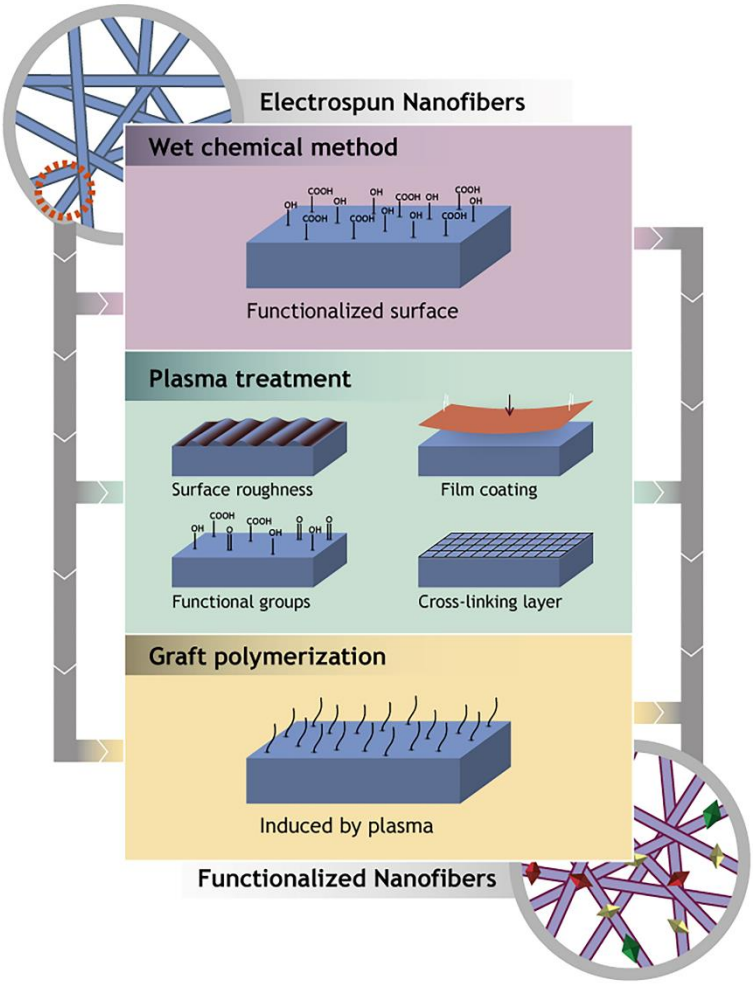

Figure 2.6. Representation of the main surface modification techniques used up to now to improve the surface nanofibers properties: wet chemical method, plasma treatment and graft polymerization.

The plasma treatment of electrospun polymeric nanofibers has been commonly employed to tailor surface adhesion and optimise wetting properties by changing the surface chemical composition [112]. Depending on the type of plasma used (*e.g.* oxygen, ammonia, argon), diverse functional groups can be added to the polymer surface in order to improve the biocompatibility of a material [109]. Besides introducing functional groups, plasma treatments can also be used to control surface roughness and induce processes like crosslink formation, graft polymerization and thin film coating of the polymeric surface [109, 113]. Jeong *et al*. prepared electrospun SF nanofibers and then treated them with oxygen plasma to increase their hydrophilicity. The results obtained revealed a higher cell adhesion and proliferation, for both normal human epidermal keratinocytes and fibroblasts, on the surface of functionalized nanofibrous membranes [114].

Graft polymerization involves the covalent immobilization of bioactive molecules at the nanofiber's surface to enhance cell adhesion, proliferation and differentiation [115]. In 2013, Gautam *et al*. fabricated a tri-polymer PCL/gelatin/collagen type I, by grafting collagen type I on electrospun PCL/gelatin mesh to improve fibroblast and keratinocytes cells adhesion and proliferation [116]. Graft polymerization may require the use of initiators to start the grafting of a monomer on the membrane surface, like when using Ultraviolet (UV) irradiation [117]. Plasma treatment is able, by itself, to generate free radicals on the polymeric matrix and therefore initiate the polymerization reaction. Park *et al*. produced electrospun biodegradable nanofibrous meshes with PGA, PLLA and PLGA. These nanofibrous surfaces were chemically modified by *in situ* graft polymerization of acrylic acid using oxygen plasma treatment. The results obtained revealed that the surface-modified membranes showed a significant improvement in cell attachment and proliferation, due to the incorporation of the hydrophilic functional groups [118].

2.6.2 Surface functionalized nanofibrous meshes to be used as drug delivery systems

A number of nanomaterials provide an excellent platform for local delivery of therapeutic agents due to their functionality and inherent nanoscale morphological characteristics [119, 120]. The optimization of different electrospinning parameters (*e.g.* the raw materials, viscosity, applied voltage, flow rate, temperature, humidity, etc.) allows the production of the nanofibers with specific features, such as mean diameter, surface area/volume ratio, porosity, wettability, and mechanical properties [37, 59, 73]. Furthermore, the nanofibers drug loading can be performed using different methodologies that comprise the incorporation of the biologic active agents before the electrospinning process be performed, through blend, co-axial, and emulsion electrospinning [121, 122]. Moreover, the nanofibers surface can also be modified by physical adsorption, layer-by-layer (LbL) assembly and chemical immobilization of biomolecules (as illustrated in Figure 2.7) [121-123]. By combining these strategies, researchers can control the encapsulation of multiple biomolecules. Depending on the role of a biomolecule in the

healing process, the drug release profile can be tailored through the incorporation method used [124]. For example, the physical adsorption of biomolecules into nanofibers is frequently associated with burst releases and short diffusion times, whereas the co-axial electrospinning allows a more controlled and sustained release profile [125, 126]. On the other hand, if the different molecules are incorporated into nanofibers by the same method, the drug release profile will be dependent on the diffusion coefficient of each molecule. In these cases, the rate of biomolecule diffusion out of the polymeric matrix will be affected by several factors like polymer swelling, polymer erosion, biomolecular dissolution/diffusion characteristics, biomolecules distribution inside the matrix and biomolecule/polymer ratio [127-129].

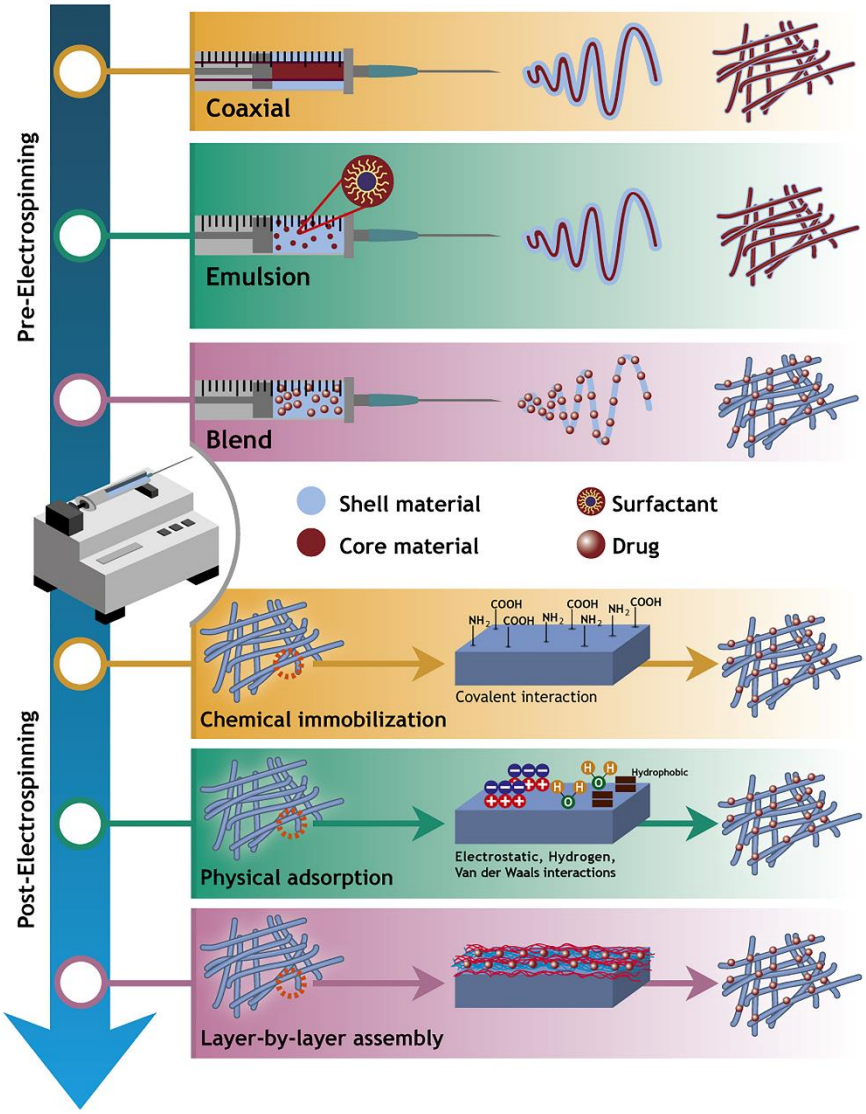

Figure 2.7. Illustration of the surface modification techniques used to produce a nanofiber-based drug delivery carrier: pre-electrospinning (blend, co-axial and emulsion electrospinning) and post-electrospinning (physical adsorption, layer-by-layer assembly and chemical immobilization).

2.6.2.1 Pre-electrospinning surface modification techniques

The blend electrospinning method involves the encapsulation of bioactive molecules that are dissolved or dispersed in the polymeric solution. Then, hybrid fibres are produced when this mixture is electrospun [130]. The encapsulation of the biomolecules within the fibres, assures their sustained release and also avoids the occurrence of an early burst release [131]. Li *et al*. mixed PVA with sodium alginate (SA) and organic rectorite (OREC) (which is recognized as a bacterial inhibitor) and then produced an electrospun nanofibrous mesh. The *in vitro* data showed that the OREC improved the bactericidal activity of the nanofibers [132]. Chouhan *et al*. developed non-mulberry SF based electrospun mats functionalized with EGF and ciprofloxacin (CIF) to be used as wound dressings. The results obtained showed that NMS-based mats are biocompatible, display antimicrobial activity and can perform a controlled drug release [133].

Despite the versatility of the blend electrospinning, one major disadvantage of the fibers fabricated with this methodology is the loss of function and activity of the incorporated biomolecules, which compromises the therapeutic effectiveness of the system [131]. To overcome this shortcoming, core-shell fibres have been produced through co-axial and emulsion electrospinning. This type of nanofibers displays an enhanced encapsulation efficiency (EE) of drug/bioactive molecules and avoids the direct contact of the biomolecules with the external environment, which is fundamental for unstable biological agents to maintain their biologic activity [134, 135].

In co-axial electrospinning, different syringe pumps and coaxial needles are used to produce the core, where the bioactive components are usually loaded, and the shell that provides protection and assures a sustained release of the encapsulated molecules [101]. Maleki *et al*. compared the capacity of tetracycline hydrochloride (TCH)-loaded PLGA core-shell nanofibers (produced with a co-axial electrospinning system) with blend fibres (prepared with the same materials) for a sustained drug release [136]. The core shell nanostructures revealed better results.

Emulsion electrospinning can also be used to manufacture core-shell nanofibers without requiring a specific needle setup. This method relies on a chemical separation through the creation of an emulsion within a single solution and the subsequent organisation of the emulsified droplets into two distinct phases, as the solvent evaporates from the electrospun fibres [137]. Wang *et al*. produced and EGF-loaded PCL/hyaluronan nanofibrous mesh, using an emulsion electrospinning technique. Their findings showed that the resulting modified hyaluronan-based membranes can encapsulate and release EGF, which is fundamental for skin tissue engineering [138].

2.6.2.2 Post-electrospinning surface modification techniques

Different approaches have been employed to immobilize biomolecules or small cell recognition motifs onto the surfaces of electrospun polymeric nanofibers. Drug immobilization on the nanofiber's surface that is stronger and offers a more stable linkage can be achieved by physical immobilization through simple physical adsorption, LbL assembly or by chemical immobilization techniques [109].

Physical surface adsorption is the simplest approach for the preparation of surfaces with well-defined properties, and does not rely on chemical processing [139]. Generally, weak nonspecific intermolecular interactions (like those found in electrostatic interactions, hydrogen bonding, hydrophobic interactions and Van der Waals forces) are established between the surface and peptide sequences [140]. One strategy used for a successful physical immobilization on the surface is based on the use of materials with a high surface area-to-volume ratio, as presented by electrospun polymeric nanofibers. The typical porous structure of these matrices results in a higher drug loading capacity per unit mass than for any other morphologies [109]. Casper *et al*. produced electrospun Polyethylene glycol (PEG) nanofibers functionalized with low molecular weight heparin, a highly sulfated glycosaminoglycan that binds GFs, for applications in drug delivery and wound repair. The analysis of their results suggests the conclusion that this functionalization method enables the binding of the bFGF on the surface of PEG nanofibers [141].

Over the past few decades, **LbL assembly** has attracted research attention due to its ability to exert nanometer control over film thickness and provide a simple, useful and versatile methodology for material surface modification [142]. Generally, LbL assembly is a cyclical process embracing the alternated depositing of polymers exhibiting opposite charges at their surface to formulate a coating of polyelectrolyte multilayers or free-standing film. The depositing process can be repeated until a multilayer film of the desired thickness is assembled [109, 142, 143]. In the assembly process, electrostatic attraction is the main driving force, although, hydrogen bonding, hydrophobic, covalent and biological interactions can also play a vital role [109]. This build-up can precisely control the composition, morphology and structure of the film [143]. In recent studies, LbL assembly has been used in a wide range of applications in the biomedical field, including wound healing. Huang *et al*. produced cellulose acetate (CA) nanofibrous mats that were used as a substrate for LbL films composed of positively charged CS derivative, lysozyme (antibacterial agent)- N-[(2-hydroxy-3-trimethyl-ammonium) propyl], and negatively charged SA. The results obtained showed that the average diameter of fibers increased with the number of coating bilayers applied. Moreover, the produced fibers exhibited antimicrobial activity [144]. Similarly, Xin *et al*. developed novel cellulose nanofibrous mats coated with SF (negatively charged) and lysozyme (positively charged). The *in vitro* and *in vivo* assays demonstrated that the mats can promote both healing in wounds and avoidance of wound infection [145]. Huang *et al*. reported the production of biomimetic nanofibrous matrices that

were coated using LbL assembly of CS (positively charged) and Type I collagen (negatively charged). The LbL structured nanofibrous membranes displayed enhanced *in vitro* cell migration and promoted *in vivo* skin re-epithelialization and vascularisation. These results demonstrate the potential of LbL structured nanofibrous matrices to restore the structural and functional properties of skin [146].

Although the LbL assembly process is simple and mild, it can be affected by many factors such as the concentration and ionic strength of the polyelectrolyte solution as well as the pH, temperature, assembly time and molecular weight of the polymers used [143]. In addition, as the driving force is a result of electrostatic interactions, they are easily leached out, when incubated over an extended period, from the surface of the modified nanofibers. Therefore, chemical immobilization of bioactive molecules is favored over physical immobilization [109]. In order to fabricate biomimetic materials that can withstand long-term survival, a stable covalent binding of functional biomolecules is required to maintain their bioactivity [139]. To accomplish that, chemical immobilization of primary amine and carboxylate groups have been extensively employed to immobilize bioactive molecules onto the surface of nanofibers for wound healing [109]. In addition, hydrophilic linkers have also been used to bind bioactive molecules, which can be recognized by cells. For this purpose, Choi *et al*. produced PCL/PEG electrospun nanofibers functionalized with amine groups on their surfaces, using PEG linkers. Then, in order to use these nanofibrous mats in the treatment of diabetic foot ulcers, EGF was chemically bound to the surface of the meshes. The results obtained showed that the EGF functionalized nanofibers exerted a superior therapeutic effect on wound healing in comparison to control groups. In addition, EGF-receptor was highly expressed in keratinocytes, due to the stimulation exerted by the EGF nanofiber group, showing their suitability to be used as skin substitute [147].

2.7 Bioactive molecules that have been incorporated into electrospun membranes aiming to improve the healing process

2.7.1 Molecules with antimicrobial activity

After skin infections occur, microorganisms' invasion prompt the deterioration of the granulation tissue, GFs and ECM components (*e.g.* collagen, elastin, and fibrin), compromising the healing process [148, 149]. Thus, in order to prevent such deleterious effects, it is imperative to use wound dressings capable of preventing bacterial penetration into the wound as well as to support skin regeneration (as illustrated in Figure 2.8). In the following topics, the different antimicrobial agents (*e.g.* antibiotics, silver nanoparticles (AgNPs) and natural extracts-derived products) that have been loaded into electrospun nanofibers for enhancing their antibacterial properties are overviewed.

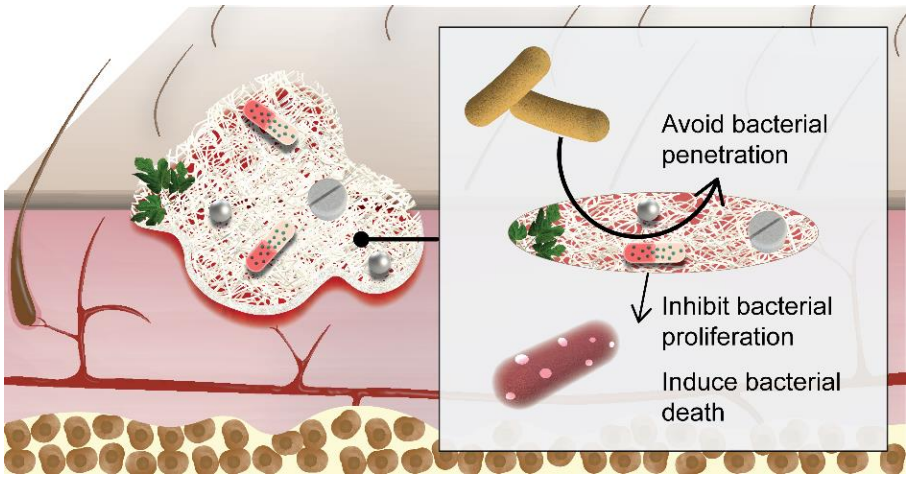

Figure 2.8. Illustration of the main antimicrobial agents (antibiotics, silver nanoparticles and natural extracts-derived products) incorporated into the electrospun nanofibers and their role in the healing process.

2.7.1.1 Antibiotics

In the clinic antibiotics are widely used, mainly those administered through oral administration, for preventing/treating microbial colonization/contamination of open wounds. Nevertheless, this therapeutic approach presents several disadvantages such as rapid elimination from blood stream, degradation, and narrow therapeutic windows. In this way, to overcome these limitations, researchers have been exploring the topical administration of antibiotics through their incorporation in wound dressings. CIF, gentamycin, tetracycline, and silver sulfadiazine (SSD) have been incorporated into electrospun membranes, which displayed a controlled release of antibiotics from the nanofibers to provide an aseptic environment at the wound site as well as for promoting the re-epithelialization and new tissue formation (please see Table 2.3) [150-155]. Alavarse *et al.* incorporated TCH, at a concentration of 5mg/mL, into PVA/CS (80/20 v/v) electrospun nanofibers [153]. A blend of polymer-antibiotic was initially electrospun and then crosslinking using glutaraldehyde (GA) vapor (0.5% for 4 h). This crosslinking step lead to an increase in the fibers mean diameter, from 119 ± 33 nm to 309 ± 68 nm. Further, the authors observed that 80% of TCH was released from PVA/CS nanofibers in Phosphate-buffered saline (PBS) solution (pH 7.4), after 24 h, which corresponds to the critical period for the establishment of wound infections. Moreover, the antimicrobial activity of PVA/CS/TCH membranes was characterized using *Escherichia coli* (*E. coli*), *Staphylococcus epidermis* (*S. epidermis*) and *Staphylococcus aureus* (*S. aureus*) as model bacteria. The obtained results showed that the incorporation of TCH into the PVA/CS nanofibrous membranes can inhibit the bacterial growth, during 24 h. Additionally, the authors reported inhibitory halos with a diameter of 8.8 ± 0.4 mm for *E. coli*, 15.6 ± 0.3 mm for *S. epidermis* and 19.6 ± 0.2 mm for *S. aureus*, which contrasts with the absence of inhibitory activity displayed by the non-functionalized membranes. In addition, these researchers also noticed that when the drug-loaded nanofibrous membranes were added to rabbit aortic smooth muscle cells, they did

not affect the cell viability for at least 72 h. Torres-Giner *et al*. produced PLA nanofibers loaded with gentamicin using three different approaches based on the incorporation of gentamicin 5 wt% into PLA nanofibers, PLA-collagen blends or in the collagen core of the collagen-PLA coaxial nanofibers [155]. Their results revealed that PLA fibers containing gentamicin presented a bimodal size distribution with an average diameters of 1106 ± 182 nm and 281 ± 55 nm; gentamicin loaded PLA-collagen blends had fibers with diameters of 168 ± 53 nm; and coaxial PLA-collagen-PLA/gentamicin presented fibers with mean diameter values of 561.43 ± 104 nm and 131.07 ± 39 nm. Moreover, the gentamicin release profile exhibited by all formulations was similar, *i.e*. the antibiotic presented a fast diffusion in the first 24 h, followed by a sustained release until reach the equilibrium after 50 h. Nevertheless, the PLA fibers released 19% of the drug after 24 h, increasing to 33% after the 50 h of incubation. On the other hand, PLA-collagen blends released 78% and 98% of gentamicin after 24 h and 50 h, respectively. Coaxial PLA-collagen-PLA nanofibers released 41% and 59% of gentamicin after 24 h and 50 h, respectively. Further, these researchers also determined the lowest concentration of gentamicin required to prevent the bacterial growth and to kill the bacteria, which are defined as minimal inhibitory concentration (MIC) and minimum bactericidal concentration (MBC), respectively. So, the PLA-collagen blends presented MIC values of 0.25, 5 and 0.5 mg and MBC values of 5, 50 and 25 mg for *S. epidermis*, *Pseudomonas aeruginosa* (*P. aeruginosa*) and *E. coli*, respectively. In turn, the PLA-collagen-PLA coaxial fibers displayed a slightly lower bactericidal activity, exhibiting MIC values of 1, 10, and 0.5 mg and MBC values of 7.5, 50, and 25 mg. PLA fibers presented the lowest antimicrobial activity for the tested bacteria, showing MIC values of 2.5, 25 and 0.5 mg and MBC values of 10, 100, and 50 mg. Moreover, the electrospun PLA-based fibers were also able to provide a matrix that promotes cell proliferation. Li and their co-workers loaded CIF (0.9%) into thermoresponsive electrospun fiber mats produced with poly(di(ethylene glycol) methyl ether methacrylate) (PDEGMA)/ poly(L-lactic acid-*co*-ε-caprolactone (P(LLA-CL) [156]. The CIF incorporation into the meshes leads to a variation on the nanofibers size, *i.e*. the non-loaded nanofibers presented diameters ranging from 948 ± 132 nm to 476 ± 189 nm, whilst the fibers containing CIF presented diameters ranging from 330 ± 118 nm to 437 ± 141 nm. Further, the release profile of CIF was characterized by an initial burst (45% of the drug was released in 10 h) that span up to 170 h, reaching a maximum cumulative release of 85%. This behaviour leads to the formation of inhibitory halos, with a diameter of 5.35 ± 0.51 cm and 5.21 ± 0.44 cm for *E. coli* and *S. aureus*, respectively, after 24 h of incubation. These values increased to 5.45 ± 0.81 cm and 5.62 ± 0.53 cm after 72 h of incubation, thus revealing that the antibacterial activity of the fibers remained for at least three days. Moreover, the *in vitro* assays also demonstrated that the nanofibers promote the adhesion and proliferation of L929 fibroblasts. In the *in vivo* assays, the fibers loaded with CIF induced a reduction of the wound area (5.7 ± 0.8% of the original area), a higher expression of CD34 (a marker used to select vascular endothelial cells) and the formation of a thicker epidermis in comparison to commercially available gauzes [156].

Mohseni and their collaborators incorporated SSD into PVA nanofibers for conferring them antimicrobial activity [157]. To accomplish that, different concentrations of SSD (1, 5 and 10 wt%) were added to the PVA solution before the electrospinning process be performed. Afterwards, the nanofibers' diameter was measured and the authors verified that the average diameter of PVA nanofibers increased with the incorporation of SSD, from 360 nm to 450, 530, and 700 nm for the PVA/SSD (1%), PVA/SSD (5%), PVA/SSD (10%) fibers, respectively. Further, the authors observed that 70% of the SSD was released during the first 7 days of incubation, reaching a value close to 100%, after 14 days. Additionally, the membranes displayed a bactericidal activity dependent on the SSD concentration. Inhibitory halos with a diameter of 2 ± 0.2 mm, 3.9 ± 0.5 mm, and 4.2 ± 0.3 mm were obtained for PVA/SSD (1%), PVA/SSD (5%), and PVA/SSD (10%) membranes, respectively (as showed in Figure 2.9), when they were added to *S.aureus*. On the other side, these researchers also verified that the incorporation of SSD decreased the mechanical properties of the membranes (the elastic modulus decreased from 56.07 MPa to 36.19 MPa for PVA/SSD (1%), 27.52 MPa for PVA/SSD (5%), and 18.14 MPa for PVA/SSD (10%)) and increased the hydrophilic character of their surfaces.

a)

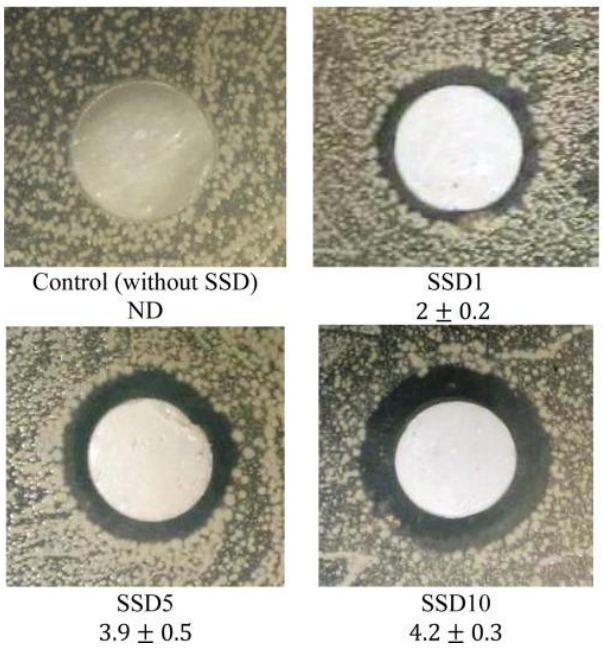

b)

Commercialized wound dressing	Inhibition Zone
Biohesive Ag	0.2 ± 0.1
Aquacel® Ag	0.6 ± 0.2
Algisite Ag	1 ± 0.2
Mepilex® Ag	ND
PolyMem® Ag	ND

Figure 2.9. Characterization of the antibacterial activity of SSD loaded PVA electrospun mats against *S.aureus*. The inhibitory halos produced by the electrospun nanofibers containing different concentrations of SSD are presented in (a) and the bactericidal activity of commercially available wound dressings are shown in (b). Reproduced from [157] with permission from Wiley.

However, in recent years researchers and clinicians have been facing the emerging of multidrug resistant bacteria that arise as consequence of the continued administration of antibiotics. In fact, more than 70% of the bacteria responsible for wound infections are resistant to at least one of the antibiotics used nowadays in the clinic [158]. Such drawback demands the development of new antimicrobial alternatives that can be used for the treatment of skin infections.

Table 2.3. Overview of different antibiotics incorporated into electrospun membranes to be used as wound dressing.

Antibiotic	Polymer	Incorporation method	Fiber diameter (nm)	Release profile	Antibacterial assays	Main conclusions	Ref.
TCH	PVA /CS	Blend electrospinning	-PVA/CS: 138± 23 nm; -PVA/CS/TCH: 119 ± 33 nm.	-The release profile of TCH displayed an initial burst release (80%), after 2 h.	-The zone of inhibition obtained was 8.8 ± 0.4 mm, 15.6 ± 0.3 mm and 19.6 ± 0.2 mm for *E. coli*, *S. epidermidis* and *S. aureus*, respectively.	-The TCH-loaded PVA/CS membranes showed good biocompatibility in contact with rabbit aortic smooth muscle cells; -The scratch assay demonstrated a higher cell migration rate (about 8%/h and 6%/h) during the initial 12 h of incubation.	[153]
	ZN/ PCL	Blend electrospinning	-ZN 3L: 0.99±0.36 μm; -ZN/PCL 3L: 1.51±0.65 μm.	-In ZN/PCL 3L fibers the TCH was gradually released, reaching the 19% in the first 3 h; -After 20 days, 27% of TCH was released from the nanofibers.	-The 3L matrices significantly reduced the number of living cells (from 100% to ≈ 35%) in the biofilms of Methicillin-resistant *Staphylococcus aureus* (*MRSA*)252; -For *MRSA* (ATCC 25923), the 3L matrices mediated a reduction in the viable cells from 100% to 27%.	-For the first time, TCH loaded matrices were applied in *ex vivo* pig skin models growing *MRSA*252 or ATCC 25923; -The ZN/PCL nanofibers loading with TCH were biocompatible with human fibroblast FEK4 skin cells.	[159]
Gentamicin	PLA/ Collagen	Blend electrospinning and coaxial electrospinning	Blend fibers: -PLA-collagen/ gentamicin: 168 ± 53 nm; Coaxial fibers: - PLA-collagen/ gentamicin: 561 ± 104 nm	-In blend PLA-collagen fibers, 78% and 98% of gentamicin was released after 24 h and 50 h, respectively; - In coaxial PLA-collagen-PLA, 41% and 59% of gentamicin was	-The blend fibers presented MIC values of 0.25, 5 and 0.5 mg and MBC values of 5, 50 and 25 mg for *S. epidermidis*, *P. aeruginosa* and *E. coli* respectively;	-The *S. epidermidis* presented a superior susceptibility towards gentamicin, followed by *E. coli* and *P.aeruginosa*; -The electrospun PLA-based fibers promoted a matrix favourable for cell	[155]

			and 131 ± 39 nm.	released after 24 h and 50 h, respectively.	-The coaxial fibers displayed MIC values of 1, 10 and 0.5 mg and MBC values of 7.5, 50 and 25 mg respectively.	proliferation during 14 days.	
	CS	-Gentamicin was loaded into liposomes; -Surface chemical immobilization of drug-loaded liposomes at surface of membranes	Not available	-The release of gentamicin from liposomes immobilized at the surface of CS membranes was characterized by a steady release rate after 16 h, which stabilized until 24 h.	-The diameter of inhibition zones exhibited by samples was 21.6 mm, 22.1 mm and 14.1 mm for *S. aureus, E. coli* and *P. aeruginosa*, respectively; -The broth dilution method demonstrated a Log(reduction)= 3.87 ± 0.33 for *S. aureus*, 4.87 ± 0.21 for *E. coli*, and 4.20 ± 0.24 for *P. aeruginosa*.	-The gentamicin released from liposomes immobilized at surface of electrospun CS membranes avoided the growth of *S. aureus*, *E. coli* and *P. aeruginosa*.	[160]
CIF	PLGA/ alginate microparticles (ALG)	Blend electrospinning	-ALG(1%) /PLGA: 673 ± 243 nm; -ALG(1%) /PLGA-CIP: 877 ± 431 nm.	-A burst release of CIP occurred in the first 7 days, which was followed by a slow release for up to 40-50 days.	-The MIC of CIF (1%) was 0.125 µg/mL against *S.aureus*; -The CIP-loaded nanofibers exhibited an inhibition zone ranging from 35-45 mm, in contact with *S.aureus*.	-The addition of SA enhanced the wettability, water uptake potential, facilitating the release of CIP at the early diffusion phase.	[161]
	PDEGMA/ P(LLA-CL)	Blend electrospinning	-Fibers without CIF: 948 ± 132 nm to 476 ± 189 nm -Fibers with CIF: 437 ± 141 nm to 330 ± 118 nm	-CIF displayed a burst release (45%) at first 10 h, followed by a gradual release over 170 h; -The final cumulative release of CIF was 81%-85%.	-The diameter of the inhibition zones exhibited by CIF-loaded fibers was 5.35 ± 0.51 cm and 5.21 ± 0.44 cm for *E. coli* and S. *aureus*, respectively; -After 72 h, the diameter of inhibition zones increased for 5.45 ±0.81 cm and 5.62 ± 0.53 cm	*-In vivo* assays revealed that the fibers loaded with CIF had better wound healing performance in comparison with commercial gauze; -The fibers promoted the adhesion and proliferation of L929 fibroblasts.	[156]

					for *E. coli* and *S. aureus*, respectively.		
SSD	PCL/PVA	Blend electrospinning	-PVA: 360 nm; -1-10 wt% SSD/PVA: 450-700 nm.	-The release profile of silver showed a burst release in the initial 24 h; -70% of silver was released during the first week, followed by a gradual release during the second week.	-The largest inhibition halo against *S.aureus* (4.2 ± 0.3 mm) was observed in 10 wt% SSD/PVA membranes, while the smallest inhibition zone (2.0 ± 0.2 mm) was presented by 1 wt% SSD/PVA fibers.	-The cellular proliferation was strongly influenced by SSD concentration, where the highest amount of SSD promoted the lowest cell proliferation; -All the membranes showed good mechanical properties (young modulus: 56.07 to 18.14 MPa) and wettability (contact angle inferior to 90).	[157]

2.7.1.2 Silver nanoparticles

The recent advances of nanotechnology-based therapies have paved the way for fighting microorganisms' multidrug resistance. In particular AgNPs have been emerging as a promising alternative to the use of antibiotics. In fact, the excellent antimicrobial properties displayed by AgNPs have been already tested against 650 different strains of bacteria [162-164]. So far, four mechanisms have been proposed to explain the antimicrobial activity of this type of nanoparticles: (i) AgNPs are able to adhere onto the surface of bacterial cell wall, causing changes in cell membrane structure and permeability, that lead to the leakage of the cellular content; (ii) AgNPs can enter into cell cytoplasm and induce damages in the intracellular structures (such as mitochondria, vacuoles, ribosomes) and biomolecules (*e.g.* protein, lipids, and Deoxyribonucleic acid (DNA)); (iii) AgNPs can mediate the production of reactive oxygen species (ROS) and free radicals; and (iv) AgNPs can modulate the signal transduction pathways, inducing the phosphorylation of various proteins in bacteria and ultimately trigger the cell death [165-167]. The antibacterial activity unveiled by AgNPs encouraged the researchers to produce different silver-based wound dressings that are already available in the market, like Acticoat®, Aquacel Ag®, Silvasorb®, and Silvercel™ [163]. Furthermore, AgNPs have been also incorporated into electrospun membranes to confer them antimicrobial properties (see Table 2.4 for further details). Aadil and colleagues produced PVA-lignin nanofibers containing AgNPs (with diameters ranging from 10 to 50 nm) using the electrospinning technique [168, 169]. The diameter of the produced nanofibers varied between 128 and 291 nm and the presence of the AgNPs within these nanofibers was confirmed through the observation of the two characteristic diffraction peaks at 33 and 47° in the X-ray spectrum, corresponding to the {111} and {200} planes of silver, respectively. Moreover, the antimicrobial activity of the produced membranes was checked against *E. coli* and *Bacillus circulans*. Santos *et al.* immobilized AgNPs on the surface of PCL/ poly((2-dimethylamino)ethyl methacrylate) (PDMAEMA) nanofibrous membranes, following the methodology proposed by Dong *et al.* [170, 171]. Further, the AgNPs size and nanoparticles content on the PCL/PDMAEMA were optimized by varying the pH values (1, 3, 5, 7, and 9) of the growth solution. In fact, the diameter of AgNPs decreased from 1020 ± 60 nm at pH 1 to 64 ± 3 nm at pH 9. On the other side, the pH also influenced the amount of AgNPs adsorbed at the surface of the nanofibers, i.e, 0.59 ppm, 7.40 ppm, 10.1 ppm, 3.40 ppm, and 0.12 ppm of silver was adsorbed at the nanoparticles surface at pH 1, 3, 5, 7 and 9, respectively. Thus, AgNPs showed the maximum adsorption at pH 5, which was attributed to the increased electrostatic interactions that occur between the positively charged amino groups of PDMAEMA and the negatively charged carboxylate groups of citrate present on the surface of AgNPs. Moreover, the results obtained revealed that the biocompatibility of the meshes increased after the AgNPs immobilization and they were able to inhibit the growth of *S. aureus*, *P. aeruginosa*, and *E. coli* [171].

Lee *et al.* produced CS nanofibers containing different amounts of AgNPs (0, 0.7, 1.3, 2 and 4%) [172]. To accomplish that, AgNPs were produced directly in the CS solution, through the chemical reduction of silver nitrate using sodium borohydride. The obtained spherical AgNPs presented an average diameter of 10 ± 2 nm and presented a narrowed wavelength band at 408 nm in UV-Vis absorption spectra, which is characteristic of small-diameter AgNPs. Further, the AgNPs formation was also confirmed by X-ray diffraction being observed the presence of peaks at 38.0°, 44.3°, 64.5° and 77.2°, characteristic of the {111}, {200}, {220} and {311} planes of the AgNPs with a face centered cubic structure. The obtained data showed that a higher content of AgNPs induces a decrease in the nanofibers' diameter from 460 ± 80 nm (at 0%) to 126 ± 28 nm (at 4%). However, nanofibers containing 4% of AgNPs displayed beads and a tangled surface morphology, thus causing their removal from the antibacterial assays. *P.aeruginosa* and *MRSA* were used as model bacteria to characterize the antimicrobial activity of the produced nanofibers, as can be observed in Figure 2.10. The diameter of the inhibitory halo increased from 0 mm to 16.07 mm, 16.58 mm, and 16.73 mm in *P.aeruginosa* and from 0 mm to 14.9 mm, 15.42 mm and 15.75 mm in *MRSA* when increasing amounts of AgNPs were incorporated in the nanofibers (0, 0.7, 1.3 and 2%, respectively). Despite the promising bactericidal activity displayed by silver loaded nanofibrous membranes, there are some handicaps that avoid their widespread in the clinic [173]. Indeed, the AgNPs have some degree of cytotoxicity and the long-term interactions with the human body, besides the nanoparticles fate, is poorly understood. In this field, several studies have been focused on understanding the possible toxic effects of metallic nanoparticles for skin tissue. The metallic nanoparticles-skin interaction (*i.e.* penetration and toxicity) are largely influenced by different physicochemical properties such as the particle type, size, shape, surface coating, charge, stability, and protein corona among others [174-176]. Once the metal nanoparticles become infiltrated into the skin, they can trigger several toxic effects by inducing cell oxidative stress, apoptosis and mitochondrial dysfunction, as well as membrane and DNA damage. In addition, the metallic ions released from the nanoparticles may cause skin sensitization and irritation [177-179]. However, until now the data available concerning the toxicity of metallic nanoparticles is insufficient, demanding in-depth studies to evaluate their biosafety.

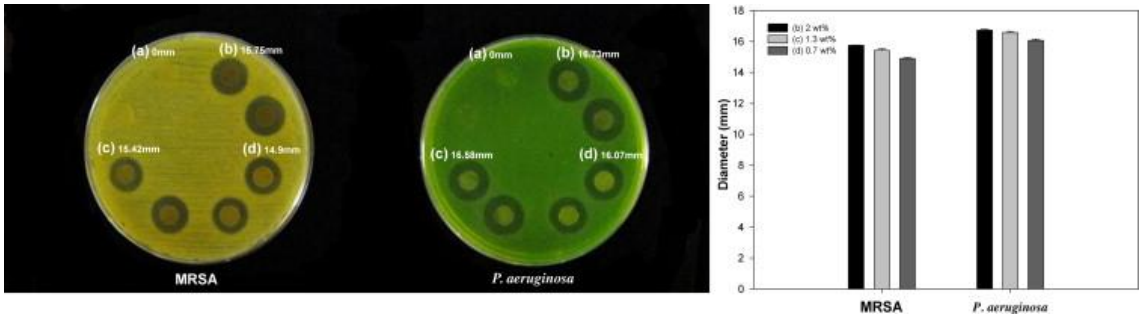

Figure 2.10. Analysis of the antibacterial activity of CS/AgNPs membranes against *MRSA* (dark yellow) and *P. aeruginosa* (green): visualization and measurement of the inhibitory halos of the membranes containing AgNPs at a concentration of 0% (a), 2% (b), 0.7% (c) and 1.3% (d). Reproduced from [172] with permission from Elsevier.

Table 2.4. Description of different electrospun meshes incorporating silver nanoparticles aimed to be used as wound dressing.

Bioactive molecule	Polymer	Incorporation method	Fiber diameter (nm)	Antibacterial assays	Main conclusions	Ref.
AgNPs	PVA/lignin	Blend electrospinning	-PVA/lignin/ AgNPs: 128- 291 nm.	-The zone of inhibition was 1.1 ± 0.05 cm against *E. coli* and 1.3 ± 0.08 cm against *B.circulans*.	-The nanofibers presented yellow and uniform appearance, due to the presence of lignin and AgNPs; -The TEM analysis revealed that AgNPs presented a diameter ranging from 10 to 50 nm.	[168]
	PCL/PDMAEMA	Blend electrospinning and *in situ* formation and immobilization of AgNPs	-PCL/PDMAEMA (80:20): 410 ± 160 nm; - PCL/PDMAEMA (50:50): 330 ± 170 nm.	-The membranes containing AgNPs showed inhibition halos against *S. aureus*, *P. aeruginosa*, and *E. coli*.	-The AgNPs immobilization was more efficient at pH 5 (≈ 25% of adsorption efficiency); -The AgNP immobilization improved the biocompatibility of the membranes.	[171]
	CS	Blend electrospinning	-CS = 460 ± 80 nm; -CTS/AgNPs (4%) = 349 ± 56 nm; -CTS/AgNPs (1.3%): 337 ± 49 nm; -CS/AgNPs (2%): 238 ± 46 nm; -CS/AgNPs (4%): 126 ± 28 nm.	-CTS/AgNPs nanofibers containing 0.1, 1.3 and 2% of AgNPs presented inhibition halos of: 16.07 mm, 16.58 mm and 16.73 mm, against *P.aeruginosa*; 14.9 mm, 15.42 mm and 15.75 mm against *MRSA*, respectively.	-The TEM analysis revealed that the spherical AgNPs with diameter of 10 ± 2 nm were well dispersed in the fibers; -The increase in the AgNPs concentration improved the nanofibers antibacterial effect.	[172]

	Collagen	Blend electrospinning	Not available	-After 48 h, the inhibition zones were: 3.2 ± 0.3 cm in *S.aureus* and 2.3 ± 0.3 cm in *P.aeruginosa*; -The MIC values of AgNPs against *S.aureus* and *P.aeruginosa* were 5.8 ± 0.3 µg/ml and 7.4 ± 0.2 µg/ml respectively.	-The entrapment efficiency of AgNPs into nanofibers was 88.1 ± 0.7%; -The AgNP loaded nanofibers showed excellent wound-healing efficacy due to their intrinsic antibacterial, anti-inflammatory, controlled drug release profile and hemostatic properties.	[180]
	CS/PVA	Blend electrospinning	-CS/PVA: 155 nm; -CS/PVA/ 0.25% AgNPs: 148 nm; -CS/PVA/ 0.5% AgNPs: 144 nm; -CS/PVA/ 1% AgNPs: 139 nm.	-The inhibition zones against *E. coli* were 7.7, 13.3 and 9.0 mm in CS/PVA/AgNPs (0.25, 0.5 and 1%) respectively; -The inhibition zones against *S.aureus* were 9.1, 14.3 and 8.5 mm in CS/PVA/AgNPs (0.25, 0.5 and 1%) respectively.	-The CS/PVA/AgNPs (0.5%) nanofibers showed the highest tensile strength; -The cumulative release of Ag from the electrospun nanofibers was 40, 56 and 36% after 16 days for nanofibers loaded with 0.25, 0.5 and 1% of AgNPs, respectively.	[181]
	PVA/CS oligosaccharides (COS)	Blend electrospinning	-PVA/COS (2:1): 192.57 ± 59.30 nm; -PVA/ COS-AgNPs: 130.13 ± 43.55 nm.	-The PVA/COS-AgNP nanofibers showed clear inhibition zones against *S. aureus* and *E. coli*.	-The Ag was rapidly released during the first 8 h (≈ 80%), which continued gradually thereafter (≈ 100% after 120 h); -The cytotoxicity tests showed that PVA/COS-AgNPs presented excellent *in vitro* biocompatibility in contact with fibroblasts cells; -The PVA/COS-AgNPs nanofibers accelerated the early stages of wound healing.	[182]

	CS/PEO	Blend electrospinning	-CS/PEO: 302 ± 56nm; -CS/PEO/Ag (2%): 277 ± 46nm; -CS/PEO/Ag (4%): 258 ± 31nm; -CS/PEO/Ag (8%): 333 ± 56nm.	-The inhibition zones against *E. coli* (≈ 25 mm) were higher than those against *S. aureus* (≈ 15 mm).	-The release profile of Ag from the nanofibers exhibited an initial fast release in first 12 h, followed by a sustained release until the 72 h; -*In vitro* cytotoxicity assays indicated that CS/PEO/Ag nanofibers presented excellent cytocompatibility in contact with pig iliac endothelial cells.	[183]

2.7.1.3 Natural extracts-derived products

To overcome the limitations associated with the use of antibiotics and AgNPs, researchers have been testing a wide variety of natural products that have been loaded into electrospun membranes (Table 2.5). Amidst them, plant extracts and essential oils (EOs) have been screened as potential sources of novel antimicrobial compounds [184-188]. The antimicrobial properties exhibited by EOs is mainly attributed to the presence of active constituents such as terpenes, terpenoids, and other aromatic and aliphatic constituents [189, 190]. Moreover, the hydrophobic character of the EOs and their components promote the partition of the lipids present in the cell membrane, increasing their permeability and consequently leading to the bacterial cells death due to the leakage of essential molecules and ions [188, 191, 192]. Therefore, the EOs can act as powerful tools to circumvent the bacterial multi-drug resistance [8]. Liakos *et al*. reported the incorporation of three different EOs (cinnamon (CN), lemongrass (LG) and peppermint (PM)) into CA electrospun nanofibers [193]. The produced fibers were free from defects or beaded structures, presenting a mean diameter of 4.2 ± 2.1 μm, 0.9 ± 0.3 μm, 2.8 ± 1.1 μm, and 2.3 ± 0.8 μm for pure CA, CA/5-CN, CA/5-LG, and CA/5-PM, respectively. Furthermore, while the pure CA fibers were colonized by *E. coli* and *Candida albicans*, leading to the formation of biofilms. Fibers loaded with 6.2 and 25% w/w of EOs were able to impair *E. coli* growth since a clear inhibition zone was observed around the samples. On the other hand, the inhibition of *C.albicans* growth was only accomplished when the EOs concentration was increased to about 40% w/w.

Besides the utilization of EOs, propolis extracts (a resinous mixture produced by honey bees) also displays antibacterial, antifungal, antiviral, antioxidant, and anti-inflammatory properties due to the presence of a wide variety of chemical compounds, such as flavonoid aglycones, phenolic acids, and ester derivatives [194]. Kim *et al*. prepared a blend of propolis extract (5, 10 and 30% wt) and PU 10% wt to create a nanofibrous membrane aimed to be used as a wound dressing [195]. The incorporation of the propolis was responsible for an increase in the fibers average diameter 204.4, 321.4, 377.2 and 556.6 nm for PU fibers containing 0, 5, 10, and 30% of propolis, respectively. A higher content of propolis extracts within the PU nanofibers induced a superior bactericidal activity against *E. coli*, with the highest inhibitory effect being registered for the PU membrane containing 30 wt% of propolis [195].

AV and CS comprise other examples of sources from natural compounds displaying antimicrobial activity [196-198]. The amino acids, salicylic acid, ascorbic acid, vitamin A (Vit-A), and vitamin E (Vit-E) found in AV confers it antibacterial, anti-inflammatory, and antioxidant activity [199, 200]. On the other hand, CS is a natural-derived polysaccharide that promotes collagen synthesis and exhibits bactericidal and hemostatic properties [197, 201]. Despite different mechanisms have been proposed for explaining the antimicrobial activity presented by CS, the most accepted mechanism is based on the establishment of electrostatic interactions between positively charged amine groups of CS and the negatively charged groups present in the

bacterial cell wall, leading to an increased cell wall permeability, leakage of intracellular constituents and the dissipation of the ionic gradients of bacteria [197, 202, 203]. In 2016, Sarhan and collaborators studied the antibacterial and wound healing activity of honey, by performing its incorporation into PVA/CS nanofibers [204]. The results obtained demonstrated that higher contents of honey (10, 20 and 30%) induced the formation of fibers with increased diameters (284 ± 97 nm, 371 ± 110 nm, and 464 ± 185 nm, respectively). Moreover, the nanofibers containing 30% of honey were the ones unveiling a higher antibacterial activity against *S.aureus* and *E. coli*.

Table 2.5. List of several types of electrospun membranes incorporating products derived from natural extracts to provide antibacterial properties.

Bioactive molecule	Polymer	Incorporation method	Fiber diameters	Antibacterial assays	Main findings	Ref.
Thymol (THY)	PCL/PVA	Co-axial electrospinning	-PCL/PVA nanofibers: 238 ± 23 nm; -PCL/PVA/THY (5%) nanofibers: 477 ± 51 nm; -PCL/PVA/THY (10%) nanofibers: 798 ± 88 nm.	-The presence of THY in the fibers core resulted in the growth inhibition of *S.aureus* and *E. coli* (> 99%).	-The THY incorporation induced a decrease in the tensile strength and increased the porosity and pore size; -The fibroblast cells remained viable (>90%) in contact with nanofibers during 7 days.	[205]
CN, clove and lavender	PVA/SA	Blend electrospinning	Not available	-A higher concentration of the oils resulted increased inhibition zones against *S.aureus*; -The fibers containing 1.5% of CN oil, clove oil or lavender oil exhibited a inhibition zone against *S.aureus* of 27.6 mm, 26.6 mm and 20.6 mm, respectively.	-FTIR spectra exhibited the peaks of oils and polymers, indicating the successful incorporation of oils into the fibers; -Nanofibers containing CN oil showed better antimicrobial properties against *S.aureus* in comparison to clove and lavender oil.	[206]
Rosemary(R) and oregan (Or)	CA	Blend electrospining	-CA nanofibers: ≈ 800 nm; -CA_5%R nanofibers: ≈ 1200 nm; -CA_5% Or nanofibers: ≈ 1300 nm.	-In *S.aureus*, both EOs (at 5% of concentration) presented similar results, with $1x10^9$ CFU/mL of viable microbial cells after 24 h of incubation; -In *E. coli*, the fibers containing Or presented a lower number of viable bacterial cells (≈ 1×10^6 CFU/ml), exhibiting an improved antibacterial effect; -In *C.albicans*, the fibers containing Or exhibited a pronounced	-The Ramman spectrum revealed that R and Or EOs were efficiently incorporated into electrospun fibers; -The Or was more effective against *S. aureus*, *E. coli* and *C.albicans* in comparison with the R.	[207]

				antibacterial effect (about 100 CFU/ml of viable cells).		
CN	Polyvinylpyrrolidone (PVP)	Emulsion electrospinning	-PVP nanofibers: 323.0 ± 69.9 nm; -PVP/4% of CN: 401.4 ± 108.7 nm.	-The largest inhibition halos were observed for the PVP/4% of CN membranes on *S.aureus*; -For *E. coli*, the PVP/2% of CN presented the higher inhibition zone; -For *C.albicans*, the zone diameters were similar for PVP containing 2%, 3% and 4% of CN.	-The PVP nanofibers containing 2, 3 and 4% of CN exhibited excellent antibacterial effects against *S.aureus*, *E. coli* and *C.albicans*; -No zone inhibition was visualized for *P.aeruginosa*; -The antibacterial activity increased with the size of the electrospun membrane.	[208]
CN, LG and PM	CA	Blend electrospinning	-CA nanofibers: 4.2 ± 2.1 µm; -CA/5-CN nanofibers: 0.9 ± 0.3 µm; -CA/5-LG nanofibers: 2.8 ± 1.1 µm; -CA/5-PM nanofibers:2.3 ± 0.8 µm.	-The fibers incorporating 6.2 and 25% of EOs were able to inhibit the proliferation of *E. coli*; -The fibers containing 40% of EOs hindered the growth of *C.albicans*.	-The effective encapsulation of the EOs into the fibers was demonstrated by Raman spectroscopy; -The fibers encapsulating low amounts of EOs were able to inhibit the formation of *E. coli* biofilms; -The nanofibers did not induce any cytotoxic effect in contact with fibroblasts and human keratinocytes.	[193]
Lavender	Polyacrylonitrile (PAN)	Blend electrospinning	-PAN nanofibers: ≈ 143.4 nm; -PAN/lavender (0.1%) nanofibers: ≈ 141.4 nm;	-PAN/lavender nanofibers presented a clear zone of inhibition with 14-15mm of the diameter, against *S.aureus* and *K.pneunoniae*; -The MIC determined for lavender oil was 100 $\mu g.mL^{-1}$;	-The cell viability of mouse fibroblasts remained near 100% till 200 $\mu g.mL^{-1}$ of lavender; -The drug release kinetics was fitted to	[209]

			-PAN/lavender (0.3%): ≈ 88.55 nm.	-The zone inhibition (13-14 mm) remained unaltered for more than 30 days.	the Higuchi model, and 38% of the lavender oil was released from nanofibers, within 24 h of incubation.	
Tea tree and manuka	PLA	Blend electrospinning	Not available	-The PLA nanofibers without EO and incorporating tea tree oil were not able to inhibit the *S. epidermis* proliferation; -The PLA nanofibers containing manuka oil presented an inhibition zone of 2 cm in diameter.	-The Raman spectroscopy analysis showed that the main components of manuka oil were stable after electrospinning process; -In tea tree oil was observed a strong reduction in the intensity of the Raman spectroscopy characteristic peaks;	[210]
Propolis	PU	Blend electrospinning	-PU nanofibers: 204.4 nm; -PU/propolis (5%) nanofibers: 321.4 nm; -PU/propolis (10%) nanofibers: 377.2 nm; -PU/propolis (30%) nanofibers: 556.6 nm.	-The PU membrane containing 30% of propolis exhibited the largest inhibition zone in contact with *E. coli*.	-The tensile strength of the nanofibers decreased when the concentration of propolis increased; -The propolis incorporation within nanofibers increased the hydrophilicity of the composite PU membranes; -The membranes allowed the proliferation and adhesion of fibroblast cells.	[195]
AV	Gelatin (Gel); PCL	Blend electrospinning; Co-electrospinning	-Gel/AV nanofibers: 124.8 ± 43.1 nm.	-The Gel/AV-PCL presented an inhibition zone of 20 mm and 15 mm for *S.aureus* and *E. coli*, respectively; -The Gel/AV-PCL nanofibers presented > 99% and 85.63%	-The membranes containing 10% of AV showed the highest biodegradation rate (up to 29% after 4 weeks immersion);	[211]

				antibacterial activity against *S.aureus* and *E. coli*, respectively.	-The AV incorporation improved the fibroblast proliferation in comparison to PCL and Gel-PCL membranes.	
Manuka honey (MH)	SF	Blend electrospinning	-SF nanofibers: 484.28 ± 101.04 nm; -SF/MH (10%) nanofibers: 843.92 ± 146.30 nm; -SF/MH (30%) nanofibers: 1149.43 ± 205.03 nm; -SF/MH (50%) nanofibers: 1547.72 ± 338.60 nm; -SF/MH (70%) nanofibers: 2229.33 ± 399.20 nm.	-The MH (10%), MH (30%), MH (50%) and MH (70%)/SF nanofibrous membranes presented inhibition zones against *E. coli* (2.5 mm, 4.2 mm, 5.7 mm and 7.6 mm); *S.aureus* (1.1 mm, 1.7 mm, 2.7 mm and 4.5 mm); *P.aeruginos*a (1.3 mm, 3.7 mm, 6.3 mm and 8.3 mm); *MRSA* (0.7mm, 1.6 mm, 5.5 mm and 6.7 mm), respectively; -The bacterial inhibition efficacy against *E. coli* was (1%, 10%, 24%, 37% and 51%), *S.aureus* (1%, 6%, 12%, 23% and 29%), *P.aeruginosa* (1%, 8%, 19%, 42% and 57%) and *MRSA* (2%, 7%, 13%, 32% and 40%) for MH (10%), MH (30%), MH (50%) and MH (70%)/SF nanofibrous membranes, respectively.	-The increase in MH amount incorporated into SF fibrous matrices did not affect the cell viability; -The MH incorporation enhanced the adhesion and spreading of fibroblasts at membranes' surface; -*In vivo* assays, the MH/SF nanofibrous membranes improved the healing process, showing a similar effect to that of the AquacelAg dressing.	[212]
Honey/CS	PVA	Blend electrospinning	Not available	-The antibacterial activity was dependent on the CS concentration; -The complete bacterial inhibition was achieved (8.25 for *S.aureus* and 2.9 for *E. coli*) after 48 h of incubation, with the 5.5% of CS.	-The nanofibers displayed antibacterial activity against *S.aureus* but poor antibacterial activity against *E. coli*; -The nanofibers containing 3.5% of CS and 20% honey presented the highest swelling (197%); -The degradation rate of membranes was inversely related to the CS concentration present within nanofibers.	[213]

Honey	PVA/CS	Blend electrospinning	-PVA/CS/honey (10%) nanofibers: 284 ± 97 nm; -PVA/CS/honey (20%) nanofibers: 371 ± 110 nm; -PVA/CS/ honey (30%) nanofibers: 464 ± 185 nm.	-At bacterial concentration of 1 x 10^8 CFU/ml, the honey just improved the antibacterial activity against *S. aureus*. In *E. coli* assays, no significant improvements were observed.	-The nanofibers containing honey (30%) presented the higher swelling capacity; -The nanofibers degradation increased with higher concentrations of honey.	[204]
CS	PCL/P(MMA-MA)	Coating	-PCL nanofibers: 500 nm; -PCL/P(MMA-MA) nanofibers: 350 nm.	-The CS-coated fibers promoted the death of *E. coli*, within 1 h after the beginning of the experiment; -No growth of bacterial colonies were observed in CS-covered fibers after incubation in a bacterial solution.	-The coating of CS circumvented the difficulty of directly electrospinning CS; -The blend between PCL and P(MMA-MA) allowed the deposition of more CS.	[196]
***Garcinia mangostana* (GM)**	CS-EDTA/PVA	Blend electrospinning	-CS-EDTA/PVA nanofibers: 205.5 ± 36.06 nm; -CS-EDTA/PVA/GM (1%-3%) nanofibers: 207.8 ± 34.30 nm-251.3 ± 47.95 nm.	-The 1% GM, 2% GM and 3% GM membranes MIC and MBC values were 2 mg/mL, 1 mg/mL and 0.5 mg/mL for *S.aureus* and *E. coli*, respectively.	-The lower swelling ability (96.67%) was noticed in nanofibers containing 3% of GM; -The cumulative release of GM from nanofibers reached 80% after 60 min of incubation; -The membranes are non-toxic and accelerated the healing process.	[214]

2.7.2 Molecules with biological activity

To improve the healing process, researchers have been incorporating bioactive molecules into electrospun membranes [11, 19, 215, 216]. The controlled and targeted release of biological molecules (*e.g.* GFs, vitamins, and anti-inflammatory molecules) at the wound site is fundamental for the regulation of the wound healing process (as illustrated in Figure 2.11) [119].

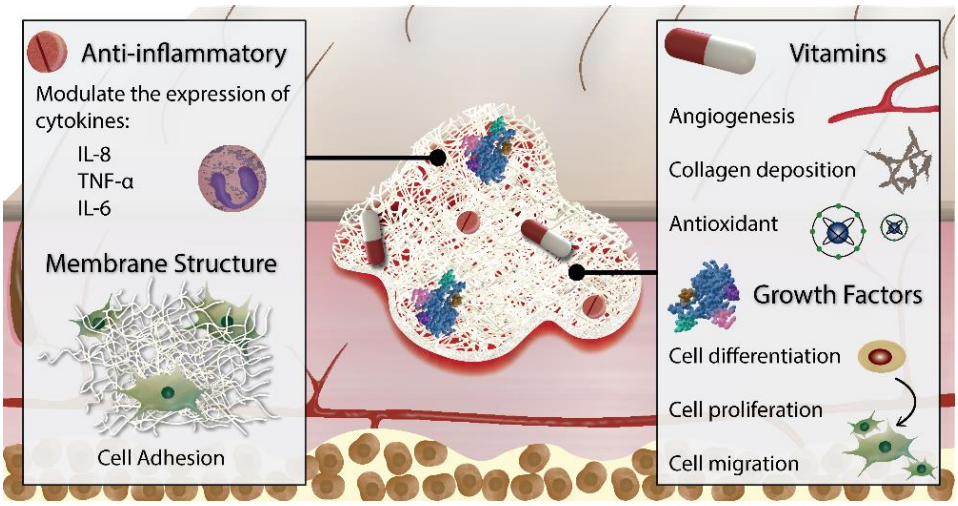

Figure 2.11. Illustration of the different molecules that have been incorporated into electrospun nanofibers and their main roles in the wound healing process.

2.7.2.1 Growth factors

GFs are biologically active polypeptides that are able to regulate the cell growth, differentiation, proliferation, migration and metabolism during the wound healing process [217]. All phases of the wound healing process are controlled by a wide variety of GFs and cytokines, particularly, EGF, PDGF, TGF-β, FGF, and vascular endothelial growth factor (VEGF) [218-221]. These molecules play a critical role in the formation of the granulation tissue, in the modulation of the inflammatory response (*e.g.* PDGF, TGF-β, and interleukins (*e.g.* IL-1 and IL-6)) as well as in the promotion of angiogenesis (*e.g.* EGF and VEGF). Moreover, GFs are also required for the ECM formation and remodelling as well as for the re-epithelialization processes (*e.g.* FGF, EGF, and VEGF) [220]. Nevertheless, the topical administration of GFs presents several drawbacks such as low *in vivo* stability, restricted absorption through the skin, elimination by exudation before reaching the wounded area, and undesirable side effects due to high local and/or systemic levels. Therefore, the loading of GFs into nanofibers is regarded as an appealing strategy for improving the wound healing process [129, 222]. In Table 2.6 are presented different electrospun membranes functionalized with GFs aimed to be used as wound dressings.

Norouzi *et al.* explored the application of the multi-jet electrospinning technique to create core-shell nanofibrous membranes containing PLGA-EGF and gelatin for improving skin regeneration [63]. The produced membranes presented PLGA-EGF and gelatin nanofibers with diameters of 390 ± 75 nm and 175 ± 45 nm, respectively. Further, the combination of PLGA and gelatin nanofibers improved the swelling ability of the membranes, from 23 ± 4% for pure PLGA fibers to 130 ± 10% for PLGA/gelatin nanofibrous membranes. Additionally, the release of EGF from these membranes occurred through an initial burst release, followed by the sustained release over 9 days. Moreover, these membranes were also able to improve the blood clotting, cell adhesion, and proliferation as well as enhance the collagen type I and III expressions (the expression levels of this protein were 22 and 25 times higher than in the normal cells).

Piran and their coworkers encapsulated PDGF into Chitosan nanoparticles (CS-NPs) and then blended them on a PCL solution, that was subsequently electrospun [223]. The data obtained showed that the addition of CS-NPs to the PCL solution lead to an increase on the fibers mean diameter (0.76 ± 0.37 μm, 1.22 ± 0.78 μm, and 1.21± 0.66 μm for PCL, PCL/CS-NPs and PCL/CS-NPs(PDGF) membranes, respectively). Furthermore, the PDGF release occurred in a controlled and sustained manner, with 12% of PDGF being released after 24 h and reaching a maximum of 83% after 1 week. Besides, it was also reported that the presence of PDGF into PCL/CS-NPs(PDGF) membranes can trigger an higher expression of PDGFRß gene, more than 2-fold, which will improve the fibroblast cells migration to the injured site. Jin *et al.* incorporated multiple epidermal induction factors (EIF) like EGF, insulin, hydrocortisone and retinoic acid on gelatin/ PLLCL nanofibers using two different approaches: EIF were directly mixed with gelatin/PLLCL composition, resulting in blend nanofibers (gelatin/PLLCL/EIF (b)); or loaded into core-shell fibers of gelatin and PLLCL (gelatin/PLLCL/EIF (cs)) [224]. The authors obtained uniform nanofibers of PLLCL, gelatin/PLLCL, gelatin/PLLCL/EIF (b) gelatin/PLLCL/EIF (cs) with fiber diameters of 456 ± 62 nm, 382 ± 100 nm, 299 ± 46 nm and 366 ± 125 nm, respectively. Further, the authors also observed that in the gelatin/PLLCL/EIF (b) nanofibers, produced through blend electrospinning, occurs an initial burst release of EGF (first three days) that stabilized until day 6, reaching the maximum of 77.8% after 15 days of incubation, which is appropriate for promoting cell proliferation. On the other side, the cumulative release profile of EGF from core-shell gelatin/PLLCL/EIF (cs) nanofibers, did not display the initial burst release, and a stable and sustained diffusion of EGF was observed (50.9% of the total amount was released after 15 days). This controlled release of EGF from nanofibers resulted in 43.6% higher proliferation of adipose-derived stem cells (ADSCs) on core-shell gelatin/PLLCL/EIF (cs) nanofibers than that on the blend gelatin/PLLCL/EIF (b) counterparts. Moreover, the rate of cell proliferation on gelatin/PLLCL/EIF (cs) and gelatin/PLLCL/EIF (b) from day 5 to 15 was 560% and 404%, respectively. Additionally, the researchers also noticed that the amount of differentiated epidermal cells on gelatin/PLLCL/EIF (cs) was superior to that observed on gelatin/PLLCL/EIF (b) membrane, 62.2% and 43.0%, respectively (as shown in Figure 2.12).

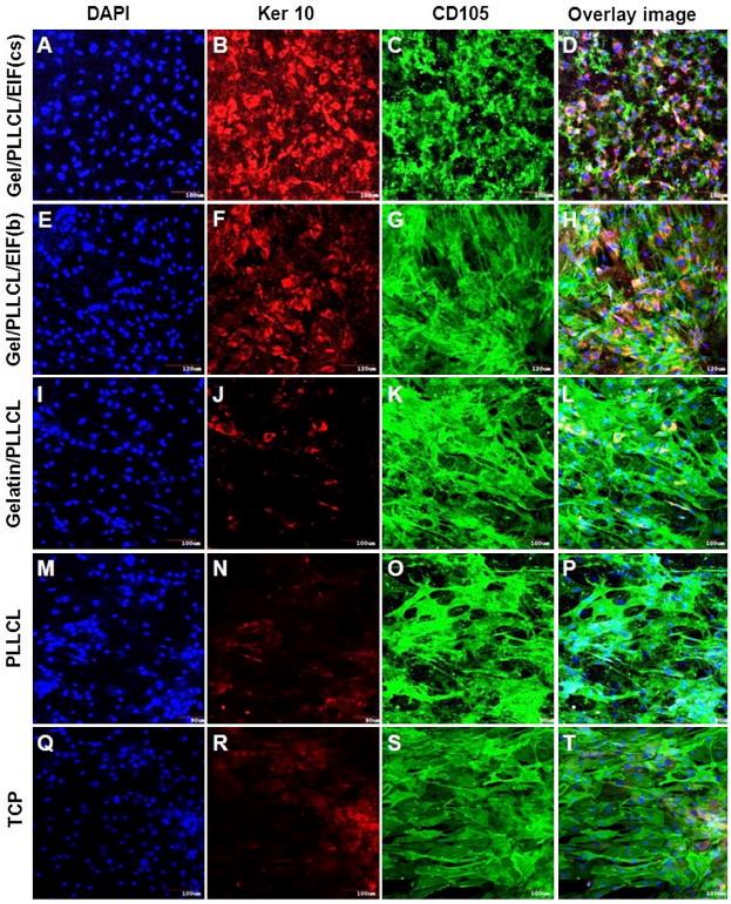

Figure 2.12. Characterization of the adipose-derived stem cells (ADSCs) epidermal differentiation after 15 days of cells being seeded in contact with different materials. Dual immunocytochemical analysis of the expression of ker 10 (red channel) and CD 105 (green channel) on Gel/PLLCL/EIF (cs) (A-D); Gel/PLLCL/EIF (b) (E-H); Gelatin/PLLCL (I-L); PLLCL (M-P); and TCP (Q-T) at 20x magnification. Reproduced from [224] with permission from Elsevier.

Table 2.6. Examples of the growth factors incorporated into electrospun meshes to be used in wound management.

Growth factor	Polymer	Incorporation method	Fiber diameter	Release profile	Main Findings	Ref.
PDGF	CS/PEO/Fb	Blend electrospinning	-CS/PEO: 269.9 ± 68.4 nm; -CS/PEO/Fb: 202.3 ± 113.2 nm.	-Cumulative release of PDGF after 48 h of incubation was 1.8 ± 0.7, 4.4 ± 1.8, 11.4 ± 4.8 ng of PDGF/mL for initially incorporated concentrations of 2, 4, and 8 µg/mL.	-The sustained released of PDGF during 48 h promoted the fibroblast migration; -The dermal fibroblast migration was functionally equivalent to a single 50 ng/mL dose of PDGF.	[225]
rhEGF	PLGA/AV	Emulsion electrospinning	-PLGA: 561.61 ± 124.28 nm; -PLGA/AV: 486.99 ±114.73 nm; -PLGA/AV/EGF: 356.03 ± 112.05 nm.	-The release profile of rhEGF from nanofibers exhibited an initial burst release (35%) within the first 8 h, followed by a slower release phase (50%) up to 7 days.	-The cell proliferation in PLGA/AV/EGF nanofibers reached a threefold increase in comparison to the control; -*In vivo* assays showed that the animals treated with PLGA/AV/EGF and PLGA/AV nanofibers presented an increased reepithelization; -The PLGA/AV/EGF nanofibers decreased the duration of the inflammatory phase.	[198]
bFGF, EGF, VEGF and PDGF	- EGF: collagen; -bFGF: HA; -PDGF and VEGF:gelatin nanoparticles.	Blend electrospinning	-Collagen nanofibers: 534 ± 128 nm; -HA nanofibers: 486 ± 151 nm.	-Gradual slow release for PDGF and VEGF from gelatin nanoparticles during 30 days; - bFGF was rapidly released from HA nanofibers, 90% in 5 days; -EGF was rapidly released from collagen nanofibers, 60% in 5 days.	-The initial release of bFGF and EGF mimicked the early stage of the wound healing process, while the slow controlled release of VEGF and PDGF imitated the late stage of skin regeneration; -*In vivo* assays demonstrated the capability of the nanofibers to promote the re-epithelialization, dermal reconstruction and vascularization in diabetic rats.	[216]
VEGF and PDGF	-VEGF: CS/PEO nanofibers; -PDGF: PLGA nanoparticles.	Blend electrospinning	-1:1 CS/PEO: 116 ± 39 nm; -1:2 CS/PEO: 132 ± 39 nm.	-The release profile of VEGF from nanofibers exhibited a burst release (63%) within 1 h. After 1 day, 100% of VEGF was released; -28% of PDGF was released from PLGA nanoparticles at	-The membranes loaded with GFs showed a faster cell growth (140.9 ± 0.8% for day 5 and 156.6 ± 6.6% for day 7) in comparison with control groups; -VEGF improved the angiogenesis, while PDGF enhanced the epithelium regeneration, collagen deposition and functional tissue remodelling.	[219]

				2 h, followed by a sustained release (40%) for 7 days.		
PDGF	CS-NPs in PCL nanofibers	Blend electrospinning	-PCL: 0.76 ± 0.37 μm; -PCL/NP:1.22 ± 0.78 μm; -PCL/NP(PDGF): 1.21± 0.66 μm.	-12% of PDGF was released in first 24 h, following a sustained release during one week (about 83% of PDGF released).	-The released PDGF induced the cell alignment on nanofibrous matrix; -The expression of PDGFRß gene was higher in cells seeded in contact with PCL/NP(PDGF) nanofibers; -The controlled release of PDGF had high potential to induce the proliferation and migration of fibroblast cells.	[223]
EGF, insulin, hydrocortisone, and retinoic acid	gelatin/PLLCL	- Blend electrospinning: gelatin/PLLCL (b); -Co-axial electrospinning: gelatin/PLLCL (cs).	-PLLCL: 456 ± 62 nm; -gelatin/PLLCL: 382 ± 100 nm; -gelatin/PLLCL/EIF (b): 299 ± 46 nm; gelatin/PLLCL/EIF (cs): 366 ± 125 nm.	-gelatin/PLLCL/EIF (b): 77.8% of EGF released after 15 days; -gelatin/PLLCL/EIF (cs): 50.9% of EGF released after 15 days.	-The cell proliferation of ADSCs was higher (43.6%) in gelatin/PLLCL/EIF (cs) than in gelatin/PLLCL/EIF (b); -The percentage of differentiated epidermal cells was 62.2% and 43.0% for gelatin/PLLCL/EIF (cs) and gelatin/PLLCL/EIF (b) membranes, respectively.	[224]
EGF	PLGA/gelatin	Emulsion electrospinning	-PLGA: 630 ± 80 nm -Gelatin: 175 ± 45 nm -PLGA/EGF/ gelatin: 390 ± 75 nm	-The release profile of EGF exhibits a burst release (in first day), followed by a sustained release over 9 days (total release of EGF was 4.2 ± 0.2 ng/mL).	-The MTT assay revealed that the fibroblast proliferation was higher on PLGA/EGF/gelatin membranes; -The cell infiltration and the expression of collagen type I and III genes was also higher in EGF loaded nanofibers; -The PLGA/EGF/gelatin membranes also demonstrated auspicious blood clotting and platelet adhesion in comparison to the commercial wound dressing (Hansplast).	[63]
	PCL/HA	Emulsion electrospinning	-PCL: 272 ± 38 nm; -PCL/HA: 184 ± 6 nm; -PCL/HA/EGF: 149 ± 4.5 nm.	-The EGF release profile exhibited an early burst release in 4 days (35 ± 1.5%); -The release profile of EGF stabilized over 25 days, reaching 43.5 ± 1.2%.	-The HA mediated increase of the membranes hydrophilicity promoted the release of EGF; -The release of EGF and HA promoted cell infiltration, regulate the collagen and TGF-	[138]

					ß1 gene expression and increase the ratio of collagen III to collagen I; -PCL/HA/EGF membranes accelerated the epidermis regeneration in the early phases of wound healing; -The wounds treated with PCL/HA/EGF membranes presented a thicker and more organized epidermis layer in the early phases of wound healing.	
bFGF and EGF	PCL-PEG/PCL	-bFGF: coaxial electrospinning; -EGF:Chemical immobilization.	Not available	-The release profile of bFGF displays an initial burst release, 30% of bFGF is released in the first 12 h; -The surface-immobilized EGF is scarcely released, less than 2% of immobilized EGF was released in 7 days.	-The nanofibrous membranes containing GFs promoted the wound healing process and improved re-epithelialization of wounded tissues; -The membranes increased the accumulation of collagen and matrix of keratin.	[226]

2.7.2.2 Vitamins

The delivery of vitamins, particularly Vit-A, C and E to the wound site can improve the healing process [70, 227]. Vit-A increases the number of macrophages and monocytes present at the wound site, stimulating the re-epithelialization and the collagen synthesis [228, 229]. The antioxidant and anti-inflammatory activity, as well as the capacity to promote the angiogenesis and reduce scarring of Vit-E also contributes to enhance the wound healing [230]. An overview of different works reporting the incorporation of vitamins into electrospun nanofibers aimed for wound healing applications is shown in Table 2.7.

Taepaiboon *et al*. prepared CA solutions containing Vit-E (5 wt%) or Vit-A (0.5 wt%) that were used to produce nanofibrous membranes [231]. Their results revealed that the percentage of vitamins incorporated within the fiber mats was 83% and 45% for Vit-E and Vit-A, respectively. The incorporation of these molecules induced a decrease in the nanofibers mean diameter from 265 ± 39 nm (for CA nanofibers) to 253 ± 41 nm (for CA fibers containing Vit-E) and 247 ± 31 nm (for CA fibers containing Vit-A). Further, the release profile of vitamins from CA electrospun membranes in two different acetate buffer solutions (B/T medium (containing 0.5 vol% Tween 80) and B/T/M medium (containing 0.5 vol% Tween 80 and 10 vol% methanol)) was evaluated. The maximum release of Vit- E and Vit-A in B/T medium was ≈ 52% and ≈ 34% after 24 h, whereas when the sample was incubated in B/T/M medium this value increased to ≈ 95% and ≈ 96%, respectively. Sheng *et al*. explored the incorporation of a PEGylated derivative of Vitamin E (TPGS) into SF nanofibers for enhancing the wound healing process [232]. To accomplish that, different blends containing TPGS (2, 4 and 8% w/w) and SF (25% w/v) were electrospun. The produced membranes exhibited a burst release of TPGS, during the first 30 min, followed by a slow and controlled diffusion of this molecule over the following 72 h. Moreover, L929 cells remained viable and proliferated at the surface of TPGS loaded SF nanofibers. In 2018, Kheradvar *et al*. reported the development of SF_PVA_AV nanofibers containing starch nanoparticles loaded with Vitamin E (VE-SNPs) [233]. The produced VE-SNPs presented a round shape morphology, a mean diameter of 44.7 nm and an EE of 91.63%. The SF_PVA_AV (40, 50, and 10 v/v) nanofibers presented a mean fiber diameter of 298.23 ± 6.92 nm. These nanofibers displayed an initial rapid release of Vit-E within the first 4 h, followed by a sustained release over 144 h. Furthermore, the increased content of VE-SNPs loaded into the membranes resulted in a higher antioxidant activity (34.7 ± 2.05% (for 1 mg) and 66.27 ± 3.7% (for 5 mg)). On the other hand, *in vitro* assays also demonstrated the biocompatible profile of the electrospun membranes, since they were able to promote fibroblasts adhesion, spreading and proliferation. Vitamin C (Vit-C) also plays an important role during the wound healing process, namely promotes the synthesis of collagen, encourages the keratinocytes differentiation and angiogenesis as well as provides protection against damages induced by UV radiation [234]. Moreover, the Vit-C deficiency leads to an impaired immune response and an increased susceptibility to wound infection [235]. Fan and their collaborators incorporated Vit-C into SF

nanofibrous matrices [236]. Their results showed that the incorporation of Vit-C into SF nanofibers increased the fibers average diameter, from 362 ± 121 nm to 416 ± 133 nm (1 wt% Vit-C) and 506 ± 68 nm (for 3 wt% Vit-C). Further, the release profile of Vit-C from SF nanofibers displayed a burst release behaviour during the initial 20 min and then reached a plateau (≈ 60% for 1 wt% Vit-C and 70% for 3 wt% Vit-C) after 250 min. In addition, the incorporation of Vit-C into the membranes promoted higher cell viability and increased expression of some key functional genes (*Col1a1*, *Gpx1*, and *Cat*).

Table 2.7. Examples of several vitamins that have been incorporated into electrospun nanofibers to improve the wound healing process.

Vitamins	Polymer	Incorporation method	Fiber diameter (nm)	EE (%)	Main conclusions	Ref.
Vit-A and Vit-E	Gelatin	Blend electrospinning	-Gelatin: 757 ± 161 nm; -Gelatin loaded with Vitamins: 566 ± 163 nm.	-Vit-E: 73.1 ± 3.2%; -Vit- A: 71.4 ± 5.5%.	-The gelatin nanofibers exhibited a sustained release of vitamins for more than 60 h; -The fibers promoted the adhesion and proliferation of L929 fibroblasts; -The Vit-E protected the Vit-A from oxidation process.	[215]
	CA	Blend electrospinning	-CA: 265 ± 39 nm; -CA/Vit-E: 253 ± 41 nm; -CA/ Vit-A: 247 ± 31 nm.	-Vit-E: 83%; -Vit-A: 45%.	-In B/T medium, the maximum release of Vit- E at 24 h was ≈ 52%, whereas for Vit-A ≈ 34% was released at 6 h; -In B/T/M medium the maximum release of the Vit-E at 24 h was ≈ 95%, whereas for Vit-A 96% was released at 6 h.	[231]
Vit-E	SF	Blend electrospinning	-SF/Vit-E (2%): 722.52 ± 300 nm; -SF/Vit-E (4%): 387.9 ± 114 nm; -SF/Vit-E (8%): 384.3 ± 161 nm.	-SF/Vit-E (2%): 65.82%; -SF/Vit-E (4%): 78.59%; -SF/Vit-E (8%): 70.02%.	-The Vit-E displayed a burst release (during the first 30 min), followed a slow drug release over the subsequent 72 h; -The Vit-E loaded SF nanofibrous promoted the adhesion and proliferation of L929 cells; -The Vit-E loaded SF membranes were capable to protect the cells from damage induced by ROS.	[232]
	SF/PVA/AV	Vit-E loaded into starch nanoparticles and blend with electrospinning solution	-SF/PVA/AV: 298.23 ± 6.92 nm.	-Vit-E into startch nanoparticles: 91.63%.	-The release profile of Vit-E consisted of an initial rapid release, followed by a slow release for 144 h; -The increase of Vit-E content resulted in higher antioxidant activity;	[233]

					-The fibroblasts cells remained viable, adhering and proliferating in contact with electrospun membranes.	
Vit-C	Carboxymethyl chitosan (CMCS/PEO	Blend electrospinning	-CMCS/PEO: 165 nm; -CMSCS/PEO/Phenytoin sodium (PHT-Na): 125 nm.	Not available	-The kinetics of drug release from the polymeric matrix was explained by the Fickian diffusion mechanism; -The membranes containing PHT-Na and Vit-C promoted a higher accumulation of stem cells (from 1.8 x 10^5 to 8.3 x 10^5 cells/mL).	[237]
	SF	Blend electrospinning	-SF: 362 ± 121 nm; -SF/Vit-C (1%): 416 ± 133 nm; -SF/Vit-C (3%): 506 ± 68 nm.	Not available	-The release profile of Vit-C from SF nanofibers exhibited a burst peak during the initial 20 min; -The Vit-C promoted a higher fibroblast viability and increased the mRNA level of key functional genes (*Col1a1*, *Gpx1* and *Cat*).	[236]
	PLLCL/ SF	Blend electrospinning	-PLLCL/SF: 275 ± 50 nm; -PLLCL/SF/TCH/Vit-C: 265 ± 97 nm.	Not available	-The PLLCL/SF membrane had a water contact angle of 98 ± 1.2°, whereas the PLLCL/SF/TCH/Vit-C showed 54 ± 2.5°; -An increased secretion of collagen was observed in the presence of nanofibers loaded with Vit-C; -The Vit-C promoted an augmented expression of F-actin.	[238]

2.7.2.3 Molecules exhibiting anti-inflammatory activity

The inflammatory phase of the wound healing process begins almost simultaneously with the haemostasis, in order to prevent blood and fluid losses as well as to remove dead tissues and avoid infection [21, 23]. In this phase, inflammatory cells (*i.e.* monocytes, macrophages, and neutrophils) play a crucial role in the wound cleansing, since they are responsible for removing all non-viable cells, bacteria-filled neutrophils, damaged ECM, and bacteria from the wound site. Moreover, these inflammatory cells are also involved in the production of GFs (like EGF, TGF-β, and FGF), that are responsible for attracting fibroblasts and smooth muscle cells into the wound [23]. However, when an exuberant and prolonged inflammatory process occurs, the continuous attraction of neutrophils and macrophages leads to the excessive production of inflammatory mediators, free radicals, and cytotoxic enzymes, which interrupt the physiological healing mechanisms and damage the surrounding tissue [69, 239, 240]. Therefore, the incorporation of anti-inflammatory molecules into wound dressings is a key approach for the treatment of skin injuries, since these molecules are capable of inhibiting the development of chronic inflammation and to avoid the accumulation of free radicals [17, 241, 242]. In Table 2.8 examples of different anti-inflammatory molecules that have been incorporated into electrospun membranes aimed to be applied as wound dressings are provided.

Among the different molecules used, curcumin was one of the first anti-inflammatory agents incorporated into electrospun nanofibers [243]. Curcumin is able to decrease the release of inflammatory cytokines from monocytes and macrophages (interleukin (IL)-8 and tumour necrosis factor (TNF)-α) as well as inhibit the enzymes associated with inflammation (cyclooxygenase (COX)-2 and lipoxygenase) [244, 245]. Merrell *et al.* developed PCL nanofibers loaded with curcumin for being applied as wound dressings [246]. Their results showed that the incorporation of curcumin (3 and 17% w/w) changed the nanofibers size diameter distribution from 300-400 nm (for PCL nanofibers) to 200-800 nm (for PCL/curcumin nanofibers). Moreover, the produced nanofibers performed the release of curcumin for 3 days, prompting a cytoprotective effect on human fibroblast cell line (HFF-1 cells), when they were incubated with hydrogen peroxide. Further, the curcumin-loaded PCL nanofibrous mats reduced the pro-inflammatory response of mouse peritoneal macrophages stimulated with lipopolysaccharide (LPS). The expression of IL-6 was reduced from ≈ 1220 pg/mL on the cells treated with PCL nanofibers to ≈ 600 pg/mL and 400 pg/mL for the cells treated with PCL fibers containing 3% and 17% of curcumin, respectively. Additionally, the animals treated with curcumin-loaded PCL nanofibers showed almost 80% of wound closure at day 10, contrasting with the 60% registered for mice treated with PCL nanofibers.

Nonsteroidal anti-inflammatory drugs are another type of molecules that are usually used to treat inflammation as well as control pain and fever [247]. Among them, the application of ibuprofen (IBP) has been widely reported, however, the continued oral administration or large doses of IBP may have associated side effects, such as kidney damage and gastric ulcers.

Therefore, the topical administration of IBP may have a positive impact on the treatment of skin injuries [248-250]. Mohiti-Asli *et al.* incorporated IBP into PLA nanofibers for promoting the regeneration of full thickness wounds [251]. The incorporation of IBP resulted in the production of nanofibers with higher fiber diameters, *i.e.* 10%, 20% and 30% of IBP-loaded nanofibers displayed a diameter of 329.11 ± 249.62 nm, 478.31 ± 167.61 nm, and 585.38 ± 131.51 nm, respectively. Moreover, these nanofibrous mats were able to support the cell adhesion and proliferation, particularly the PLA nanofibrous mat with 20% of IBP. The authors also observed that the PLA nanofibrous mat containing 20% of IBP could be degraded when applied in full-thickness wounds in mice, supporting simultaneously the wound closure (60% wound contraction after 14 days).

Chrysin (Chr), a natural flavonoid present in various plant extracts, has also been incorporated into nanofiber based wound dressings due to its anti-inflammatory properties [252, 253]. The Chr suppresses the LPS-induced COX-2 expression, inhibits the nitric oxide (NO) synthase as well as the release of NO and pro-inflammatory cytokines such as Tumor necrosis factor-α (TNF-α) and IL-1ß. Deldar and coworkers incorporated Chr into PCL/PEG nanofibrous membranes to produce a wound dressing that displays antioxidant and anti-inflammatory activities [254]. The inclusion of Chr, at 5 or 15 wt%, into PCL/PEG nanofibers changed the nanofibers diameter distribution from 300-400 nm (PCL/PEG membranes) to 250-650 nm (PCL/PEG/Chr membranes). Further, the Chr was released from the nanofibers in a sustained manner over 72 h, independently of the loaded amount. This behaviour resulted in the reduction of the expression of pro-inflammatory cytokines in 67%, 52% and 72% for IL-6, IL-1ß, and TNF-α, respectively, when J774A1 cells were in contact with PCL/PEG nanofibrous membranes loaded with Chr 15% (w/w). Additionally, a decrease on the NO production by macrophage cells was also noticed from 29.53 μM to 15.50 μM (for PCL/PEG/Chr 5% nanofibers) and to 12.52 μM (for PCL/PEG/Chr 15% nanofibers). Such results supported the Chr-loaded PCL/PEG nanofibrous membranes capacity to inhibit the inflammatory process.

Table 2.8. Description of some examples of electrospun membranes functionalized with anti-inflammatory molecules to improve the healing process.

Anti-inflammatory molecule	Polymer	Incorporation method	Fiber diameters	Release profile	Anti-inflammatory assay	Main findings	Ref.
Diclofenac (DLF)	DLF was incorporated into ZN nanoparticles and posteriorly blend with PVA	Blend electrospinning	-PVA nanofibers: 202.41 ± 25.54 nm; -PVA/ZN NPs: 311.18 ± 45.56 nm; -PVA/ZN NPs-DLF: 324.42 ± 72.80 nm.	-In the first stage, 36% of DLF was released from NPs after 8 h; -The release profile of DLF reached a plateau after 3 days, in which 80% of the drug was released.	Not available	-The NPs were well dispersed and distributed uniformly within nanofibers; -The membrane was biocompatible in contact with fibroblasts, improving its proliferation and spreading.	[255]
IBP	PLA	Blend electrospinning	-PLA/IBP (10%): 329.11 ± 249.62 nm; -PLA/IBP (20%): 478.31 ± 167.61 nm; -PLA/ IBP(30%): 585.38 ± 131.51 nm.	-0.25 mg of IBP released from PLA/IBP (30%) nanofibers after 336 h.	Not available	-The greatest cell viability and proliferation was recorded in nanofibers containing 20 wt% IBP; -The incorporation of IBP into PLA nanofibers promoted an increased viability and proliferation of both HEK and HDF.	[251]
Ketoprofen	PCL/ gelatin	Emulsion electrospining	-PCL/ ketoprofen: 345 nm; -PCL/ gelatin/ketoprofen: 272 nm.	-PCL /ketoprofen: initial burst release profile that reached a plateau (90%) after 12 min; -PCL/gelatin/ Ketoprofen: continuous and sustained	Not available	-Ketoprofen-containing electrospun membranes are biocompatible in contact with L929 mouse fibroblast cells; -The cell growth was 1.93 and 3.07 times higher in PCL/gelatin nanofibers in comparison with PCL membranes and tissue culture	[256]

				release for 4 days.		polystyrene plates, respectively.	
Polypropylene fumarate (PPF)	Phosphino carboxylic acid polymer (POCA)	Blend electrospinning	-POCA/PDF: 0.8 ± 0.1 μm.	Not available	-IL-6 and IL-1β expression was 4 and 24 times inferior in POCA/PDF electrospun membranes group; -MPO values and the inflammation process decreased (skin thickness:14.3 ± 2.5 μm), when the burn was covered with POCA/PDF dressing.	-The presence of fumarate reduces the cytokines and neutrophils production; -The skin treated with POCA:PDF membranes exhibited a thin epidermal layer and low number of inflammatory cells.	[257]
Curcumin	PCL	Blend electrospinning	-PCL: range 300-400 nm; -PCL/curcumin: 200-800 nm.	-PCL/curcumin (17%): 35 μg was released at 3 days; -PCL/curcumin (3%): 20 μg was released at 3 days.	-The IL-6 release decreased in the PCL/curcumin (7%) nanofibers group.	-The ORAC assay also demonstrated the antioxidant properties of curcumin-loaded fibers; -The membranes were biocompatible and displayed a cytoprotective effect towards human fibroblasts cells; -*In vivo* assays demonstrated the ability of PCL/curcumin nanofibers to improve the rate of wound closure in a diabetic mouse model.	[246]

Naproxen (NAP)	CA	-Blend electrospinning: CA/NAP **(NF-1)**; -Co-axial electrospinning: core (NAP/CA) and sheath (CA) **(NF-2)**; core (NAP loaded liposomes and sodium hyaluronate) and sheath (CA) **(NF-3)**.	-NF-1: 409.3 ± 152.5 nm; -NF-2: 419.2 ± 178.2 nm; -NF-3: 359.4 ± 126.2 nm.	-NF-1: 90.9% of NAP is released in 8 h; -NF-2: 80.3% of NAP is released in 8 h; -NF-3: 47.1% of NAP is released within 8 h, following a slow and sustained release for 12 days.	Not available	-The drug release from NF-1 and NF-2 nanofibers occur by a non-Fickian diffusion mechanism; -In NF-3 nanofibers, the drug release shows specific behaviour, in which a burst release occurs in first 8 h, and then a sustained drug release occurs for the following 12 days.	[258]
Chr	PCL/PEG	Blend electrospinning	-PCL/PEG: 300 - 400 nm; -PCL/PEG/Chr: 250-650 nm.	-PCL/PEG/Chr (5%): 25 µg of Chr was released after 3 days; -PCL/PEG/Chr (15%): 43 µg of Chr was released after 3 days.	-The macrophages incubated with PCL/PEG/Chr (15%) presented a 67%, 52% and 72% reduction in the Il-6, Il-1ß and TNF-α expression, respectively; -The cells NO production decreased with the Chr content, 16.22 µM and 14.60 µM for PCL/PEG/Chr (5%) and (15%), respectively.	-The nanofibers were biocompatible and exhibited antioxidant activity; -The cytoprotective effect of Chr-loaded nanofibrous membranes towards human fibroblast cells was also demonstrated; -The anti-inflammatory capability of Chr-loaded nanofibrous mats was evidenced by the macrophages decreased expression of IL-6, IL-1ß, TNF-α and NO.	[254]

Montelukast	Poly(methyl vinyl etherco-maleic acid) (PMVEMA)/ PLGA	Blend electrospinning	-PMVEMA/ PLGA/ Montelukast: 101.1- 283 nm.	-The cumulative drug release was faster on the increased amount of montekulast.	Not available	-The addition of the montekulast into PMVEMA/PLGA nanofibers did elicit any cytotoxicity effect, allowing the cells adhesion and proliferation; -The nanofibers promoted an increased platelet adhesion in comparison to the negative control.	[259]
Dexamethasone (DEX)	-SF/PEO; -SF/PEO/ DEX1 (1 mg/mL); -SF/PEO/ DEX2 (2 mg/mL).	Blend and Emulsion electrospinning	-SF/PEO: 446.25 ± 113.93 nm; -SF/PEO /DEX1: 511.11 ± 109.03 nm; -SF/PEO/ DEX2: 528.50 ± 148.00 nm.	-Using blend electrospinning: the release of DEX from SF/PEO/DEX2 was 30% in the first 2 h and 8% after 24 h; -Using emulsion electrospinning: the release of DEX from SF/PEO/DEX2 was 21% in the first 2 h and 42% after 24 h.	-The release DEX can reduce porcine hip artery endothelial cell (PIECs) inflammatory damage, which was induced by LPS.	-Core-shell structure provided a slow release of drug from nanofibers; -The incorporation of DEX provided a protective effect to the nanofibers on PIECS damaged by LPS.	[260]

2.8 Asymmetric membranes as ideal wound dressings

It is well known that the protection of a skin injury is primordial to avoid infections and dehydration of the patient. Up to recent years, researchers were only concerned in promoting the protection of the wound using occlusive wound dressings such as Opsite® (film of adhesive acrylic), Omiderm® (hydrophilized membrane of PU), or Xeroform™ (traditional gauze). However, these wound dressings are characterized by its lack of permeability to water, which leads to exudate accumulation, tissue maceration, or occurrence of infections [261]. To overcome such limitations, porous wound dressings were developed. Nevertheless, the open structure exhibited by these wound dressings demonstrated a low efficacy in the prevention of bacteria penetration (originating wound infections) and present increased evaporative water losses, which may result in wound dehydration. In addition, these dressings require regular replacement, increasing the risk of wound infection as well as inducing further damage at the wound site [262, 263].

Such drawbacks triggered the development of new wound dressings, like asymmetric membranes, acellular matrices capable of impairing bacterial penetration and simultaneously avoid the wound dehydration as well as exudate accumulation [263]. Hinrichs *et al*. reported for the first time the application of an asymmetric PU membrane, mimicking the properties and structural organization of epidermis and dermis layers, in the wound healing [264]. In this approach, the membrane top layer presented interconnected micropores that were able to avoid bacterial penetration, rapid wound dehydration as well as exudate accumulation. In addition, the bottom layer was conceived to display a high fluid absorption capacity, allow gaseous exchange as well as promote cell migration and proliferation [261, 265]. Further, it is worth to notice that the membrane layers can be loaded with diverse biomolecules (bioactive and antibacterial agents) to improve their performance in the wound healing process. The main properties and functions of asymmetric membranes to be used as wound dressing are illustrated in Figure 2.13.

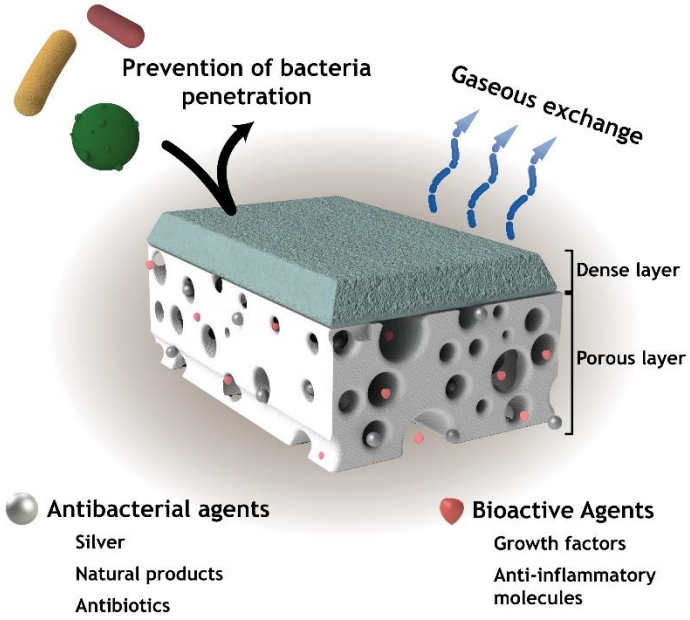

Figure 2.13. Illustration of the main features displayed by asymmetric membranes aimed to improve the wound healing.

2.8.1 General properties of asymmetric membranes aimed to be used as wound dressings

Despite the asymmetric membranes potential to reproduce the structure of the skin epidermis and dermis layers, there are several key properties that these membranes must fulfil to be applied in the treatment of skin injuries, namely the porosity, water uptake ability, wettability (contact angle), WVTR, mechanical properties, antimicrobial activity, and release profile.

2.8.1.1 Porosity

The wound dressings porosity will modulate the cells migration and adhesion, as well as the nutrients and waste products exchange between the 3D construct and the surrounding environment [266]. Usually, overall porosity values between 60 to 90% are desired for enhancing the wound healing [267]. Nevertheless, more than the overall porosity, the researchers must also consider the pore size as a limiting factor. In this way, the top layer of the membrane should contain pores with a mean diameter inferior to the bacterial size (*i.e.* inferior to 500 nm) to avoid the wound infection [268]. On the other side, the bottom layer should possess interconnected pores with a mean diameter superior to 20 μm to facilitate the cells penetration and the exchange of nutrients and waste products [269].

2.8.1.2 Wettability

The cells are more prone to adhere and proliferate in moderate hydrophilic wound dressings (water contact angle (WCA) around 40°-70°) than in hydrophilic (WCA < 20°) or hydrophobic

ones (WCA >90°) [79, 242, 270]. The inner layer of asymmetric membranes usually displays a hydrophilic character that confers to them the capacity to adsorb the wound exudate. The external layer of an asymmetric membrane presents a hydrophobic character to avoid patient dehydration as well as bacterial wound contamination [105, 271, 272].

2.8.1.3 Water uptake ability and WVTR

The wound dressing must be capable of absorb the excessive exudate and simultaneously maintain a moist environment [273]. In this way, an ideal wound dressing normally presents a water absorption in the range of 100-900% (of its initial weight), which avoid the tissue maceration caused by the fluids' accumulation and the formation of scar tissue [261, 274].On the other side, the gaseous exchanges that happen between the wound and the environment are crucial for the healing process to occur. In fact, wound dressings must be compatible with the transmission of the water vapor to avoid the exudate retention. However, high-WVTR can also result in the wound dehydration [274, 275]. Therefore, it is recommended that wound dressing present a WVTR comprehended between 2000-2500 g/m^2, a value that corresponds to half of that observed in granulating wounds (5100 g/m^2) [274]. Additionally, the permeability of wound dressings to O_2/CO_2 exchanges will impact on the cell metabolism, proliferation, and collagen synthesis. Further, the CO_2 accumulation induces the acidification of the wound media, impairing the regeneration of the wound peripherical regions, while favoring the growth of anaerobic bacteria. In this way, an O_2 permeation rate ranging from 456 to 1840 L/m^2 has been often referred as ideal to promote the wound healing [201, 276, 277].

2.8.1.4 Mechanical properties

A wound dressing should be flexible, stable, and confer mechanical support to protect the wound from external threats as well as be compatible with cell adhesion [278]. For that purpose, the wound dressing must present a mechanical behavior similar to that found in native skin, *i.e.* it should display a young modulus under torsion 0.42 to 0.85 MPa, under extension 4.6 to 20 MPa, and 0.05 to 0.15 MPa in suction tests [279].

2.8.1.5 Antimicrobial activity

The colonization of the wound by bacteria can interrupt or delay the healing process and even progress to life-threatening complications [106, 280]. The wound dressing can avoid the bacteria penetration and wound colonization through its structural properties (pore size, wettability, and surface charge) [106, 281, 282] or through the addition of antibacterial agents (*e.g.* AgNPs and antibiotics) [105, 201, 272, 283].

2.8.1.6 Release profile

The properties of wound dressings can be optimized to encapsulate bioactive agents (*e.g.* GFs, antibacterial molecules, and anti-inflammatory agents) as well as to display a specific release profile in order to promote the wound healing [284]. For example, the encapsulation of anti-inflammatory agents aims to ameliorate the inflammatory phase of the wound healing and its release should occur in a controlled fashion during the first 12 h (peak of the inflammatory phase) after the injury occur [241, 242].

2.8.2 Techniques and materials used in the production of asymmetric membranes

Different techniques, such as wet-phase inversion method, dry/wet method, supercritical carbon dioxide ($scCO_2$)-assisted phase inversion technique, electrospinning, and bioprinting have been explored to produce asymmetric membranes (Figure 2.14).

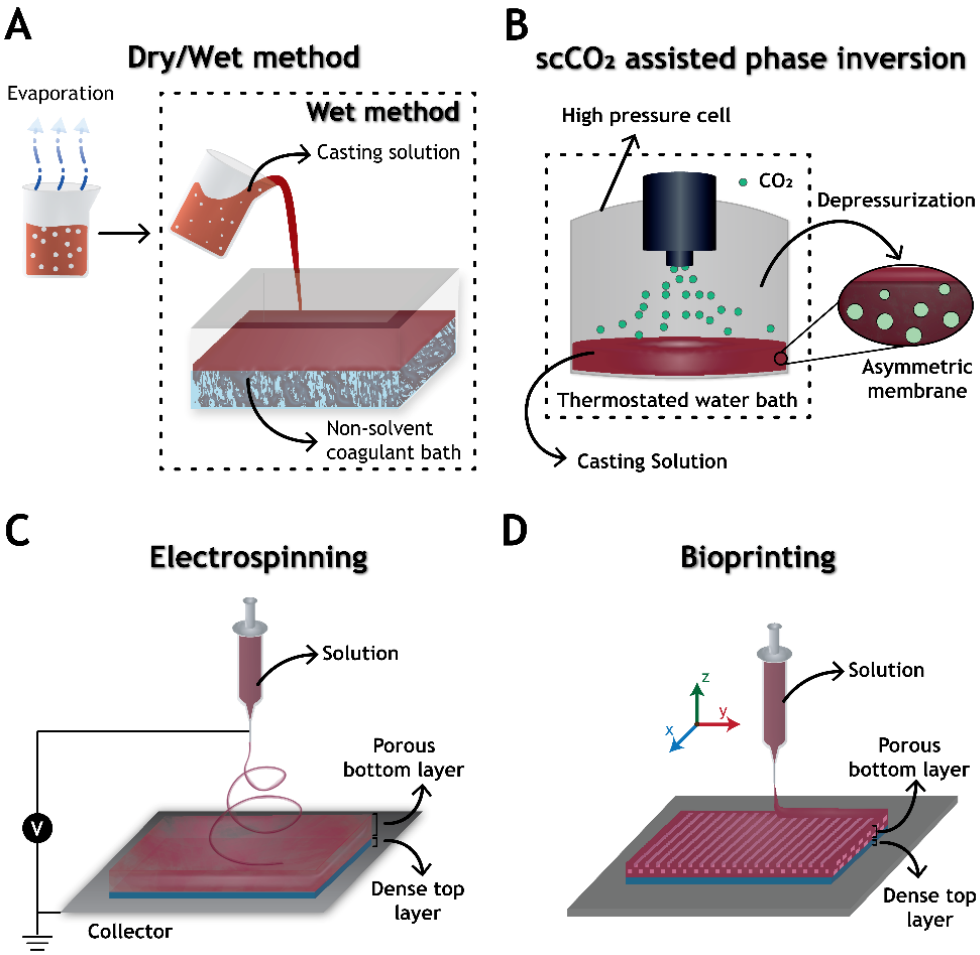

Figure 2.14. Representation of the main techniques used to produce asymmetric membranes: wet and dry/wet method (A), $scCO_2$-assisted phase inversion (B), electrospinning (C), and bioprinting (D).

The wet-phase inversion method (Figure 2.14A) involves the casting polymer immersion in a non-solvent coagulant bath, promoting the polymer precipitation and consequently the membrane formation. In this methodology, the duration of the phase separation process has a direct impact on the production of a porous sub-layer with a compact top layer [274]. However, the produced membrane often presents a thin top layer (with a thickness inferior to 1 μm) and several defects. In turn, the dry/wet-phase inversion (Figure 2.14A) initiates the membrane production with a pre-evaporation process before the polymer immersion into the coagulation bath. Such process increases the density of the polymeric solution and create a denser top layer able to protect the wound against external contamination [201, 285].

$scCO_2$-assisted phase inversion technique (Figure 2.14B) promotes the precipitation of a polymeric solution, under CO_2 supercritical conditions, producing an asymmetric membrane. The $scCO_2$ solubilizes in the casting solution promotes the removal of solvent from the polymeric solution and the membrane production occurs through the polymer precipitation [242, 286]. In this technique, it is possible to tailor the membrane properties (morphology, porosity, mechanical properties, and hydrophilicity) by tuning the processing conditions (*e.g.* casting solution concentration, the polymers ratio and the depressurization rate).

The electrospinning technique (Figure 2.14C) allows the production of interconnected fibrous membranes with structural features that resemble those exhibited by the ECM. During the production process, a polymeric solution is loaded into a syringe and subjected to a high voltage electric field, which promotes the ejection of the polymer towards a collector, originating the nanofibers. Such process is influenced by the properties of the polymeric solution (such as conductivity, surface tension, viscosity, and solvent), processing variables (flow rate, voltage, and distance between the capillary and collector) and environmental conditions (temperature and humidity) [37, 74]. Further, the asymmetric membranes can also be tailored by optimizing the nanofibers deposition (*e.g.* size, density, and orientation) and the materials used [287, 288]. More recently, new production techniques such as bioprinting started to be explored to incorporate skin cells (*e.g.* keratinocytes and fibroblasts) in asymmetric membranes [289, 290]. Bioprinting (Figure 2.14D) enables the simultaneous deposition of biomaterials and multiple cell types, providing flexibility in the design and production of customizable patient-specific tissue-engineered constructs. The bioprinting allows the asymmetric membranes production through the printing of distinctive layers incorporating the respective skin cells (keratinocytes into top layer, and fibroblasts in bottom layer) [291, 292]. The main advantages and disadvantages of asymmetric membranes production techniques are summarized in Table 2.9.

Table 2.9. Advantages and disadvantages of the main techniques used to produce asymmetric membranes.

Production method	Advantages	Disadvantages	Ref.
Wet-phase inversion	-Simple technique.	-The top layer of the asymmetric membrane often displays a reduced thickness (< 1 μm), compromising its protective function; -A limited number of polymers can be used.	[274]
Dry/wet- phase inversion	-The pre-evaporation process before the polymer immersion allows the production of a denser top layer capable to provide protection against external microorganisms.	-The pre-evaporation process requires the use of volatile solvents; -The excess of the toxic residues must be removed through additional treatments; -It is a time-consuming process; -A limited number of polymers can be used.	[201, 285]
scCO_2-phase inversion	-Easy, fast and green technology -The produced membranes are dry and solvent-free; -The membrane properties (morphology, porosity, mechanical properties and hydrophilicity) can be tailored by tuning the processing conditions (like casting solution concentration, the polymers ratio and the depressurization rate; - Several polymers can be used.	-It is required a specialized high-pressure apparatus.	[241, 242, 286, 293]
Electrospinning	-Simple technique; -The produced membranes are dry and solvent-free; -The membrane properties of the membranes can be optimized through controlling the different parameters such as solution concentration, voltage, humidity, temperature and distance to tip from collector; -The asymmetric membrane can be produced by tailoring the nanofibers deposition and materials used; -Several polymers can be used.	-It is required a specialized equipments: DC power supply and syringe pump; -The control of the all processing variables and environmental conditions is highly required.	[105, 265, 272]
Bioprinting	-Reproducible and flexible technique; -It allows the production of customizable patient-specific tissue-engineered constructs; -It is possible to incorporate viable living cells during the production of the membranes.	-It is required a specialized 3D printer that operates under sterile conditions; -Limited number of polymers and solvents can be used.	[289-291, 294]

Besides the production techniques, the raw materials used in the production of the asymmetric membranes has a tremendous impact on their properties. The selection of the polymers reflects on the desired properties and on the role of each layer during the wound healing process. In this way, the dense top layer is idealized to act as a physical barrier that provides protection to the wound site from external damages (*e.g.* physical, chemical, and bacterial agents) and avoids the dehydration of the patient. To accomplish that, the researchers often select synthetic polymers such as PU [264], PCL [106], PVA [241, 242], PLGA [295], since they display excellent mechanical properties, thermal stability, and a suitable degradation profile, hydrophobicity and allow the production of the structures with low porosity. Contrarily, in the bottom layer it is desired the presence of the bioactive polymers capable of interacting with cells, encouraging the cell adhesion and proliferation and simultaneously impair the occurrence of skin infections. For this, natural polymers arise as a viable alternative, since they can exhibit peptide sequences on their surfaces that are recognized by cell surface receptors and, consequently, encourage cell adhesion and proliferation [81]. CS, CA, collagen, AV, and HA are some examples of the natural polymers that have been used in the production of asymmetric membranes [105, 106, 242, 296].

2.9 References

1. Arasteh S, Kazemnejad S, Khanjani S, Heidari-Vala H, Akhondi MM, Mobini S. Fabrication and characterization of nano-fibrous bilayer composite for skin regeneration application. Methods. 2015; 99: 3-12.
2. Clark RA, Ghosh K, Tonnesen MG. Tissue engineering for cutaneous wounds. Journal of Investigative Dermatology. 2007;127(5):1018-29.
3. Metcalfe AD, Ferguson MW. Tissue engineering of replacement skin: the crossroads of biomaterials, wound healing, embryonic development, stem cells and regeneration. Journal of the Royal Society Interface. 2007;4(14):413-37.
4. Brohem CA, da Silva Cardeal LB, Tiago M, Soengas MS, de Moraes Barros SB, Maria-Engler SS. Artificial skin in perspective: concepts and applications. Pigment cell & melanoma research. 2011;24(1):35-50.
5. Gaffal E, Cron M, Glodde N, Bald T, Kuner R, Zimmer A, Lutz B, Tüting T. Cannabinoid 1 receptors in keratinocytes modulate proinflammatory chemokine secretion and attenuate contact allergic inflammation. The Journal of Immunology. 2013;190(10):4929-36.
6. Zhong S, Zhang Y, Lim C. Tissue scaffolds for skin wound healing and dermal reconstruction. Wiley Interdisciplinary Reviews: Nanomedicine and Nanobiotechnology. 2010;2(5):510-25.
7. Böttcher-Haberzeth S, Biedermann T, Reichmann E. Tissue engineering of skin. Burns. 2010;36(4):450-60.
8. Simões D, Miguel SP, Ribeiro MP, Coutinho P, Mendonça AG, Correia IJ. Recent advances on antimicrobial wound dressing: A review. European journal of pharmaceutics and biopharmaceutics. 2018;127:130-41.
9. Agrawal P, Soni S, Mittal G, Bhatnagar A. Role of polymeric biomaterials as wound healing agents. The international journal of lower extremity wounds. 2014:1534734614544523.

10. Rho KS, Jeong L, Lee G, Seo B-M, Park YJ, Hong S-D, Roh S, Cho JJ, Park WH, Min B-M. Electrospinning of collagen nanofibers: effects on the behavior of normal human keratinocytes and early-stage wound healing. Biomaterials. 2006;27(8):1452-61.
11. Boateng JS, Matthews KH, Stevens HN, Eccleston GM. Wound healing dressings and drug delivery systems: a review. Journal of pharmaceutical sciences. 2008;97(8):2892-923.
12. Strecker-McGraw MK, Jones TR, Baer DG. Soft tissue wounds and principles of healing. Emergency medicine clinics of North America. 2007;25(1):1-22.
13. Atiyeh BS, Ioannovich J, Al-Amm CA, El-Musa KA. Management of acute and chronic open wounds: the importance of moist environment in optimal wound healing. Current pharmaceutical biotechnology. 2002;3(3):179-95.
14. Li J, Chen J, Kirsner R. Pathophysiology of acute wound healing. Clinics in dermatology. 2007;25(1):9-18.
15. Sen CK, Gordillo GM, Roy S, Kirsner R, Lambert L, Hunt TK, Gottrup F, Gurtner GC, Longaker MT. Human skin wounds: a major and snowballing threat to public health and the economy. Wound Repair and Regeneration. 2009;17(6):763-71.
16. Tchemtchoua VT, Atanasova G, Aqil A, Filée P, Garbacki N, Vanhooteghem O, Deroanne C, Noël A, Jérome C, Nusgens B. Development of a chitosan nanofibrillar scaffold for skin repair and regeneration. Biomacromolecules. 2011;12(9):3194-204.
17. Boateng J, Catanzano O. Advanced Therapeutic Dressings for Effective Wound Healing—A Review. Journal of pharmaceutical sciences. 2015;104(11):3653-80.
18. Yolanda M-M, Maria A-V, Amaia F-G, Marcos P-B, Silvia PL, Dolores E, Jesús O-H. Adult stem cell therapy in chronic wound healing. J Stem Cell Res Ther. 2014;4(162):2.
19. Schneider A, Wang X, Kaplan D, Garlick J, Egles C. Biofunctionalized electrospun silk mats as a topical bioactive dressing for accelerated wound healing. Acta Biomaterialia. 2009;5(7):2570-8.
20. Mayet N, Choonara YE, Kumar P, Tomar LK, Tyagi C, Du Toit LC, Pillay V. A comprehensive review of advanced biopolymeric wound healing systems. Journal of pharmaceutical sciences. 2014;103(8):2211-30.
21. Beldon P. Basic science of wound healing. Surgery (Oxford). 2010;28(9):409-12.
22. Enoch S, Leaper DJ. Basic science of wound healing. Surgery (Oxford). 2008;26(2):31-7.
23. Moura LI, Dias AM, Carvalho E, de Sousa HC. Recent advances on the development of wound dressings for diabetic foot ulcer treatment—A review. Acta biomaterialia. 2013;9(7):7093-114.
24. Menke NB, Ward KR, Witten TM, Bonchev DG, Diegelmann RF. Impaired wound healing. Clinics in dermatology. 2007;25(1):19-25.
25. Yamaguchi Y, Yoshikawa K. Cutaneous wound healing: an update. The Journal of dermatology. 2001;28(10):521-34.
26. Varghese MC, Balin AK, Carter DM, Caldwell D. Local environment of chronic wounds under synthetic dressings. Archives of dermatology. 1986;122(1):52-7.
27. Alvarez OM, Mertz PM, Eaglstein WH. The effect of occlusive dressings on collagen synthesis and re-epithelialization in superficial wounds. Journal of Surgical Research. 1983;35(2):142-8.
28. Sarabahi S. Recent advances in topical wound care. Indian journal of plastic surgery: official publication of the Association of Plastic Surgeons of India. 2012;45(2):379.
29. MacNeil S. Progress and opportunities for tissue-engineered skin. Nature. 2007;445(7130):874-80.

30. Alrubaiy L, Al-Rubaiy KK. Skin substitutes: a brief review of types and clinical applications. Oman medical journal. 2009;24(1):4.
31. Horch RE, Kopp J, Kneser U, Beier J, Bach AD. Tissue engineering of cultured skin substitutes. Journal of cellular and molecular medicine. 2005;9(3):592-608.
32. Varkey M, Ding J, Tredget EE. Advances in Skin Substitutes—Potential of Tissue Engineered Skin for Facilitating Anti-Fibrotic Healing. Journal of functional biomaterials. 2015;6(3):547-63.
33. Singh A, Shenoy Y. Skin substitutes: an Indian perspective. Indian journal of plastic surgery: official publication of the Association of Plastic Surgeons of India. 2012;45(2):388.
34. Tsao C-T, Leung M, Chang JY-F, Zhang M. A simple material model to generate epidermal and dermal layers in vitro for skin regeneration. Journal of materials chemistry B. 2014;2(32):5256-64.
35. Balasubramani M, Kumar TR, Babu M. Skin substitutes: a review. Burns. 2001;27(5):534-44.
36. Vyas KS, Vasconez HC, editors. Wound healing: biologics, skin substitutes, biomembranes and scaffolds. Healthcare; 2014; 2(3):356-400.
37. Pereira RF, Barrias CC, Granja PL, Bartolo PJ. Advanced biofabrication strategies for skin regeneration and repair. Nanomedicine. 2013;8(4):603-21.
38. Shahrokhi S, Arno A, Jeschke MG. The use of dermal substitutes in burn surgery: acute phase. Wound Repair and Regeneration. 2014;22(1):14-22.
39. Gallico III GG, O'Connor NE, Compton CC, Kehinde O, Green H. Permanent coverage of large burn wounds with autologous cultured human epithelium. New England Journal of Medicine. 1984;311(7):448-51.
40. Vacher D, Autologous epidermal sheets production for skin cellular therapy. Annales pharmaceutiques françaises; 2003;61(3):203-6.
41. Moustafa M, Simpson C, Glover M, Dawson R, Tesfaye S, Creagh F, Haddow D, Short R, Heller S, MacNeil S. A new autologous keratinocyte dressing treatment for non-healing diabetic neuropathic foot ulcers. Diabetic medicine. 2004;21(7):786-9.
42. Navarro F, Stoner M, Park C, Huertas J, Lee H, Wood F, Orgill D. Sprayed keratinocyte suspensions accelerate epidermal coverage in a porcine microwound model. Journal of Burn Care & Research. 2000;21(6):513&hyhen.
43. Tausche AK, Skaria M, Böhlen L, Liebold K, Hafner J, Friedlein H, Meurer M, Goedkoop RJ, Wollina U, Salomon D. An autologous epidermal equivalent tissue-engineered from follicular outer root sheath keratinocytes is as effective as split-thickness skin autograft in recalcitrant vascular leg ulcers. Wound repair and regeneration. 2003;11(4):248-52.
44. Ramos-e-Silva M, Ribeiro de Castro MC. New dressings, including tissue-engineered living skin. Clinics in dermatology. 2002;20(6):715-23.
45. Johnsen, Ermuth, Tanczos, Bannasch, Horch, Zschocke, Peschen, Schöpf, Vanscheidt, Augustin. Treatment of therapy-refractive ulcera cruris of various origins with autologous keratinocytes in fibrin sealant. Vasa. 2005;34(1):25-9.
46. Tsai C, Lin S, Lai C, Lin T. The use of composite acellular allodermis-ultrathin autograft on joint area in major burn patients--one year follow-up. The Kaohsiung journal of medical sciences. 1999;15(11):651-8.
47. van Zuijlen PP, van Trier AJ, Vloemans JF, Groenevelt F, Kreis RW, Middelkoop E. Graft survival and effectiveness of dermal substitution in burns and reconstructive surgery in a one-stage grafting model. Plastic and reconstructive surgery. 2000;106(3):615-23.

48. Lawin PB, Silverstein P, Still Jr JM. EZ DERM™ A Porcine Heterograft Material. American journal of clinical dermatology. 2002;3(7):507-.

49. Yannas I, Burke JF. Design of an artificial skin. I. Basic design principles. Journal of biomedical materials research. 1980;14(1):65-81.

50. Whitaker IS, Prowse S, Potokar TS. A critical evaluation of the use of Biobrane as a biologic skin substitute: a versatile tool for the plastic and reconstructive surgeon. Annals of plastic surgery. 2008;60(3):333-7.

51. Noordenbos J, Doré C, Hansbrough JF. Safety and Efficacy of TransCyte* for the Treatment of Partial-Thickness Burns. Journal of Burn Care & Research. 1999;20(4):275-81.

52. Kim P, Dybowski K, Steinberg J. A closer look at bioengineered alternative tissues. Podiatry Today. 2006;19(7):38-55.

53. Caravaggi C, De Giglio R, Pritelli C, Sommaria M, Dalla Noce S, Faglia E, Mantero M, Clerici G, Fratino P, Dalla Paola L. HYAFF 11-based autologous dermal and epidermal grafts in the treatment of noninfected diabetic plantar and dorsal foot ulcers a prospective, multicenter, controlled, randomized clinical trial. Diabetes Care. 2003;26(10):2853-9.

54. Shevchenko RV, James SL, James SE. A review of tissue-engineered skin bioconstructs available for skin reconstruction. Journal of the Royal Society Interface. 2010;7(43):229-58.

55. Eaglstein WH, Alvarez OM, Auletta M, Leffel D, Rogers GS, Zitelli JA, Norris JE, Thomas I, Irondo M, Fewkes J. Acute Excisional Wounds Treated with a Tissue-Engineered Skin (Apligraf). Dermatologic surgery. 1999;25(3):195-201.

56. Still J, Glat P, Silverstein P, Griswold J, Mozingo D. The use of a collagen sponge/living cell composite material to treat donor sites in burn patients. Burns. 2003;29(8):837-41.

57. Uccioli L. A clinical investigation on the characteristics and outcomes of treating chronic lower extremity wounds using the tissuetech autograft system. The international journal of lower extremity wounds. 2003;2(3):140-51.

58. Jayaraman K, Kotaki M, Zhang Y, Mo X, Ramakrishna S. Recent advances in polymer nanofibers. Journal of Nanoscience and Nanotechnology. 2004;4(1-2):52-65.

59. Braghirolli DI, Steffens D, Pranke P. Electrospinning for regenerative medicine: a review of the main topics. Drug discovery today. 2014;19(6):743-53.

60. Bhardwaj N, Kundu SC. Electrospinning: a fascinating fiber fabrication technique. Biotechnology advances. 2010;28(3):325-47.

61. Huang Z-M, Zhang Y-Z, Kotaki M, Ramakrishna S. A review on polymer nanofibers by electrospinning and their applications in nanocomposites. Composites science and technology. 2003;63(15):2223-53.

62. Kumbar S, James R, Nukavarapu S, Laurencin C. Electrospun nanofiber scaffolds: engineering soft tissues. Biomedical Materials. 2008;3(3):034002.

63. Norouzi M, Shabani I, Ahvaz HH, Soleimani M. PLGA/gelatin hybrid nanofibrous scaffolds encapsulating EGF for skin regeneration. Journal of biomedical materials research Part A. 2015;103(7):2225-35.

64. Sood A, Granick MS, Tomaselli NL. Wound dressings and comparative effectiveness data. Advances in wound care. 2014;3(8):511-29.

65. Ma Z, Kotaki M, Inai R, Ramakrishna S. Potential of nanofiber matrix as tissue-engineering scaffolds. Tissue engineering. 2005;11(1-2):101-9.

66. Vasita R, Katti DS. Nanofibers and their applications in tissue engineering. International Journal of nanomedicine. 2006;1(1):15.
67. Min B-M, Lee G, Kim SH, Nam YS, Lee TS, Park WH. Electrospinning of silk fibroin nanofibers and its effect on the adhesion and spreading of normal human keratinocytes and fibroblasts in vitro. Biomaterials. 2004;25(7):1289-97.
68. Yang Y, Xia T, Zhi W, Wei L, Weng J, Zhang C, Li X. Promotion of skin regeneration in diabetic rats by electrospun core-sheath fibers loaded with basic fibroblast growth factor. Biomaterials. 2011;32(18):4243-54.
69. Abrigo M, McArthur SL, Kingshott P. Electrospun nanofibers as dressings for chronic wound care: advances, challenges, and future prospects. Macromolecular Bioscience. 2014;14(6):772-92.
70. Zahedi P, Rezaeian I, Ranaei-Siadat SO, Jafari SH, Supaphol P. A review on wound dressings with an emphasis on electrospun nanofibrous polymeric bandages. Polymers for Advanced Technologies. 2010;21(2):77-95.
71. Peršin Z, Ravber M, Stana Kleinschek K, Knez Ž, Škerget M, Kurečič M. Bio-nanofibrous mats as potential delivering systems of natural substances. Textile Research Journal. 2017;87(4):444-59.
72. Hassiba AJ, El Zowalaty ME, Nasrallah GK, Webster TJ, Luyt AS, Abdullah AM, Elzatahry AA. Review of recent research on biomedical applications of electrospun polymer nanofibers for improved wound healing. Nanomedicine. 2016;11(6):715-37.
73. Ray SS, Chen S-S, Li C-W, Nguyen NC, Nguyen HT. A comprehensive review: electrospinning technique for fabrication and surface modification of membranes for water treatment application. RSC Advances. 2016;6(88):85495-514.
74. Sundaramurthi D, Krishnan UM, Sethuraman S. Electrospun nanofibers as scaffolds for skin tissue engineering. Polymer Reviews. 2014;54(2):348-76.
75. Pan H, Li L, Hu L, Cui X. Continuous aligned polymer fibers produced by a modified electrospinning method. Polymer. 2006;47(14):4901-4.
76. Pham QP, Sharma U, Mikos AG. Electrospinning of polymeric nanofibers for tissue engineering applications: a review. Tissue engineering. 2006;12(5):1197-211.
77. Sill TJ, von Recum HA. Electrospinning: applications in drug delivery and tissue engineering. Biomaterials. 2008;29(13):1989-2006.
78. Khil MS, Cha DI, Kim HY, Kim IS, Bhattarai N. Electrospun nanofibrous polyurethane membrane as wound dressing. Journal of Biomedical Materials Research Part B: Applied Biomaterials. 2003;67(2):675-9.
79. Kumbar SG, Nukavarapu SP, James R, Nair LS, Laurencin CT. Electrospun poly (lactic acid-co-glycolic acid) scaffolds for skin tissue engineering. Biomaterials. 2008;29(30):4100-7.
80. Tallawi M, Rosellini E, Barbani N, Cascone MG, Rai R, Saint-Pierre G, Boccaccini AR. Strategies for the chemical and biological functionalization of scaffolds for cardiac tissue engineering: a review. Journal of the Royal Society Interface. 2015;12(108):20150254.
81. Mele E. Electrospinning of natural polymers for advanced wound care: towards responsive and adaptive dressings. Journal of Materials Chemistry B. 2016;4(28):4801-12.
82. Ju HW, Lee OJ, Lee JM, Moon BM, Park HJ, Park YR, Lee MC, Kim SH, Chao JR, Ki CS. Wound healing effect of electrospun silk fibroin nanomatrix in burn-model. International journal of biological macromolecules. 2016;85:29-39.

83. Lin J, Li C, Zhao Y, Hu J, Zhang L-M. Co-electrospun nanofibrous membranes of collagen and zein for wound healing. ACS applied materials & interfaces. 2012;4(2):1050-7.
84. Mano J, Silva G, Azevedo HS, Malafaya P, Sousa R, Silva S, Boesel L, Oliveira JM, Santos T, Marques A. Natural origin biodegradable systems in tissue engineering and regenerative medicine: present status and some moving trends. Journal of the Royal Society Interface. 2007;4(17):999-1030.
85. Sionkowska A. Interaction of collagen and poly (vinyl pyrrolidone) in blends. European Polymer Journal. 2003;39(11):2135-40.
86. Marsano E, Vicini S, Skopiǹska J, Wisniewski M, Sionkowska A, editors. Chitosan and poly (vinyl pyrrolidone): compatibility and miscibility of blends. Macromolecular Symposia; 2004: Wiley Online Library.
87. Piza M, Constantino C, Venancio E, Mattoso L. Interaction mechanism of poly (o-ethoxyaniline) and collagen blends. Polymer. 2003;44(19):5663-70.
88. Venugopal JR, Zhang Y, Ramakrishna S. In vitro culture of human dermal fibroblasts on electrospun polycaprolactone collagen nanofibrous membrane. Artificial organs. 2006;30(6):440-6.
89. Duan H, Feng B, Guo X, Wang J, Zhao L, Zhou G, Liu W, Cao Y, Zhang WJ. Engineering of epidermis skin grafts using electrospun nanofibrous gelatin/polycaprolactone membranes. Int J Nanomedicine. 2013;8:2077-84.
90. Zhou Y, Yang D, Chen X, Xu Q, Lu F, Nie J. Electrospun water-soluble carboxyethyl chitosan/poly (vinyl alcohol) nanofibrous membrane as potential wound dressing for skin regeneration. Biomacromolecules. 2007;9(1):349-54.
91. Gu S-Y, Wang Z-M, Ren J, Zhang C-Y. Electrospinning of gelatin and gelatin/poly (l-lactide) blend and its characteristics for wound dressing. Materials Science and Engineering: C. 2009;29(6):1822-8.
92. Liu S-J, Kau Y-C, Chou C-Y, Chen J-K, Wu R-C, Yeh W-L. Electrospun PLGA/collagen nanofibrous membrane as early-stage wound dressing. Journal of Membrane Science. 2010;355(1):53-9.
93. Suganya S, Venugopal J, Ramakrishna S, Lakshmi B, Dev VG. Naturally derived biofunctional nanofibrous scaffold for skin tissue regeneration. International journal of biological macromolecules. 2014;68:135-43.
94. Kataphinan W, Dabney S, Reneker D, Smith D, Akron U, inventors. Electrospun Skin masks and uses thereof patent WO2001026610 A1. 2001.
95. Smith DJ, Reneker DH, McManus AT, Schreuder-Gibson HL, Mello C, Sennett MS, inventors; Google Patents, assignee. Electrospun fibers and an apparatus therefor patent US6753454B1. 2004.
96. Yarin AL, Sett S, Lee M, Sinha-Ray S, inventors; Google Patents, assignee. Biodegradable plant wound dressing composed of electrospun nanofibers patent US20160219874A1. 2016.
97. Antunes B, Moreira A, Gaspar V, Correia I. Chitosan/arginine–chitosan polymer blends for assembly of nanofibrous membranes for wound regeneration. Carbohydrate polymers. 2015;130:104-12.
98. Cai Z-x, Mo X-m, Zhang K-h, Fan L-p, Yin A-l, He C-l, Wang H-s. Fabrication of chitosan/silk fibroin composite nanofibers for wound-dressing applications. International journal of molecular sciences. 2010;11(9):3529-39.

99. Charernsriwilaiwat N, Rojanarata T, Ngawhirunpat T, Opanasopit P. Electrospun chitosan/polyvinyl alcohol nanofibre mats for wound healing. International wound journal. 2014;11(2):215-22.
100. Kim SE, Heo DN, Lee JB, Kim JR, Park SH, Jeon SH, Kwon IK. Electrospun gelatin/polyurethane blended nanofibers for wound healing. Biomedical Materials. 2009;4(4):044106.
101. Li L, Qian Y, Jiang C, Lv Y, Liu W, Zhong L, Cai K, Li S, Yang L. The use of hyaluronan to regulate protein adsorption and cell infiltration in nanofibrous scaffolds. Biomaterials. 2012;33(12):3428-45.
102. Lee JM, Chae T, Sheikh FA, Ju HW, Moon BM, Park HJ, Park YR, Park CH. Three dimensional poly (ε-caprolactone) and silk fibroin nanocomposite fibrous matrix for artificial dermis. Materials Science and Engineering: C. 2016;68:758-67.
103. Zhang Y, Venugopal J, Huang Z-M, Lim C, Ramakrishna S. Characterization of the surface biocompatibility of the electrospun PCL-collagen nanofibers using fibroblasts. Biomacromolecules. 2005;6(5):2583-9.
104. Augustine R, Malik HN, Singhal DK, Mukherjee A, Malakar D, Kalarikkal N, Thomas S. Electrospun polycaprolactone/ZnO nanocomposite membranes as biomaterials with antibacterial and cell adhesion properties. Journal of Polymer Research. 2014;21(3):1-17.
105. Figueira DR, Miguel SP, de Sá KD, Correia IJ. Production and characterization of polycaprolactone-hyaluronic acid/chitosan-zein electrospun bilayer nanofibrous membrane for tissue regeneration. International journal of biological macromolecules. 2016;93:1100-10.
106. Miguel SP, Ribeiro MP, Coutinho P, Correia IJ. Electrospun Polycaprolactone/aloe Vera_Chitosan Nanofibrous asymmetric membranes aimed for wound healing applications. Polymers. 2017;9(5):183.
107. Lu Y, Li X, Zhou X, Wang Q, Shi X, Du Y, Deng H, Jiang L. Characterization and cytotoxicity study of nanofibrous mats incorporating rectorite and carbon nanotubes. RSC Advances. 2014;4(63):33355-61.
108. Hilal N, Khayet M, Wright CJ. Membrane modification: Technology and applications: CRC press; 2012.
109. Yoo HS, Kim TG, Park TG. Surface-functionalized electrospun nanofibers for tissue engineering and drug delivery. Advanced drug delivery reviews. 2009;61(12):1033-42.
110. Croll TI, O'Connor AJ, Stevens GW, Cooper-White JJ. Controllable surface modification of poly (lactic-co-glycolic acid)(PLGA) by hydrolysis or aminolysis I: physical, chemical, and theoretical aspects. Biomacromolecules. 2004;5(2):463-73.
111. Khorsand-Ghayeni M, Sadeghi A, Nokhasteh S, Molavi A, editors. Collagen modified PLGA nanofibers as wound-dressing. The International Conference on Nanostructures; 2016.
112. Grace JM, Gerenser LJ. Plasma treatment of polymers. Journal of dispersion science and technology. 2003;24(3-4):305-41.
113. Yoshida S, Hagiwara K, Hasebe T, Hotta A. Surface modification of polymers by plasma treatments for the enhancement of biocompatibility and controlled drug release. Surface and Coatings Technology. 2013;233:99-107.
114. Jeong L, Yeo I-S, Kim HN, Yoon YI, Jang DH, Jung SY, Min B-M, Park WH. Plasma-treated silk fibroin nanofibers for skin regeneration. International Journal of Biological Macromolecules. 2009;44(3):222-8.

115. Xu Z, Wan L, Huang X. Surface Modification by Graft Polymerization. Surface Engineering of Polymer Membranes. 2009:80-149.
116. Gautam S, Chou C-F, Dinda AK, Potdar PD, Mishra NC. Surface modification of nanofibrous polycaprolactone/gelatin composite scaffold by collagen type I grafting for skin tissue engineering. Materials Science and Engineering: C. 2014;34:402-9.
117. Burtovyy O, Klep V, Turel T, Gowayed Y, Luzinov I. Polymeric Membranes: Surface Modification by" Grafting to" Method and Fabrication of Multilayered Assemblies. ACS Publications; 2009. ACS Symposium Series;Vol. 1016.
118. Park H, Cannizzaro C, Vunjak-Novakovic G, Langer R, Vacanti CA, Farokhzad OC. Nanofabrication and microfabrication of functional materials for tissue engineering. Tissue engineering. 2007;13(8):1867-77.
119. Chen S, Liu B, Carlson MA, Gombart AF, Reilly DA, Xie J. Recent advances in electrospun nanofibers for wound healing. Nanomedicine. 2017;12(11):1335-52.
120. Song F, Li X, Wang Q, Liao L, Zhang C. Nanocomposite hydrogels and their applications in drug delivery and tissue engineering. Journal of biomedical nanotechnology. 2015;11(1):40-52.
121. Ding Y, Li W, Zhang F, Liu Z, Zanjanizadeh Ezazi N, Liu D, Santos HA. Electrospun Fibrous Architectures for Drug Delivery, Tissue Engineering and Cancer Therapy. Advanced functional materials. 2018; 29(2):1802852.
122. Hu X, Liu S, Zhou G, Huang Y, Xie Z, Jing X. Electrospinning of polymeric nanofibers for drug delivery applications. Journal of controlled release. 2014;185:12-21.
123. Balaji A, Vellayappan M, John A, Subramanian A, Jaganathan S, Supriyanto E, Razak S. An insight on electrospun-nanofibers-inspired modern drug delivery system in the treatment of deadly cancers. RSC advances. 2015;5(71):57984-8004.
124. Im JS, Yun J, Lim Y-M, Kim H-I, Lee Y-S. Fluorination of electrospun hydrogel fibers for a controlled release drug delivery system. Acta biomaterialia. 2010;6(1):102-9.
125. Saraf A, Baggett LS, Raphael RM, Kasper FK, Mikos AG. Regulated non-viral gene delivery from coaxial electrospun fiber mesh scaffolds. Journal of Controlled Release. 2010;143(1):95-103.
126. Zamani M, Prabhakaran MP, Ramakrishna S. Advances in drug delivery via electrospun and electrosprayed nanomaterials. International journal of nanomedicine. 2013;8:2997.
127. Chou S-F, Carson D, Woodrow KA. Current strategies for sustaining drug release from electrospun nanofibers. Journal of Controlled Release. 2015;220:584-91.
128. Grassi M, Grassi G. Mathematical modelling and controlled drug delivery: matrix systems. Current drug delivery. 2005;2(1):97-116.
129. Ji W, Sun Y, Yang F, van den Beucken JJ, Fan M, Chen Z, Jansen JA. Bioactive electrospun scaffolds delivering growth factors and genes for tissue engineering applications. Pharmaceutical research. 2011;28(6):1259-72.
130. Manuel CBJ, Jesús VGL, Aracely SM. Electrospinning for Drug Delivery Systems: Drug Incorporation Techniques. Electrospinning-Material, Techniques, and Biomedical Applications: InTech; 2016.
131. Kim P-H, Cho J-Y. Myocardial tissue engineering using electrospun nanofiber composites. BMB reports. 2016;49(1):26.
132. Li W, Li X, Chen Y, Li X, Deng H, Wang T, Huang R, Fan G. Poly (vinyl alcohol)/sodium alginate/layered silicate based nanofibrous mats for bacterial inhibition. Carbohydrate polymers. 2013;92(2):2232-8.

133. Chouhan D, Chakraborty B, Nandi SK, Mandal BB. Role of non-mulberry silk fibroin in deposition and regulation of extracellular matrix towards accelerated wound healing. Acta biomaterialia. 2017;48:157-74.
134. Jiang Y-N, Mo H-Y, Yu D-G. Electrospun drug-loaded core–sheath PVP/zein nanofibers for biphasic drug release. International journal of pharmaceutics. 2012;438(1):232-9.
135. Liao I, Chew S, Leong K. Aligned core-shell nanofibers delivering bioactive proteins. Nanomedicine. 2006;1(4):465-71.
136. Maleki M, Latifi M, Amani-Tehran M, Mathur S. Electrospun core–shell nanofibers for drug encapsulation and sustained release. Polymer Engineering & Science. 2013;53(8):1770-9.
137. McClellan P, Landis WJ. Recent applications of coaxial and emulsion electrospinning methods in the field of tissue engineering. BioResearch open access. 2016;5(1):212-27.
138. Wang Z, Qian Y, Li L, Pan L, Njunge LW, Dong L, Yang L. Evaluation of emulsion electrospun polycaprolactone/hyaluronan/epidermal growth factor nanofibrous scaffolds for wound healing. Journal of biomaterials applications. 2016;30(6):686-98.
139. Vladkova TG. Surface engineered polymeric biomaterials with improved biocontact properties. International Journal of polymer science. 2010;2010.
140. Bellmann C. Surface modification by adsorption of polymers and surfactants. Polymer Surfaces and Interfaces: Springer; 2008. p. 235-59.
141. Casper CL, Yamaguchi N, Kiick KL, Rabolt JF. Functionalizing electrospun fibers with biologically relevant macromolecules. Biomacromolecules. 2005;6(4):1998-2007.
142. Richardson JJ, Björnmalm M, Caruso F. Technology-driven layer-by-layer assembly of nanofilms. Science. 2015;348(6233):aaa2491.
143. Shi Q, Qian Z, Liu D, Liu H. Surface Modification of Dental Titanium Implant by Layer-by-Layer Electrostatic Self-Assembly. Frontiers in physiology. 2017;8:574.
144. Huang W, Li X, Xue Y, Huang R, Deng H, Ma Z. Antibacterial multilayer films fabricated by LBL immobilizing lysozyme and HTCC on nanofibrous mats. International journal of biological macromolecules. 2013;53:26-31.
145. Xin S, Li X, Wang Q, Huang R, Xu X, Lei Z, Deng H. Novel layer-by-layer structured nanofibrous mats coated by protein films for dermal regeneration. Journal of biomedical nanotechnology. 2014;10(5):803-10.
146. Huang R, Li W, Lv X, Lei Z, Bian Y, Deng H, Wang H, Li J, Li X. Biomimetic LBL structured nanofibrous matrices assembled by chitosan/collagen for promoting wound healing. Biomaterials. 2015;53:58-75.
147. Choi JS, Leong KW, Yoo HS. In vivo wound healing of diabetic ulcers using electrospun nanofibers immobilized with human epidermal growth factor (EGF). Biomaterials. 2008;29(5):587-96.
148. Han G, Ceilley R. Chronic wound healing: a review of current management and treatments. Advances in therapy. 2017;34(3):599-610.
149. Siddiqui AR, Bernstein JM. Chronic wound infection: facts and controversies. Clinics in dermatology. 2010;28(5):519-26.
150. Dhand C, Venkatesh M, Barathi VA, Harini S, Bairagi S, Leng EGT, Muruganandham N, Low KZW, Fazil MHUT, Loh XJ. Bio-inspired crosslinking and matrix-drug interactions for advanced wound dressings with long-term antimicrobial activity. Biomaterials. 2017;138:153-68.

151. Yazdanbakhsh M, Rashidi A, Rahimi M, Khajavi R, Shafaroodi H. The Effect of Impregnated Alpha-Cellulose Nanofibers with Ciprofloxacin Hydrochloride on Staphylococcus aureus In Vitro and Healing Process of Wound in Rat. Regenerative engineering and translational medicine. 2018;4(4):247-56.
152. Ceylan M, Yang S-Y, Asmatulu R. Effects of gentamicin-loaded PCL nanofibers on growth of Gram positive and Gram negative bacteria. International journal of applied microbiology and biotechnology research. 2017;5(5):40-51.
153. Alavarse AC, de Oliveira Silva FW, Colque JT, da Silva VM, Prieto T, Venancio EC, Bonvent J-J. Tetracycline hydrochloride-loaded electrospun nanofibers mats based on PVA and chitosan for wound dressing. Materials science and engineering: C. 2017;77:271-81.
154. Semnani D, Poursharifi N, Banitaba N, Fakhrali A. Electrospun polyvinylidene pyrolidone/gelatin membrane impregnated with silver sulfadiazine as wound dressing for burn treatment. Bulletin of materials science. 2018;41(3):72.
155. Torres-Giner S, Martinez-Abad A, Gimeno-Alcañiz JV, Ocio MJ, Lagaron JM. Controlled delivery of gentamicin antibiotic from bioactive electrospun polylactide-based ultrathin fibers. Advanced engineering materials. 2012;14(4):B112-B22.
156. Hu J, Kai D, Ye H, Tian L, Ding X, Ramakrishna S, Loh XJ. Electrospinning of poly (glycerol sebacate)-based nanofibers for nerve tissue engineering. Materials Science and Engineering: C. 2017;70:1089-94.
157. Mohseni M, Shamloo A, Aghababaei Z, Vossoughi M, Moravvej H. Antimicrobial wound dressing containing silver sulfadiazine with high biocompatibility: in vitro study. Artificial organs. 2016;40(8):765-73.
158. Ranghar S, Sirohi P, Verma P, Agarwal V. Nanoparticle-based drug delivery systems: promising approaches against infections. Brazilian archives of biology and technology. 2014;57(2):209-22.
159. Alhusein N, Blagbrough IS, Beeton ML, Bolhuis A, Paul A. Electrospun zein/PCL fibrous matrices release tetracycline in a controlled manner, killing Staphylococcus aureus both in biofilms and ex vivo on pig skin, and are compatible with human skin cells. Pharmaceutical research. 2016;33(1):237-46.
160. Monteiro N, Martins M, Martins A, Fonseca NA, Moreira JN, Reis RL, Neves NM. Antibacterial activity of chitosan nanofiber meshes with liposomes immobilized releasing gentamicin. Acta biomaterialia. 2015;18:196-205.
161. Liu X, Nielsen LH, Kłodzińska SN, Nielsen HM, Qu H, Christensen LP, Rantanen J, Yang M. Ciprofloxacin-loaded sodium alginate/poly (lactic-co-glycolic acid) electrospun fibrous mats for wound healing. European journal of pharmaceutics and biopharmaceutics. 2018;123:42-9.
162. Wilkinson L, White R, Chipman J. Silver and nanoparticles of silver in wound dressings: a review of efficacy and safety. Journal of wound care. 2011;20(11):543-9.
163. Preem L, Kogermann K. Electrospun Antimicrobial Wound Dressings: Novel Strategies to Fight Against Wound Infections. In: Springer C, editor. Recent Clinical Techniques, Results, and Research in Wounds. 2018.
164. Song J, Birbach NL, Hinestroza JP. Deposition of silver nanoparticles on cellulosic fibers via stabilization of carboxymethyl groups. Cellulose. 2012;19(2):411-24.

165. Tian J, Wong KK, Ho CM, Lok CN, Yu WY, Che CM, Chiu JF, Tam PK. Topical delivery of silver nanoparticles promotes wound healing. ChemMedChem: Chemistry Enabling Drug Discovery. 2007;2(1):129-36.
166. Dakal TC, Kumar A, Majumdar RS, Yadav V. Mechanistic basis of antimicrobial actions of silver nanoparticles. Frontiers in microbiology. 2016;7:1831.
167. Zhang S, Tang Y, Vlahovic B. A review on preparation and applications of silver-containing nanofibers. Nanoscale research letters. 2016;11(1):80.
168. Aadil KR, Mussatto SI, Jha H. Synthesis and characterization of silver nanoparticles loaded poly (vinyl alcohol)-lignin electrospun nanofibers and their antimicrobial activity. International journal of biological macromolecules. 2018;120:763-7.
169. Aadil KR, Prajapati D, Jha H. Improvement of physcio-chemical and functional properties of alginate film by Acacia lignin. Food packaging and shelf life. 2016;10:25-33.
170. Dong H, Wang D, Sun G, Hinestroza JP. Assembly of metal nanoparticles on electrospun nylon 6 nanofibers by control of interfacial hydrogen-bonding interactions. Chemistry of materials. 2008;20(21):6627-32.
171. Santos FG, Bonkovoski LC, Garcia FP, Cellet TS, Witt MA, Nakamura CV, Rubira AF, Muniz EC. Antibacterial Performance of a PCL–PDMAEMA Blend Nanofiber-Based Scaffold Enhanced with Immobilized Silver Nanoparticles. ACS applied materials & interfaces. 2017;9(11):9304-14.
172. Lee SJ, Heo DN, Moon J-H, Ko W-K, Lee JB, Bae MS, Park SW, Kim JE, Lee DH, Kim E-C. Electrospun chitosan nanofibers with controlled levels of silver nanoparticles. Preparation, characterization and antibacterial activity. Carbohydrate polymers. 2014;111:530-7.
173. Akter M, Sikder MT, Rahman MM, Ullah AA, Hossain KFB, Banik S, Hosokawa T, Saito T, Kurasaki M. A systematic review on silver nanoparticles-induced cytotoxicity: Physicochemical properties and perspectives. Journal of advanced research. 2017;9:1-16.
174. Tak YK, Pal S, Naoghare PK, Rangasamy S, Song JM. Shape-dependent skin penetration of silver nanoparticles: does it really matter? Scientific reports. 2015;5:16908.
175. Filon FL, Bello D, Cherrie JW, Sleeuwenhoek A, Spaan S, Brouwer DH. Occupational dermal exposure to nanoparticles and nano-enabled products: Part I—Factors affecting skin absorption. International journal of hygiene and environmental health. 2016;219(6):536-44.
176. Wang M, Lai X, Shao L, Li L. Evaluation of immunoresponses and cytotoxicity from skin exposure to metallic nanoparticles. International journal of nanomedicine. 2018;13:4445.
177. Sufian MM, Khattak JZK, Yousaf S, Rana MS. Safety issues associated with the use of nanoparticles in human body. Photodiagnosis and photodynamic therapy. 2017;19:67-72.
178. Ge W, Zhao Y, Lai F-N, Liu J-C, Sun Y-C, Wang J-J, Cheng S-F, Zhang X-F, Sun L-L, Li L. Cutaneous applied nano-ZnO reduce the ability of hair follicle stem cells to differentiate. Nanotoxicology. 2017;11(4):465-74.
179. Sharma V, Singh SK, Anderson D, Tobin DJ, Dhawan A. Zinc oxide nanoparticle induced genotoxicity in primary human epidermal keratinocytes. Journal of nanoscience and nanotechnology. 2011;11(5):3782-8.
180. Rath G, Hussain T, Chauhan G, Garg T, Goyal AK. Collagen nanofiber containing silver nanoparticles for improved wound-healing applications. Journal of drug targeting. 2016;24(6):520-9.

181. Liu Y, Liu Y, Liao N, Cui F, Park M, Kim H-Y. Fabrication and durable antibacterial properties of electrospun chitosan nanofibers with silver nanoparticles. International journal of biological macromolecules. 2015;79:638-43.
182. Li C, Fu R, Yu C, Li Z, Guan H, Hu D, Zhao D, Lu L. Silver nanoparticle/chitosan oligosaccharide/poly (vinyl alcohol) nanofibers as wound dressings: a preclinical study. International journal of nanomedicine. 2013;8:4131.
183. Wang X, Cheng F, Gao J, Wang L. Antibacterial wound dressing from chitosan/polyethylene oxide nanofibers mats embedded with silver nanoparticles. Journal of biomaterials applications. 2015;29(8):1086-95.
184. Burt S. Essential oils: their antibacterial properties and potential applications in foods—a review. International journal of food microbiology. 2004;94(3):223-53.
185. Brochot A, Guilbot A, Haddioui L, Roques C. Antibacterial, antifungal, and antiviral effects of three essential oil blends. MicrobiologyOpen. 2017;6(4):e00459.
186. Bachir RG, Benali M. Antibacterial activity of the essential oils from the leaves of Eucalyptus globulus against Escherichia coli and Staphylococcus aureus. Asian pacific journal of tropical biomedicine. 2012;2(9):739-42.
187. Liu Q, Meng X, Li Y, Zhao C-N, Tang G-Y, Li H-B. Antibacterial and antifungal activities of spices. International journal of molecular sciences. 2017;18(6):1283.
188. Chouhan S, Sharma K, Guleria S. Antimicrobial activity of some essential oils—present status and future perspectives. Medicines. 2017;4(3):58.
189. Akthar MS, Degaga B, Azam T. Antimicrobial activity of essential oils extracted from medicinal plants against the pathogenic microorganisms: a review. Journal Issues ISSN. 2014;2350:1588.
190. Koroch AR, Juliani HR, Zygadlo JA. Bioactivity of essential oils and their components. Flavours and fragrances: Springer; 2007. p. 87-115.
191. Bajpai VK, Sharma A, Baek K-H. Antibacterial mode of action of Cudrania tricuspidata fruit essential oil, affecting membrane permeability and surface characteristics of food-borne pathogens. Food control. 2013;32(2):582-90.
192. Lv F, Liang H, Yuan Q, Li C. In vitro antimicrobial effects and mechanism of action of selected plant essential oil combinations against four food-related microorganisms. Food research international. 2011;44(9):3057-64.
193. Liakos I, Rizzello L, Hajiali H, Brunetti V, Carzino R, Pompa P, Athanassiou A, Mele E. Fibrous wound dressings encapsulating essential oils as natural antimicrobial agents. Journal of materials chemistry B. 2015;3(8):1583-9.
194. Banskota AH, Tezuka Y, Kadota S. Recent progress in pharmacological research of propolis. Phytotherapy research. 2001;15(7):561-71.
195. Kim JI, Pant HR, Sim H-J, Lee KM, Kim CS. Electrospun propolis/polyurethane composite nanofibers for biomedical applications. Materials science and engineering: C. 2014;44:52-7.
196. Croisier F, Sibret P, Dupont-Gillain CC, Genet MJ, Detrembleur C, Jérôme C. Chitosan-coated electrospun nanofibers with antibacterial activity. Journal of materials chemistry B. 2015;3(17):3508-17.
197. Miguel SP, Ribeiro MP, Brancal H, Coutinho P, Correia IJ. Thermoresponsive chitosan–agarose hydrogel for skin regeneration. Carbohydrate polymers. 2014;111:366-73.

198. Garcia-Orue I, Gainza G, Gutierrez FB, Aguirre JJ, Evora C, Pedraz JL, Hernandez RM, Delgado A, Igartua M. Novel nanofibrous dressings containing rhEGF and Aloe vera for wound healing applications. International journal of pharmaceutics. 2017;523(2):556-66.
199. Hamman J. Composition and applications of Aloe vera leaf gel. Molecules. 2008;13(8):1599-616.
200. Eshun K, He Q. Aloe vera: a valuable ingredient for the food, pharmaceutical and cosmetic industries—a review. Critical reviews in food science and nutrition. 2004;44(2):91-6.
201. Mi FL, Wu YB, Shyu SS, Schoung JY, Huang YB, Tsai YH, Hao JY. Control of wound infections using a bilayer chitosan wound dressing with sustainable antibiotic delivery. Journal of Biomedical Materials Research. 2002;59(3):438-49.
202. Kong M, Chen XG, Xing K, Park HJ. Antimicrobial properties of chitosan and mode of action: a state of the art review. International journal of food microbiology. 2010;144(1):51-63.
203. Rabea EI, Badawy ME-T, Stevens CV, Smagghe G, Steurbaut W. Chitosan as antimicrobial agent: applications and mode of action. Biomacromolecules. 2003;4(6):1457-65.
204. Sarhan WA, Azzazy HM, El-Sherbiny IM. The effect of increasing honey concentration on the properties of the honey/polyvinyl alcohol/chitosan nanofibers. Materials science and engineering: C. 2016;67:276-84.
205. Koushki P, Bahrami SH, Ranjbar-Mohammadi M. Coaxial nanofibers from poly (caprolactone)/poly (vinyl alcohol)/Thyme and their antibacterial properties. Journal of industrial textiles. 2018;47(5):834-52.
206. Rafiq M, Hussain T, Abid S, Nazir A, Masood R. Development of sodium alginate/PVA antibacterial nanofibers by the incorporation of essential oils. Materials research express. 2018;5(3):035007.
207. Liakos IL, Holban AM, Carzino R, Lauciello S, Grumezescu AM. Electrospun fiber pads of cellulose acetate and essential oils with antimicrobial activity. Nanomaterials. 2017;7(4):84.
208. Kesici Güler H, Cengiz Çallıoğlu F, Sesli Çetin E. Antibacterial PVP/cinnamon essential oil nanofibers by emulsion electrospinning. The journal of the textile institute. 2018:1-9.
209. Balasubramanian K, Kodam KM. Encapsulation of therapeutic lavender oil in an electrolyte assisted polyacrylonitrile nanofibres for antibacterial applications. RSC advances. 2014;4(97):54892-901.
210. Zhang W, Huang C, Kusmartseva O, Thomas NL, Mele E. Electrospinning of polylactic acid fibres containing tea tree and manuka oil. Reactive and functional polymers. 2017;117:106-11.
211. Baghersad S, Bahrami SH, Mohammadi MR, Mojtahedi MRM, Milan PB. Development of biodegradable electrospun gelatin/aloe-vera/poly (ε-caprolactone) hybrid nanofibrous scaffold for application as skin substitutes. Materials science and engineering: C. 2018;93:367-79.
212. Yang X, Fan L, Ma L, Wang Y, Lin S, Yu F, Pan X, Luo G, Zhang D, Wang H. Green electrospun Manuka honey/silk fibroin fibrous matrices as potential wound dressing. Materials & Design. 2017;119:76-84.
213. Sarhan WA, Azzazy HM. High concentration honey chitosan electrospun nanofibers: biocompatibility and antibacterial effects. Carbohydrate polymers. 2015;122:135-43.
214. Charernsriwilaiwat N, Rojanarata T, Ngawhirunpat T, Sukma M, Opanasopit P. Electrospun chitosan-based nanofiber mats loaded with Garcinia mangostana extracts. International journal of pharmaceutics. 2013;452(1-2):333-43.

215. Li H, Wang M, Williams GR, Wu J, Sun X, Lv Y, Zhu L-M. Electrospun gelatin nanofibers loaded with vitamins A and E as antibacterial wound dressing materials. RSC advances. 2016;6(55):50267-77.
216. Lai H-J, Kuan C-H, Wu H-C, Tsai J-C, Chen T-M, Hsieh D-J, Wang T-W. Tailored design of electrospun composite nanofibers with staged release of multiple angiogenic growth factors for chronic wound healing. Acta biomaterialia. 2014;10(10):4156-66.
217. Li J, Zhang YP, Kirsner RS. Angiogenesis in wound repair: angiogenic growth factors and the extracellular matrix. Microscopy research and technique. 2003;60(1):107-14.
218. Yang HS, Shin J, Bhang SH, Shin J-Y, Park J, Im G-I, Kim C-S, Kim B-S. Enhanced skin wound healing by a sustained release of growth factors contained in platelet-rich plasma. Experimental & molecular medicine. 2011;43(11):622.
219. Xie Z, Paras CB, Weng H, Punnakitikashem P, Su L-C, Vu K, Tang L, Yang J, Nguyen KT. Dual growth factor releasing multi-functional nanofibers for wound healing. Acta biomaterialia. 2013;9(12):9351-9.
220. Pierce PD, MD, Glenn F, Mustoe M, Thomas A. Pharmacologic enhancement of wound healing. Annual review of medicine. 1995;46(1):467-81.
221. Obara K, Ishihara M, Ishizuka T, Fujita M, Ozeki Y, Maehara T, Saito Y, Yura H, Matsui T, Hattori H. Photocrosslinkable chitosan hydrogel containing fibroblast growth factor-2 stimulates wound healing in healing-impaired db/db mice. Biomaterials. 2003;24(20):3437-44.
222. Ucuzian AA, Gassman AA, East AT, Greisler HP. Molecular mediators of angiogenesis. Journal of burn care & research. 2010;31(1):158-75.
223. Piran M, Vakilian S, Piran M, Mohammadi-Sangcheshmeh A, Hosseinzadeh S, Ardeshirylajimi A. In vitro fibroblast migration by sustained release of PDGF-BB loaded in chitosan nanoparticles incorporated in electrospun nanofibers for wound dressing applications. Artificial cells, nanomedicine, and biotechnology. 2018;23:1-10.
224. Jin G, Prabhakaran MP, Kai D, Ramakrishna S. Controlled release of multiple epidermal induction factors through core–shell nanofibers for skin regeneration. European journal of pharmaceutics and biopharmaceutics. 2013;85(3):689-98.
225. Yuan TT, Foushee AMD, Johnson MC, Jockheck-Clark AR, Stahl JM. Development of Electrospun Chitosan-Polyethylene Oxide/Fibrinogen Biocomposite for Potential Wound Healing Applications. Nanoscale research letters. 2018;13(1):88.
226. Choi JS, Choi SH, Yoo HS. Coaxial electrospun nanofibers for treatment of diabetic ulcers with binary release of multiple growth factors. Journal of materials chemistry. 2011;21(14):5258-67.
227. Kumar SA. Wound Healing: Current Understanding and Future Prospect. International journal of drug discovery. 2017;8(1):240-6.
228. Stechmiller JK. Understanding the role of nutrition and wound healing. Nutrition in clinical practice. 2010;25(1):61-8.
229. Stechmiller J, Cowan L, Logan K. Nutrition support for wound healing. Support line. 2009;31(4):61-8.
230. Velnar T, Bailey T, Smrkolj V. The wound healing process: an overview of the cellular and molecular mechanisms. Journal of international medical research. 2009;37(5):1528-42.

231. Taepaiboon P, Rungsardthong U, Supaphol P. Vitamin-loaded electrospun cellulose acetate nanofiber mats as transdermal and dermal therapeutic agents of vitamin A acid and vitamin E. European journal of pharmaceutics and biopharmaceutics. 2007;67(2):387-97.
232. Sheng X, Fan L, He C, Zhang K, Mo X, Wang H. Vitamin E-loaded silk fibroin nanofibrous mats fabricated by green process for skin care application. International journal of biological macromolecules. 2013;56:49-56.
233. Kheradvar SA, Nourmohammadi J, Tabesh H, Bagheri B. Starch nanoparticle as a vitamin E-TPGS carrier loaded in silk fibroin-poly (vinyl alcohol)-Aloe vera nanofibrous dressing. Colloids and surfaces B: Biointerfaces. 2018;166:9-16.
234. Pullar J, Carr A, Vissers M. The roles of vitamin C in skin health. Nutrients. 2017;9(8):866.
235. Guo Sa, DiPietro LA. Factors affecting wound healing. Journal of dental research. 2010;89(3):219-29.
236. Fan L, Wang H, Zhang K, Cai Z, He C, Sheng X, Mo X. Vitamin C-reinforcing silk fibroin nanofibrous matrices for skin care application. RSC advances. 2012;2(10):4110-9.
237. Zarandi MA, Zahedi P, Rezaeian I, Salehpour A, Gholami M, Motealleh B. Drug release, cell adhesion and wound healing evaluations of electrospun carboxymethyl chitosan/polyethylene oxide nanofibres containing phenytoin sodium and vitamin C. IET nanobiotechnology. 2015;9(4):191-200.
238. Sridhar S, Venugopal JR, Ramakrishna S. Improved regeneration potential of fibroblasts using ascorbic acid-blended nanofibrous scaffolds. Journal of biomedical materials research Part A. 2015;103(11):3431-40.
239. Hajiali H, Summa M, Russo D, Armirotti A, Brunetti V, Bertorelli R, Athanassiou A, Mele E. Alginate–lavender nanofibers with antibacterial and anti-inflammatory activity to effectively promote burn healing. Journal of materials chemistry B. 2016;4(9):1686-95.
240. Kant V, Gopal A, Pathak NN, Kumar P, Tandan SK, Kumar D. Antioxidant and anti-inflammatory potential of curcumin accelerated the cutaneous wound healing in streptozotocin-induced diabetic rats. International immunopharmacology. 2014;20(2):322-30.
241. Morgado PI, Miguel SP, Correia IJ, Aguiar-Ricardo A. Ibuprofen loaded PVA/chitosan membranes: A highly efficient strategy towards an improved skin wound healing. Carbohydrate polymers. 2017;159:136-45.
242. Morgado PI, Lisboa PF, Ribeiro MP, Miguel SP, Simões PC, Correia IJ, Aguiar-Ricardo A. Poly (vinyl alcohol)/chitosan asymmetrical membranes: Highly controlled morphology toward the ideal wound dressing. Journal of membrane science. 2014;469:262-71.
243. Ammon HP, Wahl MA. Pharmacology of Curcuma longa. Planta medica. 1991;57(1):1-7.
244. ABE Y, Hashimoto S, HORIE T. Curcumin inhibition of inflammatory cytokine production by human peripheral blood monocytes and alveolar macrophages. Pharmacological research. 1999;39(1):41-7.
245. Huang M-T, Lysz T, Ferraro T, Abidi TF, Laskin JD, Conney AH. Inhibitory effects of curcumin on in vitro lipoxygenase and cyclooxygenase activities in mouse epidermis. Cancer research. 1991;51(3):813-9.
246. Merrell JG, McLaughlin SW, Tie L, Laurencin CT, Chen AF, Nair LS. Curcumin-loaded poly (ε-caprolactone) nanofibres: Diabetic wound dressing with anti-oxidant and anti-inflammatory properties. Clinical and experimental pharmacology and physiology. 2009;36(12):1149-56.

247. Müller-Decker K, Hirschner W, Marks F, Fürstenberger G. The Effects of Cyclooxygenase Isozyme Inhibition onIncisional Wound Healing in Mouse Skin. Journal of investigative dermatology. 2002;119(5):1189-95.
248. Park Y-J, Kwon R, Quan QZ, Oh DH, Kim JO, Hwang MR, Koo YB, Woo JS, Yong CS, Choi H-G. Development of novel ibuprofen-loaded solid dispersion with improved bioavailability using aqueous solution. Archives of pharmacal research. 2009;32(5):767-72.
249. Steffansen B, Herping SP. Novel wound models for characterizing ibuprofen release from foam dressings. International journal of pharmaceutics. 2008;364(1):150-5.
250. Yuan Z, Zhao J, Zhu W, Yang Z, Li B, Yang H, Zheng Q, Cui W. Ibuprofen-loaded electrospun fibrous scaffold doped with sodium bicarbonate for responsively inhibiting inflammation and promoting muscle wound healing in vivo. Biomaterials Science. 2014;2(4):502-11.
251. Mohiti-Asli M, Saha S, Murphy S, Gracz H, Pourdeyhimi B, Atala A, Loboa E. Ibuprofen loaded PLA nanofibrous scaffolds increase proliferation of human skin cells in vitro and promote healing of full thickness incision wounds in vivo. Journal of Biomedical Materials Research Part B: Applied Biomaterials. 2017;105(2):327-39.
252. Pushpavalli G, Kalaiarasi P, Veeramani C, Pugalendi KV. Effect of chrysin on hepatoprotective and antioxidant status in D-galactosamine-induced hepatitis in rats. European journal of pharmacology. 2010;631(1-3):36-41.
253. Cho H, Yun C-W, Park W-K, Kong J-Y, Kim KS, Park Y, Lee S, Kim B-K. Modulation of the activity of pro-inflammatory enzymes, COX-2 and iNOS, by chrysin derivatives. Pharmacological research. 2004;49(1):37-43.
254. Deldar Y, Pilehvar-Soltanahmadi Y, Dadashpour M, Montazer Saheb S, Rahmati-Yamchi M, Zarghami N. An in vitro examination of the antioxidant, cytoprotective and anti-inflammatory properties of chrysin-loaded nanofibrous mats for potential wound healing applications. Artificial cells, nanomedicine, and biotechnology. 2018;46(4):706-16.
255. Ghalei S, Asadi H, Ghalei B. Zein nanoparticle-embedded electrospun PVA nanofibers as wound dressing for topical delivery of anti-inflammatory diclofenac. Journal of applied polymer science. 2018;135(33):46643.
256. Basar A, Castro S, Torres-Giner S, Lagaron J, Sasmazel HT. Novel poly (ε-caprolactone)/gelatin wound dressings prepared by emulsion electrospinning with controlled release capacity of Ketoprofen anti-inflammatory drug. Materials science and engineering: C. 2017;81:459-68.
257. Romano I, Summa M, Heredia-Guerrero JA, Spanò R, Ceseracciu L, Pignatelli C, Bertorelli R, Mele E, Athanassiou A. Fumarate-loaded electrospun nanofibers with anti-inflammatory activity for fast recovery of mild skin burns. Biomedical materials. 2016;11(4):041001.
258. Li Z, Kang H, Che N, Liu Z, Li P, Li W, Zhang C, Cao C, Liu R, Huang Y. Controlled release of liposome-encapsulated Naproxen from core-sheath electrospun nanofibers. Carbohydrate polymers. 2014;111:18-24.
259. Varshosaz J, Jahanian A, Maktoobian M. Montelukast incorporated poly (methyl vinyl ether-co-maleic acid)/poly (lactic-co-glycolic acid) electrospun nanofibers for wound dressing. Fibers and polymers. 2017;18(11):2125-34.
260. Chen W, Li D, Ei-Shanshory A, El-Newehy M, Ei-Hamshary HA, Al-Deyab SS, He C, Mo X. Dexamethasone loaded core-shell SF/PEO nanofibers via green electrospinning reduced endothelial cells inflammatory damage. Colloids and surfaces B: Biointerfaces. 2015;126:561-8.

261. Morgado PI, Aguiar-Ricardo A, Correia IJ. Asymmetric membranes as ideal wound dressings: An overview on production methods, structure, properties and performance relationship. Journal of Membrane Science. 2015;490:139-51.
262. Ribeiro MP, Espiga A, Silva D, Baptista P, Henriques J, Ferreira C, Silva JC, Borges JP, Pires E, Chaves P. Development of a new chitosan hydrogel for wound dressing. Wound repair and regeneration. 2009;17(6):817-24.
263. Jayakumar R, Prabaharan M, Kumar PS, Nair S, Tamura H. Biomaterials based on chitin and chitosan in wound dressing applications. Biotechnology advances. 2011;29(3):322-37.
264. Hinrichs W, Lommen E, Wildevuur CR, Feijen J. Fabrication and characterization of an asymmetric polyurethane membrane for use as a wound dressing. Journal of applied biomaterials. 1992;3(4):287-303.
265. Miguel SP, Figueira DR, Simões D, Ribeiro MP, Coutinho P, Ferreira P, Correia IJ. Electrospun polymeric nanofibres as wound dressings: a review. Colloids and surfaces B: Biointerfaces. 2018;169:60-71.
266. Karuppuswamy P, Venugopal JR, Navaneethan B, Laiva AL, Sridhar S, Ramakrishna S. Functionalized hybrid nanofibers to mimic native ECM for tissue engineering applications. Applied surface science. 2014;322:162-8.
267. Freyman T, Yannas I, Gibson L. Cellular materials as porous scaffolds for tissue engineering. Progress in materials science. 2001;46(3-4):273-82.
268. Mi F-L, Shyu S-S, Wu Y-B, Lee S-T, Shyong J-Y, Huang R-N. Fabrication and characterization of a sponge-like asymmetric chitosan membrane as a wound dressing. Biomaterials. 2001;22(2):165-73.
269. Lee JW, Han SS, Zo SM, Choi SM. Cellulose/poly-(m-phenylene isophthalamide) porous film as a tissue-engineered skin bioconstruct. Results in physics. 2018;9:113-20.
270. Khang G, Lee SJ, Lee JH, Kim YS, Lee HB. Interaction of fibroblast cells on poly (lactide-co-glycolide) surface with wettability chemogradient. Bio-medical materials and engineering. 1999;9(3):179-87.
271. Oliveira SM, Alves NM, Mano JF. Cell interactions with superhydrophilic and superhydrophobic surfaces. Journal of Adhesion Science and Technology. 2014;28(8-9):843-63.
272. Miguel SP, Simões D, Moreira AF, Sequeira RS, Correia IJ. Production and characterization of electrospun silk fibroin based asymmetric membranes for wound dressing applications. International journal of biological macromolecules. 2019;121:524-35.
273. Perumal G, Pappuru S, Chakraborty D, Nandkumar AM, Chand DK, Doble M. Synthesis and characterization of curcumin loaded PLA—Hyperbranched polyglycerol electrospun blend for wound dressing applications. Materials science and engineering: C. 2017;76:1196-204.
274. Chen Y, Yan L, Yuan T, Zhang Q, Fan H. Asymmetric polyurethane membrane with in situ-generated nano-TiO2 as wound dressing. Journal of applied polymer science. 2011;119(3):1532-41.
275. Elsner JJ, Zilberman M. Novel antibiotic-eluting wound dressings: An in vitro study and engineering aspects in the dressing's design. Journal of tissue viability. 2010;19(2):54-66.
276. Gordillo GM, Sen CK. Revisiting the essential role of oxygen in wound healing. The american journal of surgery. 2003;186(3):259-63.
277. Bishop A. Role of oxygen in wound healing. Journal of wound care. 2008;17(9):399-402.

278. Elsner JJ, Shefy-Peleg A, Zilberman M. Novel biodegradable composite wound dressings with controlled release of antibiotics: microstructure, mechanical and physical properties. Journal of biomedical materials research Part B: Applied Biomaterials. 2010;93(2):425-35.
279. Zahouani H, Pailler-Mattei C, Sohm B, Vargiolu R, Cenizo V, Debret R. Characterization of the mechanical properties of a dermal equivalent compared with human skin in vivo by indentation and static friction tests. Skin research and technology. 2009;15(1):68-76.
280. Joo H-S, Otto M. Molecular basis of in vivo biofilm formation by bacterial pathogens. Chemistry & biology. 2012;19(12):1503-13.
281. Ong S-Y, Wu J, Moochhala SM, Tan M-H, Lu J. Development of a chitosan-based wound dressing with improved hemostatic and antimicrobial properties. Biomaterials. 2008;29(32):4323-32.
282. Archana D, Dutta J, Dutta P. Evaluation of chitosan nano dressing for wound healing: Characterization, in vitro and in vivo studies. International journal of biological macromolecules. 2013;57:193-203.
283. Liang D, Lu Z, Yang H, Gao J, Chen R. Novel asymmetric wettable AgNPs/chitosan wound dressing: in vitro and in vivo evaluation. ACS applied materials & interfaces. 2016;8(6):3958-68.
284. Liu H, Wang C, Li C, Qin Y, Wang Z, Yang F, Li Z, Wang J. A functional chitosan-based hydrogel as a wound dressing and drug delivery system in the treatment of wound healing. RSC Advances. 2018;8(14):7533-49.
285. Mi F-L, Wu Y-B, Shyu S-S, Chao A-C, Lai J-Y, Su C-C. Asymmetric chitosan membranes prepared by dry/wet phase separation: a new type of wound dressing for controlled antibacterial release. Journal of membrane science. 2003;212(1-2):237-54.
286. Temtem M, Casimiro T, Aguiar-Ricardo A. Solvent power and depressurization rate effects in the formation of polysulfone membranes with CO2-assisted phase inversion method. Journal of membrane science. 2006;283(1-2):244-52.
287. Ng R, Zang R, Yang KK, Liu N, Yang S-T. Three-dimensional fibrous scaffolds with microstructures and nanotextures for tissue engineering. RSC advances. 2012;2(27):10110-24.
288. Zhong W, Xing MM, Maibach HI. Nanofibrous materials for wound care. Cutaneous and ocular toxicology. 2010;29(3):143-52.
289. Vijayavenkataraman S, Lu W, Fuh J. 3D bioprinting of skin: a state-of-the-art review on modelling, materials, and processes. Biofabrication. 2016;8(3):032001.
290. Lee V, Singh G, Trasatti JP, Bjornsson C, Xu X, Tran TN, Yoo S-S, Dai G, Karande P. Design and fabrication of human skin by three-dimensional bioprinting. Tissue engineering part C: methods. 2013;20(6):473-84.
291. He P, Zhao J, Zhang J, Li B, Gou Z, Gou M, Li X. Bioprinting of skin constructs for wound healing. Burns & trauma. 2018;6(1):5.
292. Koch L, Deiwick A, Schlie S, Michael S, Gruene M, Coger V, Zychlinski D, Schambach A, Reimers K, Vogt PM. Skin tissue generation by laser cell printing. Biotechnology and bioengineering. 2012;109(7):1855-63.
293. Duarte ARC, Santo VE, Alves A, Silva SS, Moreira-Silva J, Silva TH, Marques AP, Sousa RA, Gomes ME, Mano JF. Unleashing the potential of supercritical fluids for polymer processing in tissue engineering and regenerative medicine. The Journal of Supercritical Fluids. 2013;79:177-85.

294. Ng WL, Yeong WY, Naing MW. Polyelectrolyte gelatin-chitosan hydrogel optimized for 3D bioprinting in skin tissue engineering. International journal of bioprinting. 2016;2(1):53-62.
295. Franco RA, Min Y-K, Yang H-M, Lee B-T. Fabrication and biocompatibility of novel bilayer scaffold for skin tissue engineering applications. Journal of biomaterials applications. 2013;27(5):605-15.
296. Mohammadi T, Saljoughi E. Effect of production conditions on morphology and permeability of asymmetric cellulose acetate membranes. Desalination. 2009;243(1-3):1-7.

Chapter III

Electrospun Polycaprolactone/Aloe Vera_Chitosan Nanofibrous Asymmetric Membranes Aimed for Wound Healing Applications

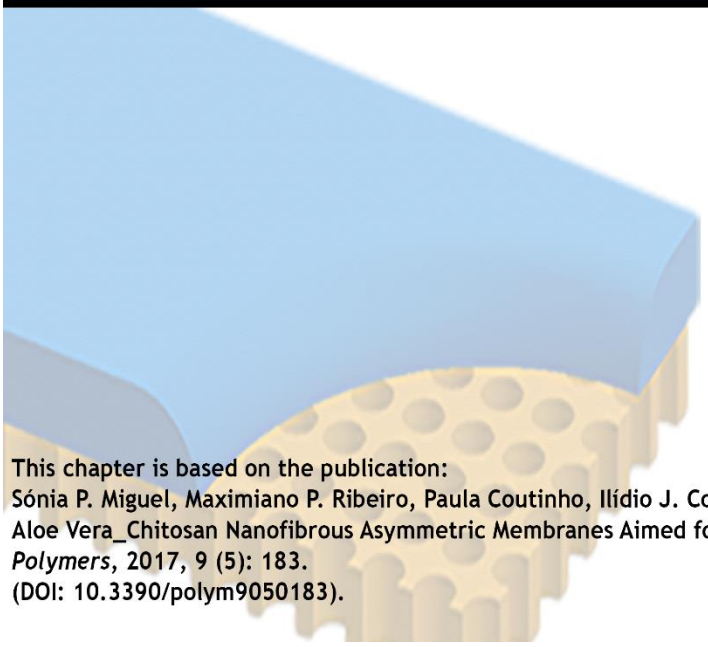

This chapter is based on the publication:
Sónia P. Miguel, Maximiano P. Ribeiro, Paula Coutinho, Ilídio J. Correia; Electrospun Polycaprolactone/ Aloe Vera_Chitosan Nanofibrous Asymmetric Membranes Aimed for Wound Healing Applications, *Polymers*, 2017, 9 (5): 183.
(DOI: 10.3390/polym9050183).

Abstract

Today, none of the wound dressings available on the market is fully capable of reproducing all the features of native skin. Herein, an asymmetric electrospun membrane was produced to mimic both layers of skin. This structure comprises a top dense layer (manufactured with polycaprolactone) that was designed to provide mechanical support to the wound and a bottom porous layer (composed of chitosan and Aloe Vera) aimed to improve the bactericidal activity of the membrane and ultimately the healing process. The results obtained revealed that the produced asymmetric membranes displayed a porosity, wettability, as well as mechanical properties similar to those presented by the native skin. Fibroblast cells were able to adhere, spread, and proliferate on the surface of the membranes and the intrinsic structure of the two layers of the membrane is capable of avoiding the invasion of microorganisms while conferring bioactive properties. Such data reveals the potential of these asymmetric membranes, in the near future, to be applied as wound dressings.

Keywords: Aloe Vera; asymmetric membranes; chitosan; electrospinning; wound dressings.

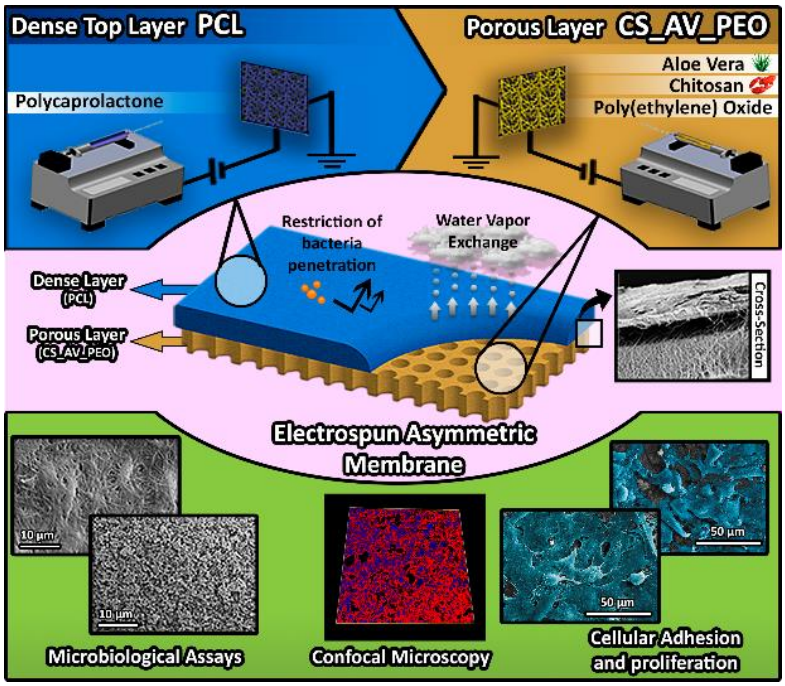

3.1 Introduction

Skin structure and functions are often compromised by traumatic events (*e.g.*, thermal burns, cuts, lacerations or surgical incisions) or chronic wounds (*e.g.* pressure ulcers or diabetic foot ulcers) [1-4]. When a large area of skin is lost, the immediate coverage of the wound is mandatory for avoiding water/blood losses, for preventing bacterial invasion, as well as decreasing the pain felt by patients [5].

Currently, autologous skin grafting remains the "gold standard" treatment used in the clinic. However, this approach cannot always be used due to the extent of the wound, limited availability of donor sites, scar formation, slow healing, and patient morbidity. Allogeneic and xenogeneic skin grafts are alternative therapeutic approaches that have been also used, although their application has associated risks of immune rejection, disease transmission, and limited availability of skin bank collection [6, 7]. To overcome these limitations, researchers have developed different skin substitutes, some of them used in the clinic. Nevertheless, none of these skin substitutes is fully capable of re-establishing the native structure and functions of skin [8, 9].

Among the skin substitutes developed so far, asymmetric membranes to be applied as wound dressings systems [10-13] have captured the attention of researchers. The top layer of these membranes can be designed to avoid bacterial invasion and also prevent wound surface dehydration, whereas the underlying layer can be conceived to remove the wound exudate and to promote cell infiltration and proliferation [8].

Heretofore, dry/wet and $scCO_2$-induced phase inversion methods have been the most used to produce asymmetric membranes [14, 15]. In recent times, electrospinning emerged as an alternative to produce bilayer membranes aimed to improve the healing process [16]. To produce electrospun membranes, a charged polymer solution is initially accelerated under a high-voltage electrostatic field, and subsequently, the fiber jet travels through the atmosphere to allow solvent evaporation, leading to the deposition of solid polymer fibers on the collector. The produced fibers display a high surface to volume ratio and porosity, properties that are crucial for increasing cell adhesion, growth, migration, differentiation, and angiogenesis [17-19].

Herein, an asymmetric membrane, composed of two distinct layers (aimed to reproduce the epidermis and dermis layers of skin), was produced through electrospinning. A synthetic polymer, PCL, was used to produce the top layer that is aimed to act as a protective barrier [13, 20]. On the other hand, CS and AV were used to manufacture the bottom layer. CS is a natural polysaccharide, known for its capacity of promoting collagen synthesis and also by exhibiting bactericidal and hemostatic properties. Such features triggered its use in the production of wound dressings, namely in HidroKi®, Patch®, Chitopack®, Tegasorb®, and

KytoCel® [16, 21-25]. Although, limited solubility of CS at physiological pH and high viscosity in acid solutions hinder its application in electrospinning. To overcome such a drawback, synthetic polymers such as PEO, PVA, PLGA have been blended with this polymer to enable the production of CS nanofibers [26-30]. AV is a member of the *Liliaceae* family and it has been widely used for the treatment of different skin disorders, like burns, infections, and other dermatologic conditions [31]. The mucilaginous gel, present in AV leaves, has a higher water content (≈ 99%), which is fundamental for wound hydration. Furthermore, different compounds like amino acids, salicylic acid, ascorbic acid, Vit-A, and Vit-E are also found in AV. Such biomolecules are responsible for conferring antibacterial, anti-inflammatory, and antioxidant properties to AV [31-33]. In addition, AV is also known for, promoting fibroblast proliferation, increasing collagen synthesis, and ultimately, enhancing the wound healing process [31-37].

3.2 Materials and Methods

3.2.1 Materials

AV leaves were obtained from 5-year-old plants (*Aloe barbadensis Miller*) that were bought from a Portuguese botanic shop. Trifluoroethanol (TFE) was purchased from Acros Organics (Jersey City, New Jersey, USA). Lysozyme from chicken egg was acquired from Alfa Aesar (Haverhill, Massachusetts, USA). Fetal bovine serum (FBS) (free from any antibiotic) was purchased from Biochrom AG (Berlin, Germany). Glacial acetic acid (AA) was obtained from LabChem (New York, NY, USA). Paraformaldehyde (PFA) was obtained from Merck, SA (Algés, Portugal). Normal Human Dermal Fibroblasts (NHDF) cells were purchased from PromoCell (Labclinics, S.A., Barcelona, Spain). 3-(4,5-Dimethylthiazol-2-yl)-5-(3-carboxymethoxyphenyl)-2 (4-sulfophenyl)-2H-tetrazolium (MTS) was bought from Promega (Madison, Wisconsin, USA). Amphotericin B, CS (low molecular weight (LMW: 50,000–190,000 Da), Dulbecco's modified Eagle's medium (DMEM-F12), Ethylenediaminetetraacetic acid (EDTA), Gentamicin, GA, Kanamycin, LB Broth, PBS, PCL (80,000 Da), PEO, Sodium hydroxide (NaOH) and Trypsin were acquired from Sigma-Aldrich (Sintra, Portugal). Quant-iT Pico Green Double-stranded deoxyribonucleic acid (dsDNA) assay kit was obtained from ThermoFisher Scientific (Waltham, Massachusetts, USA). Bovine serum albumin (BSA) was obtained from VWR International (Carnaxide, Portugal). *S. aureus* clinical isolate ATCC 25923 and *E. coli* were used as models of prokaryotic organisms to evaluate the bactericidal activity of the membranes.

3.2.2 Methods

3.2.2.1 Extraction of the AV Gel

The extraction of AV gel was performed according to a method previously described elsewhere [34, 35]. Briefly, AV leaves were initially washed with distilled water to remove any dirt from their surface and, subsequently, the skin of the leaf was carefully separated from the parenchyma using a scalpel-shaped knife (Thermo Fisher Scientific, Waltham, Massachusetts, USA). The samples obtained were then homogenized in a blender (Sigma-Aldrich, Sintra,

Portugal) and then filtered. After, the AV gel was stabilized at 65°C for 15 min and stored at 4°C for later use.

3.2.2.2 Deacetylation of chitosan

CS was purified and deacetylated through a method previously described in the literature [21]. Briefly, 500 mg of CS LMW was dispersed in 10 mL of NaOH (1M) solution, under magnetic stirring for 4 h, at 50°C. Then, the mixture was filtered using a Whatman® quantitative filter grade (Sigma-Aldrich, St. Louis, MO, USA) and a Buchner funnel to recover the deacetylated CS. The remaining material was washed extensively until the sample pH reached 7.4. Afterward, the samples were dried at 40°C overnight. The degree of deacetylation (DD) of CS was determined by using the first derivative UV-spectroscopy (1DUVS) method [38]. UV–Vis CS spectra were acquired in a Thermo Scientific Evolution 201 UV–Vis spectrophotometer (Thermo Fisher Scientific, Waltham, Massachusetts, USA).

3.2.2.3 Production of the electrospun asymmetric membranes

A conventional electrospinning apparatus adapted by us, comprising a high voltage source (Spellman CZE1000R, 0–30 kV) obtained from (Spellman, Corporate Headquarters USA) a precision syringe pump (KDS-100) (acquired from Sigma-Aldrich, Sintra, Portugal), a plastic syringe with a stainless-steel needle (21 Gauge), and an aluminum disk connected to a copper collector, was used to produce the asymmetric membranes.
The top layer of the membrane was produced with a PCL solution (7% PCL (w/v) in 80% TFE: 20% H_2O (v/v)), placed in the syringe and then electrospun at a constant flow rate of 2.5 mL/h, using a working distance of 15 cm and an applied voltage of 25 kV. After, the top layer was produced, 10 mL of CS_PEO solution—composed of 7% CS (w/v) and 8% PEO (w/v) (2:1 volume ratio) or CS_AV_PEO ((2:2:1 volume ratio), where an extract of 40% AV gel (v/v) was used) was electrospun on top of the PCL electrospun membrane at a constant flow rate of 4.0 mL/h, using a working distance of 12 cm and an applied voltage of 28 kV. The produced asymmetric membranes (PCL/CS_PEO and PCL/CS_AV_PEO) were then characterized through *in vitro* assays to evaluate their suitability to be used as wound dressings.

3.2.2.4 Attenuated total reflectance–fourier transform infrared spectroscopy analysis

The final composition of the electrospun membranes was determined by ATR-FTIR analysis. The membranes' spectra were acquired with an average of 128 scans, a spectral width ranging from 4000 and 400 cm^{-1} and a spectral resolution of 4 cm^{-1}, using a Nicolet iS10 FTIR spectrophotometer (Thermo Scientific, Waltham, MA, USA). Furthermore, the spectra of the raw materials used to produce the membranes were also acquired for comparative purposes.

3.2.2.5 Characterization of the mechanical properties of the membranes

The mechanical properties of PCL/CS_PEO and PCL/CS_AV_PEO membranes were determined with a Shimadzu AG-X Tensile Testing Machine (Tokyo, Japan) operated at room temperature (RT), under wet and dry conditions, accordingly to the guidelines established by the Standard Test Method for Tensile Properties of Polymer Matrix Composite Materials (ASTM standard D3039/ D3039 M) [15]. The tested samples (n = 5) had a width of 2 cm, a gauge length of 6 cm and a thickness ranging from 0.41 to 0.52 mm. The length between the clamps was set to 2 cm and the speed of testing was set to 2 mm/min. In wet conditions, the membranes were immersed in a PBS solution, over 24 h at 37°C. Load-extension data was recorded and the stress-strain curve of the membranes was determined through Equations (3.1) and (3.2), respectively:

$$\text{Stress} = \sigma = \frac{F}{A} \tag{3.1}$$

$$\text{Strain} = \varepsilon = \frac{\Delta l}{L} \tag{3.2}$$

where F is the applied force; A is the cross-sectional area; Δl is the change in length, and L is the length between the clamps.

3.2.2.6 Evaluation of the porosity of the produced membranes

The microporosity of the membranes was determined through a liquid displacement method [25]. Briefly, three specimens were weighed and then immersed in absolute ethanol for 1 h and later on reweighed. The membrane's porosity was determined through Equation (3.3):

$$\text{Porosity}\ (\%) = \frac{W_s - W_d}{D_{\text{ethanol}} \times V_{\text{membrane}}} \times 100 \tag{3.3}$$

where W_d is the initial weight of dry membrane and Ws is the weight of the swollen membrane, D_{ethanol} is the density of the ethanol at RT and V_{membrane} is the volume of the swollen membrane. For each sample, three replicates were used, and the presented data represents the average of the results obtained for each sample.

3.2.2.7 Determination of contact angle at the surface of the produced membranes

The contact angles at the surface of the samples were determined with a Data Physics Contact Angle System OCAH 200 apparatus (DataPhysics Instruments GmbH, Filderstadt, Germany) operating in static mode, at 25°C and using water as a reference fluid. For each sample, water drops (4 µL) were placed on the surface of the membranes. The reported contact angles are the average of at least three independent measurements.

3.2.2.8 Water vapor transmission rate

The water vapor diffusion through the PCL/CS_PEO and PCL/CS_AV_PEO membranes was evaluated accordingly to a method previously described elsewhere [25]. Briefly, the membranes

were used to seal the opening of a glass test tube (1.77 cm^2) containing 10 mL of ultrapure water to avoid its evaporation. A parafilm tape was used to attach the membrane to the glass tube. Afterward, the membranes were incubated at 37°C and at specific time points, the amount of water evaporation was obtained by determining the weight loss. The WVTR was estimated through Equation (3.4):

$$\text{Water Vapor Transmission Rate} = \frac{W_{\text{loss}}}{A} \tag{3.4}$$

where W_{loss} is the daily weight loss of water and *A* is the area of the tube opening.

3.2.2.9 Swelling and enzymatic degradation

Swelling and degradation tests were performed by immersing all samples in PBS (pH = 5) and PBS containing 13.6 mg/mL lysozyme, at 37°C , under stirring (60 RPM) for 30 days [35]. All experiments were conducted in triplicate and the solutions were changed periodically in order to guarantee that the enzyme remained active through the study. The swollen sample weights were measured after removing the water excess present at the surface of the membranes, by gently tapping the surface with filter paper. Water uptake was determined through Equation (3.5).

$$\text{Swelling ratio } (Q) = \frac{W_t}{W_0} \tag{3.5}$$

where W_t is the final weight and W_0 is the initial weight of the membranes.

The degradation profile of the samples was determined at specific time points (1, 3, 7, 14, and 30 days). To do that, samples were removed from the solution (PBS with 13.6 mg/mL lysozyme) and weighed, after being completely dried [38]. The degradation percentage at each time point was calculated according to Equation (3.6):

$$\text{Weight loss } (\%) = \frac{W_i - W_t}{W_i} \times 100 \tag{3.6}$$

where W_i corresponds to the initial weight of the sample and W_t to the weight of the sample at time *t*.

3.2.2.10 Protein adsorption

To characterize protein adsorption at the surface of the membranes, BSA was used, following a procedure described elsewhere [39]. The membranes were initially placed in a 24-well cell culture plate and 300 µL of BSA (1 mg/mL protein/phosphate buffer) was added to the surface of the electrospun membranes. The plate was then placed in a humidified incubator at 37°C at specific time points. Empty wells (tissue culture polystyrene) were used as background reference. The non-adherent BSA was removed from wells by washing them with PBS solution. Subsequently, 300 µL of 2% sodium dodecyl sulfate was added to each well and then incubated

overnight to extract adhered proteins. The concentration of the adhered proteins was determined through the micro bicinchoninic acid (BCA Kit) assay.

3.2.2.11 Characterization of the biological properties of the produced membranes

3.2.2.11.1 Characterization of cell viability and proliferation in contact with the membranes

The cytotoxic profile of produced membranes was evaluated in vitro following ISO 10993-5. Prior to cell seeding, membranes were placed into 96-well plates and then sterilized, by UV irradiation (254 nm, ≈ 7 $mW.cm^{-2}$), over 1 h. NHDF cells were used as model and seeded at a density of 10×10^3 cells per well in the presence of the membranes. Then, the plate was incubated at 37°C, in a 5% CO_2 humidified atmosphere, and the culture medium was changed every two days until the end of the assay. After 1, 3, and 7 days of incubation, a MTS assay was performed to characterize the membranes biocompatibility. Briefly, the medium of each well was removed and replaced by a mixture of 100 µL of fresh culture medium and 20 µL of MTS/PMS (phenazine methosulfate) reagent solution. Following this, cells were incubated for 4 h, at 37°C, in a 5% CO_2 atmosphere. The absorbance of each sample (n = 5) was determined at 492 nm using a microplate reader (Biorad xMark microplate spectrophotometer). Cells cultured without materials were used as a negative control (K^-), whereas cells cultured with ethanol (96%) were used as positive control (K^+).

3.2.2.11.2 dsDNA quantification

To assess the cells proliferation rate, the total DNA content was measured with a Quan-iT PicoGreen dsDNA Assay kit, following a protocol previously described in the literature [35, 40]. Briefly, NHDF cells were seeded, at a density of 10×10^3 cells/mL, in contact with the produced membranes. After 1, 3, and 7 days, the membranes were washed twice with PBS and then each membrane was transferred into a 1.5 mL Eppendorfs containing 1mL of ultra-pure water. Thereafter, the cell–membrane complexes were subjected to a freeze–thaw cycle and sonicated for 15 min, to lyse the cells. Samples and standards were prepared and mixed with a PicoGreen solution at a 200:1 ratio and placed in a 96-well plate (n = 3) [35]. The plate was incubated for 10 min in the dark and fluorescence was measured in a microplate reader using excitation and emission wavelengths of 480 nm and 520 nm, respectively. A calibration curve was performed, and samples dsDNA concentrations were determined.

3.2.2.12 Characterization of the antimicrobial properties of the membranes

3.2.2.12.1 Analysis of bacterial penetration through the top layer of the produced membranes

S. aureus and *E. coli*, gram-positive and gram-negative bacteria, were used to characterize the capacity of the membrane's top layer to avoid bacterial infiltration within their structure. To accomplish this, transwell systems (Corning Incorporated, New York, NY, USA) were modified

with a PCL membrane or a filter paper (0.22 μm) (control group) to act as the interface between the upper and lower chamber. The PCL membrane and the filter paper were inoculated with a bacterial suspension (1×10^8 colony forming units (CFU)/mL), during 24 h, at 37°C [41]. After, the optical density of the medium culture present in the lower chamber was determined. Posteriorly, the number of colonies that cross the PCL membrane/filter paper were also counted. Furthermore, the PCL membrane and filter paper were recovered and submitted to Scanning electron microscopy (SEM) analysis to evaluate the presence of the bacterial colonies on the upper and lower side of the samples.

3.2.2.12.2 Characterization of bactericidal activity of the bottom Layers (CS_PEO and CS_AV_PEO) membranes

The bactericidal activity of the PCL/CS_PEO and PCL/CS_AV_PEO membranes was also characterized using *S. aureus* and *E. coli* as bacteria models. Briefly, each membrane was added to 10 mL of LB broth at pH 6.2, containing 1×10^5 CFU/mL of early mid-log phase culture and then were incubated at 37°C, for 24 h. After the incubation period, serial dilutions were prepared and 100 μL of bacterial samples were transferred into LB agar plates. Following overnight incubation at 37°C, bacterial colonies were counted and expressed as the number of colonies forming units per mL [25, 42, 43]. The bacterial growth inhibition was calculated through Equation (3.7):

$$\text{Antibacterial efficiency } (\%) = \frac{N_0 - N}{N_0} \times 100 \tag{3.7}$$

where N_0 and N each represents the bacteria number of control and experimental group.

To further characterize the bactericidal activity of the membranes, biofilm formation on the membrane's surface was also studied. To accomplish this, the produced membranes were placed on the surface of a plate of LB agar in contact with *S. aureus* and *E. coli* (1×10^8 CFU/mL) and then incubated for 24 h, at 37°C [21]. Following this, biofilm formation at the surface of the membranes was assessed through SEM analysis.

3.2.2.13 Characterization of the morphologic features and biological performance of the electrospun membranes by SEM Analysis

Biological samples, containing cells or bacteria, were fixed for 4 h with 2.5% (v/v) GA. Following this, samples were washed three times with PBS and then dehydrated with growing concentrations of ethanol (70, 80, 90, and 100%) or freeze-dried for 3 h. Finally, all biological and non-biological samples were mounted onto aluminum stubs with Araldite glue and sputter-coated with gold using a Quorum Q150R ES sputter coater (Quorum Technologies Ltd, Laughton, East Sussex, England). SEM images were then acquired with different magnifications,

using an acceleration voltage of 20 kV, in a Hitachi S-3400N Scanning Electron Microscope (Hitachi, Tokyo, Japan).

3.2.2.14 Confocal microscopy analysis

Confocal laser scanning microscopy (CLSM), Zeiss, Oberkochen, Germany) was used to characterize cell distribution and proliferation at the surface of both layers of the produced asymmetric membranes. Cells (10×10^3 cells/mL) were seeded on the surface of CS_PEO and CS_AV_PEO layers, which were previously placed in µ-Slide 8 well Ibidi imaging plates (Ibidi GmbH, Planegg/Martinsried, Germany). After 1 and 3 days, cells were fixed with 4% PFA in PBS for 20 min and then stained with the WGA-Alexa 594® conjugate. Cells were then rinsed several times with PBS and labeled with Hoechst 33342® nuclear probe (2 µM). The 3D reconstruction and image analysis were performed using Zeiss Zen 2010 software (Zeiss, Oberkochen, Germany).

3.2.2.15 Statistical analysis

The statistical analysis of the results obtained was performed using one-way analysis of variance (ANOVA), with the Newman-Keuls post hoc test. A p value lower than 0.05 ($p < 0.05$) was considered statistically significant.

3.3 Results and Discussion

3.3.1 Characterization of the morphology of the membranes

When asymmetric membranes are aimed to be used as wound dressings, they are conceived with a dense top layer, that can protect the wound from physical damage and infection, and a porous and hydrophilic inner layer capable of absorbing the wound exudate and providing a 3D architecture that enables cell adhesion and proliferation [44].

Up to now, different techniques have been used to produce these membranes, including supercritical carbon dioxide ($scCO_2$)-assisted phase, dry/wet-phase inversion, and electrospinning [10, 45]. In this study, asymmetric membranes were produced with an electrospinning apparatus. In Figure 3.1, a denser top layer can be observed that was manufactured with PCL (an Food and Drug Administration-approved biomaterial that has a low cost, is biocompatible, and displays good mechanical properties) [16, 46-48]. This polymer confers to the top layer suitable mechanical properties, waterproof capacity, avoids bacteria penetration, and regulates the gaseous exchanges between the wound and the surrounding environment. On the other hand, the porous bottom layer was composed either of CS_PEO or CS_AV_PEO and was designed to be able to absorb the wound exudates, promote nutrient exchange, support cell proliferation, and also to confer antimicrobial properties to the membrane.

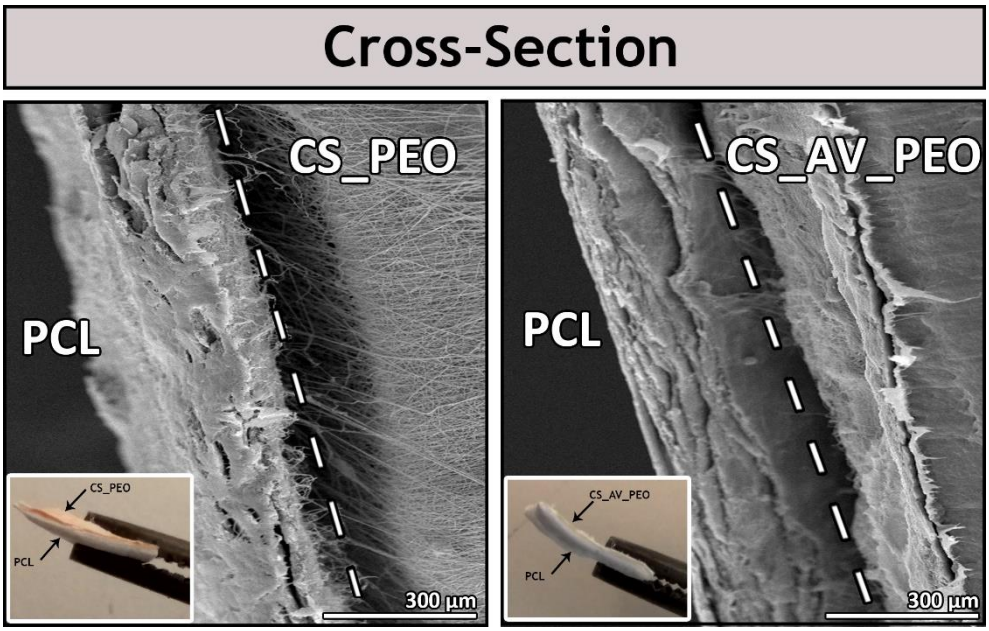

Figure 3.1. SEM and macroscopic images of the cross-section of the produced bilayer membranes (PCL/CS_PEO and PCL/CS_AV_PEO).

The higher porosity of the bottom layers of the asymmetric membranes was also confirmed by the results obtained in porosity assays (see further details in Section 3.3.4). Regarding the macroscopic images (insets of Figure 3.1), it is possible to identify the two different layers of asymmetric membrane. Such a feature will make easier the future application of the membranes at the wound site. The diameter of the electrospun nanofibers present in the membranes was determined through SEM analysis (Figure 3.2). The top layer displays randomly oriented fibers with average diameters of 385 ± 134 nm. Such a result is in agreement with the data available in the literature for membranes produced with PCL [49]. In turn, the bottom layer of membranes presented a mean diameter of 239 ± 122 nm and 152 ± 54 nm for CS_PEO and CS_AV_PEO, respectively (Figure 3.2). It seems that the incorporation of the AV gel leads to the production of thinner fibers, due to the reduction of the viscosity of the solution used for nanofiber production. Suganya and their collaborators had already reported a similar effect on the diameter of PCL nanofibers when AV was added to the PCL solution. Nanofibers with a diameter of the 215 ± 63 nm were produced when AV and PCL were blended [36]. On the other hand, Karuppuswamy *et al*. previously obtained PCL nanofibers with diameters of 346 ± 63 nm and PCL/AV nanofibers with diameters of 307 ± 42 nm [50]. Moreover, the diameters of nanofibers produced herein are within the size range displayed by collagen fibers present in natural ECM (50–400 nm). The increased roughness presented by the produced membranes leads to a higher surface area available for cell adhesion. In addition, the high porosity exhibited by the nanofibers is fundamental in preventing fluid accumulation, enhance oxygen permeation, and ultimately improve cell adhesion and proliferation [51-53].

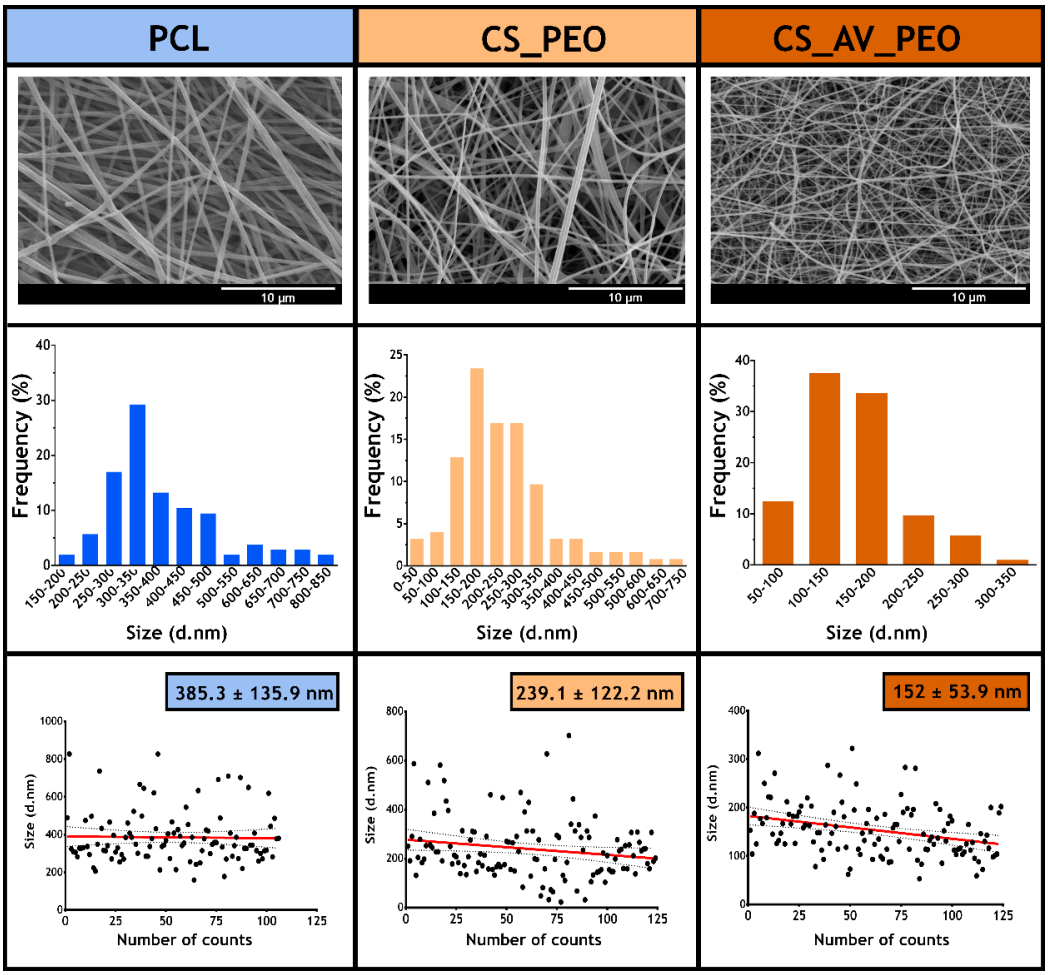

Figure 3.2. Characterization of the produced asymmetric membranes morphologic features. SEM images, fiber diameters distribution and the diameters of different fibers of the top layer (PCL) and bottom layers (CS_PEO or CS_AV_PEO) of the produced bilayer membranes are presented.

3.3.2 Attenuated total reflectance-fourier transform infrared spectroscopic analysis

The acquired ATR-FTIR spectra of raw materials and of the produced membranes are presented in Figure 3.3. The spectrum of the top layer (Figure 3.3A) presents its characteristic peaks at 2942 cm^{-1} (I) (asymmetric CH_2 stretching), 2 868 cm^{-1} (symmetric CH_2 stretching), 1723 cm^{-1} (II) (carbonyl stretching), 1292 cm^{-1} (C-O and C-C stretching), 1239 cm^{-1} (asymmetric C-O-C stretching) and 1161 cm^{-1} (symmetric C-O-C stretching) [54, 55]. In Figure 3.3B, it is possible observe the characteristic bands of PEO in the region between 2900 cm^{-1} and 2850 cm^{-1} (CH_2 (band I)) [56]. Furthermore, the spectrum of the CS_AV_PEO layer (Figure 3.3B) displays the characteristic peaks of AV at 1714 (O-acetyl esters (band II)), 1592 (asymmetrical COO^- stretching (band III)), 1246 (glucan units), 1030 (glycosidic bond), and 606 cm^{-1} (C–H ring vibration). Additionally, the bottom layer also exhibits peaks at 2876 cm^{-1} (aliphatic C–H stretch), 1586 cm^{-1} (NH_2 stretch), 1372 cm^{-1} (–C–O stretching of the primary alcohol group) and at 1028 cm^{-1} (C–O–C glycosidic bond (band IV)) that belong to CS [57, 58].

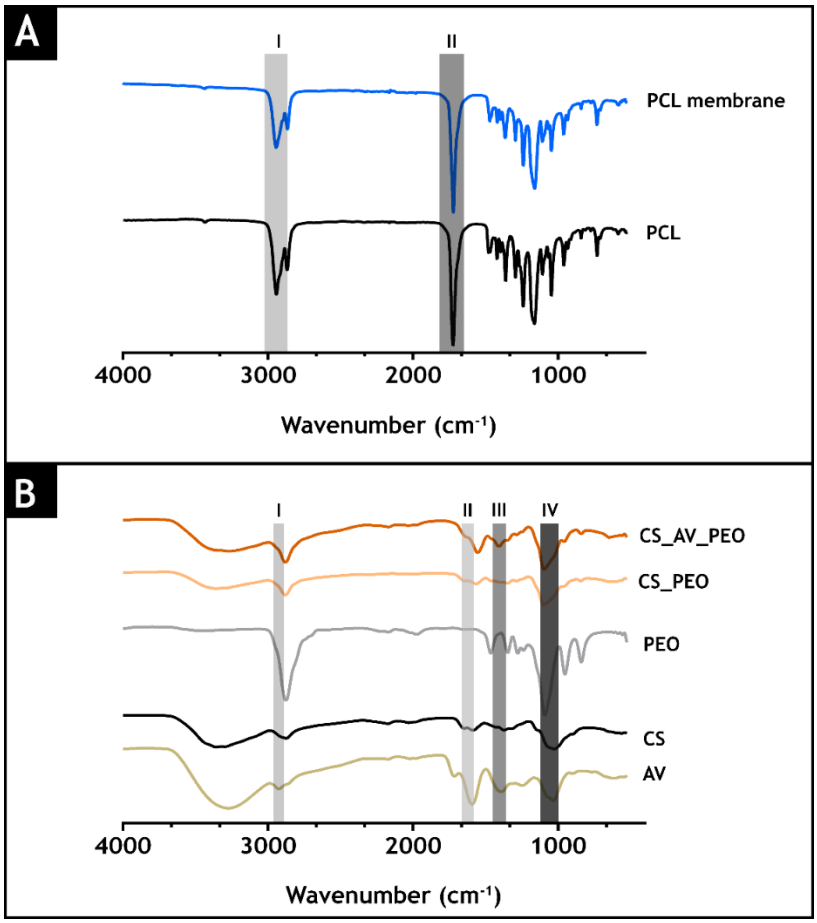

Figure 3.3. ATR-FTIR of the produced membranes and of their raw materials: top (A) and bottom layers (B).

3.3.3 Characterization of the membrane's mechanical properties

Membranes to be used as wound dressings must present mechanical properties that can support angiogenesis, the lymphatic system, nerve bundles, and other structures found in native skin [59-61]. Herein, the mechanical properties of the produced membranes were evaluated in dry and wet conditions [62].

Through the analysis of the stress-strains curves (Figure 3.4), it is possible to notice that the membranes display a two-stage fracture in the dry state. Such a result is explained by the presence of natural polymers (CS and AV) in the bottom layer that have weaker mechanical properties. In the wet state the membranes do not show the two stage break, since CS and AV are less brittle in wet conditions [15, 63]. PCL/CS_PEO membranes presented a Young Modulus of 46.89 ± 3.78 MPa in dry state, whereas in wet conditions a value of 22.76 ± 2.17 MPa was obtained (Figure 3.4). Such increase in the elasticity was also observed for PCL/CS_AV_PEO membranes, *i.e.*, 36.53 ± 1.29 MPa and 27.14 ± 3.56 MPa for the dry and wet state, respectively. Moreover, in the wet state, the PCL/CS_PEO and PCL/CS_AV_PEO membranes displayed tensile strengths of 9.40 ± 2.40 MPa and 6.23 ± 0.33 MPa, respectively.

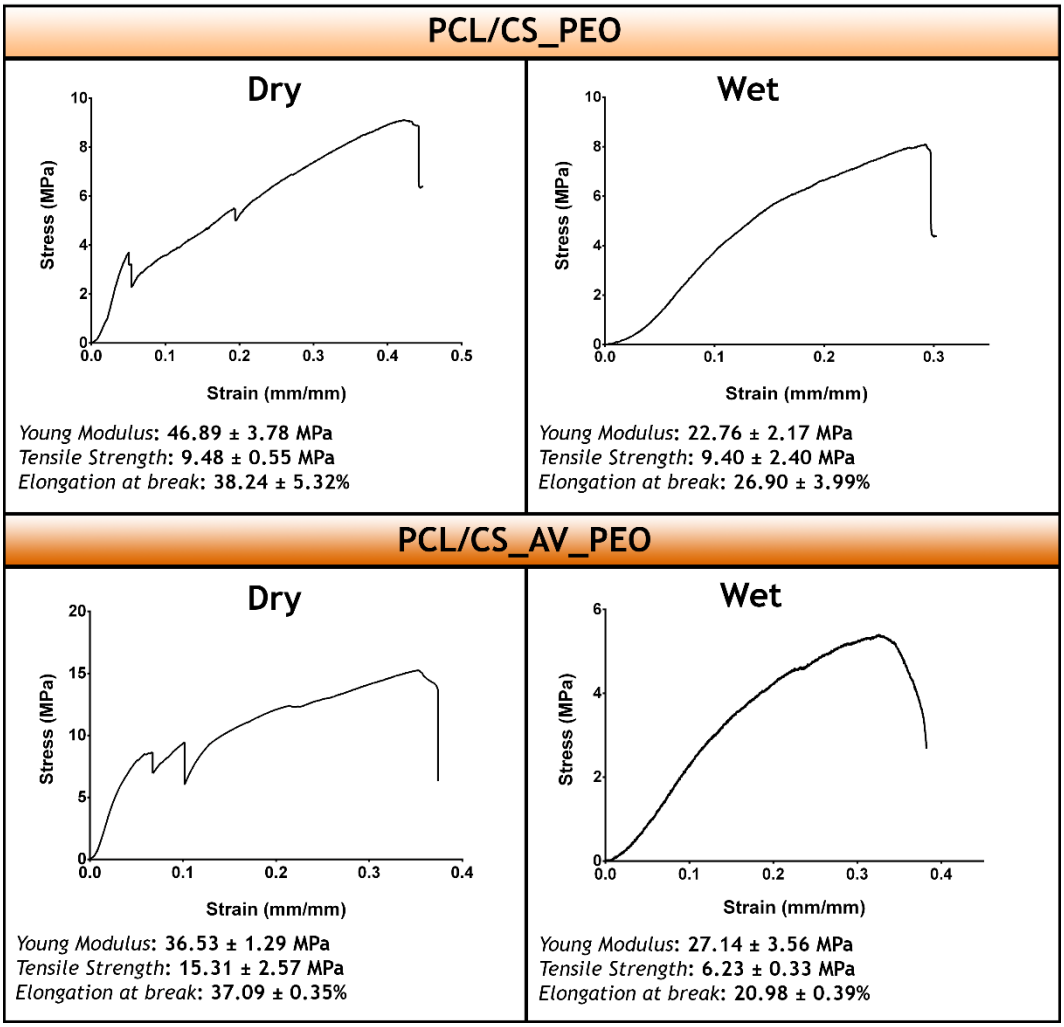

Figure 3.4. Typical stress-strain curves and mechanical properties determined for the produced membranes in dry and wet conditions. Young´s modulus, tensile strength, and elongation at break of PCL/CS_PEO and PCL/CS_AV_PEO membranes.

On the other hand, in the dry state, the PCL/CS_PEO and PCL/CS_AV_PEO membranes presented tensile strengths of 9.48 ± 0.55 MPa and 15.31 ± 2.57 MPa, respectively. The elongation-to-break assays revealed that PCL/CS_PEO and PCL/CS_AV_PEO membranes can bear a strain of 26.90 ± 3.99% and 20.98 ± 0.39% for the wet state and 38.24 ± 5.32% and 37.09 ± 0.35% for the dry state, correspondingly. Despite the samples presenting a different behavior in dry and wet conditions, the produced membranes show a Young modulus, tensile strengths, and elongation-to-break values that are very close to that displayed by native skin (Young modulus (4.6–20.0 MPa), tensile strengths (5.00–30.00 MPa) and elongation-to-break (35.00–115.00%)). This emphasizes the suitability of the produced membranes to confer adequate mechanical support during the tissue remodeling process, as well as, avoiding possible side effects resulting from the stress-shielding mechanism [60, 64]. The excellent mechanical performance of the produced membranes can be explained by the presence of PCL within the top layer. In the literature, it has been widely described that this synthetic polymer is capable of providing enhanced mechanical properties due to its chemical and thermal stability [65, 66].

3.3.4 Characterization of the membrane' porosity

In the area of tissue engineering, the porosity of a material is essential to provide void spaces for cell accommodation, migration and also for the exchange of nutrients between the 3D construct and the surrounding environment [50]. Herein, a liquid displacement method was used to determine membrane porosity (ethanol was used as displacement fluid) [67]. The data obtained is presented in Figure 3.5A and reveals that top layer (PCL) displays the lowest porosity (55 ± 5%), which is essential for avoiding microorganism penetration [15, 41]. On the other hand, the bottom layers, composed of CS_PEO or CS_AV_PEO, showed porosities of 89.5 ± 5.3 and 97.8 ± 4.5%, respectively. Such results can be explained by the higher number of spaces available between the CS_AV_PEO nanofibers, which have a lower diameter. Several researchers have previously highlighted that materials with porosities above 90% are the most appropriate for skin tissue engineering applications since they are able to provide the required space for cell accommodation, migration, nutrient exchange, and production of a new ECM [46, 68-72].

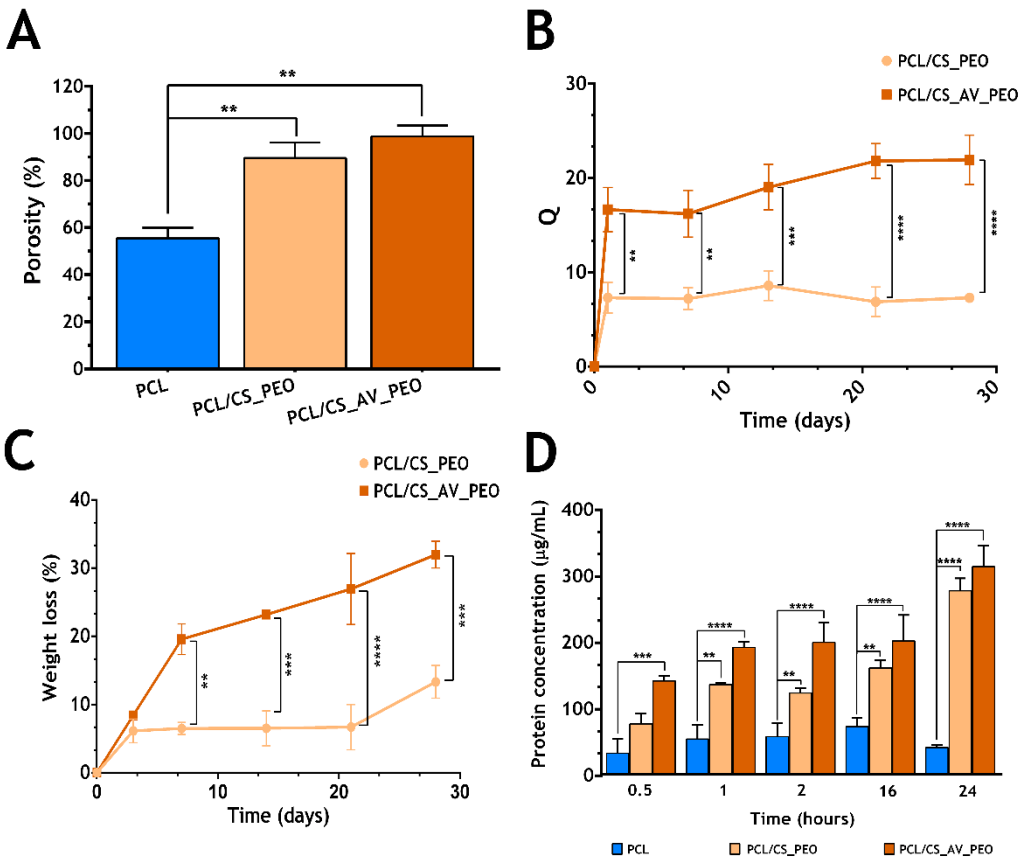

Figure 3.5. Characterization of the total porosity (A), swelling profile (B), weight loss (C), and protein adsorption (D) on the membrane's surface at different time points.

3.3.5 Membrane surface wettability

Material surface wettability is a crucial parameter that affects cell adhesion, proliferation, and differentiation [73]. The surface wettability is usually characterized by determining the WCA [74-76]. In the literature, it is described that cells are more prone to adhere, spread, and grow on moderate hydrophilic substrates (40° < WCA < 70°) than on hydrophobic (WCA > 90°) or very hydrophilic ones (WCA < 20°) [21, 77, 78].

In the present study, the membranes' top layer exhibited a hydrophobic character (WCA of 126.2° ± 1.21°), due to the presence of aliphatic polyester PCL [79, 80]. Conversely, CS_PEO and CS_AV_PEO layers presented WCA values of 75.58° ± 12.57° and 69.06° ± 3.78° which are characteristic of moderate hydrophilic materials. Such WCA values can be explained by the presence of natural polymers (CS and AV) that have functional groups like amides, esters, and hydroxyl groups which confer hydrophilic character to the bottom layer [81, 82]. During the wound healing process, hydrophilic materials are able to provide moist environments, that enhance the healing process [83].

3.3.6 Water vapor transmission rate

As described above, an ideal wound dressing besides providing a moist environment, must also avoid wound dehydration, as well as be capable of removing the wound exudate [15, 21, 43]. An accumulation of exudate at the wound site leads to the breakdown of ECM components or to the maceration of the healthy surrounding tissues, that ultimately induces more pain to the patient [84]. Furthermore, it has been reported that wound dressings with WVTRs values ranging from 2000–2500 g/m^2/day provide an adequate level of moisture and prevent exudate accumulation [85].

Herein, the produced membranes showed similar WVTR values: The PCL/CS_PEO membrane displayed a WVTR of 1452.61 ± 86.08 g/m^2/day, while the PCL/CS_AV_PEO had a value of 1252.35 ± 21.22 g/m^2/day. Although the determined WVTR values are outside the range of that displayed by an ideal dressing, there are several commercially available wound dressings that have WVTR values outside this range, like Tegaderm™ (3M, Maplewood, MN, USA), Bioclusive™ (Johnson-Johnson, New Brunswick, NJ, USA), and Op Site (Smith & Nephew, London, UK), which have WVTRs of 491 ± 44, 394 ± 12, and 792 ±32 g/m^2/day, respectively [86-89].

3.3.7 Characterization of the membranes' swelling profile

The characterization of the swelling profile of the membranes is fundamental to evaluate the capacity of these membranes to absorb the wound exudate. To accomplish that, membranes were incubated in a PBS solution and their weight was monitored at specific timepoints.

The obtained results showed that the PCL/CS_AV_PEO membrane displays a higher water absorption ratio (≈ 20) than the PCL/CS_PEO membrane (≈ 10) (Figure 3.5B). Such a result is explained by the incorporation of hydrophilic materials in the composition of membranes [21, 31, 34, 35]. Furthermore, the swelling profile displayed by the membranes is compatible with the removal of the excess of exudate from the wound, which is usually produced during the inflammatory phase of the healing process (1–3 days after the injury occurs). Based on this data, the PCL/CS_AV_PEO membranes are the ones more appropriate to absorb any excess of exudate that may be present in the wound.

3.3.8 Characterization of degradation profile of the membranes

Commercially available wound dressings are usually non-degradable and they need to be removed from the wound. Such removal can affect the healing process since it can induce the formation of scar tissue as well as increase the risk of bacterial contamination [78, 90]. To overcome this drawback, researchers started to produce biodegradable wound dressings. However, their rate of degradation must be proportional to the rate of healing or regeneration of the compromised tissue [91, 92].

Herein, the degradation profile of the developed membranes was studied using lysozyme, an enzyme found in human serum, which is capable of degrading CS-based materials in vivo [93, 94]. The results obtained revealed that after 30 days of incubation, the PCL/CS_AV_PEO and PCL/CS_PEO membranes had weight losses of ≈ 30% and ≈ 10%, respectively (Figure 3.5C). Such variation in weight is explained by AV capacity to reduce the number of interactions occurring between CS molecules, thus facilitating the enzymatic degradation [35]. Despite PCL displaying a slow degradation profile in vitro [79], it is expected that under in vivo conditions it degrades faster. A variety of enzymes, like matrix metalloproteinase (MMP-1), gelatinase-A (MMP-2), and stromelysin-1 (MMP-3) are secreted by macrophages, epidermal cells, and fibroblasts during the wound healing process and may contribute to the enzymatic breakdown of PCL [95-97].

3.3.9 Evaluation of protein adsorption on the membranes' surface

When a wound dressing is placed at the wound site, it is exposed to body fluids and almost immediately the proteins present in these fluids become adsorbed onto the dressing's surface. Protein adsorption can have a direct impact on the material's biocompatibility since it can influence cellular attachment [76, 98, 99]. Indeed, cells adhere to proteins adsorbed on material surfaces through membrane receptors that recognize specific amino acid sequences present in adhesive proteins (*e.g.* fibronectin, and vitronectin) [100].

Herein, to characterize protein adsorption to the PCL, PCL/CS_PEO and PCL/CS_AV_PEO membranes´ surface, albumin was used as a model protein (Figure 3.5D). Albumin is the most abundant protein in serum and after an injury occurs this protein is accumulated at the wound

site, during the early phase of the healing process. Subsequently, the absorbed albumin is replaced by fibronectin and vitronectin [76]. The results obtained revealed that albumin did not become adsorbed onto the PCL membrane (Figure 3.5D), as previously reported in the literature [101, 102]. Conversely, the concentration of protein adsorbed onto PCL/CS_PEO and PCL/CS_AV_PEO membranes increases with time and no statistically significant difference was noticed between these samples. Such a finding was expected since both membranes exhibit rough, porous and hydrophilic surfaces (WCA < 90°). Furthermore, other authors claim that the protein adsorption at the membranes' surface can occur through the interaction of proteins with the amine groups of CS, which have a high affinity for negatively charged groups found on proteins and cell membranes [103-105].

3.3.10 Evaluation of cell viability and proliferation in the presence of membranes

The wound healing process is known by its complexity and interaction of different cell types with matrix components that act together to re-establish the 3D structure and the functions of the damaged tissue. Herein, NHDF cells, enrolled in the synthesis of collagen, fibronectin, and other biomolecules were used to evaluate the cell response to the presence of the developed membranes [106].

Optical microscopic images of the NHDF cells in contact with membranes after 1, 3, and 7 days are presented in Figure 3.6. These images show that NHDF cells did not suffer any morphological variation when in contact with the membranes, displaying a similar shape to those of K^-, where cells were incubated with culture medium. Moreover, the cytotoxic profile of the membranes was evaluated through an MTS assay, over 1, 3, and 7 days (Figure 3.7A). The results revealed that all membranes did not induce any cytotoxic effect on NHDFs, over 7 days. Furthermore, the dsDNA quantification results (Figure 3.7B) are compliant with the data obtained in the MTS assay, suggesting that NHDFs remain viable and proliferate over at least 7 days, when they are seeded in contact with the produced membranes.

Besides being biocompatible, a wound dressing must also promote cell attachment, growth, and proliferation. Herein, the cell adhesion to the surface of the membranes was characterized by SEM analysis (Figure 3.7C). The obtained SEM images evidenced the bioadhesive character of the bottom layer of the produced membranes. After 7 days of incubation, it was possible to visualize that cells adhere and proliferate on the nanofibrous network, which is crucial for tissue regeneration [107]. Additionally, CLSM analysis was also performed and the acquired images (Figure 3.8) demonstrate that, after 3 days of incubation, the fibroblast cells have a higher attachment, proliferation, and growth when they are in contact with the PCL/CS_AV_PEO membranes, in comparison to the PCL/CS_PEO ones.

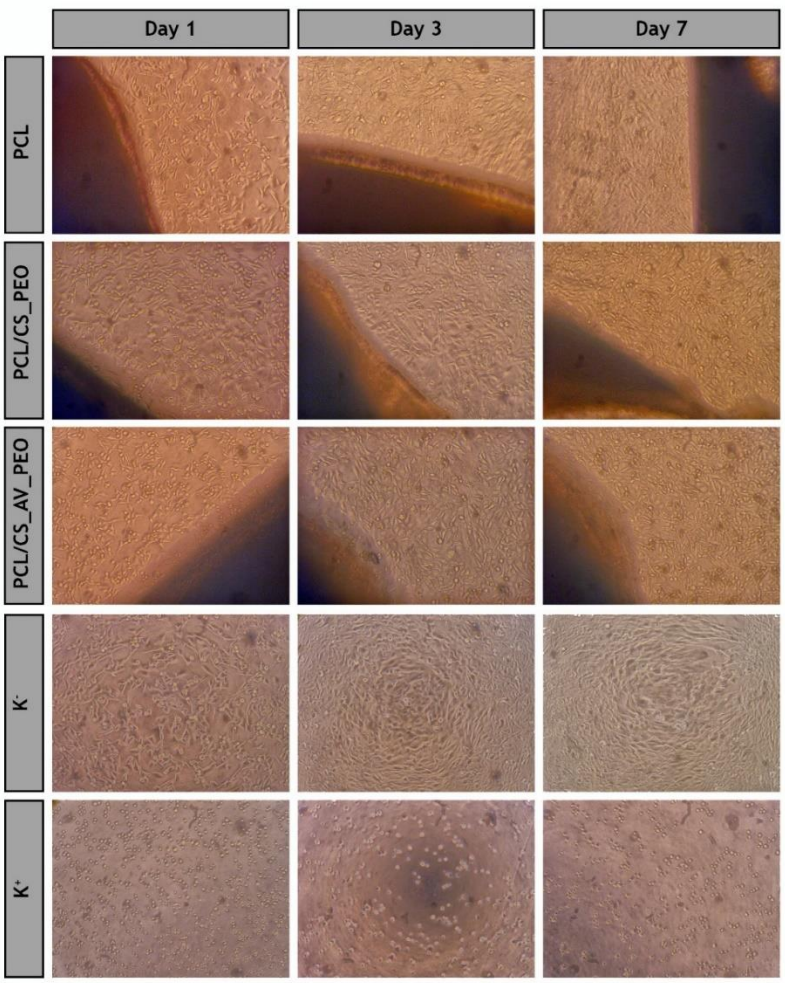

Figure 3.6. Optical microscopic images of Normal Human Dermal Fibroblast (NHDF) cells in the presence of the different produced membranes (PCL, PCL/CS_PEO and PCL/CS_AV_PEO) after 1, 3, and 7 days of incubation; K^- (negative control); K^+ (positive control).

Similar results have been already reported for other materials that have AV in their composition [108]. The exact mechanisms through which AV stimulates cell proliferation and growth factor production in fibroblasts are still unknown. Previous studies speculated that AV interacts with the growth factor receptors of the fibroblasts and stimulates cell activity and proliferation [36, 109]. Such interaction occurs between the active components, such as mannose-6-phosphate and/or acemannan, present in AV and the mannose receptor available on the fibroblast's surface [110, 111]. The results obtained through the color-coded depth analysis of the membranes showed that fibroblasts migrate to the interior of the membrane, with some cells being observed between 8–10 μm within the polymeric structure, after 3 days of incubation (Figure 3.8). Such data emphasize that the pores available on the bottom layers allow cellular internalization, and also provide an effective nutrient supply and metabolic waste removal, thus leading to the restoring of the structure and functions of the native tissue [21, 112].

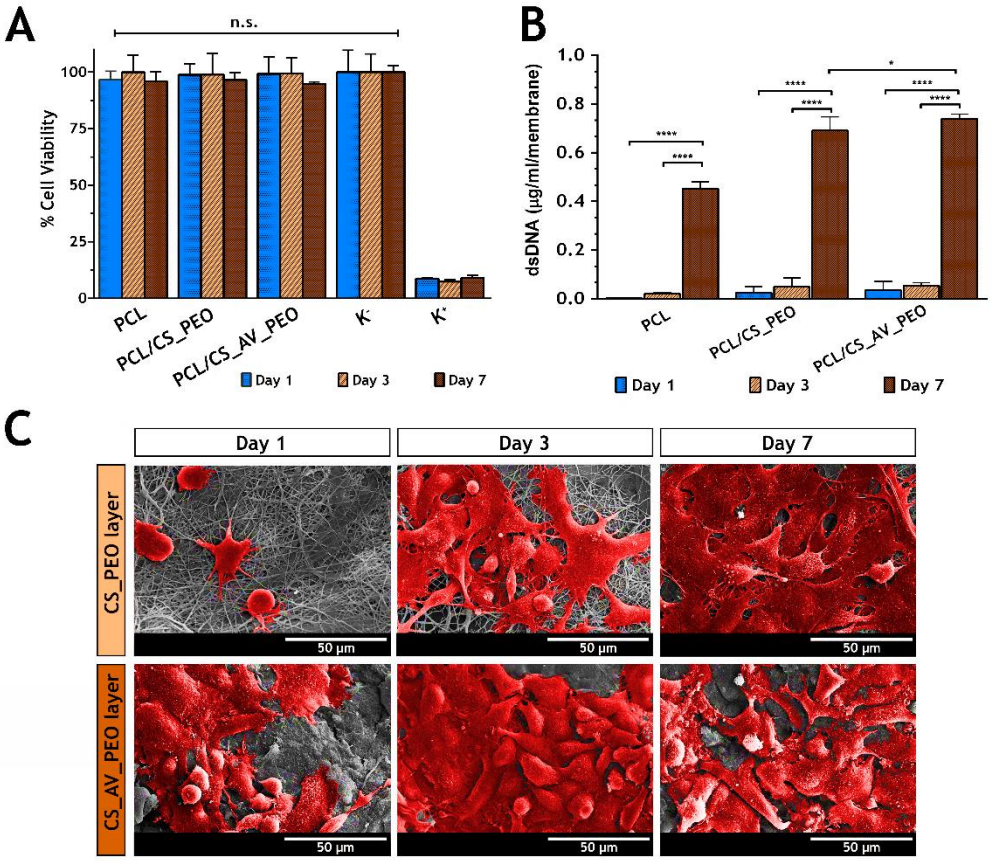

Figure 3.7. Characterization of the biological performance of the produced membranes. NHDF cell viability was evaluated when the cells were incubated with produced membranes (A) and the content of dsDNA of NHDF cells adhered to the surface of the developed membranes was determined after 1, 3, and 7 days of incubation (B). The statistical analysis of the results was performed using one-way ANOVA with Newman–Keuls test SEM micrographs of NHDF cells morphology at the surface of the different electrospun membranes after 1, 3, and 7 days are presented in (C).

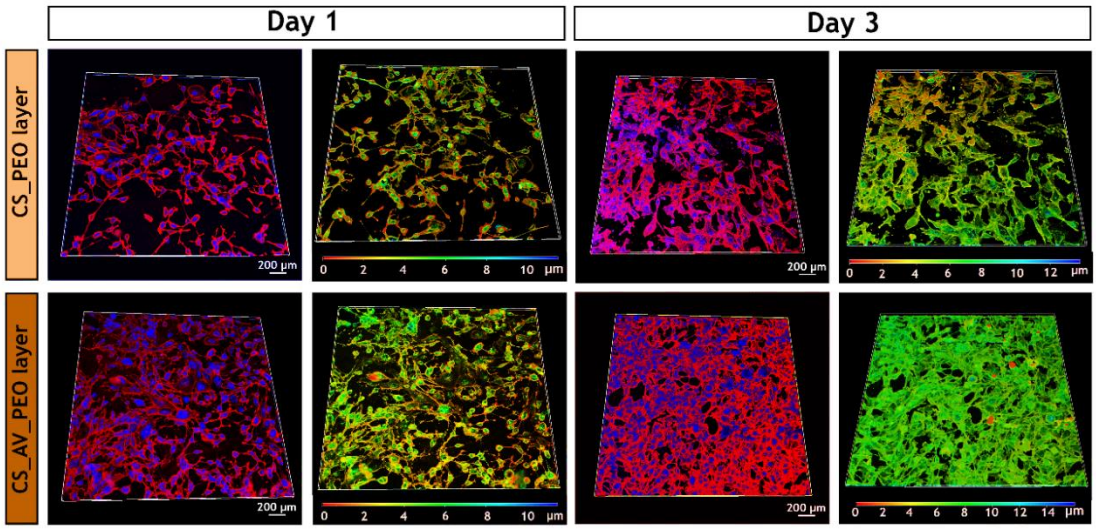

Figure 3.8. CLSM images of fibroblast cells cultured on the surface of CS_PEO and CS_AV_PEO layers and color coded depth analysis (red 0 µm, blue 10–14 µm) after 1 and 3 days. Blue channel: cell nuclei labeled Hoechst 33342®; red channel: cytoplasm stained with WGA-Alexa 594® conjugate.

3.3.11 Characterization of the antimicrobial properties of the produced membranes

Skin injuries are prone to microorganism contamination, that can often interrupt the healing process and lead to life-threatening complications. Such are the demands for wound dressings capable of avoiding bacterial invasion and growth. In this study, the antimicrobial properties of the produced membranes were characterized by using *S. aureus* (gram-positive bacterium) and *E. coli* (gram-negative bacterium) as models [113, 114]. The results presented in Figure 3.9 show that the top layer of the produced membranes acts as protective barrier, avoiding the infiltration of the model bacteria. The data obtained for this layer does not show any significant statistical difference with the control group, where filter paper (with pore size of 0.22 µm) was used.

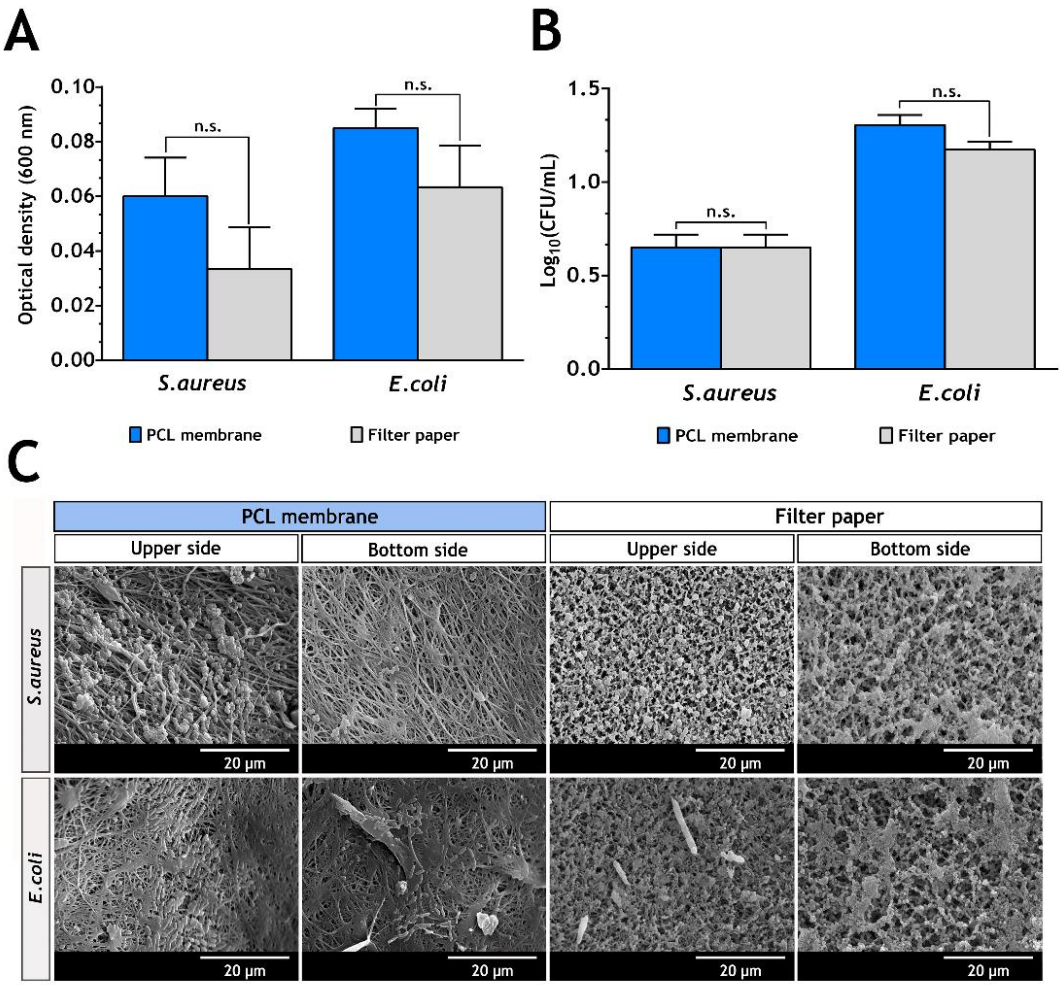

Figure 3.9. Evaluation of the bacterial infiltration through the PCL membrane and filter paper (control group). The optical density of the medium culture present in the lower chamber of the transwell system determined at 600 nm is shown in (A); The number of colony forming units of *S.aureus* and *E. coli* that cross the PCL and filter paper, after 24 h, are displayed in (B); SEM images of adhered microorganisms (*S. aureus* and *E. coli*) at the upper and lower side of the PCL membrane and filter paper are observed in (C).

SEM images also evidenced that few bacteria were able to adhere to the upper side of the top layer. Such results can be explained by the low porosity of the PCL layer, that hampers the entrance of microorganisms into the wound. Additionally, the capacity of the bottom layers (CS_PEO and CS_AV_PEO) to provide an aseptic environment at the wound site was also evaluated. To accomplish this, membranes were incubated over 24 h with bacteria. Both bottom layers (CS_PEO and CS_AV_PEO) showed an inhibitory effect on *S.aureus* and *E. coli* growth (see Figure 3.10A and 3.10B). Furthermore, no biofilm formation on the membrane's surface was noticed (see Figure 3.10C for further details) due to the intrinsic bactericidal activity of CS and AV.

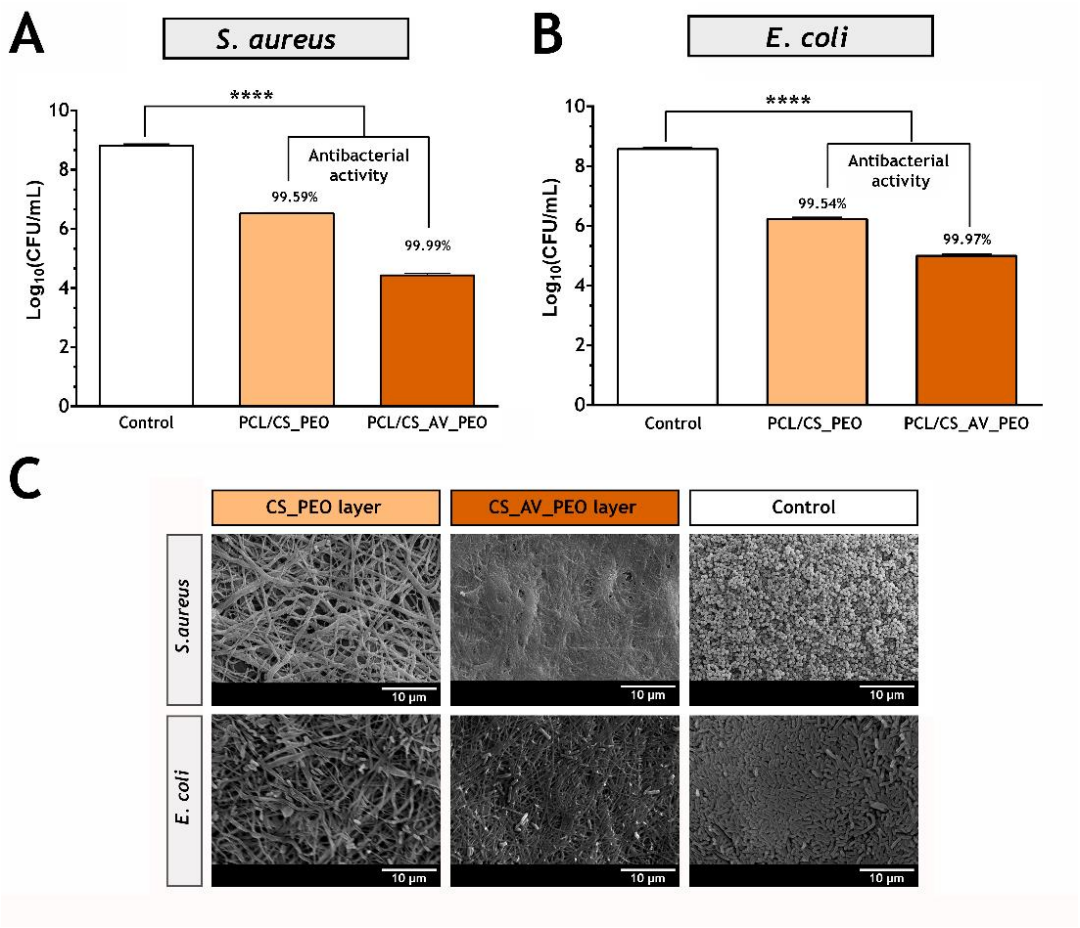

Figure 3.10. Evaluation of the produced membranes bactericidal activity. The antibacterial activity of PCL/CS_PEO and PCL/CS_AV_PEO membranes against *S. aureus* and *E. coli* is presented in (A) and (B), respectively; SEM images of *S.aureus* and *E. coli* in contact with PCL/CS_PEO and PCL/CS_AV_PEO membranes and of the negative controls are displayed in (C).

In the literature, it has been described that this polycationic polymer interacts with the negatively charged groups present at the bacteria surface, leading to an increased cell wall permeability and consequently the leakage of intracellular constituents and the dissipation of the ionic gradients that exist in bacteria [21, 115-117]. Furthermore, the positive charge density can be increased through a deacetylation process. Herein, the CS deacetylation degree was set to about 98% (see Table 3.1), *i.e.* almost all the primary amine groups of CS were

positively charged and are available to interact with the negatively charged groups present in the bacterial cell wall. Additionally, the acemannan, anthraquinones, and salicylic acid present in AV gel also contribute to the bactericidal activity displayed by the produced membranes [35, 118].

Table 3.1. Degree of deacetylation of the different chitosan samples used in this study (*n*= 3).

Sample	Nominal DD [a] (%)	Determined DD [b] (%)
(1) Comercial CS	75–85	82.02 ± 1.87
(2) Purified CS	—	97.88 ± 1.19

[a] Provided by the manufacturer; [b] Determined by 1DUVS.

3.4 Conclusions

In this study, electrospinning technology was used to produce asymmetric membranes composed of PCL, CS, PEO and in some cases AV. The asymmetric structure of the membranes was conceived to mimic skin native structure. The top layer confers protection to the wound against external threats and, simultaneously, the bottom layer encourages cell migration and proliferation. The results attained show that the incorporation of AV in a CS_PEO nanofiber system enabled the production of a bottom layer capable of providing adequate moisture at the wound site as well as promoting better and faster fibroblast attachment and proliferation. In addition, the produced membranes presented mechanical properties and antimicrobial activity that are compatible with their applications as wound dressings.

In the near future, the incorporation of other bioactive molecules (*e.g.* ECM components, vitamins or GFs) can be considered as a means to further improve the performance of these membranes in wound repair or other envisioned biomedical applications.

3.5 References

1. MacNeil S. Biomaterials for tissue engineering of skin. Materials today. 2008;11(5):26-35.
2. Peck MD. Epidemiology of burns throughout the world. Part I: Distribution and risk factors. Burns. 2011;37(7):1087-100.
3. Peck MD. Epidemiology of burns throughout the World. Part II: intentional burns in adults. Burns. 2012;38(5):630-7.
4. Madaghiele M, Demitri C, Sannino A, Ambrosio L. Polymeric hydrogels for burn wound care: Advanced skin wound dressings and regenerative templates. Burns & Trauma. 2015;2(4):153-61.
5. Rieger KA, Birch NP, Schiffman JD. Designing electrospun nanofiber mats to promote wound healing–a review. Journal of Materials Chemistry B. 2013;1(36):4531-41.
6. Nyame TT, Chiang HA, Orgill DP. Clinical applications of skin substitutes. Surgical Clinics of North America. 2014;94(4):839-50.

7. Sun BK, Siprashvili Z, Khavari PA. Advances in skin grafting and treatment of cutaneous wounds. Science. 2014;346(6212):941-5.
8. Greaves NS, Iqbal SA, Baguneid M, Bayat A. The role of skin substitutes in the management of chronic cutaneous wounds. Wound repair and regeneration. 2013;21(2):194-210.
9. Catalano E, Cochis A, Varoni E, Rimondini L, Azzimonti B. Tissue-engineered skin substitutes: an overview. Journal of Artificial Organs. 2013;16(4):397-403.
10. Morgado PI, Aguiar-Ricardo A, Correia IJ. Asymmetric membranes as ideal wound dressings: An overview on production methods, structure, properties and performance relationship. Journal of Membrane Science. 2015;490:139-51.
11. Xu H, Chang J, Chen Y, Fan H, Shi B. Asymmetric polyurethane membrane with inflammation-responsive antibacterial activity for potential wound dressing application. Journal of Materials Science. 2013;48(19):6625-39.
12. Liang D, Lu Z, Yang H, Gao J, Chen R. Novel asymmetric wettable AgNPs/chitosan wound dressing: in vitro and in vivo evaluation. ACS applied materials & interfaces. 2016;8(6):3958-68.
13. Liao N, Unnithan AR, Joshi MK, Tiwari AP, Hong ST, Park C-H, Kim CS. Electrospun bioactive poly (ε-caprolactone)–cellulose acetate–dextran antibacterial composite mats for wound dressing applications. Colloids and Surfaces A: Physicochemical and Engineering Aspects. 2015;469:194-201.
14. Hinrichs W, Lommen E, Wildevuur CR, Feijen J. Fabrication and characterization of an asymmetric polyurethane membrane for use as a wound dressing. Journal of applied biomaterials. 1992;3(4):287-303.
15. Morgado PI, Lisboa PF, Ribeiro MP, Miguel SP, Simões PC, Correia IJ, Aguiar-Ricardo A. Poly (vinyl alcohol)/chitosan asymmetrical membranes: Highly controlled morphology toward the ideal wound dressing. Journal of membrane science. 2014;469:262-71.
16. Figueira DR, Miguel SP, de Sá KD, Correia IJ. Production and characterization of polycaprolactone-hyaluronic acid/chitosan-zein electrospun bilayer nanofibrous membrane for tissue regeneration. International journal of biological macromolecules. 2016;93:1100-10.
17. Wu C, Chen T, Xin Y, Zhang Z, Ren Z, Lei J, Chu B, Wang Y, Tang S. Nanofibrous asymmetric membranes self-organized from chemically heterogeneous electrospun mats for skin tissue engineering. Biomedical Materials. 2016;11(3):035019.
18. Rim NG, Shin CS, Shin H. Current approaches to electrospun nanofibers for tissue engineering. Biomedical materials. 2013;8(1):014102.
19. Huang Z-M, Zhang Y-Z, Kotaki M, Ramakrishna S. A review on polymer nanofibers by electrospinning and their applications in nanocomposites. Composites science and technology. 2003;63(15):2223-53.
20. Estellés JM, Vidaurre A, Duenas JMM, Cortázar IC. Physical characterization of polycaprolactone scaffolds. Journal of Materials Science: Materials in Medicine. 2008;19(1):189-95.
21. Miguel SP, Ribeiro MP, Brancal H, Coutinho P, Correia IJ. Thermoresponsive chitosan–agarose hydrogel for skin regeneration. Carbohydrate polymers. 2014;111:366-73.
22. Mi FL, Wu YB, Shyu SS, Schoung JY, Huang YB, Tsai YH, Hao JY. Control of wound infections using a bilayer chitosan wound dressing with sustainable antibiotic delivery. Journal of Biomedical Materials Research. 2002;59(3):438-49.

23. Aoyagi S, Onishi H, Machida Y. Novel chitosan wound dressing loaded with minocycline for the treatment of severe burn wounds. International journal of pharmaceutics. 2007;330(1):138-45.
24. Chen J-P, Chang G-Y, Chen J-K. Electrospun collagen/chitosan nanofibrous membrane as wound dressing. Colloids and Surfaces A: Physicochemical and Engineering Aspects. 2008;313:183-8.
25. Antunes B, Moreira A, Gaspar V, Correia I. Chitosan/arginine–chitosan polymer blends for assembly of nanofibrous membranes for wound regeneration. Carbohydrate polymers. 2015;130:104-12.
26. Mogoşanu GD, Grumezescu AM. Natural and synthetic polymers for wounds and burns dressing. International journal of pharmaceutics. 2014;463(2):127-36.
27. Kim I-Y, Seo S-J, Moon H-S, Yoo M-K, Park I-Y, Kim B-C, Cho C-S. Chitosan and its derivatives for tissue engineering applications. Biotechnology advances. 2008;26(1):1-21.
28. An J, Zhang H, Zhang J, Zhao Y, Yuan X. Preparation and antibacterial activity of electrospun chitosan/poly (ethylene oxide) membranes containing silver nanoparticles. Colloid and Polymer Science. 2009;287(12):1425-34.
29. Zhang Y, Huang X, Duan B, Wu L, Li S, Yuan X. Preparation of electrospun chitosan/poly (vinyl alcohol) membranes. Colloid and Polymer Science. 2007;285(8):855-63.
30. Duan B, Yuan X, Zhu Y, Zhang Y, Li X, Zhang Y, Yao K. A nanofibrous composite membrane of PLGA–chitosan/PVA prepared by electrospinning. European Polymer Journal. 2006;42(9):2013-22.
31. Hamman JH. Composition and applications of Aloe vera leaf gel. Molecules. 2008;13(8):1599-616.
32. Eshun K, He Q. Aloe vera: a valuable ingredient for the food, pharmaceutical and cosmetic industries—a review. Critical reviews in food science and nutrition. 2004;44(2):91-6.
33. Maenthaisong R, Chaiyakunapruk N, Niruntraporn S, Kongkaew C. The efficacy of aloe vera used for burn wound healing: a systematic review. Burns. 2007;33(6):713-8.
34. Silva S, Caridade S, Mano J, Reis R. Effect of crosslinking in chitosan/aloe vera-based membranes for biomedical applications. Carbohydrate polymers. 2013;98(1):581-8.
35. Silva S, Popa EG, Gomes ME, Cerqueira M, Marques A, Caridade S, Teixeira P, Sousa C, Mano J, Reis R. An investigation of the potential application of chitosan/aloe-based membranes for regenerative medicine. Acta biomaterialia. 2013;9(6):6790-7.
36. Suganya S, Venugopal J, Mary SA, Ramakrishna S, Lakshmi B, Dev VG. Aloe vera incorporated biomimetic nanofibrous scaffold: a regenerative approach for skin tissue engineering. Iranian Polymer Journal. 2014;23(3):237-48.
37. Suganya S, Venugopal J, Ramakrishna S, Lakshmi B, Dev VG. Naturally derived biofunctional nanofibrous scaffold for skin tissue regeneration. International journal of biological macromolecules. 2014;68:135-43.
38. Muzzarelli RA, Rocchetti R. Determination of the degree of acetylation of chitosans by first derivative ultraviolet spectrophotometry. Carbohydrate Polymers. 1985;5(6):461-72.
39. Wei J, Igarashi T, Okumori N, Igarashi T, Maetani T, Liu B, Yoshinari M. Influence of surface wettability on competitive protein adsorption and initial attachment of osteoblasts. Biomedical Materials. 2009;4(4):045002.

40. Yang F, Both SK, Yang X, Walboomers XF, Jansen JA. Development of an electrospun nano-apatite/PCL composite membrane for GTR/GBR application. Acta biomaterialia. 2009;5(9):3295-304.

41. Mi F-L, Shyu S-S, Wu Y-B, Lee S-T, Shyong J-Y, Huang R-N. Fabrication and characterization of a sponge-like asymmetric chitosan membrane as a wound dressing. Biomaterials. 2001;22(2):165-73.

42. Levard C, Mitra S, Yang T, Jew AD, Badireddy AR, Lowry GV, Brown Jr GE. Effect of chloride on the dissolution rate of silver nanoparticles and toxicity to E. coli. Environmental science & technology. 2013;47(11):5738-45.

43. Lin W-C, Lien C-C, Yeh H-J, Yu C-M, Hsu S-h. Bacterial cellulose and bacterial cellulose-chitosan membranes for wound dressing applications. Carbohydrate polymers. 2013;94(1):603-11.

44. Mi F-L, Wu Y-B, Shyu S-S, Chao A-C, Lai J-Y, Su C-C. Asymmetric chitosan membranes prepared by dry/wet phase separation: a new type of wound dressing for controlled antibacterial release. Journal of Membrane Science. 2003;212(1-2):237-54.

45. Reis TC, Correia IJ, Aguiar-Ricardo A. Electrodynamic tailoring of self-assembled three-dimensional electrospun constructs. Nanoscale. 2013;5(16):7528-36.

46. Chong E, Phan T, Lim I, Zhang Y, Bay B, Ramakrishna S, Lim C. Evaluation of electrospun PCL/gelatin nanofibrous scaffold for wound healing and layered dermal reconstitution. Acta biomaterialia. 2007;3(3):321-30.

47. Merrell JG, McLaughlin SW, Tie L, Laurencin CT, Chen AF, Nair LS. Curcumin-loaded poly (ε-caprolactone) nanofibres: Diabetic wound dressing with anti-oxidant and anti-inflammatory properties. Clinical and experimental pharmacology and physiology. 2009;36(12):1149-56.

48. Venugopal JR, Zhang Y, Ramakrishna S. In vitro culture of human dermal fibroblasts on electrospun polycaprolactone collagen nanofibrous membrane. Artificial organs. 2006;30(6):440-6.

49. Zhang Y, Venugopal J, Huang Z-M, Lim C, Ramakrishna S. Characterization of the surface biocompatibility of the electrospun PCL-collagen nanofibers using fibroblasts. Biomacromolecules. 2005;6(5):2583-9.

50. Karuppuswamy P, Venugopal JR, Navaneethan B, Laiva AL, Sridhar S, Ramakrishna S. Functionalized hybrid nanofibers to mimic native ECM for tissue engineering applications. Applied surface science. 2014;322:162-8.

51. Kumbar SG, Nair LS, Bhattacharyya S, Laurencin CT. Polymeric nanofibers as novel carriers for the delivery of therapeutic molecules. Journal of nanoscience and nanotechnology. 2006;6(9-10):2591-607.

52. Khil MS, Cha DI, Kim HY, Kim IS, Bhattarai N. Electrospun nanofibrous polyurethane membrane as wound dressing. Journal of Biomedical Materials Research Part B: Applied Biomaterials. 2003;67(2):675-9.

53. Zhang Y, Lim CT, Ramakrishna S, Huang Z-M. Recent development of polymer nanofibers for biomedical and biotechnological applications. Journal of Materials Science: Materials in Medicine. 2005;16(10):933-46.

54. Catledge S, Clem W, Shrikishen N, Chowdhury S, Stanishevsky A, Koopman M, Vohra Y. An electrospun triphasic nanofibrous scaffold for bone tissue engineering. Biomedical materials. 2007;2(2):142.

55. Ghasemi-Mobarakeh L, Prabhakaran MP, Morshed M, Nasr-Esfahani M-H, Ramakrishna S. Electrospun poly (ε-caprolactone)/gelatin nanofibrous scaffolds for nerve tissue engineering. Biomaterials. 2008;29(34):4532-9.
56. Brugnerotto J, Lizardi J, Goycoolea F, Argüelles-Monal W, Desbrieres J, Rinaudo M. An infrared investigation in relation with chitin and chitosan characterization. Polymer. 2001;42(8):3569-80.
57. Inpanya P, Faikrua A, Ounaroon A, Sittichokechaiwut A, Viyoch J. Effects of the blended fibroin/aloe gel film on wound healing in streptozotocin-induced diabetic rats. Biomedical Materials. 2012;7(3):035008.
58. Chang X, Chen B, Feng Y. Water-soluble polysaccharides isolated from skin juice, gel juice and flower of Aloe vera Miller. Journal of the Taiwan Institute of Chemical Engineers. 2011;42(2):197-203.
59. Zahedi P, Rezaeian I, Ranaei-Siadat SO, Jafari SH, Supaphol P. A review on wound dressings with an emphasis on electrospun nanofibrous polymeric bandages. Polymers for Advanced Technologies. 2010;21(2):77-95.
60. Elsner JJ, Zilberman M. Novel antibiotic-eluting wound dressings: An in vitro study and engineering aspects in the dressing's design. Journal of tissue viability. 2010;19(2):54-66.
61. Elsner JJ, Shefy-Peleg A, Zilberman M. Novel biodegradable composite wound dressings with controlled release of antibiotics: microstructure, mechanical and physical properties. Journal of Biomedical Materials Research Part B: Applied Biomaterials. 2010;93(2):425-35.
62. Vatankhah E, Prabhakaran MP, Jin G, Mobarakeh LG, Ramakrishna S. Development of nanofibrous cellulose acetate/gelatin skin substitutes for variety wound treatment applications. Journal of biomaterials applications. 2014;28(6):909-21.
63. Morgado PI, Miguel SP, Correia IJ, Aguiar-Ricardo A. Ibuprofen loaded PVA/chitosan membranes: A highly efficient strategy towards an improved skin wound healing. Carbohydrate polymers. 2017;159:136-45.
64. Zahouani H, Pailler-Mattei C, Sohm B, Vargiolu R, Cenizo V, Debret R. Characterization of the mechanical properties of a dermal equivalent compared with human skin in vivo by indentation and static friction tests. Skin research and technology. 2009;15(1):68-76.
65. Chang KY, Hung LH, Chu I, Ko CS, Lee YD. The application of type II collagen and chondroitin sulfate grafted PCL porous scaffold in cartilage tissue engineering. Journal of Biomedical Materials Research Part A. 2010;92(2):712-23.
66. Xue J, Feng B, Zheng R, Lu Y, Zhou G, Liu W, Cao Y, Zhang Y, Zhang WJ. Engineering ear-shaped cartilage using electrospun fibrous membranes of gelatin/polycaprolactone. Biomaterials. 2013;34(11):2624-31.
67. Fradique R, Correia T, Miguel S, de Sá K, Figueira D, Mendonça A, Correia I. Production of new 3D scaffolds for bone tissue regeneration by rapid prototyping. Journal of Materials Science: Materials in Medicine. 2016;27(4):1-14.
68. Freyman T, Yannas I, Gibson L. Cellular materials as porous scaffolds for tissue engineering. Progress in materials science. 2001;46(3-4):273-82.
69. Dagalakis N, Flink J, Stasikelis P, Burke J, Yannas I. Design of an artificial skin. Part III. Control of pore structure. Journal of biomedical materials research. 1980;14(4):511-28.
70. Chen G, Ushida T, Tateishi T. Scaffold design for tissue engineering. Macromolecular Bioscience. 2002;2(2):67-77.

71. Griffith LG. Emerging design principles in biomaterials and scaffolds for tissue engineering. Annals of the New York Academy of Sciences. 2002;961(1):83-95.
72. Ma PX, Choi J-W. Biodegradable polymer scaffolds with well-defined interconnected spherical pore network. Tissue engineering. 2001;7(1):23-33.
73. Deligianni DD, Katsala ND, Koutsoukos PG, Missirlis YF. Effect of surface roughness of hydroxyapatite on human bone marrow cell adhesion, proliferation, differentiation and detachment strength. Biomaterials. 2000;22(1):87-96.
74. Oliveira SM, Alves NM, Mano JF. Cell interactions with superhydrophilic and superhydrophobic surfaces. Journal of Adhesion Science and Technology. 2014;28(8-9):843-63.
75. Cui W, Li X, Zhou S, Weng J. Degradation patterns and surface wettability of electrospun fibrous mats. Polymer Degradation and Stability. 2008;93(3):731-8.
76. Arima Y, Iwata H. Effect of wettability and surface functional groups on protein adsorption and cell adhesion using well-defined mixed self-assembled monolayers. Biomaterials. 2007;28(20):3074-82.
77. Khang G, Lee SJ, Lee JH, Kim YS, Lee HB. Interaction of fibroblast cells on poly (lactide-co-glycolide) surface with wettability chemogradient. Bio-medical materials and engineering. 1999;9(3):179-87.
78. Kumbar SG, Nukavarapu SP, James R, Nair LS, Laurencin CT. Electrospun poly (lactic acid-co-glycolic acid) scaffolds for skin tissue engineering. Biomaterials. 2008;29(30):4100-7.
79. Zhang Y, Ouyang H, Lim CT, Ramakrishna S, Huang ZM. Electrospinning of gelatin fibers and gelatin/PCL composite fibrous scaffolds. Journal of Biomedical Materials Research Part B: Applied Biomaterials. 2005;72(1):156-65.
80. Ranjbar-Mohammadi M, Bahrami SH. Electrospun curcumin loaded poly (ε-caprolactone)/gum tragacanth nanofibers for biomedical application. International journal of biological macromolecules. 2016;84:448-56.
81. Agnes Mary S, Giri Dev V. In vivo bioactivity of herbal-drug-incorporated nanofibrous matrixes. Journal of Applied Polymer Science. 2015;132(26).
82. Jithendra P, Rajam AM, Kalaivani T, Mandal AB, Rose C. Preparation and characterization of aloe vera blended collagen-chitosan composite scaffold for tissue engineering applications. ACS applied materials & interfaces. 2013;5(15):7291-8.
83. Atiyeh BS, Ioannovich J, Al-Amm CA, El-Musa KA. Management of acute and chronic open wounds: the importance of moist environment in optimal wound healing. Current pharmaceutical biotechnology. 2002;3(3):179-95.
84. Harris A, Rolstad B. Hypergranulation tissue: a nontraumatic method of management. Ostomy/wound management. 1994;40(5):20-2, 4, 6-30.
85. Gu S-Y, Wang Z-M, Ren J, Zhang C-Y. Electrospinning of gelatin and gelatin/poly (l-lactide) blend and its characteristics for wound dressing. Materials Science and Engineering: C. 2009;29(6):1822-8.
86. Chen Y, Yan L, Yuan T, Zhang Q, Fan H. Asymmetric polyurethane membrane with in situ-generated nano-TiO2 as wound dressing. Journal of Applied Polymer Science. 2011;119(3):1532-41.
87. Lamke L-O, Nilsson G, Reithner H. The evaporative water loss from burns and the water-vapour permeability of grafts and artificial membranes used in the treatment of burns. Burns. 1977;3(3):159-65.

88. Queen D, Gaylor J, Evans J, Courtney J, Reid W. The preclinical evaluation of the water vapour transmission rate through burn wound dressings. Biomaterials. 1987;8(5):367-71.
89. Jonkman MF, Molenaar I, Nieuwenhuis P, Bruin P, Pennings AJ. New method to assess the water vapour permeance of wound coverings. Biomaterials. 1988;9(3):263-7.
90. Li WJ, Laurencin CT, Caterson EJ, Tuan RS, Ko FK. Electrospun nanofibrous structure: a novel scaffold for tissue engineering. Journal of biomedical materials research. 2002;60(4):613-21.
91. Zhong S, Zhang Y, Lim C. Tissue scaffolds for skin wound healing and dermal reconstruction. Wiley Interdisciplinary Reviews: Nanomedicine and Nanobiotechnology. 2010;2(5):510-25.
92. Duan H, Feng B, Guo X, Wang J, Zhao L, Zhou G, Liu W, Cao Y, Zhang WJ. Engineering of epidermis skin grafts using electrospun nanofibrous gelatin/polycaprolactone membranes. International Journal of Nanomedicine. 2013;8:2077-84.
93. Henry JB, AuBuchon JP. Clinical diagnosis and management by laboratory methods. Archives of Pathology and Laboratory Medicine. 1997;121(9):1016.
94. Ren D, Yi H, Wang W, Ma X. The enzymatic degradation and swelling properties of chitosan matrices with different degrees of N-acetylation. Carbohydrate Research. 2005;340(15):2403-10.
95. Zonari A, Martins TM, Paula ACC, Boeloni JN, Novikoff S, Marques AP, Correlo VM, Reis RL, Goes AM. Polyhydroxybutyrate-co-hydroxyvalerate structures loaded with adipose stem cells promote skin healing with reduced scarring. Acta biomaterialia. 2015;17:170-81.
96. Ji C, Annabi N, Khademhosseini A, Dehghani F. Fabrication of porous chitosan scaffolds for soft tissue engineering using dense gas CO 2. Acta Biomaterialia. 2011;7(4):1653-64.
97. Mignatti P, Rifkin DB, Welgus HG, Parks WC. Proteinases and tissue remodeling. The molecular and cellular biology of wound repair. US: Springer; 1988. p. 427-74.
98. Ponche A, Ploux L, Anselme K. Protein/material interfaces: investigation on model surfaces. Journal of Adhesion Science and Technology. 2010;24(13-14):2141-64.
99. Brown RA, Phillips JB. Cell responses to biomimetic protein scaffolds used in tissue repair and engineering. International review of cytology. 2007;262:75-150.
100. Cai K, Bossert J, Jandt KD. Does the nanometre scale topography of titanium influence protein adsorption and cell proliferation? Colloids and surfaces B: Biointerfaces. 2006;49(2):136-44.
101. Chen F, Lee C, Teoh S. Nanofibrous modification on ultra-thin poly (e-caprolactone) membrane via electrospinning. Materials Science and Engineering: C. 2007;27(2):325-32.
102. Mattanavee W, Suwantong O, Puthong S, Bunaprasert T, Hoven VP, Supaphol P. Immobilization of biomolecules on the surface of electrospun polycaprolactone fibrous scaffolds for tissue engineering. ACS applied materials & interfaces. 2009;1(5):1076-85.
103. Haipeng G, Yinghui Z, Jianchun L, Yandao G, Nanming Z, Xiufang Z. Studies on nerve cell affinity of chitosan-derived materials. Journal of biomedical materials research. 2000;52(2):285-95.
104. Prasitsilp M, Jenwithisuk R, Kongsuwan K, Damrongchai N, Watts P. Cellular responses to chitosan in vitro: the importance of deacetylation. Journal of materials science: materials in medicine. 2000;11(12):773-8.
105. Bumgardner J, Wiser R, Elder S, Jouett R, Yang Y, Ong J. Contact angle, protein adsorption and osteoblast precursor cell attachment to chitosan coatings bonded to titanium. Journal of Biomaterials Science, Polymer Edition. 2003;14(12):1401-9.

106. Reinke J, Sorg H. Wound repair and regeneration. European surgical research. 2012;49(1):35-43.
107. LeBaron RG, Athanasiou KA. Extracellular matrix cell adhesion peptides: functional applications in orthopedic materials. Tissue engineering. 2000;6(2):85-103.
108. Chithra P, Sajithlal G, Chandrakasan G. Influence of Aloe vera on the healing of dermal wounds in diabetic rats. Journal of ethnopharmacology. 1998;59(3):195-201.
109. Hutter JA, Salman M, Stavinoha WB, Satsangi N, Williams RF, Streeper RT, Weintraub ST. Antiinflammatory C-glucosyl chromone from Aloe barbadensis. Journal of natural products. 1996;59(5):541-3.
110. Danhof IE, McAnalley B. Stabilized Aloe Vera-Effect on Human-Skin Cells. Drug & Cosmetic Industry. 1983;133(2):52.
111. Jettanacheawchankit S, Sasithanasate S, Sangvanich P, Banlunara W, Thunyakitpisal P. Acemannan stimulates gingival fibroblast proliferation; expressions of keratinocyte growth factor-1, vascular endothelial growth factor, and type I collagen; and wound healing. Journal of pharmacological sciences. 2009;109(4):525-31.
112. Weng L, Romanov A, Rooney J, Chen W. Non-cytotoxic, in situ gelable hydrogels composed of N-carboxyethyl chitosan and oxidized dextran. Biomaterials. 2008;29(29):3905-13.
113. Bowler P, Duerden B, Armstrong DG. Wound microbiology and associated approaches to wound management. Clinical microbiology reviews. 2001;14(2):244-69.
114. Maneerung T, Tokura S, Rujiravanit R. Impregnation of silver nanoparticles into bacterial cellulose for antimicrobial wound dressing. Carbohydrate polymers. 2008;72(1):43-51.
115. Kong M, Chen XG, Xing K, Park HJ. Antimicrobial properties of chitosan and mode of action: a state of the art review. International journal of food microbiology. 2010;144(1):51-63.
116. Rabea EI, Badawy ME-T, Stevens CV, Smagghe G, Steurbaut W. Chitosan as antimicrobial agent: applications and mode of action. Biomacromolecules. 2003;4(6):1457-65.
117. Devlieghere F, Vermeulen A, Debevere J. Chitosan: antimicrobial activity, interactions with food components and applicability as a coating on fruit and vegetables. Food microbiology. 2004;21(6):703-14.
118. Pandey R, Mishra A. Antibacterial activities of crude extract of Aloe barbadensis to clinically isolated bacterial pathogens. Applied biochemistry and biotechnology. 2010;160(5):1356-61.

Chapter IV

Production and characterization of electrospun Silk Fibroin based asymmetric membranes for wound dressing applications

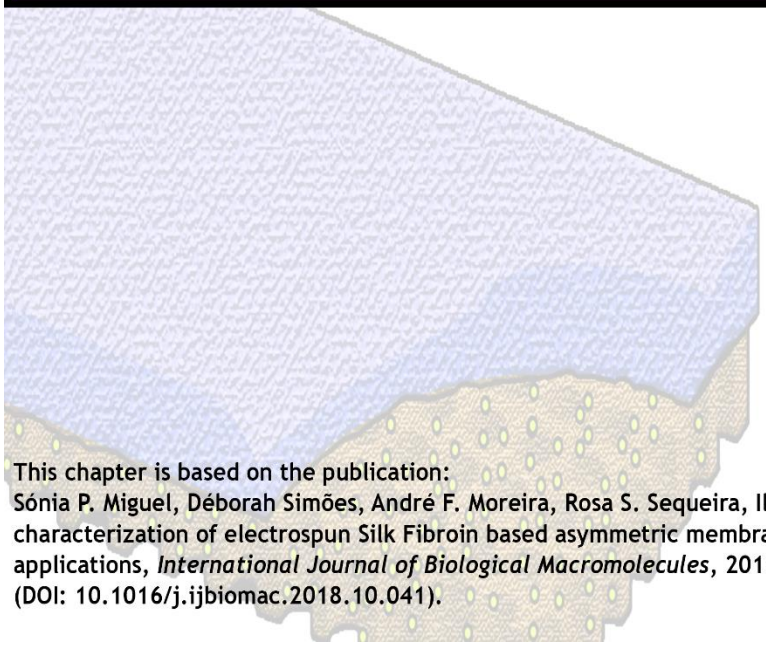

This chapter is based on the publication:
Sónia P. Miguel, Déborah Simões, André F. Moreira, Rosa S. Sequeira, Ilídio J. Correia; Production and characterization of electrospun Silk Fibroin based asymmetric membranes for wound dressing applications, *International Journal of Biological Macromolecules*, 2019, 121: 524-535. (DOI: 10.1016/j.ijbiomac.2018.10.041).

Abstract

Nowadays, wound dressings with improved properties are under development and among them, asymmetric membranes have gained an increasing interest due to their two-layered structure that mimic both the epidermis and dermis layers of the skin. Herein, a new asymmetric membrane was produced using the electrospinning technique. The top layer was produced with silk fibroin (SF) and poly(caprolactone) to reproduce the dense nature and waterproof ability of the epidermis. On the other hand, the dermis-like bottom layer was manufactured with SF and hyaluronic acid loaded with an herbal drug (thymol (THY)). All the data gathered showed that the produced electrospun asymmetric membrane exhibited the porosity, wettability, and mechanical properties suitable for the healing process. Further, the *in vitro* data also demonstrated that the human fibroblast are able to adhere and spread at the membranes' surface, thus confirming their biocompatibility. Moreover, the incorporation of THY into the bottom layer of the membrane, improved its antioxidant and antibacterial properties. Overall, the obtained results demonstrate the appropriateness of the produced membrane for wound healing applications.

Keywords: electrospun asymmetric membranes; silk fibroin; thymol.

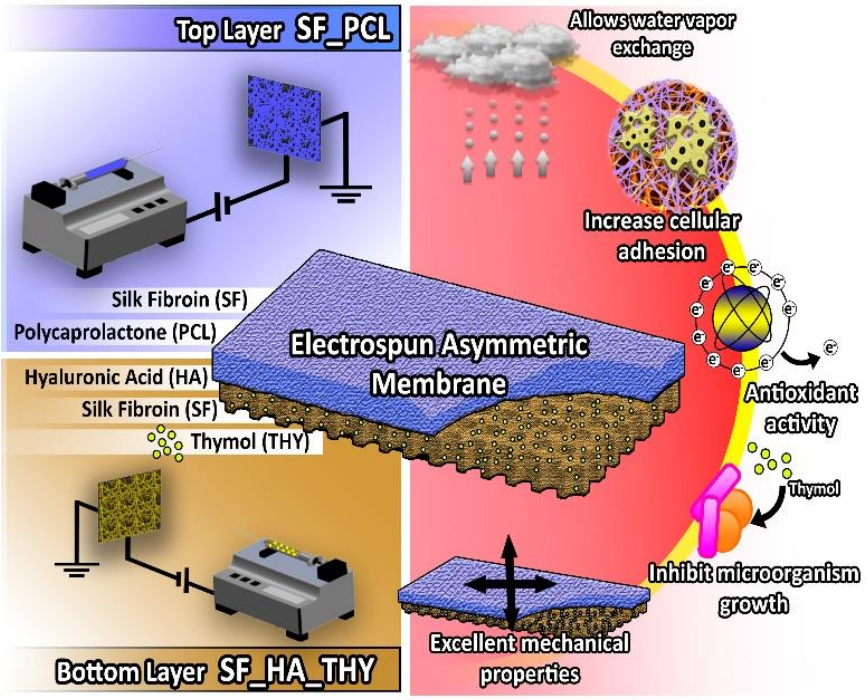

4.1 Introduction

A wound results from a sharp injury, that affects the skin' structure and disrupts the cells' crosstalk interactions and functions across the skin layers [1]. Skin injuries can represent a severe health risk to the human body since skin' functions such as thermal insulation, body fluid retention and protection from external threats can be hindered [2]. To avoid further complications, after a skin injury occurs, an immediate covering of the wound is required to protect the underlying tissues from hazard agents as well as prevent fluid loss [3].

Up to now, in the clinic, the traditional wound dressings (*e.g.* gauzes, bandages, and creams) and skin grafts have been the most used therapeutic approaches, and they act as temporary barriers. However, most of them are expensive, require frequent replacement, and are not able to fully re-establish skin structure and functions [4]. Therefore, the development of new therapeutic strategies or methodologies to assist the wound healing mechanism is extremely important. Among the different wound dressings under development, the nanofibrous membranes have received an increasing attention due to their intrinsic properties, such as high surface-to-volume ratio, interconnected pores that are compatible with cell penetration and nutrient exchange, as well as the potential to promote the hemostasis phase and wound exudate absorption [4, 5]. In addition, the nanofibers are able to mimic the structure of the proteins (*e.g.* laminin and collagen) found in the natural ECM [5].

Different techniques (self-assembly, dry/wet phase separation, electrospinning, and $scCO_2$-induced phase inversion) have been used to produce nanofibrous membranes. The electrospinning technique is one of the most explored to produce nanofibers due to its simplicity, efficacy, reproducibility and versatility. Recently, this methodology has also been employed for the manufacture of Nanofibrous Asymmetric Membranes [5, 6]. The main feature of this type of wound dressing is their two-layered structure that is able to mimic both skin layers (epidermis and dermis). In general, an asymmetric membrane displays (i) a dense and waterproof top layer that confers protection to the wound site in a similar way to the epidermis layer and (ii) a porous bottom layer that reproduces the dermis structure [6, 7].

Herein, an EAM composed of two interconnected layers was produced for enhancing the healing process. The top layer was composed of SF and poly(caprolactone) (PCL), while the bottom layer was produced by using a blend of SF with HA. SF is a fibrous protein synthesized by a variety of insects including silkworm and presents excellent biocompatibility, good water vapor permeability, biodegradability, mechanical strength, and minimal inflammatory reaction [8]. In turn, PCL is a hydrophobic synthetic polymer that exhibits a high mechanical strength. The combination of SF with PCL was used to produce a layer that presents epidermis-like properties such as the hydrophobic character, waterproof ability and mechanical resistance [6]. On the other side, the HA was selected since it is a hydrophilic and polyanionic polymer that can be found in connective tissues (*e.g.* skin, ligament, cartilage, blood vessels) and provides a high

capacity of hydration, water-sorption and water retention, as well as allows cell attachment, migration, and proliferation [5, 9]. Therefore, the production of a porous bottom layer composed of SF/HA combination should result in a dermis-like structure, capable of absorbing the wound exudate as well as promote the cell adhesion and proliferation. Furthermore, to confer antimicrobial activity to the bottom layer, THY, an herbal drug, was loaded into the nanofibers mesh [10]. THY is the major component of the EOs extracted from *Lippia gracilis* and it exhibits various biological effects such as antimicrobial, antioxidant, antinociceptive, local anesthetic, and anti-inflammatory [11]. Up to now, THY has been applied as an active antiseptic ingredient in some toothpastes, such as Euthymol® (Johnson & Johnson's). Further, when comparing to other EOs, such as carvacrol, THY shows an increased antioxidant potential [12]. However, the addition of THY into EAM and its impact on the biological properties of the wound dressing materials is poorly explored in the literature.

4.2 Materials and methods

4.2.1 Materials

Silk from cocoons of *BomByx mori* was acquired from the Portuguese Association of Parents and Friends of Mentally Disabled Citizens (APPACDM, Castelo Branco, Portugal). TFE was supplied by Acros Organics (Jersey City, NJ, USA). FBS free from any antibiotic was purchased from Biochrom AG (Berlin, Germany). HA extra low molecular weight (8000-15000 Da) was gotten from Carbosynth (Compton, UK). NHDF cells were acquired from PromoCell (Labclinics, S.A., Barcelona, Spain). MTS solution was bought from Promega (Madison, WI, USA). FA (99-100%) was acquired from Chem-Lab NV (Zedelgem, Belgium). Calcium chloride ($CaCl_2$), Sodium carbonate (Na_2CO_3) and Triton X-100 were obtained from Fisher (Hampton, New Hampshire, EUA). DMEM-F12, EDTA, gentamicin, GA, LB Broth, PEO, PBS, sodium hydroxide (NaOH), PCL (80,000 Da), THY (≥ 99.0%) and trypsin were purchased from Sigma-Aldrich (Sintra, Portugal). Quant-iT Pico Green dsDNA assay kit was obtained from ThermoFisher Scientific (Waltham, MA, USA). *S. aureus* clinical isolate (ATCC 25923) and *P. aeruginosa* obtained from a human sample were used as models of prokaryotic organisms to evaluate the bactericidal activity of the produced membranes. Propidium iodide (PI) buffer was gotten from Invitrogen (Carlsbad, Califórnia, EUA) and Calcein AM was supplied by Calbiochem (Merck Millipore, Oeiras, Portugal). Ethanol was acquired from José Manuel Gomes dos Santos (Odivelas, Portugal).

4.2.2 Methods

4.2.2.1 Silk fibroin extraction

SF was extracted from the silk cocoons by adapting a protocol previously reported in the literature [13, 14]. The adopted protocol is illustrated in Figure 4.1. Briefly, the cocoons are initially degummed, *i.e.* sericin external layer is removed, by submerging the silk cocoons in a boiling solution of Na_2CO_3 0.5% (w/v) for 2-4 h. After that, the resulting fibroin filaments were

extensively rinsed in hot distilled water (40-50°C) and dried at RT. The dried silk material was then dissolved in a ternary solvent system composed of $CaCl_2/CH_3CH_2OH/H_2O$ (1:2:8 in molar ratio) at 78°C for 4 h. Afterwards, the SF solution was centrifugated to remove any impurities and dialyzed in double distilled H_2O (18.2 MΩ). After 3 days, the purified SF solution was lyophilized for further use.

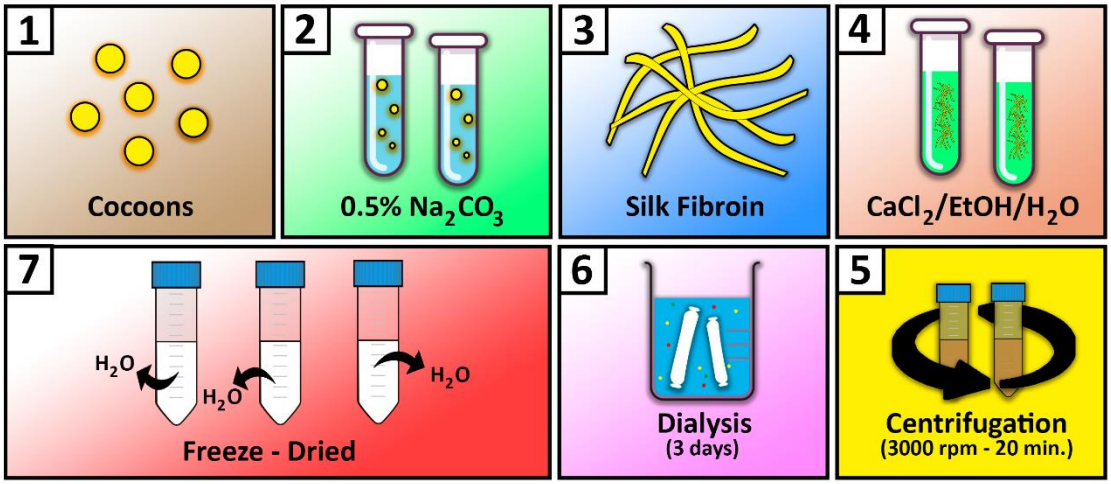

Figure 4.1. Illustration of the protocol followed to perform the silk fibroin (SF) extraction: Cocoons from *Bombyx-mori* were used to obtain SF (**1**); In the second step, cocoons were boiled in 0.5% Na_2CO_3 during 30 min (**2**); The degumming process of the cocoons was performed to obtain raw SF, by promoting the removal of sericin (**3**); The SF was dissolved in a ternary solvent ($CaCl_2$/ethanol/H_2O) at 78°C, during 4 h (4); The SF solution was centrifugated to remove any impurity (5); SF solution was dialysed against ultrapure water, for 3 days (6); The SF powder was then obtained through the freeze-drying process (7).

4.2.2.2 Production of the electrospun asymmetric membrane

The production of the **EAM membrane** was performed using a conventional electrospinning apparatus, comprised of high voltage source (Spellman CZE1000R, 0–30 kV) (obtained from Spellman, Corporate Headquarters USA) a precision syringe pump (KDS-100) (acquired from Sigma-Aldrich, Sintra, Portugal), a plastic syringe with a stainless-steel needle (21 Gauge), and an aluminium disk connected to a copper collector. The top layer (**SF_PCL**) of the membrane was produced by using a blend composed of SF (10% w/v) and PCL (10% w/v) dissolved in a solution of FA (98% v/v) and TFE (80% v/v) at 2:1 volume ratio. Then, this solution was placed in the syringe and electrospun at a constant flow rate of 1.0 mL/h, using a working distance of 10-12 cm and an applied voltage of 28 kV, until a thickness similar to the epidermis layer of the human skin (0.05-1.5 mm) was obtained. Posteriorly, the bottom layer (**SF_HA_THY**) was produced by combining the solutions of SF (10% w/v) in FA (98% v/v) and HA (20% w/v) in H_2O at 2:1 volume ratio. Subsequently, THY at a concentration of 5 mg/mL and 2 mL of PEO (8% w/v) were added to the blend. PEO was added to the blend to adjust its viscosity in order to improve its electrospinability. Afterwards, the polymeric solution was electrospun on top of the SF_PCL membrane at a constant flow rate of 2.3 mL/h, using a working distance of 12 cm and an applied voltage of 28 kV. The bottom layer without THY (**SF_HA**) was also produced for

comparative purposes. In the same way, the electrospun of the bottom layer was performed until an obtained thickness value of 1.5–4 mm (dermis layer thickness).

To improve the water stability of SF, all membranes were treated with ethanol vapor (75%) at 25°C, for 1 h and then dried under vacuum at RT for 2 h [15]. This procedure induces structural changes, through a crystallization process, being observed the transition from silk I (random coil) to silk II (ß sheet) conformation.

4.2.2.3 Attenuated total reflectance-fourier transform infrared spectroscopy analysis

The SF conformational changes (random coil to ß sheet) and final composition of the electrospun membranes were studied by ATR-FTIR analysis. The membranes' and raw materials (used in membrane production) spectra were acquired with an average of 128 scans, a spectral width ranging from 4000 and 400 cm^{-1} and a spectral resolution of 4 cm^{-1}, using a Nicolet iS10 FTIR spectrophotometer (Thermo Scientific, Waltham, MA, USA).

4.2.2.4 Characterization of the mechanical properties of the produced membranes

The mechanical properties of EAM membranes were determined with a Shimadzu AG-X Tensile Testing Machine (Tokyo, Japan) operated at RT, accordingly to the guidelines established by the Standard Test Method for Tensile Properties of Polymer Matrix Composite Materials (ASTM standard D3039/ D3039 M). For the test analysis, the samples (n = 5) were prepared with a gauge length of 6 cm, a width of 2 cm, and a thickness ranging from 1.5-1.8 mm. The length between the clamps and the speed of testing was set to 2 cm and 20 mm/min, respectively.

The mechanical assays were performed under wet and dry conditions. For the wet conditions, the membranes were immersed in a PBS solution (pH 5.5), over 24 h, at 37°C. Load-extension data was recorded and the stress–strain curve of the membranes was determined through Equations (4.1) and (4.2), respectively:

$$Stress = \sigma = \frac{F}{A} \tag{4.1}$$

$$Strain = \varepsilon = \frac{\Delta l}{L} \tag{4.2}$$

Where *F* is the applied force; A is the cross-sectional area; *Δl* is the change in length, and *L* is the length between the clamps.

4.2.2.5 Evaluation of the porosity of the produced membranes

The total porosity of the membranes was determined through a liquid displacement method. Briefly, the membranes (*n*= 3) were weighed and then immersed in absolute ethanol. After 1 h

of immersion, the samples were reweighed. The membrane's porosity was determined through Equation (4.3):

$$Porosity\ (\%) = \frac{W_s - W_d}{D_{ethanol}\, x\, V_{membrane}}\ x\ 100 \qquad (4.3)$$

Where W_d is the initial weight of the dry membrane and W_s is the weight of the swollen membrane, $D_{ethanol}$ is the density of the ethanol at RT and $V_{membrane}$ is the volume of the swollen membrane.

4.2.2.6 Determination of the contact angle at the surface of the produced membranes

The contact angles at the samples' surface were determined with a Data Physics Contact Angle System OCAH 200 apparatus (DataPhysics Instruments GmbH, Filderstadt, Germany) operating in static mode, at 25°C and using water as the reference fluid. For each sample, water drops (4 µL) were placed on the surface of the membranes. The reported contact angles are the average of at least three independent measurements.

4.2.2.7 Water vapor transmission rate

The water vapor diffusion through the SF_PCL, SF_HA_THY, and EAM membranes was evaluated accordingly to a method previously described elsewhere [6]. Briefly, the membranes were used to seal the opening of a glass test tube (1.77 cm^2) containing 10 mL of ultrapure water to avoid its evaporation. Parafilm was used to attach the membrane to the glass tube. Afterwards, the membranes were incubated at 37°C and at specific time points, the amount of water evaporated was assessed by measuring the weight loss of the test tube. Then, the WVTR for each membrane sample was estimated through Equation (4.4):

$$Water\ Vapor\ Transmission\ Rate = \frac{W_{loss}}{A} \qquad (4.4)$$

Where W_{loss} is the daily weight loss of water and A is the area of the tube opening.

4.2.2.8 Evaluation of the swelling capacity of the produced membranes

The swelling capacity of the membranes was evaluated by immersing all the samples in PBS at, pH 5 and pH 8, to mimic the pH found in native human skin and skin infection, respectively. The assays were performed in triplicate at 37°C and under stirring (60 RPM) [6]. Then, the PBS excess present at the surface of the membranes was removed by gently tapping the surface with filter paper and the weight of the swollen samples was measured. The water uptake capacity was determined through Equation (4.5).

$$Swelling\ ratio = \frac{W_t}{W_0} \qquad (4.5)$$

Where W_t is the final weight and W_0 is the initial weight of the membranes.

4.2.2.9 Determination of the weight loss of the membranes

The membranes degradation profile was characterized during 7 days. For that purpose, membrane samples were incubated in PBS solution at 37° C, under stirring (60 RPM). At different timepoints (1, 3, and 7 days), the membranes were withdrawn from solution, freeze-dried, and weighed. The membranes degradation at each time point was calculated according to Equation (4.6):

$$Weight\ loss\ (\%) = \frac{W_i - W_t}{W_i}\ x\ 100 \quad (4.6)$$

Where W_i corresponds to the initial weight of the sample and W_t to the weight of the sample at time t.

4.2.2.10 Evaluation of the antioxidant activity of the membranes

The antioxidant activity of SF_PCL, SF_HA and SF_HA_THY membranes was assessed using the 2-diphenyl-1-picrylhydrazyl (DPPH) radical scavenging assay. In this assay, DPPH free radicals are neutralized by accepting an electron or a hydrogen atom, resulting in a change of the solution color from purple to yellow [16]. Briefly, 5 mg of the electrospun mats were immersed in 3 mL of 100 μM DPPH solution in methanol. The reaction mixture was then incubated in the dark for 8 h. At different timepoints, the samples were collected, and the absorbance at 517 nm was measured using a microplate reader (Biorad xMark microplate spectrophotometer). The DPPH degradation was assessed using the following Equation (4.7):

$$DPPH\ scavenging\ (\%) = \frac{A_B - A_S}{A_S}\ x\ 100 \quad (4.7)$$

Where A_B is the absorbance of the blank samples and A_S is the absorbance of the samples incubated with the membranes.

4.2.2.11 Evaluation of the encapsulation and loading efficiency of THY within the bottom layer of produced EAM

To evaluate the encapsulation and loading efficiency of THY, the uncrosslinked SF_HA and SF_HA_THY layers were subjected to total degradation, through their immersion in FA, during 1 h, under stirring. Then, the supernatant was recovered by centrifugation at 14000 RPM for 10 min, and the absorbance was measured at 274 nm by using a Thermo Scientific Evolution 201 UV–vis spectrophotometer [10]. The THY concentration in the supernatant was determined using a standard absorbance curve (Figure 4.2A) of THY at 274 nm (y = 0.0202x + 2.153, R^2= 0.9988). On the other hand, the UV spectra were obtained for SF_HA and SF_HA_THY

samples to evaluate if the polymers have interference in the determination of the THY concentration.

From the analysis of Figure 4.2B, it is possible to observe that the polymers do not influence the recorded absorbance values during the THY loading and release assays. The EE and loading efficiency were determined using the following Equations (4.8) and (4.9):

$$EE\ (\%) = \frac{W_i - W_s}{W_i}\ x\ 100 \tag{4.8}$$

$$LE\ (\%) = \frac{W_i - W_s}{Y}\ x\ 100 \tag{4.9}$$

Where W_i is the total amount of THY added in SF_HA_THY membrane, W_s is the amount of THY in the supernatant, and Y is the total dry weight of SF_HA_THY membrane.

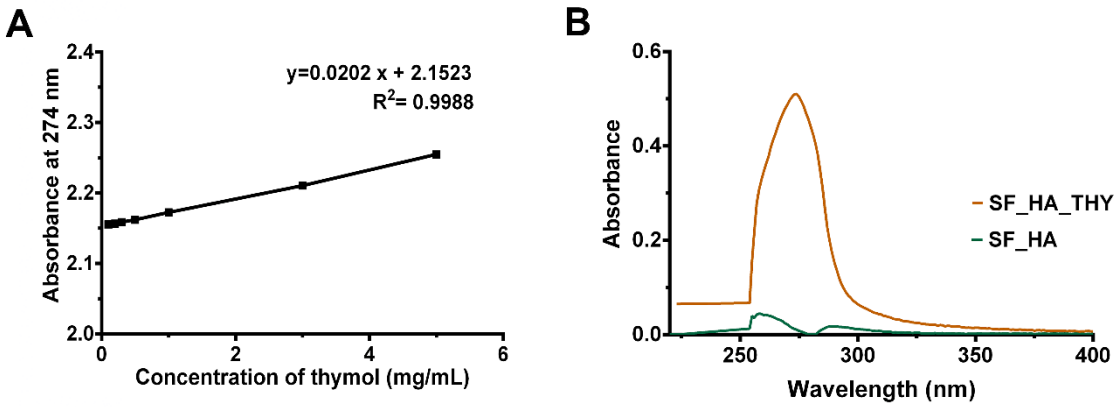

Figure 4.2. Calibration curve performed to determine the THY concentration (A); UV spectra acquired for SF_HA and SF_HA_THY layers (B).

4.2.2.12 Analysis of the drug-release kinetics

The amount of THY released from the electrospun membranes was measured according to a method previously reported in the literature [10]. The electrospun membranes (with a total weight of 5 mg) were immersed in 2 mL of PBS at pH 5 or pH 8. The samples were then incubated at 37° C under agitation (60 RPM) in an incubator shaker, to mimic the physiological conditions. At different timepoints, the samples were centrifugated and the supernatant (1 mL) absorbance was measured at 274 nm, using a Thermo Scientific Evolution 201 UV-vis spectrophotometer, to determine the amount of THY released. All experiments were performed in triplicate. Further, the drug-release kinetics exhibited by the produced membranes were also characterized by using the Peppas-Korsmeyer (4.10) and Hixon-Crowell models (4.11):

$$\text{Peppas-Korsmeyer: } \frac{M_t}{M_\infty} = Kt^n \tag{4.10}$$

$$\text{Hixon-Crowell: } Q_0^{1/3} = Q_t^{1/3} - K_s t \tag{4.11}$$

Where M_t is the cumulative amount of drug released at time t, M_∞ is the initial drug loading, K is a constant characteristic of the drug-polymer system, and n is the diffusion exponent, suggesting the nature of the release mechanism. Q_t is the amount of drug dissolved in time t and Q_0 is the initial amount of drug in the solution.

4.2.2.13 Characterization of EAM biocompatibility

4.2.2.13.1 Characterization of cell viability and proliferation when they are in contact with the produced membranes

The membranes' biocompatibility was evaluated using an MTS assay as recommended by the ISO 10993-5:2009 (Biological evaluation of medical devices- Part 5: Tests for *in vitro* cytotoxicity). Prior to cell seeding, membranes were placed into 96-well plates, occupying less than 10% of the well area, and then sterilized under UV irradiation (254 nm, ≈ 7 $mW.cm^{-2}$) for 1 h. After, NHDF cells were seeded at a density of 10×10^3 cells per well and incubated at 37°C, in an incubator with a 5% CO_2 humidified atmosphere. After 1, 3 or 7 days of incubation, the medium of each well was removed and replaced by a mixture of 100 µL of fresh culture medium and 20 µL of MTS/PMS reagent solution and incubated for 4 h, at 37°C, in a 5% CO_2 atmosphere. The absorbance of each sample (n= 5) was determined at 492 nm using a microplate reader (Biorad xMark microplate spectrophotometer). Cells incubated with ethanol (96%) were used as positive control (K^+), whereas cells incubated only with culture medium were used as a negative control (K^-).

4.2.2.13.2 dsDNA quantification assay

The total dsDNA was measured with a Quan-iT PicoGreen dsDNA Assay kit, following a protocol previously described in the literature [17]. NHDF cells were seeded, at a density of 10×10^3 cells/mL, in contact with the produced membranes. After 1, 3, and 7 days, cell lysis was induced by treating the cell-nanofibrous membranes complexes with Triton X-100 for 1 h. After, the membranes were transferred into a 1.5 mL Eppendorfs and were subjected to a freeze–thaw cycle and sonicated for 15 min. From the obtained supernatant, 100 µL were withdrawn and mixed with an equal volume of PicoGreen solution in TE buffer (1X). The plate was incubated for 10 min in the dark and the fluorescence was measured in a microplate reader using excitation and emission wavelengths of 485 nm and 535 nm, respectively. The dsDNA concentration on the different samples was determined following protocols described in literature using a calibration curve.

4.2.2.13.3 Live/dead assay

Cell survival and proliferation at the surface of the SF_PCL, SF_HA and SF_HA_THY layers were evaluated by fluorescence microscopy through a Live/Dead assay (Invitrogen, Life Technologies, Foster City, CA, USA). This method allows the simultaneous detection of both live and dead cells with calcein acetozxmethyl (calcein AM) and PI dyes, respectively. Calcein

AM is a non-fluorescent and cell membrane-permeable reagent, which is converted by the intracellular esterases to calcein, that exhibits an intense green fluorescent (ex/em: ≈ 495 nm/ 515 nm). PI is a popular red-fluorescent nuclear probe that only enter into the cells when their membranes are damaged (ex/em: ≈ 493 nm/≈ 636 nm). To perform this assay, NHDF cells (10 x 10^3 cells/mL) were seeded on the surface of the membranes, which were previously placed in µ-Slide 8 well Ibidi imaging plates (Ibidi GmbH, Planegg/Martinsried, Germany) and sterilized by UV irradiation (254 nm, ≈ 7 $mW.cm^{-2}$), over 1 h. Cells cultured without materials were used as negative control (K^-), whereas cells treated with permeabilization solution (Triton X-100) were used as positive control (K^+). After 1, 3 and 7 days, cells were incubated with the staining solution according to the manufacturer's instructions, for 15-20 min. Then, the stained cells present in the nanofibrous membranes were analyzed by fluorescence microscopy and the images were captured using Zeiss Zen 2010 software (Zeiss, Oberkochen, Germany).

4.2.2.14 Characterization of the biological performance of the electrospun membranes through SEM Analysis

NHDF cells or bacteria seeded at the surface of the produced membranes were fixed with 2.5% (v/v) GA, for 30 min. Following this, the samples were washed three times with PBS and frozen at -80°C and freeze-dried during 3h or 6 h for samples containing NHDF or bacteria, respectively. After, all samples were mounted on aluminum stubs with Araldite glue and sputter-coated with gold using a Quorum Q150R ES sputter coater (Quorum Technologies Ltd, Laughton, East Sussex, England). SEM images were acquired with different magnifications, using an acceleration voltage of 20 kV, in a Hitachi S-3400N Scanning Electron Microscope (Hitachi, Tokyo, Japan).

4.2.2.15 Evaluation of the EAM antimicrobial properties

4.2.2.15.1 Analysis of bacterial penetration through the top layer of EAM

S. aureus and *P. aeruginosa*, gram-positive and gram-negative bacteria respectively, were used to characterize the capacity of the membrane's top layer to avoid bacterial infiltration within their structure. To accomplish this, transwell systems (Corning Incorporated, New York, NY, USA) were modified with SF_PCL membrane or a filter paper (0.22 µm) (control group) to act as the interface between the upper and lower chamber. The SF_PCL membrane and the filter paper were inoculated with a bacterial suspension (1 × 10^8 CFU/mL), for 24 h, at 37°C. Afterwards, the optical density (absorbance value at 600 nm) of the culture medium present in the lower chamber was measured and the number of colonies that crossed the SF_PCL membrane/filter paper were counted. In addition, the presence of microorganisms at the upper and bottom surfaces of the SF_PCL membrane or in the filter paper were investigated through SEM.

4.2.2.15.2 Characterization of the EAM Bottom Layer antibacterial activity

The bactericidal activity of the bottom layers of SF_HA and SF_HA_THY was also characterized using *S.aureus* and *P.aeruginosa*, as models. Briefly, 25-50 mg of each sample were added to 10 mL of LB broth, at pH 6.2, containing 1 × 10^5 CFU/mL of early mid-log phase bacteria culture and then incubated at 37°C, for 24 h. After the incubation period, serial dilutions were prepared and 100 µL of bacterial samples were transferred into LB agar plates. Following overnight incubation at 37°C, bacterial colonies were counted and expressed as CFU/mL. The bacterial growth inhibition was calculated through Equation (4.12):

$$Antibacterial\ efficiency\ (\%) = \frac{N_0 - N}{N_0}\ x\ 100 \qquad (4.12)$$

Where N_0 and N each represent the bacteria number of control and experimental group, respectively.

Furthermore, a modified Kirby-Bauer technique was used to characterize the antimicrobial properties of the membranes. For this, circular membranes (n= 3) were placed on the surface of an agar plate seeded with *S. aureus* or *P.aeruginosa* (1 x 10^8 CFU/mL) and incubated for 24 h, at 37°C. After that, the inhibitory halos around the samples were photographed and the halo size determined with an image analysis software, ImageJ (NIH Image, USA). In addition, the biofilm formation at the surface of the membranes was also assessed through SEM analysis.

4.2.2.16 Statistical analysis

The statistical analysis of the obtained results was performed using ANOVA, with the Newman-Keuls post hoc test. A p value lower than 0.05 ($p < 0.05$) was considered statistically significant.

4.3 Results and discussion

4.3.1 Characterization of the morphology of the membranes

In recent years, asymmetric membranes have become the main target of different studies to develop wound dressings that can mimic the structure and functions of human skin [5, 6]. In this study, an electrospinning technique was used to produce a novel asymmetric membrane based on a silk derived biopolymer enriched with a natural compound, THY. The dense top SF_PCL layer provides mechanical support, acts as a physical barrier to protect the wound from mechanical and chemical damage, dehydration, and bacteria infiltration, as well as coordinate the gaseous exchange. On the other side, the SF_HA layer acts as a wound-dressing interface able to absorb wound exudate, promote nutrient exchange, support cell adhesion and proliferation as well as confer antimicrobial, anti-inflammatory and antioxidant properties to the membrane due to the incorporation of THY (SF_HA_THY).

The morphology of the nanofibers were analyzed by SEM and the diameters of the fibers were determined using the ImageJ software (Figure 4.3).

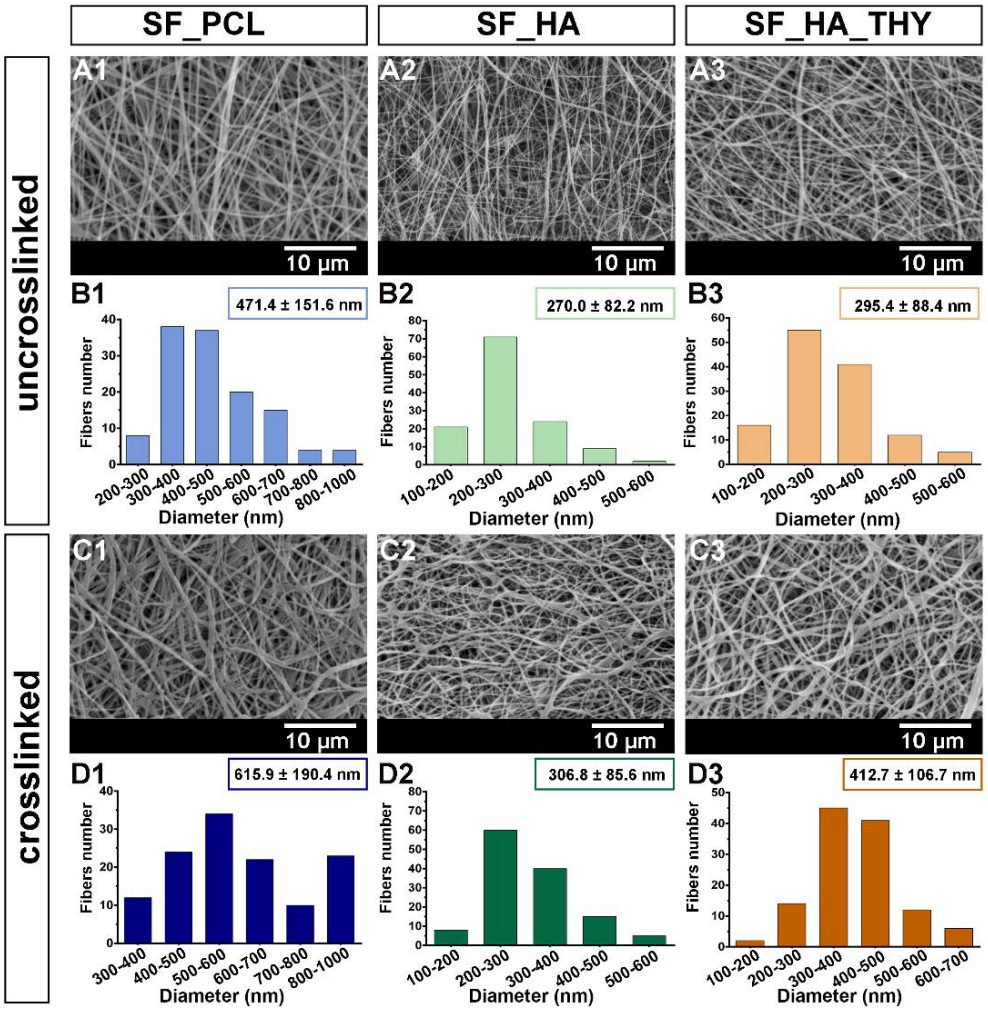

Figure 4.3. Characterization of the SF_PCL, SF_HA, and SF_HA_THY nanofibrous layers morphological properties. SEM images of the top and bottom layers, before (A1-A3) and after the crosslinking process (C1-C3). Top and bottom layers nanofibers diameter distribution before and after crosslinking are presented in (B1-B3) and (D1-D3), respectively.

The size measurements revealed that the nanofibers of the top layer display an average diameter of 471.4 ± 151.6 nm, while the SF_HA and SF_HA_THY nanofibers of the bottom layer present a mean diameter of 270.0 ± 82.2 nm and 295.4 ± 88.4 nm, respectively. Moreover, to improve the water stability of the SF a crosslinking process was performed, resulting in an increase in the SF_PCL, SF_HA, and SF_HA_THY nanofibers mean diameter to 615.9 ± 190.4 nm, 306.8 ± 85.6 nm and 412.7 ± 106.7 nm, respectively. Cross-sectional images of the EAM were also acquired (Figure 4.4) and they clearly show the bilayered organization of the produced membrane. Furthermore, the incorporation of THY did not induce any significant morphologic variations in the bottom layer of the membrane, *i.e.* size and structure. Contrarily, the crosslinking process leads to the formation of more irregular nanofibrous structures with increased density and fiber diameters, which is in agreement with the data available in the

literature for similar crosslinked nanofibrous meshes [14, 18]. Nevertheless, the nanofibers diameter is still within the range of the collagen fibrils found at the ECM (50-500 nm), which highlights the EAM capacity to mimic some of the native skin structural features and provide an interface that favours cell migration, adhesion, and proliferation [19].

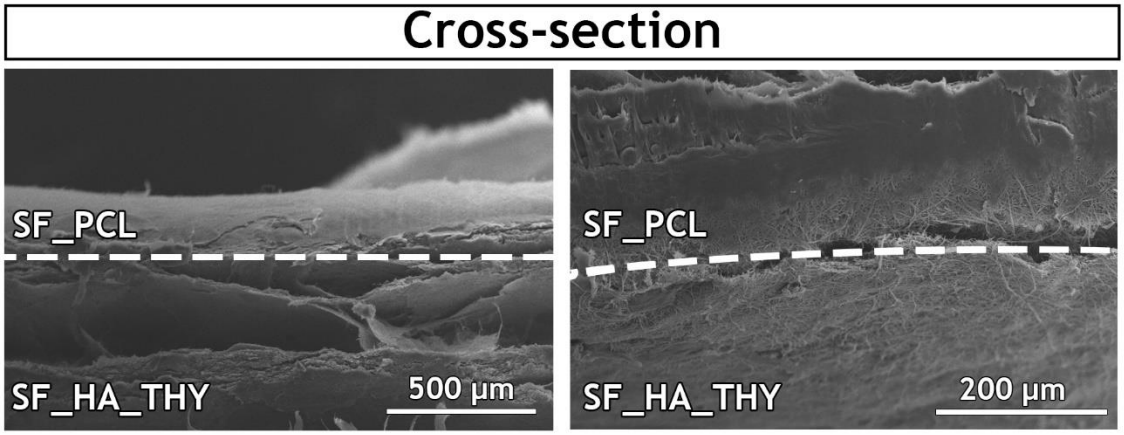

Figure 4.4. SEM images of the produced EAM cross-section (top layer: SF_PCL; bottom layer: SF_HA).

4.3.2 Attenuated total reflectance-fourier transform infrared spectroscopic analysis

As aforementioned, the aqueous stability of SF can be improved by promoting a conformational change in its structure, *i.e.* a conversion from random coil to ß-sheet through the treatment of the membrane with ethanol vapor. The structural changes in SF were confirmed by FTIR analysis. In Figure 4.5, it is possible to see that the peaks of amide I (1643 cm^{-1}) and amide II (1528 cm^{-1}) that are characteristic of the random coil conformation were shifted to 1627 cm^{-1} and 1518 cm^{-1}, respectively. This result confirms the presence of the ß-sheet conformation of SF nanofibers and consequently the improved aqueous stability of SF [14, 20]. Further, to confirm the improved water stability, the membranes were also incubated for 24 h in ultrapure water and the absorbance at 275 nm was recorded (Figure 4.6). The spectrum of the crosslinked membranes did not show a significant release of SF, while the spectrum of uncrosslinked membranes presents a broad peak, *i.e.* SF dissolution occurred.

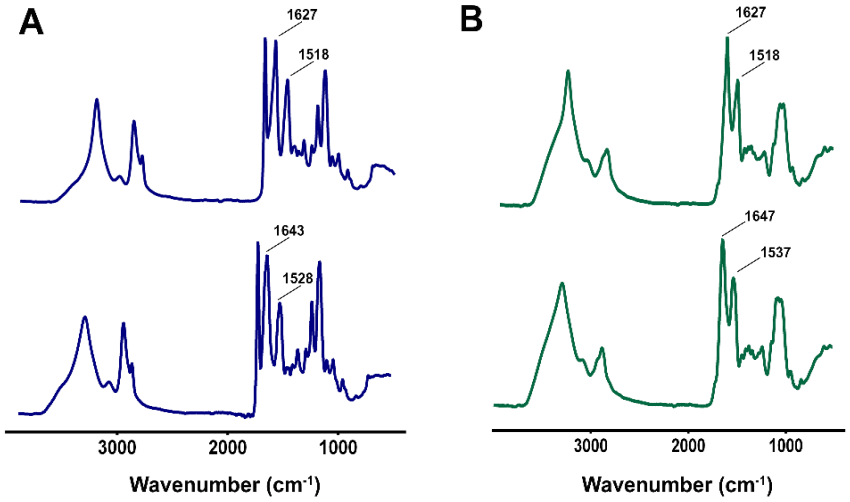

Figure 4.5. ATR_FTIR spectra of the top (A) and bottom (B) layers, showing the structural changes of silk from random coiled to ß-sheet conformation.

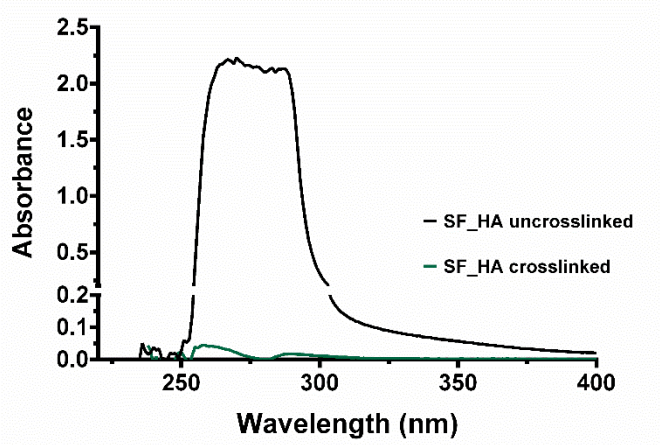

Figure 4.6. UV spectra of the uncrosslinked and crosslinked SF_HA layer after 24 h of incubation in ultrapure water.

On the other side, FTIR was also used to characterize the chemical composition of the electrospun layers produced in this work (Figure 4.7A). The spectrum of the top layer displays the characteristic peaks of SF at 3281 cm^{-1} (-OH stretching and bending vibration mode), 2942 cm^{-1} (asymmetric CH_2 stretching), 1627 cm^{-1} (amide I), and 1518 cm^{-1} (amide II) [14, 21]. Additionally, in this spectrum, the characteristic peaks of PCL are also visible at 2942 cm^{-1} (asymmetric CH_2 stretching), 1724 cm^{-1} (carbonyl stretching), 1293 cm^{-1} (C-O and C-C stretching), 1239 cm^{-1} (asymmetric C-O-C stretching) and 1163 cm^{-1} (symmetric C-O-C stretching) [21]. Similarly, the spectrum of the bottom layer (Figure 4.7B) shows the typical bands of SF, as well as the characteristic peaks of HA at 3200-3600 cm^{-1} (OH and NH stretching), 1640-1690 cm^{-1} (C=O stretching of primary amide) and 1029 cm^{-1} (C-O-C stretching) [5].

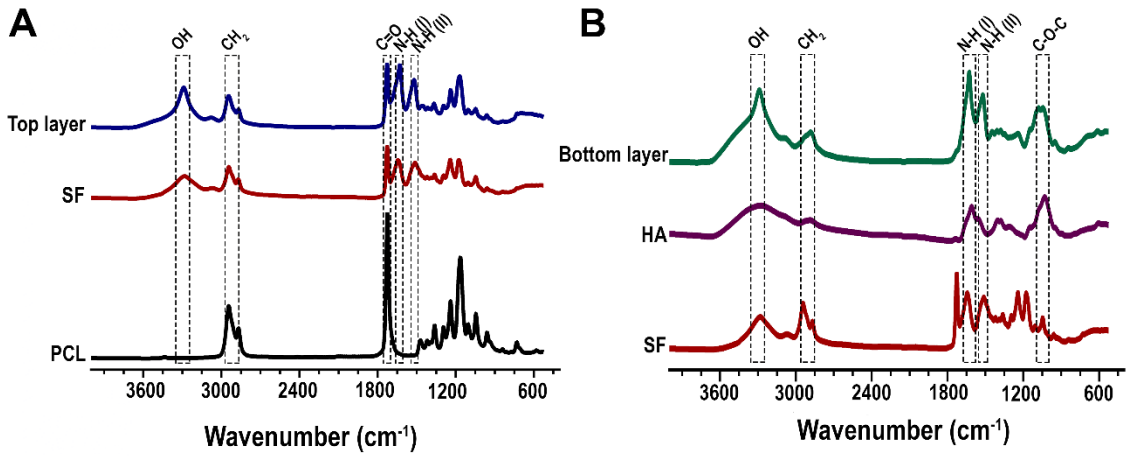

Figure 4.7. ATR_FTIR analysis of the top (A) and bottom (B) nanofibrous layers as well as of its raw materials.

Furthermore, the incorporation of THY into SF_HA nanofibers was also investigated. The spectrum presented in Figure 4.8 displays the THY characteristic peaks at 3174 cm^{-1} (stretching vibration of phenolic O-H group), 2900 cm^{-1} region (C-H stretching), 1619-1516 cm^{-1} (C-C ring stretching band), 1516-1421 cm^{-1} (OH bending vibration), 1243 cm^{-1} (C-O stretching), and 801 cm^{-1} (aromatic C-H bending) [22]. Further, the same peaks can be observed in the spectrum of the SF_HA_THY membrane, which indicates the successful entrapment of THY within the polymeric nanofibers.

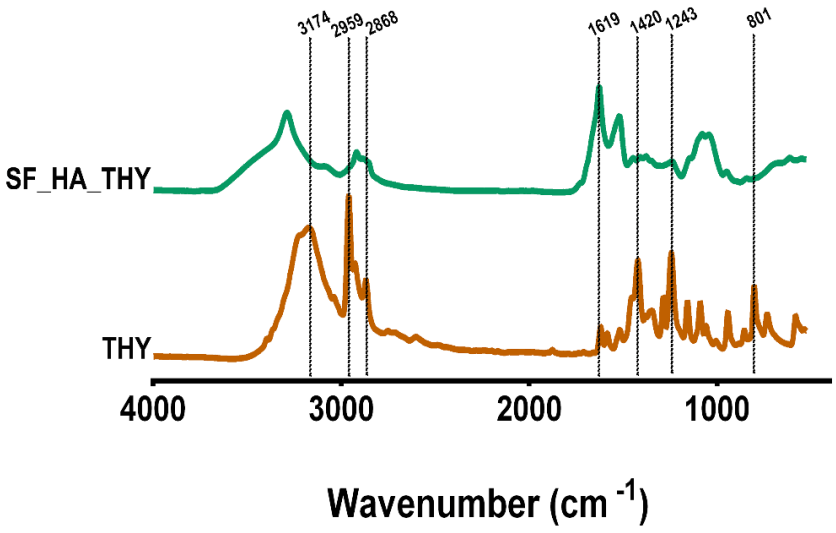

Figure 4.8. ATR_FTIR analysis of the thymol-loaded membrane bottom layer and raw thymol.

4.3.3 Characterization of the membranes' mechanical properties

The mechanical properties of the produced EAM were assessed in dry and wet conditions. The Young's modulus, tensile strength, and elongation at break for the EAM and the values reported for native skin are presented in Table 4.1. The Young's modulus obtained for EAM was 25.67 ± 6.84 MPa in a dry state, whereas in wet conditions this value decreased to 14.70 ± 4.42 MPa. Moreover, the EAM showed values of the Tensile Strength of 23.01 ± 6.73 MPa

in the dry state and 7.59 ± 1.26 MPa in wet conditions. The elongation at break assays reveal that the EAM can bear a strain of 69.27 ± 14.87% and 57.39 ± 13.78% for the dry and wet state, respectively. The obtained data, both in dry and wet conditions, emphasize the excellent mechanical properties of the EAM. In fact, the obtained Young modulus, tensile strengths, and elongation-at-break values are similar to those displayed by the native skin (as depicted in Table 4.1). Further, such results demonstrate that the EAM can tolerate all the stresses during the membrane handling and provide mechanical support during the wound healing process. The mechanical performance of EAM can be attributed to PCL and SF, which are recognized by their good mechanical properties [6, 23]. Further, Nogueira *et al*. reported that the structural transition from random coil to β-sheet conformation makes SF more resistant to water and also improves its mechanical properties [24].

Table 4.1. Young's modulus, tensile strength, and elongation at break of EAM and the native human skin [25].

		Young Modulus (MPa)	Tensile Strength (MPa)	Elongation at break (%)
EAM	Dry	25.67 ± 6.84	23.01 ± 6.73	69.27 ± 14.87
	Wet	14.70 ± 4.42	7.59 ± 1.26	57.39 ± 13.78
Native skin		4.6-20	5-30	35-115

4.3.4 Assessment of the membranes' porosity

The wound dressings' porosity affects the cellular adhesion, infiltration, and proliferation, as well as gases, nutrients and fluids exchange at the wound site [26]. Based on data available in the literature, for an effective healing process occurs, wound dressings should display porosity values within the range of 60-90% [27].

Herein, the SF_PCL and SF_HA_THY nanofibrous layers presented a total porosity of 64.28 ± 2.59% and 85.24 ± 2.47%, respectively (Figure 4.9A). Moreover, the EAM membrane displayed a total porosity of 74.78 ± 6.98%, a value that is comprehended between the porosity values of the individual membranes (top and bottom layers). The obtained porosity values are in accordance with the structural differences noticed between the top and bottom layers, as previously observed in the SEM images. In fact, the lower porosity of SF_PCL layer is justified by the increased nanofiber diameter and deposition density. Such values are in agreement with those obtained for other asymmetric membranes reported in the literature, where the top layer produced with PCL displayed the lowest porosity (55 ± 5%) and the bottom layer composed of CS_AV_PEO showed a superior porosity (97.8 ± 5%) [6]. Moreover, the obtained porosity values are compatible with the functions desired for each layer, the lower porosity of top layer will inhibit microorganism invasion whereas the highly porous bottom layer (≈ 90%) allows cell adhesion, migration, and proliferation [26].

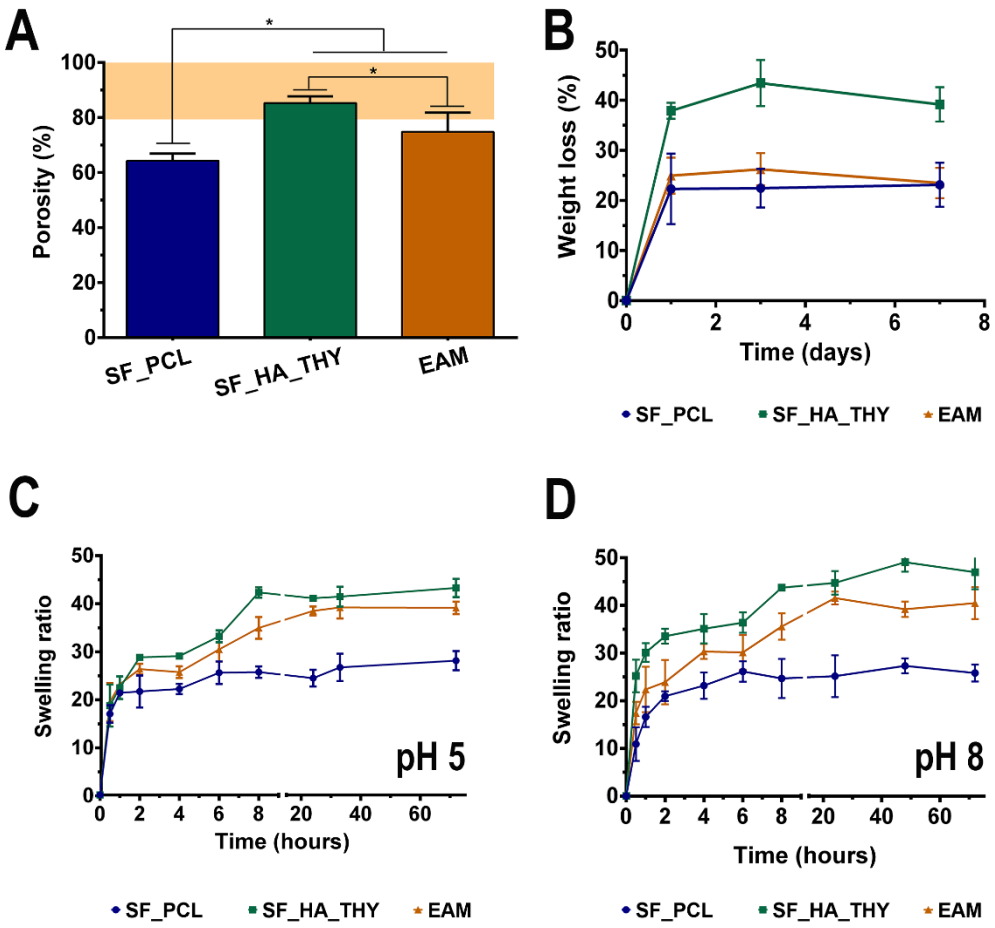

Figure 4.9. Characterization of the total porosity (A), weight loss (B), and swelling profile at pH 5 (C) and pH 8 (D), of the SF_PCL and SF_HA_THY layers and EAM at different time points (data are presented as the mean ± standard deviation, n = 5, *p < 0.05).

4.3.5 Evaluation of the produced membranes' swelling profile

Membranes' swelling capacity has a tremendous impact on its application in the wound healing process. This property is fundamental to accomplish the absorption of the wound exudate, which is essential to prevent tissue maceration and skin infection [28]. The swelling profile of the produced membranes was studied by incubating them in PBS at pH 5 (Figure 4.9C) and pH 8 (Figure 4.9D) to mimic the conditions found in the native and injured skin. The obtained results demonstrated that SF_PCL, SF_HA _THY, and EAM membranes reached their maximum water uptake capacity after 24 h. On the other hand, the swelling capacity for all the groups was higher at pH 8, *i.e.* water absorption ratio of ≈ 25, ≈ 45 and ≈ 42 for SF_PCL, SF_HA_THY, and EAM, respectively. The obtained data reveal that the bottom layer presents a higher swelling ratio in comparison with the top layer, which occurs due to the incorporation of hydrophilic compounds, like HA [29]. Further, the combination of SF_PCL and SF_HA_THY nanofibrous layers appears to result in an EAM membrane with a more controlled swelling capacity, *i.e.* have a higher swelling ratio than the top layer, however it is not as high as the

bottom layer, which allows a sustained absorption of exudates and avoids the wound dehydration. Additionally, the increased swelling capacity at pH 8 highlights the potential of EAM to remove the exudate from the wound, produced 1-3 days after the injury occurs, namely during the inflammatory phase.

4.3.6 Evaluation of the membranes' degradation profile

When a non-biodegradable biomaterial is used to cover the skin lesion, its removal from the wound can induce the formation of scar tissue and pain to the patient as well as increase the risk of bacterial contamination. In this way, wound dressings should be produced with biodegradable materials, that display a degradation profile that is similar to the skin regeneration rate [30]. Therefore, the fine-tuning of the biomaterials degradation profile is crucial to enhance the healing process [31].

SF fibers are defined as a non-degradable biomaterial, which hinders its application in the production of wound dressings. To surpass such handicap, in this study, silk based EAM degradability was tailored by adding different polymers and compounds to the SF matrix (Figure 4.9B). The degradation studies showed that the EAM membrane undergoes a weight loss of 23% during the 7 days. Further, SEM images of the EAM membrane cross-section (Figure 4.10) were acquired and revealed that the two layers remain attached together, even after incubation in PBS for 7 days. The degradation profile may be justified by the strong entanglement between the two layers that compose the EAM. Moreover, the two polymers used in the top layer (SF and PCL) present a slow degradation profile. In fact, the *in vitro* degradation of SF occurs mainly by hydrolysis, whereas PCL degrades through the action of MMPs and hydrolysis of the polyester components [32]. In turn, the HA and THY, present in the bottom layer of EAM, are characterized by suffering higher weight losses *in vivo*. HA is degraded by the action of the hyaluronidases enzymes, hydrolysis and oxidation [9]. On the other hand, THY suffers degradation through the oxidation, polymerization, disproportionation and cyclization reactions [33].

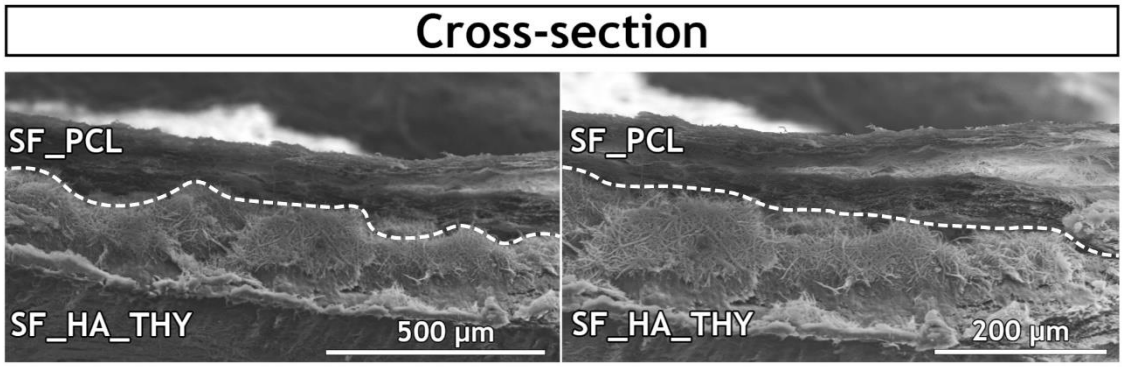

Figure 4.10. SEM images of the produced EAM cross-section after incubation in PBS solution (pH 5) for 7 days.

4.3.7 Characterization of the EAM water vapor transmission rate

The ability of a wound dressing control the water loss can be determined by the WVTR [34]. In the wound healing process, WVTR plays an important role in preventing wound dehydration and exudate accumulation, favouring the tissue regeneration [35].

The EAM membrane presented a WVTR of 2070.62 ± 102.52 mL/m^2/day. This value is superior to those found on commercial wound dressings (*e.g.* 491 ± 44 g/m^2/day for Tegaderm™ (3M), 394 ± 12 g/m^2/day for Bioclusive™ (Johnson-Johnson), and 792 ± 32 g/m^2/day for Opsite (Smith & Nephew)) [36] and to other asymmetric membranes previously described in the literature (*e.g.* asymmetric PCL/CS_AV_PEO membrane (1252.35 ± 21.22 g/m^2/day) [6], PCL_HA/CS_ZN electrospun bilayer membrane (1762.91 ± 187.50 g/m^2/day) [5] and asymmetric PVA/CS membranes produced by $scCO_2$-assisted phase inversion method (214 ± 16 g/m^2/day) [37]). In fact, according to the data available in several studies, the ideal WVTR value should be comprised between 2000-2500 mL/m^2/day to facilitate the proliferation and function of epidermal cells and fibroblasts as well as the water vapor exchanges [38].

4.3.8 Water contact angle determination

Wound dressing material wettability is one of the most important surface properties that affect its biological performance, namely protein adsorption, platelet adhesion, blood coagulation as well as cells and bacterial adhesion [39]. Herein, materials wettability was studied by determining the WCA. The SF_PCL layer exhibited a WCA value of 103.10 ± 6.57º, revealing a hydrophobic character. This result can be explained by the hydrophobicity of the PCL aliphatic polyester chains and SF ß-sheet conformation [14, 20]. Further, the SF_PCL membrane was designed to act as a physical barrier that protects the wound and also avoids bacteria infiltration. For that purpose, the application of hydrophobic surfaces (90º< WCA< 150º) has been reported as more effective [5, 39]. In turn, the SF_HA and SF_HA_THY layers presented WCA values of 26.51 ± 4.87º and 38.77 ± 5.32º, respectively. This hydrophilic character is explained by the presence of HA polymer, which is one of the most hydrophilic molecules of ECM [29]. Furthermore, the incorporation of hydrophobic essential oil (THY) resulted in a membrane with a moderate hydrophilic surface, WCA value comprehended between 40º-70º, which are considered ideal for supporting cell attachment and proliferation (see Section 4.3.11) [40].

4.3.9 Characterization of the Thymol *in vitro* release profile

Different materials and drugs have been used to produce electrospun meshes, that are aimed to be used as drug delivery systems [5, 41]. Among them, biodegradable (*e.g.* CS, PLA, PEO, PCL [5, 42]) or non-biodegradable (*e.g.* PU [43]) materials have been used to accomplish specific drug release profiles. Herein, THY (an herbal drug) was selected to be loaded into the nanofibers in order to provide antibacterial and antioxidant properties to the bottom layer of

the EAM (as illustrated in Figure 4.11A). The LE and EE values obtained for the THY incorporation in the bottom layer of the EAM were 64.8 ± 5.42% and 79.7 ± 7.19%, respectively. These results indicated that THY can be efficiently encapsulated in the SF_HA nanofibrous layer by using the electrospinning technique.

Afterwards, the THY release profile from SF_HA nanofibrous layer was characterized at pH 5 (pH of the native skin) and 8 (pH of injured skin) [7]. The obtained results (Figure 4.11B) show that the THY release from the nanofibers, at both pHs, comprises two different phases, *i.e.* a burst release in the first 8 h after immersion in PBS, followed by a gradual release up to 24 h. Such release profile can be justified by the high surface to volume ratio of the nanofibers that favours the PBS adsorption and consequently the diffusion of THY from the nanofibrous membranes to the release media. The cumulative release of THY from the bottom layers is 71.75 ± 2.06% and 91.87 ± 0.99% at pH 5 and pH 8, respectively. Such results may be explained by the higher swelling exhibited by the membranes at pH 8. Further, the increased HA degradation that occurs in alkaline conditions can favour the release of THY [44]. Nevertheless, the obtained release profile is crucial for the bottom layer to avoid the skin infections as well as to reduce the formation of ROS at wound site.

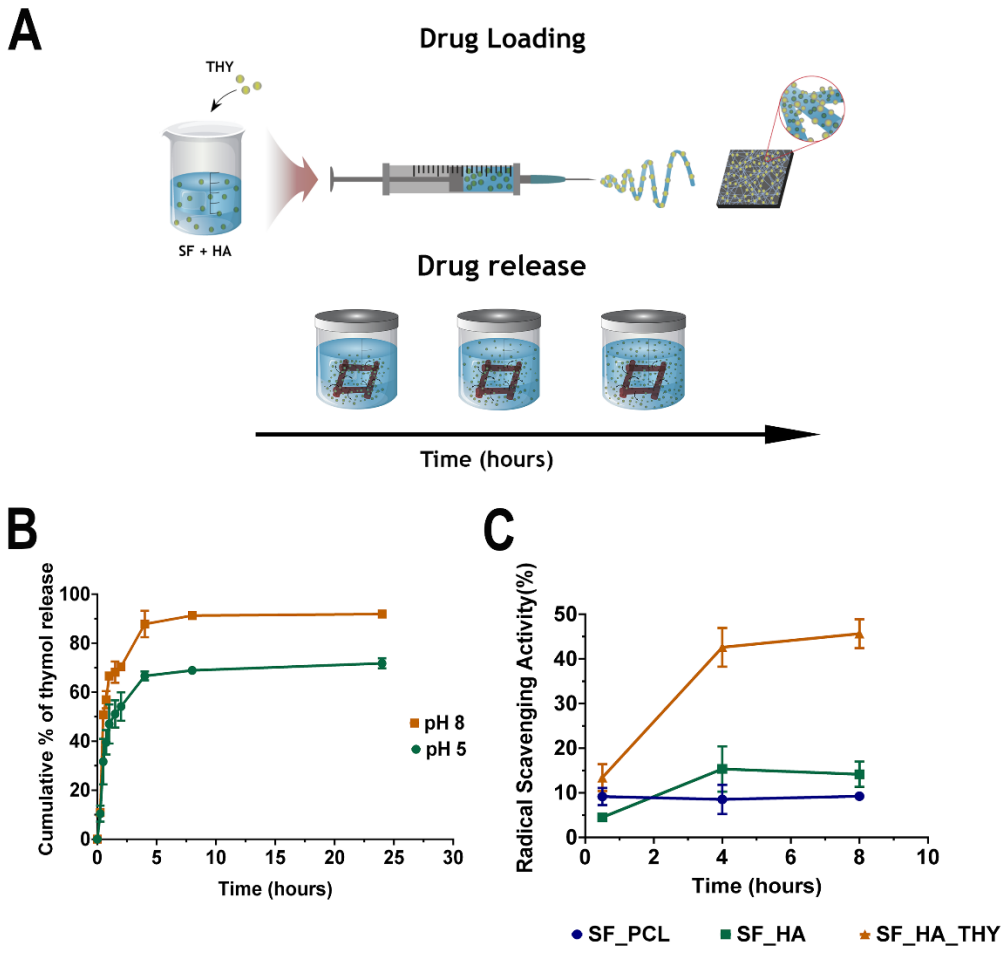

Figure 4.11. Schematic representation of the drug loading and release assays (A); evaluation of the THY *in vitro* release profile (B) and antioxidant activity (C).

Moreover, the release data was also analysed by different mathematical kinetic models to characterize the type of interactions that affect the drug release, please see Table 4.2. The mathematical model that presents the best fitting with the obtained release data is the Korsmeyer-Peppas (R^2= 0.99 (n< 0.5)). This indicates that the drug is released from the SF_HA_THY layer through a Fickian diffusion process, which occurs through the swelling of the polymeric matrix and the formation of heterogeneous regions with a quicker drug dissolution in the composite nanofiber [45]. Additionally, due to the higher weight loss of the bottom layer (as previously determined), the release mechanism could also be fitted with the Hixon-Crowell model (R^2= 0.92). Therefore, it can be concluded that the drug release from SF_HA_THY layer occurs essentially due to the THY dissolution from the polymeric matrix and the degradation of the nanofibers.

Table 4.2. Regression coefficients of the mathematical models fitting the THY release from the SF_HA_THY nanofibrous layers at pH 5 and pH 8.

		Hixon-Crowell	**Korsmeyer-Peppas**	
		R^2	R^2	n
pH 5	**SF_HA_THY**	0.92	0.99	0.29
pH 8	**SF_HA_THY**	0.92	0.99	0.20

4.3.10 Evaluation of the produced membranes' antioxidant activity

During the wound healing process, namely in the inflammatory phase, occurs the production of ROS, which are important molecules in the body defence against the microorganisms' invasion. However, when the production of ROS is excessive, the ECM proteins are degraded, and cell functions are impaired. Moreover, the ROS can prompt the proinflammatory cytokines secretion and promote the activity of MMPs, impairing the production of ECM and, consequently, delaying the healing process [46].

Herein, the antioxidant activity of the produced membranes was investigated through the DPPH assay, along 8 h. DPPH is a stable free radical, which displays a maximum absorption peak at 517 nm. In Figure 4.11C, it is observed that SF_PCL and SF_HA membranes present a reduced antioxidant activity (9.22% and 14.15%, respectively). On the other hand, SF_HA_THY membrane exhibited high DPPH scavenging activity (≈ 45.64%) after 8 h of incubation. The residual antioxidant activity of SF_PCL and SF_HA is attributed to the phenolic side chains of SF tyrosine and tryptophan amino acids residues [14]. In the bottom layer, the THY incorporation in the SF_HA nanofibers improved its antioxidant activity. In the literature, Yanishlieva and their collaborators already highlighted the antioxidant activity of THY in a lipidic mixture (*i.e.* purified triacylglycerols of lard and sunflower oil) [12]. This protective

effect of THY arises from its capacity to donate a hydrogen atom (from the phenol hydroxyl groups) to the peroxyl radicals, producing stabilized phenoxyl radicals [47].

4.3.11 Characterization of the electrospun membranes biological properties

4.3.11.1 Evaluation of the cell viability and adhesion in contact with the EAM

The cytocompatibility of the electrospun membranes was evaluated using NHDF as model cells. Fibroblasts were chosen since they are involved in the production of ECM, glycoproteins, adhesive molecules, and various cytokines that modulate the reestablishment of the damaged tissue. The optical microscopic images of the NHDF cells seeded in contact with membranes after 1, 3 and 7 days (Figure 4.12) show that cells did not suffer any morphological alteration since they exhibit a morphology similar to those present in the negative control (cells incubated only with culture medium). On the other side, cells with a spherical shape were visualized in the positive control.

Furthermore, the cytotoxic profile of the membranes was also evaluated through a MTS assay, over 1, 3 and 7 days (Figure 4.13A). The data obtained show that the produced membranes did not induce any cytotoxic effect on NHDFs, over 7 days. Moreover, the amount of THY incorporated in the membranes did not compromise the cell viability.
In addition, the membranes biocompatibility was also characterized by the dsDNA assay. The obtained results (Figure 4.13B) do not show any significative differences between the test and the control group, which suggests that the NHDFs remain viable and proliferate when seeded in contact with the produced membranes for 7 days.

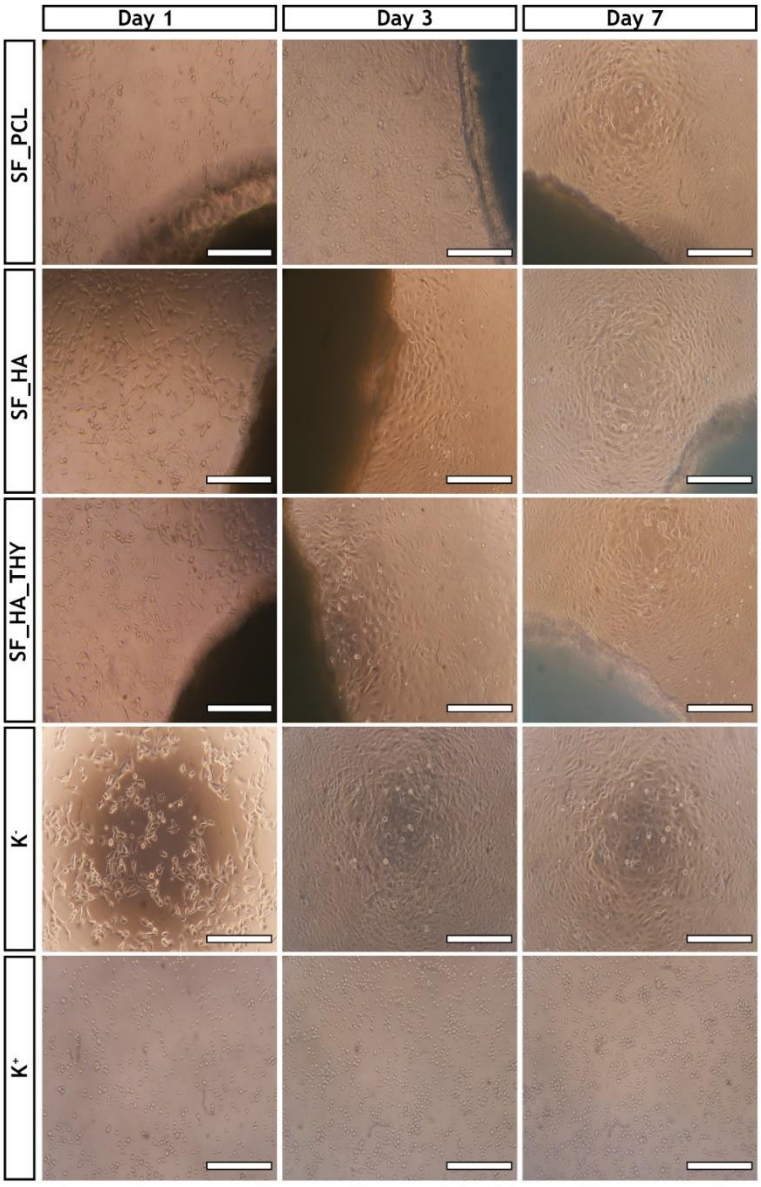

Figure 4.12. Optical microscopic images of Normal Human Dermal Fibroblast (NHDF) cells cultured in the presence of the different produced membranes (SF_PCL, SF_HA and SF_HA_THY) after 1, 3, and 7 days of incubation; K^- (negative control); K^+ (positive control). Scale bar represents 200 µm.

Moreover, the SEM images presented in Figure 4.13C show that the topography and roughness of the electrospun membranes promote cell adhesion. However, in the SF_HA and SF_HA_THY layers, the fibroblast cells appear to present more filopodia protrusions, showing higher cell adhesion and proliferation.

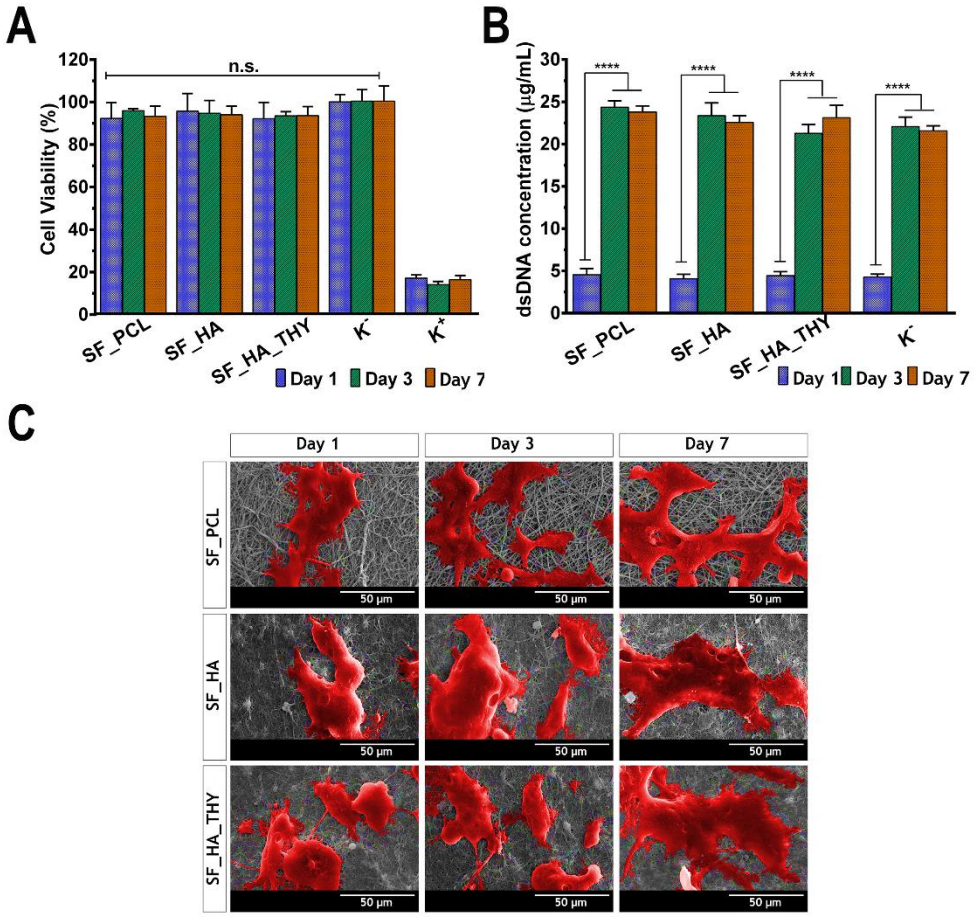

Figure 4.13. Characterization of the produced membranes cytotoxic profile. Analysis of the NHDF cell viability (A) and dsDNA content (B) after 1, 3, and 7 days of incubation with the membranes. Data are presented as the mean ± standard deviation, n = 5, ****p < 0.0001. SEM images of NHDF cells seeded at the surface of the different electrospun membranes after 1, 3, and 7 days (C).

4.3.11.2 Live/dead assay

Live/dead assay was also performed to analyse the cell survival at the surface of the membranes, by simultaneously staining live (green labelled) and dead (red labelled) cells. The CLSM images (Figure 4.14) clearly show that cells remain viable when they are seeded in contact with membranes, and their number increased along time. These results corroborate the data obtained in the MTS and dsDNA assays, thus supporting the biocompatibility of these membranes. Moreover, the SF_HA and SF_HA_THY layers present a higher number of cells. The enhanced biological properties exhibited by the bottom layers are explained by the presence of HA in its composition. In fact, HA is a protein found in skin ECM that has a high water retention capacity, stimulates the migration of inflammatory and fibroblast cells into the wounds, through its interaction with cell surface receptors CD44 [48]. Moreover, the low molecular weight of the HA used in this study also favours cell migration and adhesion [49].

Indeed, these superior biological performance of HA enriched nanofibers was also observed in a study performed by Li *et. al*, where the incorporation of HA improved the cellular

microenvironment, favouring the cellular infiltration and adhesion to the nanofibers [50]. Moreover, Selvaraj and their co-workers also demonstrated that fibroblasts proliferate and remain viable when in contact with SF electrospun membranes [14]. Overall, the obtained results clearly demonstrate the excellent biocompatibility of the produced EAM as well as support its application as a wound dressing for promoting the healing process.

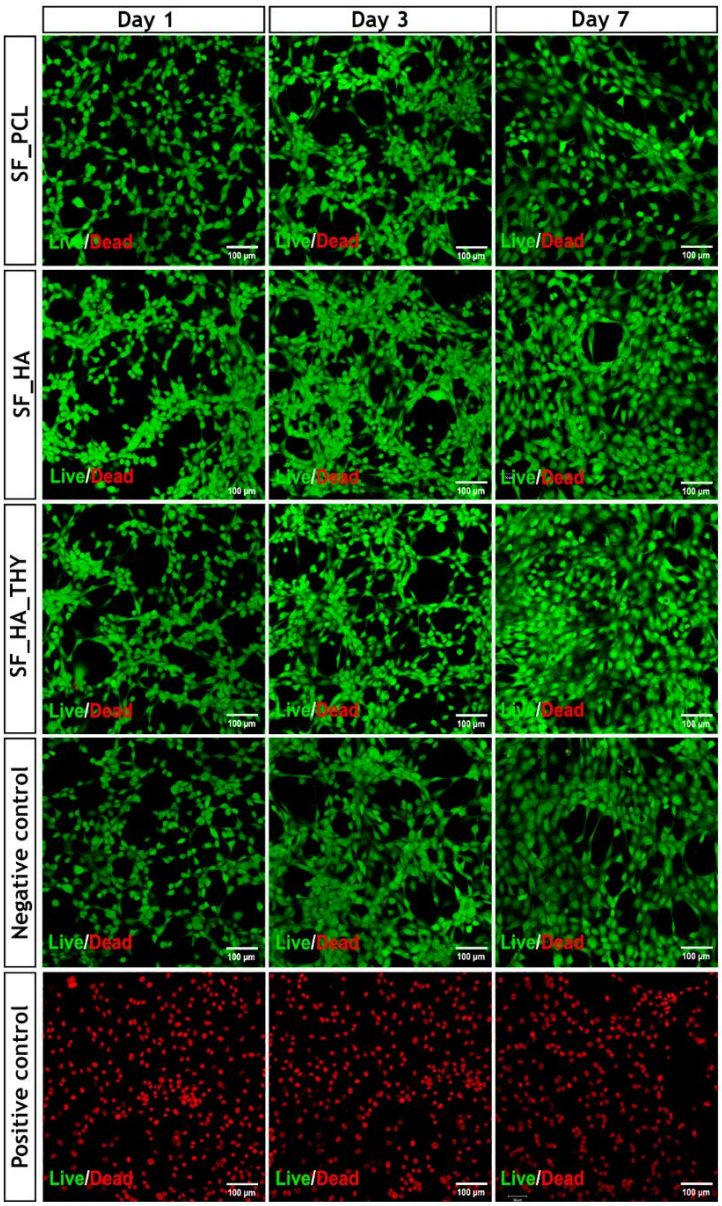

Figure 4.14. Fluorescence microscopic images from a Live-dead assay of NHDFs cultured on the surface of the produced membranes after, 1, 3 and 7 days. Green channel: viable cells labelled with Calcein; red channel: dead cells stained with Propidium iodide.

4.3.12 Evaluation of the antimicrobial properties of the membranes

Bacterial contaminations, which usually occur after a skin injury, are regarded as one of the most severe and devastating health complications. According to the available information, up to 65-80% of all infections lead to the formation of biofilms, highlighting the urgent need to develop biomaterials capable of avoiding the establishment and development of infections [51]. In this context, the antimicrobial properties of the produced membranes were evaluated by using *S.aureus* (gram-positive bacterium) and *P.aeruginosa* (gram-negative bacterium) as bacteria models. These strains were selected since they are described as the most common microorganisms found in skin infections [52]. The results presented in Figure 4.15A and 4.15B show that the top layer (SF_PCL) of the EAM membrane, acts as a protective barrier, avoiding the bacterial infiltration in both bacterial models.

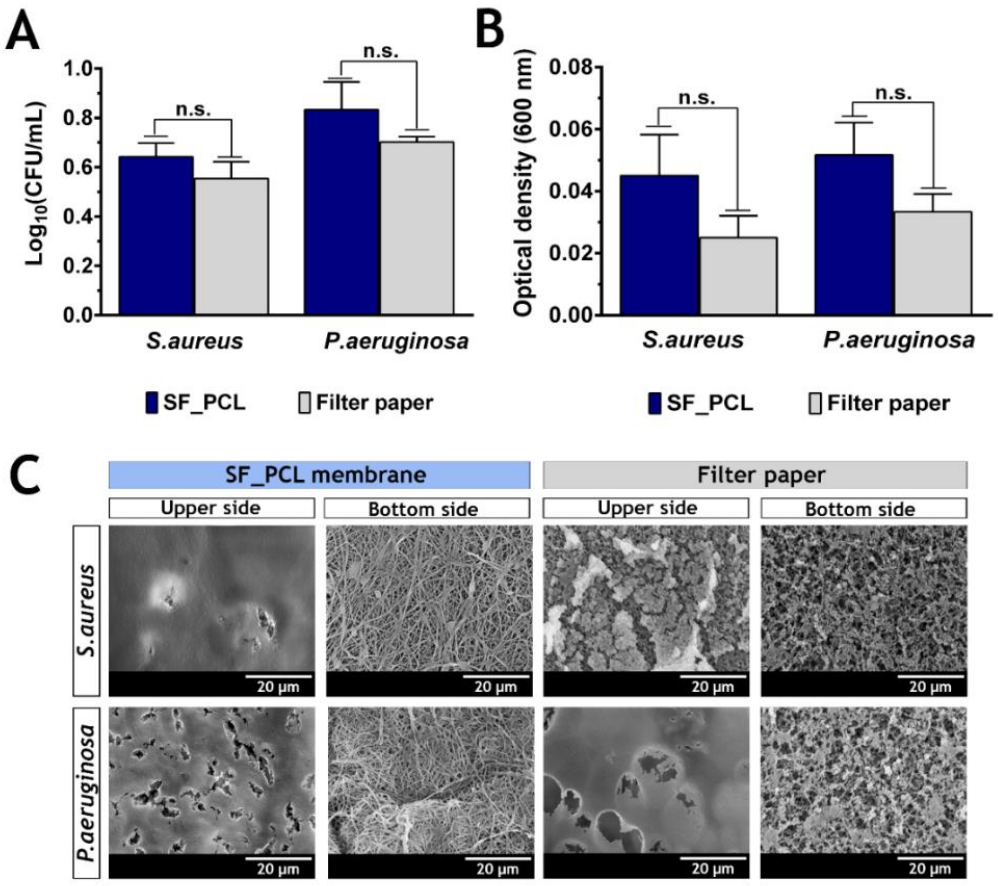

Figure 4.15. Evaluation of the bacterial infiltration through SF_PCL membrane and filter paper (control group). Determination of the number of the CFU of *S.aureus* and *P.aeruginosa* that crossed the SF_PCL membrane or filter paper, after 24 h (A). Measurement of the optical density from medium samples recovered from the lower chamber of the transwell system (B). Data are presented as the mean ± standard deviation, n = 5, n.s.= non-significant. SEM images of the microorganisms (*S.aureus* and *P.aeruginosa*) that adhered to the upper or lower side of the SF_PCL membrane and filter paper (C).

Further, the obtained results do not show any significant difference with the control group, a filter paper (pore size of 0.22 µm). Additionally, SEM images (Figure 4.15C) also demonstrate that the bacteria can adhere to the upper side of the top layer, however no bacteria were visualized at the bottom side of the nanofibrous layer, which emphasizes the capacity of the top layer to act as a filter, due to its low porosity, avoiding the microorganism's colonization of the wound. Furthermore, the antibacterial properties of the bottom layers (SF_HA and SF_HA_THY) were also evaluated. To accomplish that, bacteria models (*S.aureus* and *P.aeruginosa*) were grown in contact with the membranes and then, the number of bacterial colonies formed were counted. The obtained results show that the SF_HA_THY membranes present an increased inhibitory effect in bacterial growth, 87.42% and 58.43% for *S.aureus* and *P.aeruginosa,* when compared to SF_HA membranes, 4.05% and 3.42% for *S.aureus* and *P.aeruginosa* (Figure 4.16A and 4.16B). Furthermore, contrasting to SF_HA membranes, no biofilm formation was observed at the surface of SF_HA_THY nanofibrous layer (Figure 4.16C).

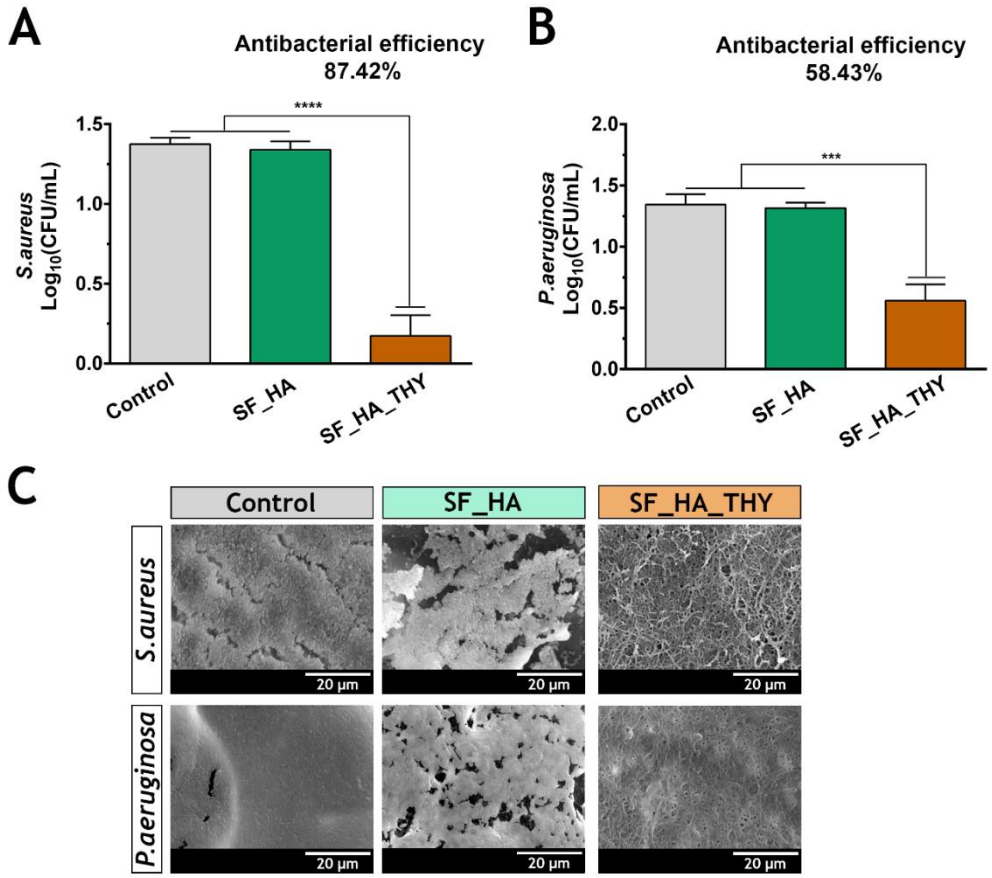

Figure 4.16. Evaluation of the SF_HA and SF_HA_THY nanofibrous layers antibacterial potential against *S.aureus* (A) and *P.aeruginosa* (B). Data are presented as the mean ± standard deviation, n = 5, ***p < 0.001, ****p < 0.0001. SEM images of control, SF_HA and SF_HA_THY nanofibrous layers incubated with *S.aureus* and *P.aeruginosa* (C).

To further assess the antibacterial potential of the membranes, the modified Kirby-Bauer assay was performed. The obtained data confirmed the excellent antimicrobial properties of the SF_HA_THY layer, which presented a 2 to 3 times larger inhibitory halo area in comparison to SF_HA layer for *S.aureus* and *P.aeruginosa*, respectively (Figure 4.17).

The results demonstrate that the incorporation of THY conferred antimicrobial properties to the bottom SF_HA layer. The antibacterial properties of EOs and their components have been already reported in the literature [53, 54]. In the majority of the cases, the EOs destabilize the cellular architecture, leading to the disruption of the cell wall structure and functions [55, 56]. The impairment of the cell wall permeability can compromise the solutes transport, the maintenance of the cell energy, and the metabolic regulation [57]. Further, the antibacterial activity of EOs can induce the reduction of the membrane potential, the disruption of the proton pumps, and depletion of the intracellular ATP [58]. However, several studies speculate that the antimicrobial activity of EOs is significantly influenced by the physicochemical characteristics of the bacterial cell wall [55, 59]. Indeed, in this study, the THY presented a superior efficacy towards *S.aureus*. In this sense, some studies suggest that the difference in the susceptibility to antimicrobials between Gram-positive and Gram-negative bacteria could be attributed to the cytoplasmic membrane and/or outer membrane cell wall structure and composition [60]. The structure of the Gram-positive bacteria cell wall facilitates the penetration of hydrophobic molecules into the cells, allowing their action on the cell wall and within the cytoplasm [60]. On the other hand, the cell wall of Gram-negative bacteria is more complex and present a higher thickness [59]. Further, the cell wall of the Gram-negative bacteria is composed primarily of LPS molecules which form a hydrophilic permeable barrier, providing protection against the effect of hydrophobic EOs [61].

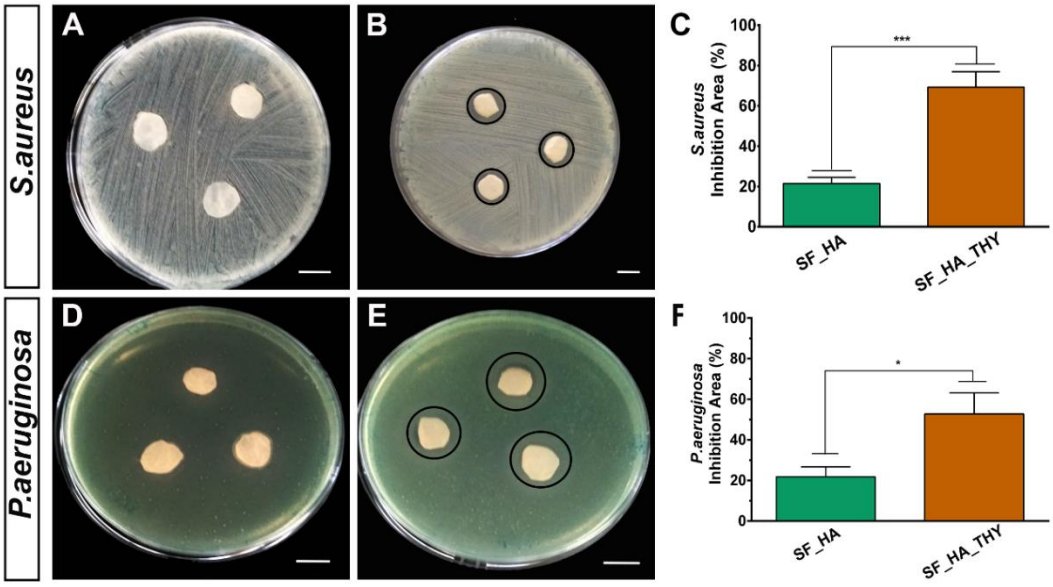

Figure 4.17. Evaluation of the EAM' bottom layer bactericidal activity. Macroscopic images and analysis of the inhibitory halos around the samples of the bottom layers, when they were put in contact with *S.aureus* (A, B, and C) and *P.aeruginosa* (D, E, and F). Data are presented as the mean ± standard deviation, n = 5, *p < 0.05, ***p < 0.001).

4.4 Conclusions

Despite the tremendous efforts made in the development of wound dressings, none of the currently available is fully capable of re-establish the skin native structure and functions. To overcome this situation, the EAMs exhibiting a skin-like layered organization and physicochemical properties arise as a highly promising approach for improving the wound healing mechanism. Herein, a bilayered EAM was produced using as the main component a silk derived biopolymer. The top layer was manufactured with SF and PCL to act as a physical barrier at the wound site, whereas the bottom layer was composed of SF, HA and THY to enhance the wound healing process and avoid the occurrence of infections at the wound site. It is worth to notice that to the best of our knowledge, this is the first time that THY is incorporated in an EAM. Moreover, the structural organization and mechanical properties exhibited by EAM are similar to those of the human native skin. Moreover, *in vitro* assays revealed that the membrane can promote the cell adhesion, proliferation and spreading. In addition, the incorporation of THY into the bottom nanofibrous layer imprinted in the EAM antioxidant and antibacterial properties that are essential for the healing process.

In the near future, the EAM and THY anti-inflammatory, local anaesthetic, antinociceptive, cicatrizing and antiseptic properties will be further characterized to reinforce the application of this membrane as a wound dressing. Moreover, the inclusion of GFs and proteins can also be considered to improve the biological performance of these membranes.

4.5 References

1. Chaudhari AA, Vig K, Baganizi DR, Sahu R, Dixit S, Dennis V, Singh SR, Pillai SR. Future prospects for scaffolding methods and biomaterials in skin tissue engineering: a review. International journal of molecular sciences. 2016;17(12):1974.
2. Sun BK, Siprashvili Z, Khavari PA. Advances in skin grafting and treatment of cutaneous wounds. Science. 2014;346(6212):941-5.
3. Pereira RF, Barrias CC, Granja PL, Bartolo PJ. Advanced biofabrication strategies for skin regeneration and repair. Nanomedicine. 2013;8(4):603-21.
4. Miguel SP, Figueira DR, Simões D, Ribeiro MP, Coutinho P, Ferreira P, Correia IJ. Electrospun polymeric nanofibres as wound dressings: a review. Colloids and surfaces B: Biointerfaces. 2018;169:60-71.
5. Figueira DR, Miguel SP, de Sá KD, Correia IJ. Production and characterization of polycaprolactone-hyaluronic acid/chitosan-zein electrospun bilayer nanofibrous membrane for tissue regeneration. International journal of biological macromolecules. 2016;93:1100-10.
6. Miguel SP, Ribeiro MP, Coutinho P, Correia IJ. Electrospun Polycaprolactone/aloe Vera_Chitosan Nanofibrous asymmetric membranes aimed for wound healing applications. Polymers. 2017;9(5):183.
7. Morgado PI, Miguel SP, Correia IJ, Aguiar-Ricardo A. Ibuprofen loaded PVA/chitosan membranes: A highly efficient strategy towards an improved skin wound healing. Carbohydrate polymers. 2017;159:136-45.

8. Wang H, Liu XY, Chuah YJ, Goh JC, Li JL, Xu H. Design and engineering of silk fibroin scaffolds with biomimetic hierarchical structures. Chemical Communications. 2013;49(14):1431-3.

9. Collins MN, Birkinshaw C. Hyaluronic acid based scaffolds for tissue engineering—A review. Carbohydrate polymers. 2013;92(2):1262-79.

10. Karami Z, Rezaeian I, Zahedi P, Abdollahi M. Preparation and performance evaluations of electrospun poly (ε-caprolactone), poly (lactic acid), and their hybrid (50/50) nanofibrous mats containing thymol as an herbal drug for effective wound healing. Journal of Applied Polymer Science. 2013;129(2):756-66.

11. Marino M, Bersani C, Comi G. Antimicrobial activity of the essential oils of Thymus vulgaris L. measured using a bioimpedometric method. Journal of Food Protection. 1999;62(9):1017-23.

12. Yanishlieva NV, Marinova EM, Gordon MH, Raneva VG. Antioxidant activity and mechanism of action of thymol and carvacrol in two lipid systems. Food Chemistry. 1999;64(1):59-66.

13. Cai Z-x, Mo X-m, Zhang K-h, Fan L-p, Yin A-l, He C-l, Wang H-s. Fabrication of chitosan/silk fibroin composite nanofibers for wound-dressing applications. International journal of molecular sciences. 2010;11(9):3529-39.

14. Selvaraj S, Fathima NN. Fenugreek Incorporated Silk Fibroin Nanofibers□ A Potential Antioxidant Scaffold for Enhanced Wound Healing. ACS applied materials & interfaces. 2017;9(7):5916-26.

15. Fan L, Wang H, Zhang K, He C, Cai Z, Mo X. Regenerated silk fibroin nanofibrous matrices treated with 75% ethanol vapor for tissue-engineering applications. Journal of Biomaterials Science, Polymer Edition. 2012;23(1-4):497-508.

16. Mishra K, Ojha H, Chaudhury NK. Estimation of antiradical properties of antioxidants using DPPH assay: A critical review and results. Food chemistry. 2012;130(4):1036-43.

17. Silva SS, Popa EG, Gomes ME, Cerqueira M, Marques A, Caridade S, Teixeira P, Sousa C, Mano J, Reis R. An investigation of the potential application of chitosan/aloe-based membranes for regenerative medicine. Acta biomaterialia. 2013;9(6):6790-7.

18. Ferreira P, Santos P, Alves P, Carvalho MP, de Sá KD, Miguel SP, Correia IJ, Coimbra P. Photocrosslinkable electrospun fiber meshes for tissue engineering applications. European Polymer Journal. 2017;97:210-9.

19. Zhao J, Han W, Chen H, Tu M, Zeng R, Shi Y, Cha Z, Zhou C. Preparation, structure and crystallinity of chitosan nano-fibers by a solid–liquid phase separation technique. Carbohydrate polymers. 2011;83(4):1541-6.

20. Kong J, Yu S. Fourier transform infrared spectroscopic analysis of protein secondary structures. Acta biochimica et biophysica Sinica. 2007;39(8):549-59.

21. Ghasemi-Mobarakeh L, Prabhakaran MP, Morshed M, Nasr-Esfahani M-H, Ramakrishna S. Electrospun poly (ε-caprolactone)/gelatin nanofibrous scaffolds for nerve tissue engineering. Biomaterials. 2008;29(34):4532-9.

22. Michalska-Sionkowska M, Walczak M, Sionkowska A. Antimicrobial activity of collagen material with thymol addition for potential application as wound dressing. Polymer Testing. 2017;63:360-6.

23. Labet M, Thielemans W. Synthesis of polycaprolactone: a review. Chemical Society Reviews. 2009;38(12):3484-504.

24. Nogueira GM, Rodas AC, Leite CA, Giles C, Higa OZ, Polakiewicz B, Beppu MM. Preparation and characterization of ethanol-treated silk fibroin dense membranes for biomaterials application using waste silk fibers as raw material. Bioresource technology. 2010;101(21):8446-51.

25. Zahouani H, Pailler-Mattei C, Sohm B, Vargiolu R, Cenizo V, Debret R. Characterization of the mechanical properties of a dermal equivalent compared with human skin in vivo by indentation and static friction tests. Skin research and technology. 2009;15(1):68-76.

26. Valipouri A, Gharehaghaji AA, Alirezazadeh A, Ravandi SAH. Porosity characterization of biodegradable porous poly (L-lactic acid) electrospun nanofibers. Materials Research Express. 2017;4(12):125002.

27. Chong EJ, Phan TT, Lim IJ, Zhang YZ, Bay BH, Ramakrishna S, Lim CT. Evaluation of electrospun PCL/gelatin nanofibrous scaffold for wound healing and layered dermal reconstitution. Acta Biomater. 2007;3(3):321-30.

28. Perumal G, Pappuru S, Chakraborty D, Nandkumar AM, Chand DK, Doble M. Synthesis and characterization of curcumin loaded PLA—Hyperbranched polyglycerol electrospun blend for wound dressing applications. Materials science and engineering: C. 2017;76:1196-204.

29. Fakhari A, Berkland C. Applications and emerging trends of hyaluronic acid in tissue engineering, as a dermal filler and in osteoarthritis treatment. Acta biomaterialia. 2013;9(7):7081-92.

30. Lu Q, Zhang B, Li M, Zuo B, Kaplan DL, Huang Y, Zhu H. Degradation mechanism and control of silk fibroin. Biomacromolecules. 2011;12(4):1080-6.

31. Rottmar M, Richter M, Mäder X, Grieder K, Nuss K, Karol A, von Rechenberg B, Zimmermann E, Buser S, Dobmann A. In vitro investigations of a novel wound dressing concept based on biodegradable polyurethane. Science and technology of advanced materials. 2015;16(3):034606.

32. Vepari C, Kaplan DL. Silk as a biomaterial. Progress in polymer science. 2007;32(8-9):991-1007.

33. Turek C, Stintzing FC. Stability of essential oils: a review. Comprehensive Reviews in Food Science and Food Safety. 2013;12(1):40-53.

34. Gupta B, Agarwal R, Alam M. Textile-based smart wound dressings. 2010.

35. Xu R, Xia H, He W, Li Z, Zhao J, Liu B, Wang Y, Lei Q, Kong Y, Bai Y. Controlled water vapor transmission rate promotes wound-healing via wound re-epithelialization and contraction enhancement. Scientific reports. 2016;6:24596.

36. Jonkman MF, Molenaar I, Nieuwenhuis P, Bruin P, Pennings AJ. New method to assess the water vapour permeance of wound coverings. Biomaterials. 1988;9(3):263-7.

37. Morgado PI, Lisboa PF, Ribeiro MP, Miguel SP, Simões PC, Correia IJ, Aguiar-Ricardo A. Poly (vinyl alcohol)/chitosan asymmetrical membranes: Highly controlled morphology toward the ideal wound dressing. Journal of membrane science. 2014;469:262-71.

38. Chen Y, Yan L, Yuan T, Zhang Q, Fan H. Asymmetric polyurethane membrane with in situ-generated nano-TiO2 as wound dressing. Journal of Applied Polymer Science. 2011;119(3):1532-41.

39. Oliveira SM, Alves NM, Mano JF. Cell interactions with superhydrophilic and superhydrophobic surfaces. Journal of Adhesion Science and Technology. 2014;28(8-9):843-63.

40. Arima Y, Iwata H. Effect of wettability and surface functional groups on protein adsorption and cell adhesion using well-defined mixed self-assembled monolayers. Biomaterials. 2007;28(20):3074-82.

41. Meng Z, Xu X, Zheng W, Zhou H, Li L, Zheng Y, Lou X. Preparation and characterization of electrospun PLGA/gelatin nanofibers as a potential drug delivery system. Colloids and Surfaces B: Biointerfaces. 2011;84(1):97-102.

42. Kim TG, Lee DS, Park TG. Controlled protein release from electrospun biodegradable fiber mesh composed of poly(epsilon-caprolactone) and poly(ethylene oxide). Int J Pharm. 2007;338(1-2):276-83.

43. Kenawy E-R, Abdel-Hay FI, El-Newehy MH, Wnek GE. Processing of polymer nanofibers through electrospinning as drug delivery systems. Nanomaterials: Risks and Benefits: Springer; 2009. p. 247-63.

44. Stern R, Kogan G, Jedrzejas MJ, Soltes L. The many ways to cleave hyaluronan. Biotechnol Adv. 2007;25(6):537-57.

45. Kumar SU, Matai I, Dubey P, Bhushan B, Sachdev A, Gopinath P. Differentially cross-linkable core–shell nanofibers for tunable delivery of anticancer drugs: synthesis, characterization and their anticancer efficacy. RSC Advances. 2014;4(72):38263-72.

46. Gangwar M, Gautam MK, Ghildiyal S, Nath G, Goel RK. Mallotus philippinensis Muell. Arg fruit glandular hairs extract promotes wound healing on different wound model in rats. BMC complementary and alternative medicine. 2015;15(1):123.

47. Mastelic J, Jerkovic I, Blažević I, Poljak-Blaži M, Borović S, Ivancčić-Baće I, Smrečki V, Žarković N, Brčić-Kostic K, Vikić-Topić D. Comparative study on the antioxidant and biological activities of carvacrol, thymol, and eugenol derivatives. Journal of agricultural and food chemistry. 2008;56(11):3989-96.

48. Neuman MG, Nanau RM, Oruña-Sanchez L, Coto G. Hyaluronic acid and wound healing. Journal of Pharmacy & Pharmaceutical Sciences. 2015;18(1):53-60.

49. Kouvidi K, Berdiaki A, Nikitovic D, Katonis P, Afratis N, Hascall VC, Karamanos NK, Tzanakakis GN. Role of receptor for hyaluronan mediated motility (RHAMM) in low molecular weight hyaluronan (LMWHA) mediated fibrosarcoma cell adhesion. Journal of Biological Chemistry. 2011:jbc. M111. 275875.

50. Li L, Qian Y, Jiang C, Lv Y, Liu W, Zhong L, Cai K, Li S, Yang L. The use of hyaluronan to regulate protein adsorption and cell infiltration in nanofibrous scaffolds. Biomaterials. 2012;33(12):3428-45.

51. Joo H-S, Otto M. Molecular basis of in vivo biofilm formation by bacterial pathogens. Chemistry & biology. 2012;19(12):1503-13.

52. Cardona AF, Wilson SE. Skin and soft-tissue infections: a critical review and the role of telavancin in their treatment. Clin Infect Dis. 2015;61 Suppl 2:S69-78.

53. Liolios C, Gortzi O, Lalas S, Tsaknis J, Chinou I. Liposomal incorporation of carvacrol and thymol isolated from the essential oil of Origanum dictamnus L. and in vitro antimicrobial activity. Food chemistry. 2009;112(1):77-83.

54. Puskarova A, Buckova M, Krakova L, Pangallo D, Kozics K. The antibacterial and antifungal activity of six essential oils and their cyto/genotoxicity to human HEL 12469 cells. Sci Rep. 2017;7(1):8211.

55. Lopez-Romero JC, González-Ríos H, Borges A, Simões M. Antibacterial effects and mode of action of selected essential oils components against Escherichia coli and Staphylococcus aureus. Evidence-Based Complementary and Alternative Medicine. 2015;2015.

56. Trombetta D, Castelli F, Sarpietro MG, Venuti V, Cristani M, Daniele C, Saija A, Mazzanti G, Bisignano G. Mechanisms of antibacterial action of three monoterpenes. Antimicrobial agents and chemotherapy. 2005;49(6):2474-8.

57. Rota C, Carraminana J, Burillo J, Herrera A. In vitro antimicrobial activity of essential oils from aromatic plants against selected foodborne pathogens. Journal of Food Protection. 2004;67(6):1252-6.

58. Turina AV, Nolan MV, Zygadlo JA, Perillo MA. Natural terpenes: self-assembly and membrane partitioning. Biophys Chem. 2006;122(2):101-13.

59. Nazzaro F, Fratianni F, De Martino L, Coppola R, De Feo V. Effect of essential oils on pathogenic bacteria. Pharmaceuticals. 2013;6(12):1451-74.

60. Tiwari BK, Valdramidis VP, O'Donnell CP, Muthukumarappan K, Bourke P, Cullen P. Application of natural antimicrobials for food preservation. Journal of agricultural and food chemistry. 2009;57(14):5987-6000.

61. Helander IM, Alakomi H-L, Latva-Kala K, Mattila-Sandholm T, Pol I, Smid EJ, Gorris LG, von Wright A. Characterization of the action of selected essential oil components on Gram-negative bacteria. Journal of agricultural and food chemistry. 1998;46(9):3590-5.

Chapter V

Production and characterization of a novel asymmetric 3D printed construct aimed for skin tissue regeneration

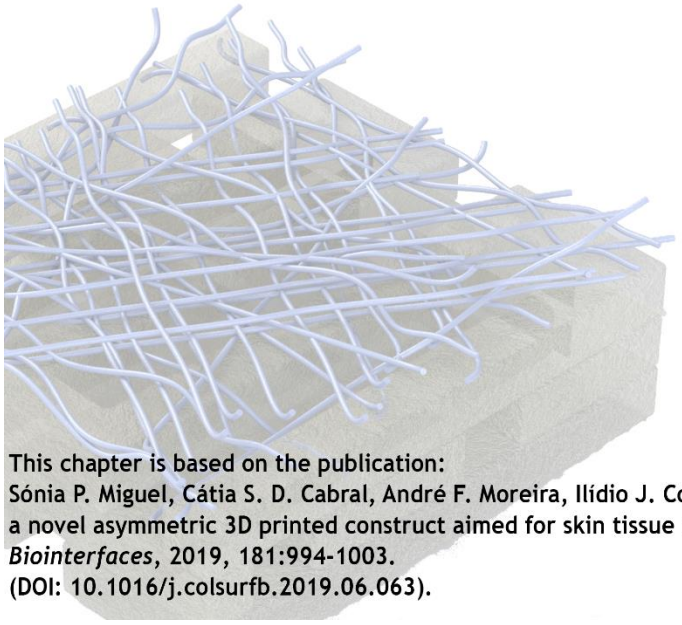

This chapter is based on the publication:
Sónia P. Miguel, Cátia S. D. Cabral, André F. Moreira, Ilídio J. Correia; Production and characterization of a novel asymmetric 3D printed construct aimed for skin tissue regeneration, *Colloids and Surfaces B: Biointerfaces*, 2019, 181:994-1003.
(DOI: 10.1016/j.colsurfb.2019.06.063).

Abstract

Skin is a complex organ that act as the first protective barrier against any external threat. After an injury occurs, its structure and functions must be re-established as soon as possible. Among different available skin substitutes (epidermal, dermal and dermo-epidermal), none of them is fully capable of reproducing/re-establishing all the features and functions of native skin. Herein, a three-dimensional skin asymmetric construct (3D_SAC) was produced using electrospinning and 3D bioprinting techniques. A poly(caprolactone) and silk sericin blend was electrospun to produce a top layer aimed to mimic the epidermis features, *i.e.* to provide a protective barrier against dehydration and hazard agents. In turn, the dermis like layer was formed by printing layer-by-layer a chitosan/sodium alginate hydrogel. The results obtained in the in vitro assays revealed that the 3D_SAC display a morphology, porosity, mechanical properties, wettability, antimicrobial activity and a cytotoxic profile that grants their application as a skin substitute during the healing process.

Keywords: Electrospinning; 3D bioprinting; Asymmetric skin construct; Skin regeneration.

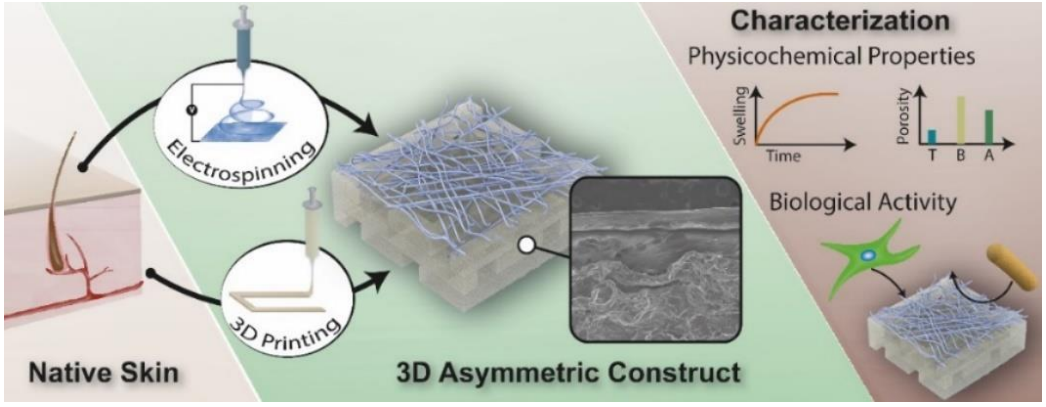

5.1 Introduction

Skin is the body first line of defence, it provides protection against external harmful agents and plays a pivotal role in the maintenance of the body homeostasis [1, 2]. Being the outermost organ of the body, it is susceptible to different types of injuries, such as acute (*e.g.*, surgical and traumatic wounds, abrasions and burns) and chronic wounds (*e.g.*, diabetic foot and pressure ulcers) [1]. Considering the wound size, extent, and depth, researchers have been developing different treatments, comprising various skin substitutes that are aimed to replace epidermis, dermis or both layers of the skin. Among them, the epidermal/dermal substitutes are the most advanced skin constructs [3]. Despite all the advancements attained so far, the currently available skin substitutes present several limitations that include poor tissue integration, due to inappropriate vascularization, deficient adhesion to the wound bed, scarring at the graft margins or incapacity to reproduce skin appendages [2, 3].

To overcome these limitations, biomaterials, bioactive molecules, cells, and modern biomanufacturing techniques have been combined to develop new advanced skin constructs [2]. Among them, the asymmetric wound dressing have captured the attention of different researchers that have been employing various techniques, such as wet phase inversion, dry/wet, $scCO_2$-assisted phase inversion and electrospinning, in their production process [4-7]. In 2010, Chen *et al.* combined the solvent evaporation, wet phase inversion, and organic-inorganic hybridization methods to produce a PU asymmetric membrane loaded with nano-TiO_2. Their results revealed that the membrane' top layer avoided bacterial penetration, whereas the porous sublayer was able to absorb high amounts of exudate [8]. In turn, Morgado *et al.* used a $scCO_2$-assisted phase inversion technique to produce CS/PVA asymmetric membranes loaded with ibuprofen, which by controlling the depressurization rate presented a thin top layer (thickness 15 μm) and a sponge bottom layer with uniform pore distribution [7]. Further, Miguel *et al.* produced a SF based asymmetric membrane using an electrospinning technique. The top layer was composed of SF and PCL, reproducing the waterproof ability of the epidermis, whereas the bottom layer constituted of SF, HA and loaded with thymol exhibited the porosity, wettability, antibacterial and antioxidant properties suitable for healing process [5]. Liang and their collaborators produced a silver nanoparticle/CS composite dressing displaying an asymmetric layered organization. To accomplish that, the authors prepared chitosan sponges loaded with AgNPs through a lyophilization process. Then, one side of sponge was modified by a thin layer of stearic acid, which confers then waterproof and anti-adhesion properties to the external layer of the asymmetric membrane [9].

Herein, a 3D_SAC was produced for the first time using both electrospinning and 3D printing techniques. The top layer was produced using the electrospinning since it allows the formation of fibers with a high surface-to-volume ratio and interconnected pores, which will allow cell penetration and nutrient exchange [10, 11]. PCL and silk sericin (SS) were selected, for the first time, to produce the top layer due to their intrinsic properties. PCL is a synthetic polymer,

widely known by its excellent mechanical resistance, biocompatibility and hydrophobicity. On the other side, SS is a biocompatible protein derived from the silk-worm cocoon with moisturizing capacity [11-14]. Further, SS can also act as antioxidant, bio-adhesive and bioactive agent, which is crucial for the healing process [15]. Moreover, Aramwith *et al*. described that SS could activate the collagen production in wounds and significantly increase the epithelialization rate [16]. Therefore, the combination of these two materials (PCL and SS) can reproduce the epidermis barrier like function.

On the other side, the 3D Bioprinting technique was used to replicate the dermis structure by promoting the sequential layer-by-layer deposition of both CS and SA [17, 18]. The 3D printing technique allows the tailoring of the hydrogel' stiffness and geometry to precisely replicate the shape of the skin lesion [17-19]. Moreover, the 3D hydrogel possesses excellent intrinsic properties, like the high ability to absorb and retain the wound exudate, promoting the cell proliferation and migration, which are required for complete reepithelization of the wound [20-23]. Moreover, this technique offers a great control on the geometry and interconnectivity of the porosity as well as a higher mechanical stability [2]. On the other side, the bottom layer was produced with CS, which is a deacetylated derivative of chitin that exhibits several attractive properties (*e.g.* antimicrobial, biocompatible, biodegradable and hemostatic activity) [6, 11, 21, 24, 25]. In fact, these properties triggered the production of several wound dressings available in the market, such as Hidroki®, Patch®, Chitopack®, Tegasorb® and KytoCel® [26]. In turn, SA is a hydrophilic, biocompatible and biodegradable polymer, which is also widely used in different biomedical applications [27-31]. In skin regeneration area, the SA enhance the absorption of wound exudates, minimizing bacterial infections, reducing adverse allergic effects, and improving the healing process [32].

Overall, the data obtained in this study revealed that the produced 3D_SAC provides a dense top layer (electrospun membrane) that can act as protective barrier against microorganisms' infiltration and dehydration, while the porous bottom layer (3D printed hydrogel), affords a suitable structure and environment for cell migration and proliferation.

5.2 Materials and Methods

5.2.1 Materials

Cocoons of BomByx mori were acquired from the Portuguese Association of Parents and Friends of Mentally Disabled Citizens (Castelo Branco, Portugal). TFE was supplied by Acros Organics (Jersey City, NJ, USA). FA (99-100%) was bought from Chem-Lab NV (Zedelgem, Belgium). Calcium chloride ($CaCl_2$), CS medium molecular weight (190 000-310 000 Da; DD: 83.35% ± 0.23), DMEM-F12, GA 25% (v/v), LB broth, PFA, PCL (80 000 Da), PBS, SA (MW= 120-190 kDa), Triton X-100 and trypsin were purchased from Sigma-Aldrich (Sintra, Portugal). NHDF cells were acquired from PromoCell (Labclinics, S.A., Barcelona, Spain). MTS solution was bought from Promega (Madison, WI, USA). Lysozyme from chicken egg was acquired from Alfa Aesar

(Haverhill, MA, USA). AA was purchased from Pronalab (Barcelona, Spain). *S. aureus* (ATCC 25923) and *P. aeruginosa* obtained from a human sample were used as models of prokaryotic organisms to evaluate the bactericidal activity of the produced layers. FBS was acquired from Biochrom AG (Berlin, Germany). Quant-iT Pico Green dsDNA assay kit and Tris Base was obtained from ThermoFisher Scientific (Waltham, MA, USA). PI buffer was bought from Invitrogen (Carlsbad, Califórnia, EUA) and Calcein AM was supplied by Calbiochem (Merck Millipore, Oeiras). Double deionized and filtered water was obtained using a Milli-Q Advantage A10 ultrapure Water Purification System (0.22 μm filtered; 18.2 MΩ/cm at 25°C).

5.2.2 Methods

5.2.2.1 Silk sericin extraction

SS was extracted from the silk cocoons by adapting the high temperature and high-pressure degumming technique previously reported in the literature [16]. Briefly, cocoons of *Bombyx mori* silkworm were cut into small pieces and submitted to an autoclave cycle (at 120°C, for 1 h), allowing the extraction of SS from the cocoons. Then, the obtained aqueous solution, denominated as heat-degraded SS, was collected, filtered and purified by centrifugation at 4500 RPM for 30 min. The SS powder was then obtained through the freeze-drying process.

5.2.2.2 Production of the membrane (Polycaprolatone_Silk sericin)

The membrane, composed of polycaprolatone and silk sericin (**PCL_SS**), was produced using a conventional electrospinning apparatus, comprised of a high voltage power supply (Spellman CZE1000R, 0–30 kV, Spellman, USA), a precision syringe pump (KDS-100, Sigma-Aldrich, Portugal), a plastic syringe with a stainless-steel needle (21 Gauge), and an aluminium disk connected to a copper collector. For that purpose, a blend solution of PCL (9% w/v in TFE (80% v/v)) and SS (3% w/v in FA (98% v/v)) was prepared at 2:1 volume ratio. Afterwards, this solution was placed in the syringe and electrospun at a constant flow rate of 1.0 mL/h, using a working distance of 10-12 cm and an applied voltage of 28 kV, until the layer displayed a thickness quite similar to that exhibited by the epidermis layer of the human skin (0.05-1.5 mm).

5.2.2.3 Production of CS_SA hydrogels

In order to produce the hydrogel, a CS 8% (w/v) solution was prepared in AA (1% v/v)), and then mixed with SA (3% (w/v)) solution at 5:1 volume ratio. After that, the CS_SA solution was crosslinked with 5% $CaCl_2$ and completely homogenized with an X10/25 Ultra-turrax. Then, the blend was loaded into a syringe (10cc Luer Lock) and extruded using a Rapid Prototyping (Fab@Home) printer. The printed 3D model was designed using a Computer aided design (CAD)/Computer aided manufacturing software (SolidWorks). The developed 3D model was composed of several layers angled at 90° with the underlying layer (0°–90°–180°), as shown in

Figure 5.1. After the 3D printing, the **CS_SA hydrogels** were crosslinked by immersion in 10% $CaCl_2$ (w/v) solution during 3 h.

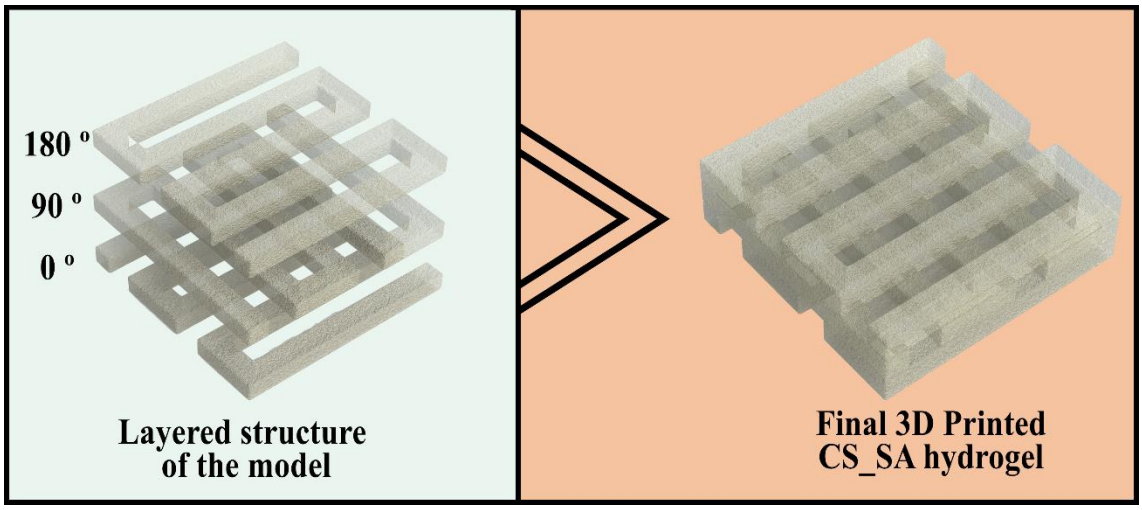

Figure 5.1. Schematic overview of the CS_SA hydrogel 3D CAD model layered structure.

Then, the printed gels were washed with double-deionized and filtered water and the excess of water was absorbed with a filter paper. The 3D skin asymmetric construct (**3D_SAC**) was obtained by the electrospinning of the PCL_SS membrane on the top of the CS_SA hydrogel.

5.2.2.4 Characterization of the layers' morphology and physicochemical properties

The surface morphology of both layers of the produced membranes was characterized through SEM. In brief, the samples were mounted on aluminium stubs with Araldite glue and sputter-coated with gold using a Quorum Q150R ES sputter coater (Quorum Technologies Ltd, Laughton, East Sussex, England). Then, SEM images were acquired with different magnifications, using an acceleration voltage of 20 kV, in a Hitachi S-3400N Scanning Electron Microscope (Hitachi, Tokyo, Japan). Through these images and using ImageJ software, the top layer' fibers diameters and pore sizes as well as bottom layer' pores sizes were measured.

On the other side, the final composition of the both layers (membrane and hydrogel) was characterized through attenuated total reflectance-fourier transform infrared spectroscopy (ATR_FTIR) analysis. The spectra of the membrane, hydrogel, and raw materials were acquired with an average of 128 scans, a spectral width between 4 000 and 400 cm^{-1} and a spectral resolution of 4 cm^{-1}, using a Nicolet iS10 FTIR spectrophotometer (Thermo Scientific, Waltham, MA, USA).

5.2.2.5 Characterization of the mechanical properties of the top and bottom layer of 3D_SAC

5.2.2.5.1 Evaluation of the tensile properties of the top layer

The tensile properties of PCL_SS membrane were evaluated using a Shimadzu AG-X Tensile Testing Machine (Tokyo, Japan), accordingly to the guidelines set by the Standard Test Method for Tensile Properties of Polymer Matrix Composite Materials (ASTM standard D3039/ D3039 M). The samples (*n*= 5) were prepared with a gauge length of 8 cm, a width of 2 cm, and thickness ranging from 0.3-0.5 mm. The length between clamps and the speed of testing was set to 2 cm and 20 mm/min, respectively. The membrane tensile properties were determined at RT, after their immersion in a PBS solution (pH 5.5), over 24 h, at 37°C. Load-extension data was recorded and the stress–strain curve of the membranes was determined through Equations (5.1) and (5.2), respectively:

$$Stress = \sigma = \frac{F}{A} \quad (5.1)$$

$$Strain = \varepsilon = \frac{\Delta l}{L} \quad (5.2)$$

where *F* is the applied force; *A* is the cross-sectional area; *Δl* is the change in length, and *L* is the length between the clamps.

5.2.2.5.2 Determination of bottom layer' compressive properties

The compressive properties of the 3D hydrogels were evaluated at RT using a Shimadzu AG-X Tensile Testing Machine (Tokyo, Japan), with a crosshead speed of 2 mm/min and a load cell of 5kN, as previously described [17]. The CS_SA hydrogel' compressive strength (C_s) was determined using the Equation (5.3):

$$Cs = \frac{F}{w \times l} \quad (5.3)$$

Where *F* corresponds to the load at the time of fracture, *w* and *l* represent the width and length of the gels, respectively.

In turn, the Young modulus was calculated by the stress-strain relation, using Equation (5.4):

$$YM = \frac{C_S}{H_d} \quad (5.4)$$

Where C_s is the gel compressive strength and H_d represents the height deformation at maximum load.

5.2.2.6 Evaluation of the porosity of the layers and 3D_SAC

The total porosity of the PCL_SS, CS_SA, and 3D_SAC was evaluated through the liquid displacement method, according to a protocol described in the literature [11, 33]. Each sample (*n*= 5) was weighted and immersed in absolute ethanol for 1 h. Subsequently, the samples were re-weighted, and the porosity was calculated taking into account the amount of ethanol absorbed, Equation (5.5):

$$Porosity\ (\%) = \frac{W_s - W_d}{D_{EtOH} - V_{sample}} \times 100 \quad (5.5)$$

where W_d is the initial weight of the dry samples and W_s is the weight of the swollen samples, $D_{ethanol}$ is the density of the ethanol at RT and V_{sample} is the volume of the swollen sample.

5.2.2.7 Evaluation of the swelling profile of the layers and 3D_SAC

The swelling behaviour of the 3D_SAC and individual layers (PCL_SS and CS_SA) was evaluated by immersion in Tris-HCl buffer (pH 5) under stirring (60 RPM), at 37 ºC [11, 34]. At predetermined timepoints, the sample was recovered, the solution excess was removed, and the weight was measured. Then, the swelling ratio was obtained through the Equation (5.6):

$$Swelling\ ratio = \frac{W_t}{W_0} \quad (5.6)$$

Where W_t corresponds to the final weight and W_0 is the initial weight of the samples.

5.2.2.8 Characterization of the degradation profile of the layers and 3D_SAC

The degradation profile of samples was monitored along 7 days. To accomplish that, PCL_SS, CS_SA, and 3D_SAC were immersed in Tris-HCl buffer containing 13.6 mg/L lysozyme, under stirring (50 RPM), at 37 ºC, as described in our previous report [11]. Lysozyme is an enzyme found in human serum and it is involved in the hydrolyzation of N-acetyl glucosamine groups presented in CS backbone [11, 35]. At predetermined intervals, the samples were removed from the solution, freeze-dried and weighed. The percentage of degradation of each sample at specific time points was calculated according to Equation (5.7):

$$Weight\ loss\ (\%) = \frac{W_i - W_t}{W_i}\ x\ 100 \quad (5.7)$$

Where W_i is the initial weight of the sample and W_t is the weight of the sample at time t.

5.2.2.9 Determination of the water vapor transmission rate

The 3D_SAC WVTR was evaluated following a method previously described [5, 11]. In brief, the samples (*n*= 5) were used to seal the opening of a glass test tube (1.77 cm^2) containing 10 mL

of double-deionized and filtered water. To prevent unspecific water losses, the 3D_SAC was gently attached to the tubes with parafilm tape. Afterwards, the samples were incubated at 37 ºC and the water evaporation from each test tube was monitored by measuring the weight losses in each tube. Then, the WVTR was estimated through Equation (5.8):

$$Water\ Vapor\ Transmission\ Rate = \frac{W_{loss}}{A} \quad (5.8)$$

Where W_{loss} is the daily weight loss of water and A is the area of the tube opening.

5.2.2.10 Evaluation of the wettability

The contact angles at the surface of the top (PCL_SS membrane) and bottom (CS_SA hydrogel) layers of 3D_SAC were determined using a Data Physics Contact Angle System OCAH 200 apparatus (DataPhysics Instruments GmbH, Germany) operating in static mode at 25°C (water was used as the reference fluid). The reported contact angles are the average of at least three independent measurements of water drops (4 µL) placed at various locations in the surface of the sample.

5.2.2.11 Characterization of the 3D_SAC layers' biological properties

5.2.2.11.1 Characterization of the cell viability and proliferation when they were in contact with produced layers

The PCL_SS and CS_SA layers' biocompatibility was assessed through an MTS assay performed according to the ISO 10993-5 (Biological evaluation of medical devices- Part 5: Tests for *in vitro* cytotoxicity). In brief, membranes and hydrogels (n= 5) were placed into 96-wells plates, occupying < 10% of the well area, and sterilized under UV irradiation (254 nm, ≈ 7 mW.cm^{-2}) for 1 h. Then, NHDF cells were seeded in the presence of the layers at a density 10×10^3 cells/well and incubated at 37 ºC, in 5% CO_2 humidified atmosphere. After 1, 3 and 7 days of incubation, the medium was removed and cells were incubated with a mixture of 100 µL of fresh culture medium and 20 µL of MTS, for 4 h (37 ºC, 5% CO_2). Then, the absorbance of the samples was measured at 490 nm, using a microplate reader (Bio-Rad xMark microplate spectrophotometer). Cells incubated only with culture medium were used as a negative control (K^-), while cells incubated with ethanol (70%) were used as the positive control (K^+).

5.2.2.11.2 dsDNA Quantification assay

Cells proliferation in contact with layers was further characterized by measuring the total dsDNA using the Quant-iT PicoGreen dsDNA Assay kit (Invitrogen, USA) [5, 17]. Briefly, NHDF cells were cultured in the presence of the PCL_SS and CS_SA (n= 5), at a density of 20 × 10^3 cells/well. After 1, 3 and 7 days, cell lysis was induced by adding Triton X-100 (1 mL) to the samples, for 1 h. Thereafter, a cell scraper was used to harvest the remaining adhered cells and the cell-material complexes were transferred into 1.5 mL tubes. The samples were

then subjected to a freeze-thaw cycle, sonicated for 15 min, and then centrifuged at 14 000 g, for 15 min, at RT. Subsequently, the supernatant was recovered and 100 µL were mixed with an equal volume of the PicoGreen solution (1:200 dilution of the PicoGreen reagent in 1X TE Buffer). After 10 min of incubation, the fluorescence of samples was measured in a microplate reader, using the excitation and emission wavelengths of 485 nm and 535 nm, respectively. Further, a calibration curve was also performed to allow the quantification of the dsDNA present in the different samples.

5.2.2.11.3 Live/dead assay

Cell viability at the surface of PCL_SS and CS_SA layers was also characterized through a Live/Dead assay (Invitrogen, Life Technologies, USA). To accomplish that, NHDF cells (10 x 10^3 cells/well) were seeded on the surface of PCL_SS and CS_SA layers previously placed in µ-Slide 8 well Ibidi imaging plates (Ibidi GmbH, Germany). After 1, 3 and 7 days, cells were incubated with the sainting solution (following the manufacturer's instructions) for 15-20 min. Then, the samples were imaged using a Zeiss LSM 710 laser scanning confocal microscope (Carl Zeiss SMT Inc., USA).

5.2.2.11.4 Characterization of the cell migration into CS_SA hydrogel through confocal microscopic analysis

CLSM analysis was used to evaluate the cell migration within 3D CS_SA hydrogels. To accomplish that, NHDF (10 × 10^3 cells/well) were seeded on µ-Slide 8 well Ibidi imaging plates (Ibidi, Germany) containing the CS_SA hydrogels. After 24 h of incubation, the samples were treated with a permeabilization solution (Triton X-100) and the cell nucleus was stained with PI (15mM) during 15 min, at 37° C. After that, the samples were washed and fixed with 4% PFA for 15 min, at RT. Imaging experiments were then performed in a Zeiss LSM 710 laser scanning confocal microscope (Carl Zeiss SMT Inc., USA), where consecutive z-stacks were acquired. 3D reconstruction and image analysis were performed in Zeiss Zen 2010.

5.2.2.12 Characterization of the produced membranes antimicrobial activity

5.2.2.12.1 Analysis of the bacterial penetration through the PCL_SS membrane (top layer)

The bacterial infiltration assay with gram-positive (S. *aureus*) and gram-negative (*P. aeruginosa*) bacteria was performed to evaluate the top layer efficacy in avoiding bacteria penetration. To accomplish that, transwell systems (Corning Incorporated, USA) were modified with PCL_SS membrane or filter paper (0.22 µm), which act as interface between the upper and lower chambers. Then, the upper chamber was inoculated with a bacterial suspension (1×10^8 CFU)/mL), during 24 h, at 37 ºC. The optical density (absorbance value at 600 nm) of the culture medium placed in the lower chamber was measured and the number of colonies that transposed the membrane or the filter paper were counted. Furthermore, SEM images

were acquired to evaluate the presence of microorganisms on the upper and bottom surfaces of the PCL_SS membrane and in the filter paper.

5.2.2.12.2 Characterization of bactericidal activity of the CS_SA hydrogel (bottom layer)

The antibacterial activity of CS_SA hydrogel was also characterized using *S. aureus* and *P. aeruginosa*. For this purpose, 25-50 mg of each sample (*n*= 3) were added to 10 mL of LB broth, at pH 6.2, containing $1x10^5$ CFU/mL of early mid-log phase bacteria culture, and posteriorly incubated for 24 h, at 37°C. Then, serial dilutions were prepared and 100 µL of bacterial samples were seeded on LB agar plates. After overnight incubation at 37ºC, the bacterial colonies were counted and expressed as CFU/mL and the bacterial growth inhibition was determined through Equation (5.9):

$$Antibacterial\ efficency\ (\%) = \frac{N_0 - N}{N_0} \times 100 \quad (5.9)$$

Where N_0 and N represent the bacteria number of control and experimental group, respectively.

In addition, a modified Kirby-Bauer technique was also used to evaluate the antibacterial performance of the CS_SA hydrogel. Circular disks of hydrogel (*n*= 3) were placed on the surface of an agar plate seeded with *S. aureus* and *P. aeruginosa* (1 x 10^8 CFU/mL) and incubated for 24 h, at 37°C. Afterwards, the inhibition area was photographed and measured using an image analysis software, ImageJ (NIH Image, USA). Furthermore, the biofilm formation at the layers' surface was also investigated by SEM analysis.

5.2.2.13 Characterization of the cell and bacterial adhesion at the surface of the 3D_SAC top and bottom layers through SEM analysis

SEM analysis was performed to evaluate both cellular and bacterial adhesion to the surface of the materials, as previously reported by Miguel *et al*. [5]. In brief, the layers containing NDHF cells or bacteria were fixed with 2.5% (v/v) GA, for 30min. Subsequently, the samples were frozen at -80 ºC and freeze-dried for 3h (samples seeded with eukaryotic cells) or 6 h (samples in contact with bacteria). Before the SEM images acquisition, all samples were prepared and visualized through SEM analysis, as previously described in section 5.2.2.4.

5.2.2.14 Statistical analysis

The statistical analysis of the obtained results was performed using ANOVA, with the Newman-Keuls *post hoc* test. A p value lower than 0.05 ($p < 0.05$) was considered statistically significant.

5.3 Results and discussion

5.3.1 Characterization of the produced layers morphology

Artificial 3D structures have triggered the attention of researchers for tissue regeneration purposes. Matrices that closely mimic the ECM favour cell proliferation and differentiation as well as allow nutrients, metabolites and soluble factors diffusion [36]. In this study, an asymmetric 3D construct composed of a dense and mechanical resistant top layer and a porous and bioactive bottom layer was produced using both electrospinning and 3D bioprinting techniques. The production of the nanofibrous top layer by electrospinning technique aimed to promote the cell-cell and cell-ECM interactions that occur at nano-scale level [10, 37]. The high surface-to-volume ratio presented by the electrospun nanofibers favours the interaction between integrin receptors available on cell surface and nanofibrous membrane, triggering a cascade of four events: cell attachment, cell spreading, reorganization of actin cytoskeleton and formation of focal adhesions [22]. Further, this layer also works as a barrier against microorganism infiltration, as well as enables the drainage of the wound exudate and gaseous exchanges. Such properties are crucial to avoid the occurrence of skin infections and wound dehydration [5, 11].

On the other hand, the 3D printed hydrogel provides a 3D structure with a porosity and microenvironment suitable for cell migration and proliferation [2, 23]. Moreover, the hydrogel's hydrophilic polymer chains absorb high levels of exudate, keeping a moist environment at wound site whilst absorbing excessive exudate [21, 22].

SEM analysis was performed to fully characterize both layers of the asymmetric skin construct (see Figure 5.2 for further details). The PCL_SS top layer displayed a highly interconnected mesh composed of fibers with a mean diameter of 318.6 ± 93.75 nm, with a mean pore size of 629.45 ± 150.34 nm. In turn, the CS_SA hydrogel bottom layer presented macropores with a mean diameter of the 976.6 ± 141.69 μm. Moreover, the cross-sectional images of 3D_SAC revealed that the thickness of the top and bottom layers was 0.55 ± 0.16 mm and 1.59 ± 0.19 mm, respectively. Such results demonstrate that the combination of both techniques allowed the production of membranes that reproduce the morphological features of the epidermis and dermis layers. The top layer nanofibers diameters are within the range of the collagen fibrils found at the ECM of human skin (50-500 nm) [10]. Further, the thickness of the top layer was tailored by optimizing the continuous deposition of the nanofibers until reaching a thickness similar to that exhibited by the epidermis layer (0.5-1.5 mm) [1]. In turn, the thickness of the bottom layer was controlled by the design of the 3D CAD model (Figure 5.1), that allow to define the height of the 3D structures is within the range of the native dermis layer (0.6–3 mm), by controlling the number of printed layers [1]. Moreover, the existence of macropores in the bottom layer (CS_SA hydrogel) is essential for cell nutrition and proliferation as well as for formation of new tissues and nutrients/oxygen diffusion into the

wound site [21, 23]. Indeed, according to Loh and coworkers, the pore size and total porosity are parameters that have a direct impact on cell viability and proliferation, and consequently on the healing process [38].

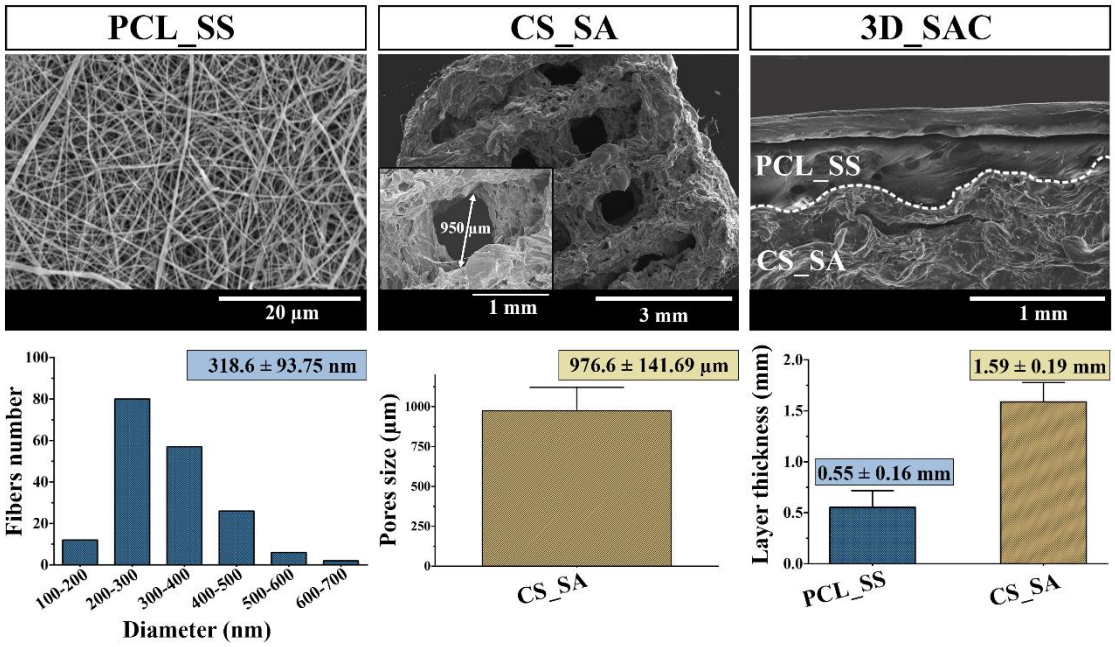

Figure 5.2. Morphological analysis of the 3D_SAC' layers. SEM images of the top (PCL_SS), bottom (CS_SA) layer and cross-section of the 3D_SAC. Analysis of the top layer fiber' size distribution, bottom layer mean pore size and layer thickness.

5.3.2 Attenuated total reflectance-Fourier transform infrared spectroscopic analysis

The chemical composition of the produced membrane and hydrogel was characterized by FTIR analysis. The spectrum of the top layer (Figure 5.3A) displays the characteristic peaks of SS at 1631 cm^{-1} (Amide I, which arises from the C=O stretching vibrations of the peptide linkages), at 1527 cm^{-1} (Amide II, that derives from N-H bending and the C-N stretching vibration), at 1239 cm^{-1}(Amide III, represents primarily the C-N stretching vibration linked to N-H bending vibration). Furthermore, the presence of the amide I peak at 1631 cm^{-1} also show that the SS possess a ß-sheet conformation [39, 40]. Such data is in accordance with the work published by Tsukada, which reported that the SS recovered by this extraction protocol (hot water) mainly presents ß-sheet structures, due to the lyophilization process, with 10% of α-helice conformation [41]. In addition, the PCL_SS spectrum also presents the PCL characteristic peaks at 2942 cm^{-1} (asymmetric CH_2 stretching), 1724 cm^{-1} (carbonyl stretching), 1293 cm^{-1} (C-O and C-C stretching), 1239 cm^{-1} (asymmetric C-O-C stretching) and 1139 cm^{-1} (symmetric C-O-C stretching) [5, 11, 33].

On the other hand, the characteristic peaks of the bottom layer's components are presented in Figure 5.3B. The peaks of CS appear at 3293 cm^{-1} (- OH stretch), 2871 cm^{-1} (aliphatic C–H stretch), 1648 cm^{-1} (NH_2 stretch), 1374 cm^{-1} (–C–O stretching of the primary alcohol group) and at 1026 cm^{-1} (C–O–C glycosidic bond) [11, 12, 17]. Further, the peaks of the SA are presented between 3000-3700 cm^{-1} (-OH stretch of water and -OH groups of the G and M units of alginate) and at 1597 cm^{-1} and 1406 cm^{-1} (C=O stretching vibration of the carboxylic group of alginate) [29].

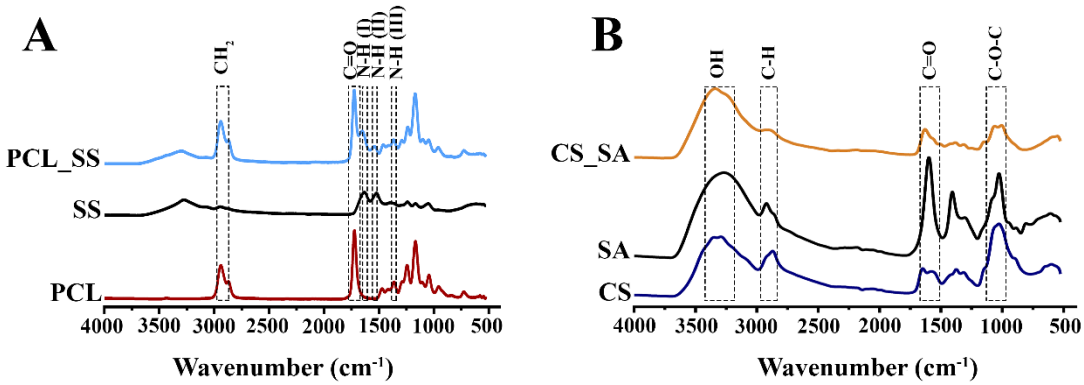

Figure 5.3. ATR-FTIR analysis of the top (PCL_SS membrane) (A) and bottom (CS_SA hydrogel) (B) layers and their respective raw materials.

5.3.3 Evaluation of the 3D_SAC mechanical properties

Wound dressings must display mechanical properties that allow them provide mechanical support that is required to protect the wound from external threats [4, 42]. Herein, the mechanical properties of the top layer were evaluated through the tensile assays, whereas the bottom layer' mechanical performance was characterized using a compressive assay. In relation to the PCL_SS top layer, the obtained values for tensile strength, Young's modulus, and elongation at break, in wet state, were 34.92 ± 7.39 MPa, 27.92 ± 8.09 MPa, and 155.37 ± 5.71%, respectively. On the other side, the bottom layer (CS_SA hydrogel) displayed a compressive strength and Young's modulus of 0.16 ± 0.05 MPa and 0.05 ± 0.01 MPa, respectively. These results confirm the excellent mechanical properties of the top layer, that present similar tensile strengths (5-30 MPa), Young modulus (4.6- 20 MPa), and elongation at break (35-115%) values to those displayed by the native skin [5, 7, 11]. Such mechanical performance can be attributed to the PCL, a synthetic polymer well known by its mechanical strength [43]. In turn, the CS_SA hydrogel presented a lower mechanical performance, which can be attributed to the higher porosity of this layer (Figure 5.2 and 5.4A). In fact, the production of porous scaffolds with a best compromise between porosity and mechanical strength is still one the major challenges faced by the researchers [44]. Further, the hydrogel was produced only with natural polymers (CS and SA), which are widely recognized by their weak mechanical properties [45, 46].
However, the CS_SA hydrogel exhibited compressive strength values quite similar to the native skin (0.2-7 MPa). Additionally, these results are in accordance with compressive strength and Young modulus values (0.46 ± 0.22 MPa and 8.16 ± 1.75 MPa, respectively) reported in literature

by Liu *et al.* for CS_alginate hybrid scaffolds [47]. The mechanical properties exhibited by the produced layers emphasized their suitability for being applied during the healing process.

5.3.4 Determination of the layers and skin construct porosity

Biomaterials' porosity is a key parameter for their application in tissue engineering. An interconnected pore structure and high porosity are essential features to ensure cellular penetration and the adequate nutrients diffusion within the construct and to ECM produced by these cells [36, 48]. Herein, the total porosity was determined using a liquid displacement method [5, 11]. The obtained results revealed that the PCL_SS membrane and the CS_SA hydrogel have a porosity of 56.66 ± 2.47% and 99.08 ± 5.31% respectively, whereas the 3D_SAC display a total porosity of 79.13 ± 2.55%, a value comprehended between the individual layers (Figure 5.4A). Such results are in accordance with the morphological variations observed in SEM images (Figure 5.2). In fact, the electrospun top membrane provides a nano-scale and a polymeric dense network composed by the interconnected fibers, that display a low porosity, which avoids microorganisms invasion [49]. Further, the low porosity displayed by the top layer is crucial to this layer to act as a protective barrier [5]. On the other hand, the 3D printed hydrogel exhibits a highly porous polymeric structure with macropores that are compatible with cell migration and proliferation, as well as absorption of the excess of the exudate from the wound site. Additionally, the CS_SA hydrogel high porosity is in agreement with those reported in the literature for CS hydrogels, where the porosity values range from 75%-85% [50]. Further, the CS_SA hydrogel exhibited a porosity value similar to those displayed by the acellular dermal matrix (68.3 ± 5.8%) [51].

However, it is worth to notice that the biomaterials porosity has a direct impact on the mechanical properties of the 3D networks, *i.e.*, the biomaterials structural stability is impaired by an increased porosity. Indeed, Venugopal and co-workers evaluated this influence on the production of PCL/nanohydroxyapatite/collagen nanofibers. Their results revealed that an increase in the pore size from 2-15 μm to 5-50 μm, promoted an augment on porosity from 72.3% to 89.7% and a decrease on the tensile strength from 2.72 MPa to 1.28 MPa [52]. So, in this work, the combination of the 3D hydrogel with the electrospun membrane enabled the production of a 3D_SAC displaying a porosity within the preferred range (60-90%), which is fundamental to promote cell accommodation and migration [24].

5.3.5 Characterization of the layers and skin construct swelling profile

The healing process was associated with the production of wound exudate, which is a complex mixture of water, soluble inflammatory mediators, proteases, GFs, and electrolytes [33]. However, an abnormal production of wound exudate (resultant from the prolonged inflammation stage, wound bed infection, and chronic healing) leads to tissue maceration and excoriation in the periwound region. Further, an excessive amount of exudate impairs the cellular migration towards to the wound bed, avoiding the proper tissue replacement and hence

extending the healing period [47]. Herein, the capacity of the individual layers and 3D_SAC to absorb the wound exudate was characterized by evaluating their swelling profile (Figure 5.4B). The results clearly demonstrate that the CS_SA hydrogel layer presents the higher swelling ratio (≈ 43) after 10 h of immersion, whereas the PCL_SS membrane and 3D_SAC only reach their maximum swelling ratio (≈ 29 and ≈ 30, respectively) after 18 h of incubation.

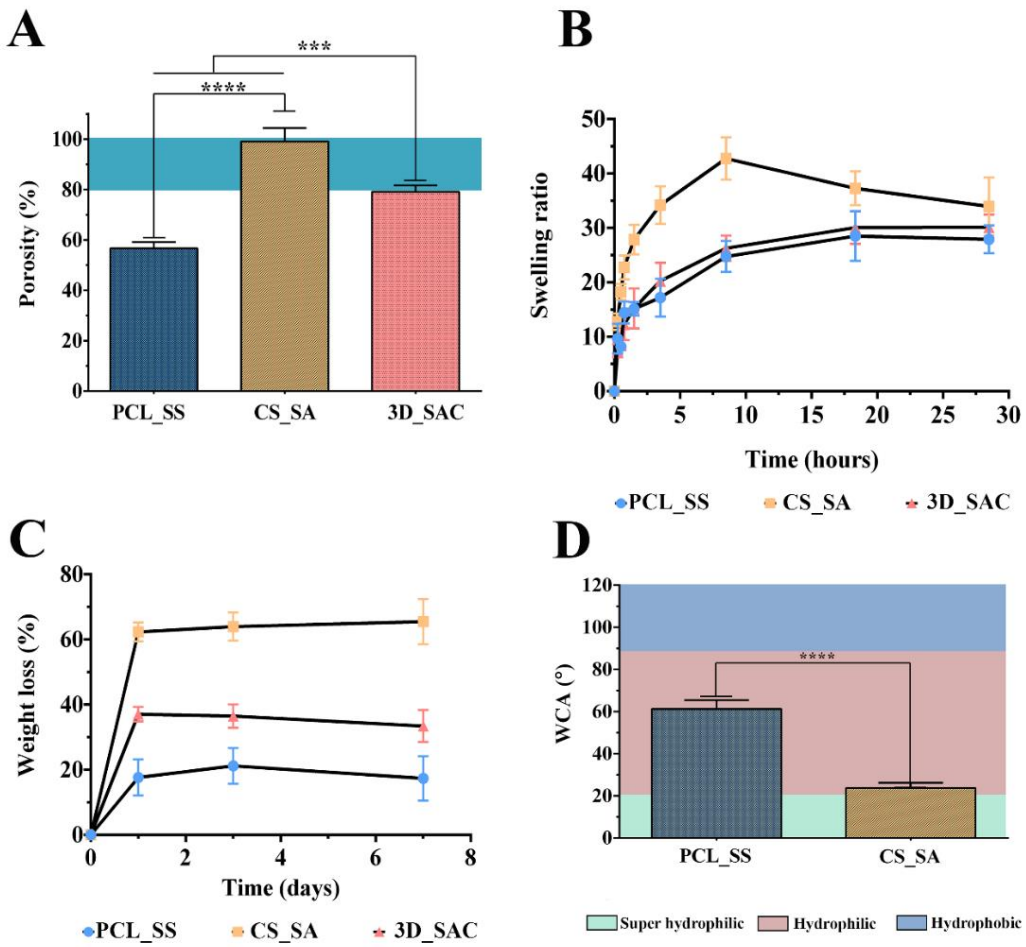

Figure 5.4. Evaluation of the total porosity (A), swelling profile (B), weight loss profile (C) and the wettability (D) of the PCL membrane, CS_SA gel, and 3D_SAC. Data are presented as the mean ± standard deviation, n = 5, **p < 0.01, ***p<0.0001.

The higher swelling ratio of the hydrogel layer can be explained by the presence of hydrophilic groups (amine, hydroxyl, and carboxyl) on CS and SA backbones that can be easily hydrated [11, 19, 31]. As previously described by Raja and Fathima, the -NH_2 and -OH groups located at each *N*-acetyl-glucosamine and glucosamine residues of the CS and SA backbone interact with water molecules through hydrogen bonding [22]. However, the continuous swelling cause the loss of the mechanical integrity and compressive stress to surrounding tissue [53]. Herein, the greater swelling ratio of hydrogel was controlled through the presence of the PCL_SS membrane, as demonstrated by the data obtained for 3D_SAC. Further, the 3D_SAC swelling profile is compatible with the adsorption of the wound exudate, which combined with the

capacity to allow gaseous exchanges (*e.g.* water vapor transmission) should allow the maintenance of an environment moisture in values that promote the healing process.

5.3.6 Evaluation of the layers and skin construct degradation profile

Most of the commercially available wound dressings are non-degradable, requiring their replacement/removal and consequently favouring the scar tissue formation and leading to an increased risk of bacterial contamination [54]. Due to that, the development of biodegradable structures that display a degradation profile compatible with the rate of skin regeneration is a key requirement of wound dressings [12, 42]. Herein, the degradation profiles of the individual layers and asymmetric skin construct were evaluated using lysozyme, an enzyme found in human serum that can degrade CS-based materials [35]. After 7 days of incubation in Tris buffer solution (containing lysozyme), the CS_SA hydrogel presented the highest weight loss (65.44 ± 6.93%), whereas the PCL_SS membrane displayed the lowest one (17.33 ± 6.81%), and the 3D_SAC had an intermediate weight loss of 33.39 ± 6.81% (Figure 5.4C). The improved stability of PCL_SS membrane can be attributed to the PCL, an aliphatic polyester that suffer low degradation through hydrolysis or by the action of MMPs [5, 43]. In turn, the SS present on the top layer is mainly decomposed through hydrolytic degradation processes. Such, is explained by the highly hydrophilic character of SS side chains (hydroxyl, carboxyl, and amino groups) [48]. In opposition, the accelerated degradation prolife of the 3D hydrogel can be justified by i) the CS degradation mediated by the lysozyme hydrolyzation of the N-acetyl glucosamines groups [35]; ii) the SA disintegration by gradual replacement of calcium by sodium ions present in the medium; and iii) the weak ionic interaction established between the amino groups of CS and the carboxyl groups of SA [47]. Further, the SA can also become depolymerized through the spontaneous alkaline elimination of its glyosidic linkages that occur *in vivo* [19, 31].

Herein, the strong entanglement between the two layers (PCL_SS membrane and CS_SA hydrogel) allowed the production of the 3D_SAC with a weight loss value comprehended between the weight losses displayed by the individual layers. In Figure 5.5, the cross-section of the 3D_SAC can be visualized after 1, 3 and 7 days of incubation. These images demonstrate that despite the decrease in the bottom and top layers density (more perceptible in bottom layer), they remain attached during at least 7 days.

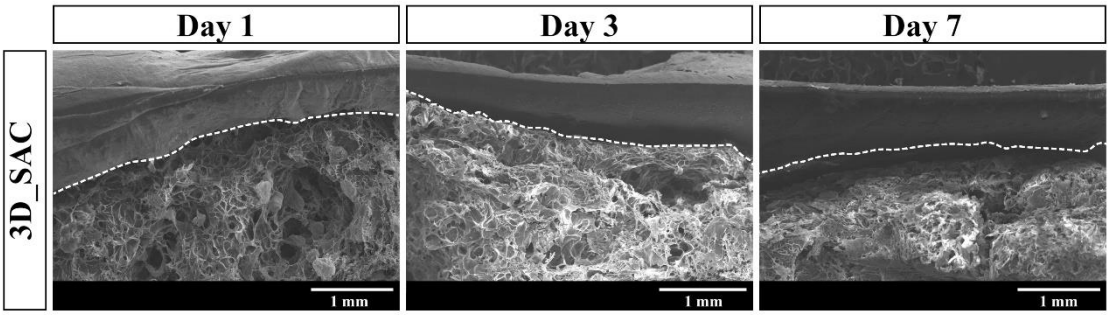

Figure 5.5. SEM images of the 3D_SAC cross-sections after their incubation in Tris-buffered saline solution (pH 5) for 1, 3, and 7 days.

5.3.7 Determination of the skin asymmetric construct WVTR

The maintenance of a moist environment at the wound bed is crucial for an effective healing to occur. In fact, a moist environment avoids patient dehydration as well as enhances the angiogenesis and the collagen synthesis [20]. The wound dressings' WVTR is also an important feature to maintain a moist environment at wound site, favouring the cell proliferation. In fact, the 3D_SAC presented a WVTR value of 1737.85 ± 192.12 mL/m^2/day, which is similar to those found on other asymmetric membranes previously produced (*e.g.* asymmetric PCL/CS_AV_PEO membrane (1252.35 ± 21.22 g/m^2/day) [11], PCL_HA/ CS_ZN electrospun bilayer membrane (1762.91 ± 187.50 g/m^2/day) [12] and SF based asymmetric membrane (2070.62 ± 102.52 mL/m^2/day) [5]). Further, the 3D_SAC capacity to provide a suitable moisture environment is superior to that displayed by commercial wound dressings (*e.g.* 285 ± 8 g/m^2/day for Comfeel (Coloplast A/S); 394 ± 12 g/m^2/day for Bioclusive (Johnson-Johnson); and 792 ± 32 g/m^2/day for Op Site (Smith & Nephew) [55]). In addition, according to the literature, the wound dressings with WVTR values comprehended between 2000 and 2500 mL/m^2/day are more prone to maintain a favourable environment for cell proliferation and water vapor exchanges [7, 8, 46].

5.3.8 Characterization of the layers' wettability

The biological response to the biomaterial implantation is closely related to the cellular interaction at the biomaterials' surface [56]. Among the different surface features, the surface wettability has a direct impact on the cell adhesion process [57]. In this way, the wound dressing wettability was also evaluated through the determination of the WCA at the layers' surface (Figure 5.4D). The PCL_SS membrane presented a WCA value of 61.27 ± 4.15°, indicating a moderate hydrophilic character (40° <WCA< 70°) [11, 57]. Such result can be explained by the presence of highly hydrophilic hydroxyl, carboxyl, and amino groups on SS backbone [13, 14], that counterbalance the hydrophobicity of the PCL aliphatic polyesters chains [11, 43]. On the other side, the bottom layer of the asymmetric skin construct (CS_SA hydrogel) exhibited a WCA value of 23.75 ± 2.46 °, revealing a superhydrophilic character (WCA≈ 20°). Such result can be explained by the high percentage of hydrophilic groups

(*e.g.* amine, hydroxyl, and carboxy) on CS and SA backbones [47]. According to the literature, cell adhesion-mediating ECM proteins (*e.g.* vitronectin, fibronectin, collagen or laminin) are more prone to become adsorbed on hydrophilic surfaces [56, 57].

5.3.9 Characterization of the 3D_SAC layers' biological properties

The cytotoxic profile of asymmetric skin construct was evaluated through the incubation of the PCL_SS membrane and CS_SA hydrogel in contact with NHDF, which were used as model cells. Fibroblasts were selected to perform these assays, since they are involved in the production of ECM components (collagen and fibronectin), cytokines and GFs, which are essential for the reestablishment of the damaged tissue' structure. Optical microscopic images of NHDF cells seeded in contact with the layers after 1, 3 and 7 days are presented in Figure 5.6. Such images revealed that the NHDF cells do not suffer any morphological variation when seeded in contact with samples. Cells display a similar morphology to that of the negative control (cells seeded only in contact with culture medium).

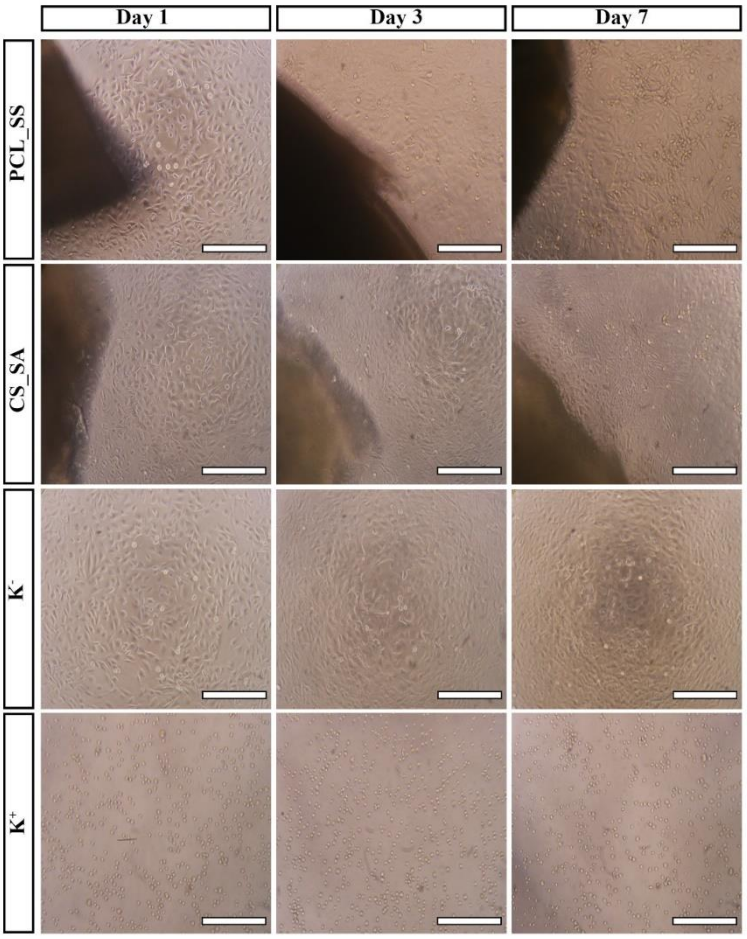

Figure 5.6. Optical microscopic images of Normal Human Dermal Fibroblast (NHDF) cells cultured in the presence of the produced layers (PCL_SS and CS_SA) of 3D_SAC for 1, 3, and 7 days; K^- (negative control); K^+ (positive control). Scale bar represents 200 μm.

Moreover, the cytotoxic profile of the 3D_SAC' layers was also evaluated through the MTS assay over 1, 3 and 7 days (Figure 5.7A). Such results show that both layers did not elicit any cytotoxic effect on NHDFs, over the 7 days. Further, the dsDNA quantification results (Figure 5.7B) corroborated the data obtained in the MTS assay, thus revealing that the NHDFs remained viable and proliferated in contact with the produced layers for 7 days.

Apart from the biocompatibility, a wound dressing must also favour cell attachment, growth, and proliferation. The SEM images presented in Figure 5.7C show that the surface topography of both layers was able to promote the cell adhesion and proliferation. Indeed, after 7 days, the cells presented the typical fibroblastic morphology, exhibiting a smooth arrangement, and established interconnections between each other, forming a continuous cell layer. Additionally, the number of NHDF cells adhered on the layers' surface increased overtime, which further supports membranes biocompatibility.

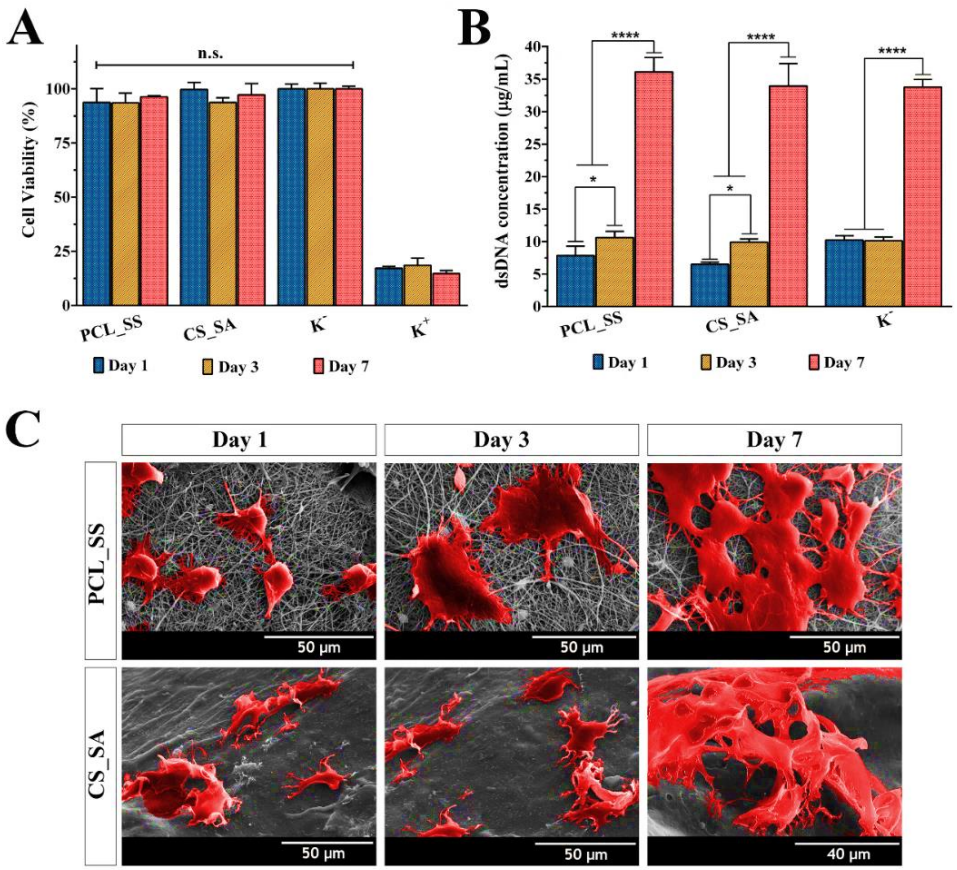

Figure 5.7. Characterization of the 3D_SAC' layers cytotoxic profile. Analysis of the NHDF cell viability (A) and dsDNA content (B) after 1, 3, and 7 days of incubation. Representative pseudo-coloured SEM images of NHDF cells seeded at the surface of the top and bottom layers of skin asymmetric construct after 1, 3, and 7 days (C). Data are presented as the mean ± standard deviation, n = 5, ****p< 0.0001; the groups assigned with n.s. were not statistically significant.

Live/dead assays were also performed to further characterize the 3D_SAC' layers cytocompatibility through the staining of live and dead cells with calcein and PI, respectively [5, 33].

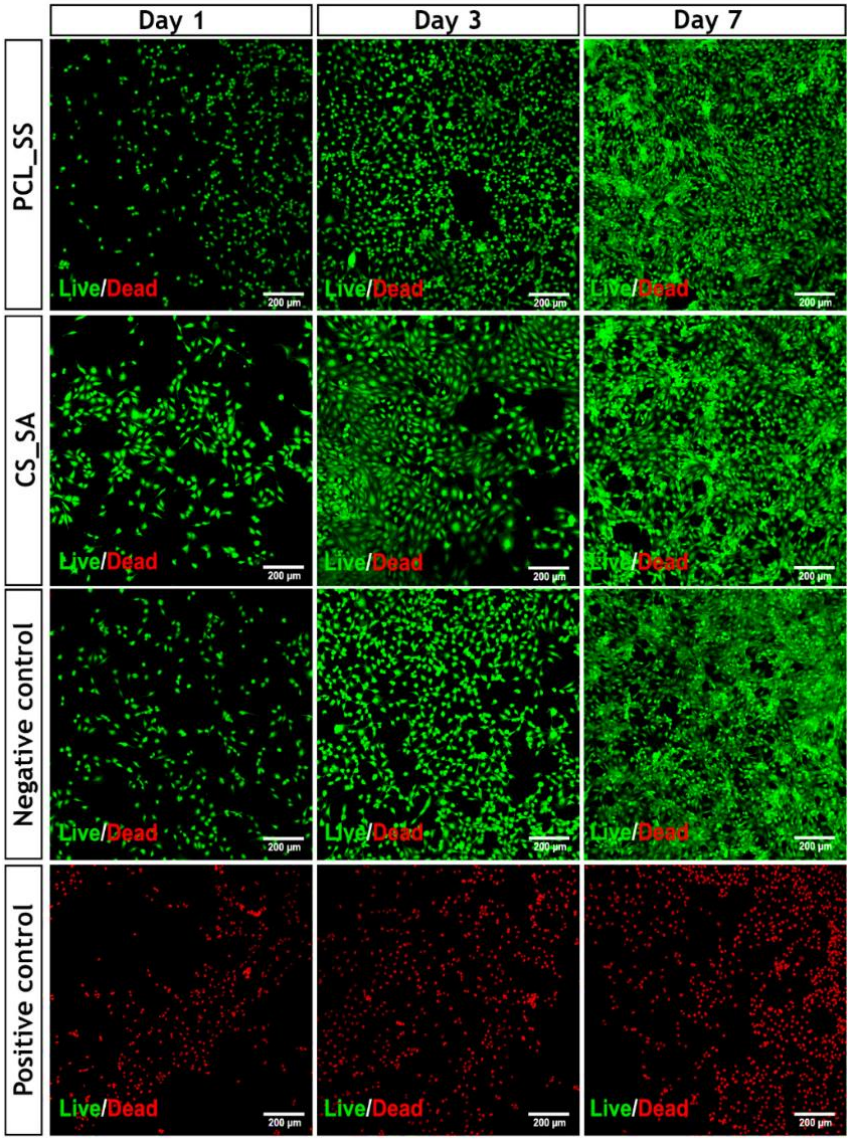

Figure 5.8. CLSM images from the live/dead assay of NHDFs cultured on the surface of the PCL/SS membrane (top layer) and CS_SA hydrogel (bottom layer) after 1, 3 and 7 days. Green channel: viable cells labelled with Calcein; red channel: dead cells stained with Propidium iodide.

The CLSM images (Figure 5.8) clearly show that the cells remained viable (green channel) and presented an uniform cell distribution throughout the both layers of the 3D_SAC. Such results can be explained by the presence of SS and CS in the composition of the top and bottom layers, respectively. In fact, Tsubouchi *et al.* found that SS enhanced the attachment of primary cultured human skin fibroblasts on petri dishes coated with SS [58]. SS besides displaying a hydrophilic character also possess various amino acid on its backbone (*e.g.* serine, glycine, and aspartic acid) that are known for their capability to promote cell adhesion, spreading and proliferation, and thereby improving the healing process [16].

On the other hand, in the bottom layer, the interaction of the cell membrane GAGs with the amine groups of CS present in CS_SA hydrogel promotes cell adhesion [21, 59]. Moreover, the CS provides a 3D network that promotes cell proliferation and tissue organization [60].

Fibroblast cells migration and proliferation within CS_SA hydrogel (bottom layer) was also characterized through confocal microscopy analysis (Figure 5.9). The CLSM images presented in Figure 5.9B show that the cells were able to migrate into the interior of CS_SA hydrogel. Cellular internalization is further noticeable in the orthogonal projection shown in Figure 5.9C. In addition, the depth colour coding images (Figure 5.9D) also confirm that the NHDF cells migrated into hydrogels interior through their pores. Such results confirm that the porous structure of the printed CS_SA hydrogel was suitable for the accommodation and proliferation of NHDFs, as well as to allow an effective nutrient supply and metabolic waste removal, processes that are essential for an effective cell growth and subsequently skin regeneration occur [21, 61]. When the NHDFs reach the wound site, they start to produce and secrete ECM proteins (essentially collagen type III) and GFs (*e.g.*, TGF-1, FGF and VEGF) that play pivotal roles in the restoration of the injured skin' structure [12]. Together, these results demonstrate that the 3D_SAC mimic the native human skin structure and promote the healing process.

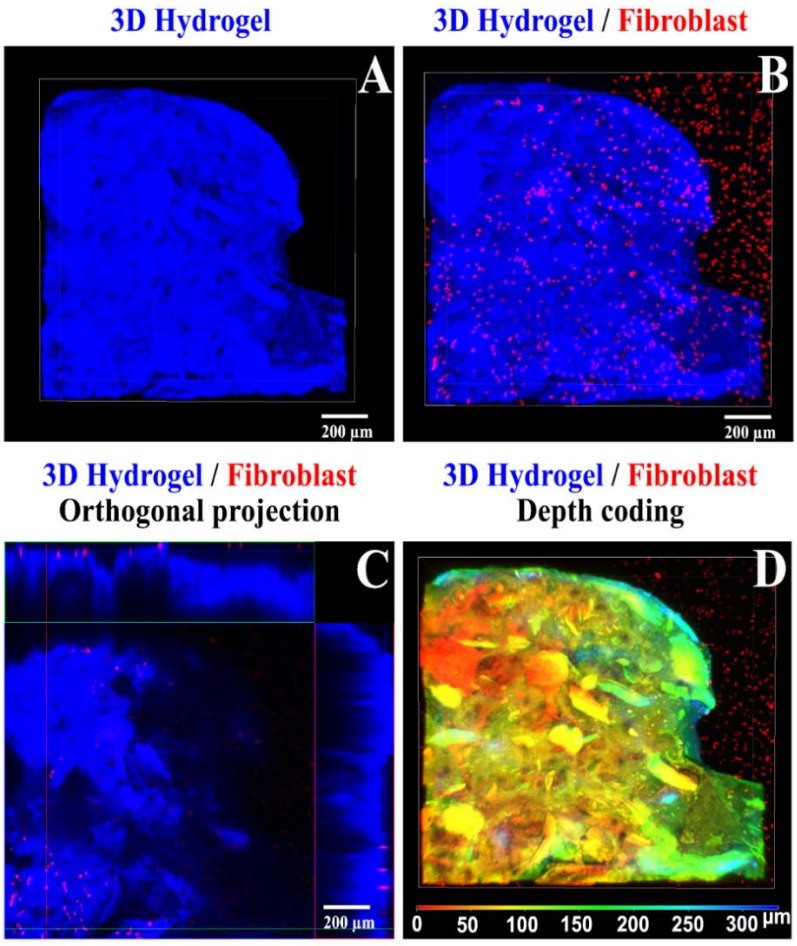

Figure 5.9. CLSM images of the cells within CS_SA hydrogel. 3D reconstruction images (A and B) and orthogonal projection (C) of the cells seeded in contact with the hydrogel. Depth colour coding CLSM image of the hydrogel (D).

5.3.10 Evaluation of the antimicrobial properties of the produced layers

A wound is highly susceptible to bacterial contamination, leading to the infection that can often impair the healing process, leading to high rates of morbidity and mortality [33]. Once bacteria adhered to wound surface, a cascade of events occur, leading to the formation of biofilms [26]. In this way, it is crucial to develop wound dressings showing antimicrobial activity that are capable of inhibiting bacteria growth. In this study, the antimicrobial properties of the produced layers of 3D_SAC were characterized using *S.aureus* and *P.aeruginosa*, as models of gram-positive and gram-negative bacteria, respectively. These bacterial strains were selected since they are the most common pathogen found in skin infections [5, 26]. The membrane top layer (PCL_SS), which will be in direct contact with the external environment, was conceived to avoid microbial invasion of the wound site. The results presented in Figure 5.10A and 5.10B show that the top layer of 3D_SAC, acts as protective barrier, hampering the infiltration of the both bacteria. Further, it is noticeable that there is no significant difference with the control group, a filter paper (pore size of 0.22 µm, which is usually used for sterilization purposes).

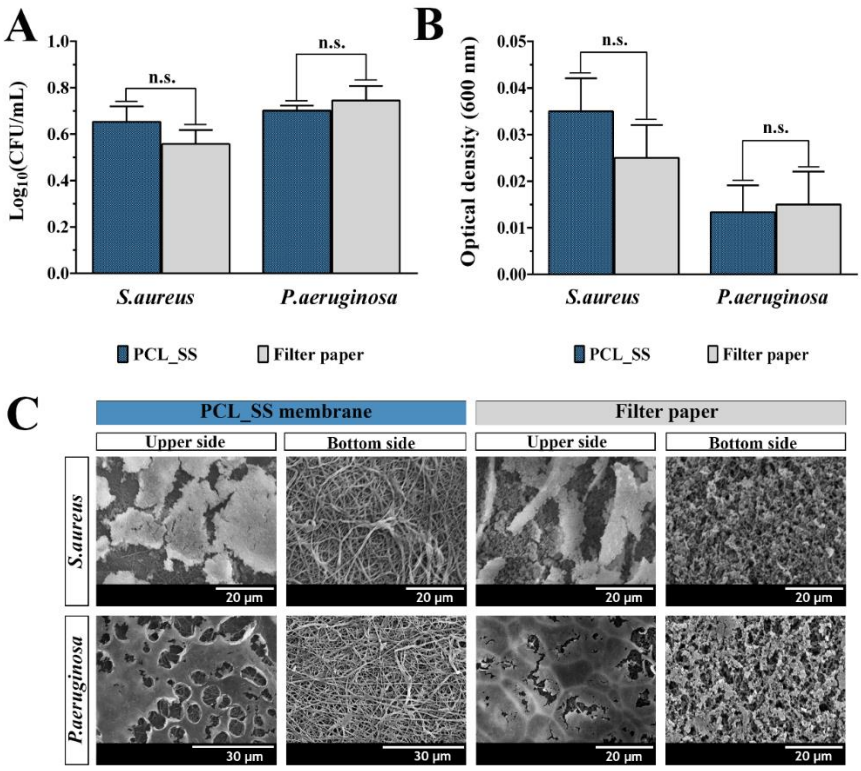

Figure 5.10. Evaluation of the bacterial infiltration through the PCL_SS membrane and filter paper (control group). Determination of the number of CFU of *S. aureus* and *P. aeruginosa* that crossed the PCL_SS membrane or filter paper, after 24 h (A). Optical density of medium samples recovered from the lower chamber of the transwell system (B). Data are presented as the mean ± standard deviation, n = 5, n.s. = non-significant. SEM images of the microorganisms (*S. aureus* and *P. aeruginosa*) that adhered to the upper or lower side of the PCL_SS membrane and filter paper are presented in (C).

In addition, the SEM images (Figure 5.10C) revealed that despite some bacteria can adhere to the upper side of the top layer, no bacteria penetration to the bottom side of the nanofibrous layer occurred. Such results highlighted the capacity of the top layer to act as a barrier, due to its low porosity, that hampers the microorganisms' colonization of the wound site [4]. Further, despite of few works reporting the antibacterial properties of SS, different authors proposed that the bactericidal activity presented by this protein results from the interaction of the protonated amino groups of SS with the negatively charged groups available on the bacterial cell wall (surface components like LPS and proteoglycans) [25, 39]. Moreover, SS with low molecular weight could penetrate the bacterial cells directly resulting in the loss of the cell's integrity, as already reported in works performed by Doakhan *et al*. [62], and Zhao *et al*. [25].

Additionally, the bottom layer (CS_SA hydrogel) capacity to provide an aseptic environment to the wound was also evaluated. To accomplish that, hydrogels were incubated over 24 h with bacteria models (*S.aureus* and *P.aeruginosa*) and then the number of colonies formed were counted. The results revealed that the CS_SA hydrogel exhibited an inhibitory effect on bacterial growth of 90.91% and 66.85% for *S.aureus* and *P.aeruginosa* (Figure 5.11A and 5.11B), respectively. To further assess the antibacterial activity of the bottom layer, the modified Kirby-Bauer assay was also performed. The results corroborated the antibacterial activity of the bottom layer, since an inhibition area of ≈ 92% and ≈ 45% was determined for *S.aureus* and *P.aeruginosa*, respectively (Figure 5.11C). Further, no biofilm formation was noticed at the surface of the CS_SA layer, when it was incubated with the microorganisms (Figure 5.11D). In contrast, biofilm formation occurred in the control samples, where bacteria were seeded on contact with agar plate (without the CS_SA hydrogel). The bactericidal activity of the 3D_SAC bottom layer can be explained by the presence of CS in the hydrogels' formulation, which is widely described in the literature as material with antimicrobial properties. For example, Antunes *et al*. produced CS-based wound dressings and they obtained an inhibitory effect of ≈ 50% and ≈ 16.5% for *E. coli* and *S.aureus* [24]. In a similar way, Nguyen and their collaborators produced co-axial PLA/CS nanofibers and they obtained an antibacterial efficiency between 100% and 52% for *E. coli* [63]. Different mechanisms have been proposed to explain the antimicrobial activity of CS. Although, the most one, purposes that the electrostatic interactions occurring between the positively charged amine groups of CS and the negatively charged groups available on the bacterial cell wall are responsible for CS bactericidal effect [26, 64]. Such interactions will increase the cell wall permeability, and consequently, allow the leakage of the intracellular constituents that lead to the disruption of the ionic gradients found within the bacteria. Further, the CS can also promote the formation of a polymeric envelope around the bacteria, leading to the inhibition of cell exchanges and nutrients absorption [4, 21, 26, 64].

It is worth to notice that the antibacterial effect of CS is influenced by the structure and composition of the bacterial cell wall. In fact, the data obtained revealed that the CS_SA

hydrogel presented a more pronounced antibacterial effect towards *S.aureus* (gram-positive bacteria), as shown in Figure 5.11. Similar observations have also been reported by other researchers in the literature [17, 65]. Gram-negative bacteria (*P.aeruginosa*) cell wall is more complex and thicker, possessing an outer membrane composed of LPS and proteins. As a phospholipid bilayer, the lipid portion of the outer membrane is largely impermeable to charged macromolecules, such as CS [65].

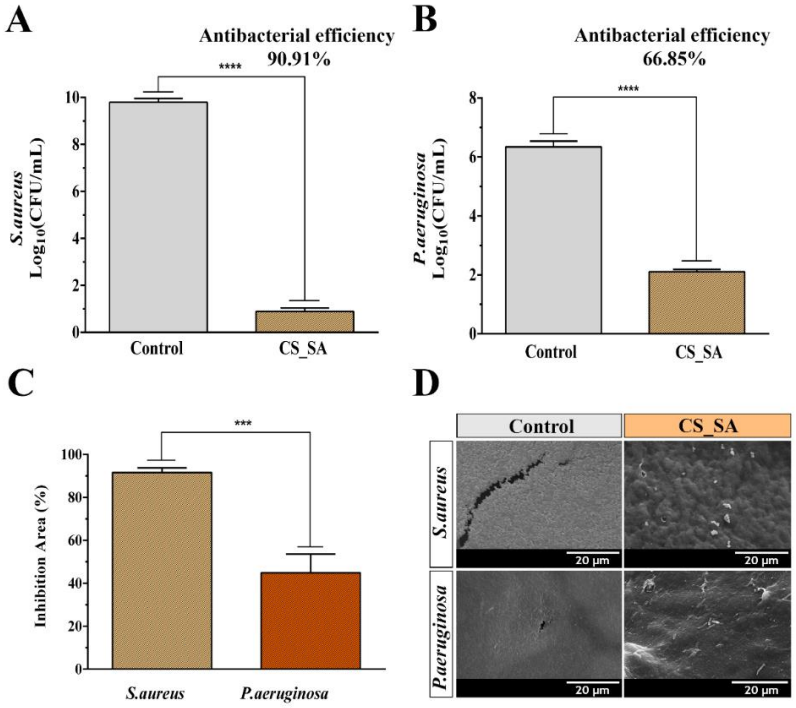

Figure 5.11. Evaluation of the CS_SA layer antibacterial properties against *S. aureus* (A) and *P. aeruginosa* (B). Data are presented as the mean ± standard deviation, n = 5, ***p < 0.001, ****p < 0.0001. Determination of the inhibition area displayed by the bottom layer, when placed in contact with both bacterial models (C). SEM images of control and CS_SA hydrogel incubated with *S. aureus* and *P. aeruginosa* (D).

5.4 Conclusions

The asymmetric membranes potential to be used in wound dressing applications has been recognized in different reports available in the literature. In fact, the reproduction of native skin' structure allows them to mimic the epidermis and dermis' functions, avoiding the microbial invasion and simultaneously, promoting the cell adhesion and proliferation. Despite the several dermo-epidermal skin substitutes available in the market, none of them is able to fully capable of mimicking the structure and functions of the skin layers, while promoting the healing process.

In this work, it was reported for the first time, the production of a 3D asymmetric skin construct combining the electrospinning and 3D bioprinting technology. The epidermis layer was mimicked through the production of a dense and interconnected polymeric nanofibrous

membrane (PCL_SS), which act as physical protective barrier to the wound site. The top layer was able to avoid the microorganisms' infiltration and present excellent mechanical properties (tensile strength, young modulus, and elongation at break), quite similar to those displayed by native human skin. On the other side, the bottom layer (CS_SA hydrogel) obtained by using a 3D Bioprinting technique exhibited an adequate porosity, wettability and biological properties for supporting cell adhesion, migration, and proliferation, as well as, inhibit the *S.aureus* and *P.aeruginosa* growth. In the near future, the incorporation of bioactive molecules (*e.g.* GFs, proteins, vitamins, anti-inflammatory drugs, and cells) into PCL_SS membrane and CS_SA hydrogel can be performed for improving the 3D asymmetric skin construct' performance on the wound healing process. Furthermore, *in vivo* assays may be pursued to fully depict the therapeutic potential of the 3D_SAC for enhancing the skin regeneration, emphasizing the suitability of this asymmetric 3D skin construct for the treatment of the skin injuries, which affect millions of patients worldwide.

5.5 References

1. Kolarsick PA, Kolarsick MA, Goodwin C. Anatomy and physiology of the skin. Journal of the Dermatology Nurses' Association. 2011;3(4):203-13.
2. Vijayavenkataraman S, Lu W, Fuh J. 3D bioprinting of skin: a state-of-the-art review on modelling, materials, and processes. Biofabrication. 2016;8(3):032001.
3. Morgado PI, Aguiar-Ricardo A, Correia IJ. Asymmetric membranes as ideal wound dressings: An overview on production methods, structure, properties and performance relationship. Journal of Membrane Science. 2015;490:139-51.
4. Miguel SP, Moreira AF, Correia IJ. Chitosan based-asymmetric membranes for wound healing: A review. International journal of biological macromolecules. 2019;127:460-75.
5. Miguel SP, Simões D, Moreira AF, Sequeira RS, Correia IJ. Production and characterization of electrospun silk fibroin based asymmetric membranes for wound dressing applications. International journal of biological macromolecules. 2019;121:524-35.
6. Mi F-L, Wu Y-B, Shyu S-S, Chao A-C, Lai J-Y, Su C-C. Asymmetric chitosan membranes prepared by dry/wet phase separation: a new type of wound dressing for controlled antibacterial release. Journal of Membrane Science. 2003;212(1-2):237-54.
7. Morgado PI, Lisboa PF, Ribeiro MP, Miguel SP, Simões PC, Correia IJ, Aguiar-Ricardo A. Poly (vinyl alcohol)/chitosan asymmetrical membranes: Highly controlled morphology toward the ideal wound dressing. Journal of membrane science. 2014;469:262-71.
8. Chen Y, Yan L, Yuan T, Zhang Q, Fan H. Asymmetric polyurethane membrane with in situ-generated nano-TiO2 as wound dressing. Journal of Applied Polymer Science. 2011;119(3):1532-41.
9. Liang D, Lu Z, Yang H, Gao J, Chen R. Novel asymmetric wettable AgNPs/chitosan wound dressing: in vitro and in vivo evaluation. ACS applied materials & interfaces. 2016;8(6):3958-68.
10. Miguel SP, Figueira DR, Simões D, Ribeiro MP, Coutinho P, Ferreira P, Correia IJ. Electrospun polymeric nanofibres as wound dressings: a review. Colloids and surfaces B: Biointerfaces. 2018;169:60-71.

11. Miguel SP, Ribeiro MP, Coutinho P, Correia IJ. Electrospun Polycaprolactone/aloe Vera_Chitosan Nanofibrous asymmetric membranes aimed for wound healing applications. Polymers. 2017;9(5):183.
12. Figueira DR, Miguel SP, de Sá KD, Correia IJ. Production and characterization of polycaprolactone-hyaluronic acid/chitosan-zein electrospun bilayer nanofibrous membrane for tissue regeneration. International journal of biological macromolecules. 2016;93:1100-10.
13. Zhang Y-Q. Applications of natural silk protein sericin in biomaterials. Biotechnology advances. 2002;20(2):91-100.
14. Lamboni L, Gauthier M, Yang G, Wang Q. Silk sericin: a versatile material for tissue engineering and drug delivery. Biotechnology Advances. 2015;33(8):1855-67.
15. Cuttle L, Kempf M, Phillips GE, Mill J, Hayes MT, Fraser JF, Wang X-Q, Kimble RM. A porcine deep dermal partial thickness burn model with hypertrophic scarring. Burns. 2006;32(7):806-20.
16. Aramwit P, Kanokpanont S, Nakpheng T, Srichana T. The effect of sericin from various extraction methods on cell viability and collagen production. International Journal of Molecular Sciences. 2010;11(5):2200-11.
17. Cabral CS, Miguel SP, de Melo-Diogo D, Louro RO, Correia IJ. In situ green reduced graphene oxide functionalized 3D printed scaffolds for bone tissue regeneration. Carbon. 2019;146:513-23.
18. Dababneh AB, Ozbolat IT. Bioprinting technology: a current state-of-the-art review. Journal of Manufacturing Science and Engineering. 2014;136(6):061016.
19. Fradique R, Correia TR, Miguel S, De Sa K, Figueira D, Mendonça A, Correia I. Production of new 3D scaffolds for bone tissue regeneration by rapid prototyping. Journal of Materials Science: Materials in Medicine. 2016;27(4):69.
20. Fan L, Yang H, Yang J, Peng M, Hu J. Preparation and characterization of chitosan/gelatin/PVA hydrogel for wound dressings. Carbohydrate polymers. 2016;146:427-34.
21. Miguel SP, Ribeiro MP, Brancal H, Coutinho P, Correia IJ. Thermoresponsive chitosan–agarose hydrogel for skin regeneration. Carbohydrate polymers. 2014;111:366-73.
22. Saraiva SM, Miguel SP, Ribeiro MP, Coutinho P, Correia IJ. Synthesis and characterization of a photocrosslinkable chitosan–gelatin hydrogel aimed for tissue regeneration. RSC Advances. 2015;5(78):63478-88.
23. Wang S, Lee JM, Yeong WY. Smart hydrogels for 3D bioprinting. International Journal of Bioprinting. 2015;1(1).
24. Antunes BP, Moreira AF, Gaspar V, Correia I. Chitosan/arginine–chitosan polymer blends for assembly of nanofibrous membranes for wound regeneration. Carbohydrate polymers. 2015;130:104-12.
25. Zhao R, Li X, Sun B, Zhang Y, Zhang D, Tang Z, Chen X, Wang C. Electrospun chitosan/sericin composite nanofibers with antibacterial property as potential wound dressings. International journal of biological macromolecules. 2014;68:92-7.
26. Simões D, Miguel SP, Ribeiro MP, Coutinho P, Mendonça AG, Correia IJ. Recent advances on antimicrobial wound dressing: A review. European journal of pharmaceutics and biopharmaceutics. 2018;127:130-41.
27. bing Jin X, sheng Sun Y, Zhang K, Wang J, ping Shi T, dong Ju X, quan Lou S. Ectopic neocartilage formation from predifferentiated human adipose derived stem cells induced by adenoviral-mediated transfer of hTGF beta2. Biomaterials. 2007;28(19):2994-3003.

28. Bouhadir KH, Alsberg E, Mooney DJ. Hydrogels for combination delivery of antineoplastic agents. Biomaterials. 2001;22(19):2625-33.
29. Diogo G, Gaspar V, Serra I, Fradique R, Correia I. Manufacture of ß-TCP/alginate scaffolds through a Fab@ home model for application in bone tissue engineering. Biofabrication. 2014;6(2):025001.
30. Ruvinov E, Leor J, Cohen S. The promotion of myocardial repair by the sequential delivery of IGF-1 and HGF from an injectable alginate biomaterial in a model of acute myocardial infarction. Biomaterials. 2011;32(2):565-78.
31. Valente J, Valente TAM, Alves P, Ferreira P, Silva A, Correia I. Alginate based scaffolds for bone tissue engineering. Materials science and engineering: C. 2012;32(8):2596-603.
32. Aderibigbe B, Buyana B. Alginate in wound dressings. Pharmaceutics. 2018;10(2):42.
33. Simões D, Miguel SP, Correia IJ. Biofunctionalization of electrospun poly (caprolactone) fibers with Maillard reaction products for wound dressing applications. Reactive and Functional Polymers. 2018;131:191-202.
34. Maia J, Ribeiro MP, Ventura C, Carvalho RA, Correia IJ, Gil MH. Ocular injectable formulation assessment for oxidized dextran-based hydrogels. Acta biomaterialia. 2009;5(6):1948-55.
35. Ren D, Yi H, Wang W, Ma X. The enzymatic degradation and swelling properties of chitosan matrices with different degrees of N-acetylation. Carbohydrate Research. 2005;340(15):2403-10.
36. Khademhosseini A, Langer R. Microengineered hydrogels for tissue engineering. Biomaterials. 2007;28(34):5087-92.
37. Chen S, Liu B, Carlson MA, Gombart AF, Reilly DA, Xie J. Recent advances in electrospun nanofibers for wound healing. Nanomedicine. 2017;12(11):1335-52.
38. Loh QL, Choong C. Three-dimensional scaffolds for tissue engineering applications: role of porosity and pore size. Tissue Engineering Part B: Reviews. 2013;19(6):485-502.
39. Gupta D, Agrawal A, Rangi A. Extraction and characterization of silk sericin. Indian Journal of Fibre & Textile Research (IJFTR). 2014;39(4):364-72.
40. Martínez DCC, Zuluaga CL, Restrepo-Osorio A, Álvarez-López C. Characterization of sericin obtained from cocoons and silk yarns. Procedia engineering. 2017;200:377-83.
41. Tsukada M. Thermal decomposition behavior of sericin cocoon. Journal of Applied Polymer Science. 1978;22(2):543-54.
42. Elsner JJ, Shefy-Peleg A, Zilberman M. Novel biodegradable composite wound dressings with controlled release of antibiotics: microstructure, mechanical and physical properties. Journal of Biomedical Materials Research Part B: Applied Biomaterials. 2010;93(2):425-35.
43. Labet M, Thielemans W. Synthesis of polycaprolactone: a review. Chemical Society Reviews. 2009;38(12):3484-504.
44. Hollister SJ. Porous scaffold design for tissue engineering. Nature materials. 2005;4(7):518.
45. Shanmugasundaram N, Ravichandran P, Reddy PN, Ramamurty N, Pal S, Rao KP. Collagen-chitosan polymeric scaffolds for the in vitro culture of human epidermoid carcinoma cells. Biomaterials. 2001;22(14):1943-51.
46. Morgado PI, Miguel SP, Correia IJ, Aguiar-Ricardo A. Ibuprofen loaded PVA/chitosan membranes: A highly efficient strategy towards an improved skin wound healing. Carbohydrate polymers. 2017;159:136-45.

47. Li Z, Ramay HR, Hauch KD, Xiao D, Zhang M. Chitosan–alginate hybrid scaffolds for bone tissue engineering. Biomaterials. 2005;26(18):3919-28.
48. Wang Z, Zhang Y, Zhang J, Huang L, Liu J, Li Y, Zhang G, Kundu SC, Wang L. Exploring natural silk protein sericin for regenerative medicine: an injectable, photoluminescent, cell-adhesive 3D hydrogel. Scientific reports. 2014;4:7064.
49. Mi F-L, Shyu S-S, Wu Y-B, Lee S-T, Shyong J-Y, Huang R-N. Fabrication and characterization of a sponge-like asymmetric chitosan membrane as a wound dressing. Biomaterials. 2001;22(2):165-73.
50. Sudheesh Kumar P, Lakshmanan V-K, Anilkumar T, Ramya C, Reshmi P, Unnikrishnan A, Nair SV, Jayakumar R. Flexible and microporous chitosan hydrogel/nano ZnO composite bandages for wound dressing: in vitro and in vivo evaluation. ACS applied materials & interfaces. 2012;4(5):2618-29.
51. Wang Y, Xu R, He W, Yao Z, Li H, Zhou J, Tan J, Yang S, Zhan R, Luo G. Three-dimensional histological structures of the human dermis. Tissue Engineering Part C: Methods. 2015;21(9):932-44.
52. Venugopal J, Vadgama P, Kumar TS, Ramakrishna S. Biocomposite nanofibres and osteoblasts for bone tissue engineering. Nanotechnology. 2007;18(5):055101.
53. Serra I, Fradique R, Vallejo M, Correia TR, Miguel S, Correia I. Production and characterization of chitosan/gelatin/β-TCP scaffolds for improved bone tissue regeneration. Materials Science and Engineering: C. 2015;55:592-604.
54. Zhong S, Zhang Y, Lim C. Tissue scaffolds for skin wound healing and dermal reconstruction. Wiley Interdisciplinary Reviews: Nanomedicine and Nanobiotechnology. 2010;2(5):510-25.
55. Jonkman MF, Molenaar I, Nieuwenhuis P, Bruin P, Pennings AJ. New method to assess the water vapour permeance of wound coverings. Biomaterials. 1988;9(3):263-7.
56. Bacakova L, Filova E, Parizek M, Ruml T, Svorcik V. Modulation of cell adhesion, proliferation and differentiation on materials designed for body implants. Biotechnology advances. 2011;29(6):739-67.
57. Oliveira SM, Alves NM, Mano JF. Cell interactions with superhydrophilic and superhydrophobic surfaces. Journal of Adhesion Science and Technology. 2014;28(8-9):843-63.
58. Tsubouchi K, Igarashi Y, Takasu Y, Yamada H. Sericin enhances attachment of cultured human skin fibroblasts. Bioscience, biotechnology, and biochemistry. 2005;69(2):403-5.
59. Ribeiro MP, Espiga A, Silva D, Baptista P, Henriques J, Ferreira C, Silva JC, Borges JP, Pires E, Chaves P. Development of a new chitosan hydrogel for wound dressing. Wound repair and regeneration. 2009;17(6):817-24.
60. Jayakumar R, Prabaharan M, Kumar PS, Nair S, Tamura H. Biomaterials based on chitin and chitosan in wound dressing applications. Biotechnology advances. 2011;29(3):322-37.
61. Kathuria N, Tripathi A, Kar KK, Kumar A. Synthesis and characterization of elastic and macroporous chitosan–gelatin cryogels for tissue engineering. Acta biomaterialia. 2009;5(1):406-18.
62. Doakhan S, Montazer M, Rashidi A, Moniri R, Moghadam M. Influence of sericin/TiO2 nanocomposite on cotton fabric: Part 1. Enhanced antibacterial effect. Carbohydrate polymers. 2013;94(2):737-48.

63. Nguyen TTT, Chung OH, Park JS. Coaxial electrospun poly (lactic acid)/chitosan (core/shell) composite nanofibers and their antibacterial activity. Carbohydrate Polymers. 2011;86(4):1799-806.

64. Arkoun M, Daigle F, Heuzey M-C, Ajji A. Mechanism of action of electrospun chitosan-based nanofibers against meat spoilage and pathogenic bacteria. Molecules. 2017;22(4):585.

65. Helander I, Nurmiaho-Lassila E-L, Ahvenainen R, Rhoades J, Roller S. Chitosan disrupts the barrier properties of the outer membrane of Gram-negative bacteria. International journal of food microbiology. 2001;71(2-3):235-44.

Chapter VI

Concluding Remarks and Future Trends

6. Concluding Remarks and Future Perspectives

6.1 Concluding Remarks

Skin injuries are known as a major health problem. Up to now, different therapeutic approaches have been developed to enhance the healing process, namely by providing protection to the wound site against external agents and dehydration. The research outcomes already allowed the development of 3D constructs (hydrogels, scaffolds, sponges, membranes) with different morphologies, structures and loaded with different bioactive molecules or cells that in some cases are currently used in the clinic. However, these skin substitutes are still unable to fully reproduce skin's native structure and functions. Such fact propelled the search for new alternative therapeutic solutions. Among them, the membranes produced through the electrospinning technique have captured the attention of the researchers due to the versatility, low cost, and capacity to incorporate different bioactive/antimicrobial molecules, that play crucial roles for improving the wound healing process. Further, to reproduce the skin's native structure, the researchers started to produce asymmetric membranes that possess two distinct layers that mimic both the epidermis and dermis features. However, the production of the asymmetric membranes has been essentially performed by using the wet/dry and $scCO_2$-assisted phase inversion methods.

Herein, the electrospinning technique potential to produce asymmetric membranes for wound dressing applications was explored. To accomplish that, different combinations of natural (CS, SF, HA, SS, SA) and synthetic (PCL) polymers were used to produce asymmetric structures. Further, the nanofibers were enriched with a natural extract (AV) and an essential oil (THY) to improve the biological properties of the produced wound dressings. In addition, the electrospinning technique was also combined with the 3D printing in order to obtain an asymmetric skin construct, displaying an electrospun membrane in the top layer, and a 3D printed hydrogel in the bottom layer.

In the first study performed on this PhD thesis, the asymmetric membrane with a CS/AV bottom layer and a PCL top layer was produced through the sequential deposition of electrospun fibers. The PCL dense top layer was able to avoid the *S. aureus* and *E. coli* infiltration, as well as provide mechanical support to the wound site. On the other side, the AV incorporation into the CS nanofibers allowed the production of a bottom layer that confers a moist environment at the wound site and improves the fibroblasts adhesion/proliferation. Further, the antimicrobial properties of CS and AV inhibited the microorganisms' growth at the surface of the bottom layer.

In the second study (chapter 4), an SF-based asymmetric electrospun membrane loaded with THY was successfully produced and characterized. The obtained results demonstrated that the top layer composed of SF and PCL presented similar properties to the epidermis layer, *i.e.*,

hydrophobic character, high mechanical resistance and impermeability. On the other hand, the SF_HA bottom layer incorporating the THY was able to mimic the features of the dermis layer. The obtained results evidence that the produced asymmetric electrospun membranes possess suitable porosity and mechanical properties to be applied as wound dressings. Further, the *in vitro* assays demonstrated that the NHDF adhere and proliferate at the membranes' surface. On the other side, the THY incorporation into the bottom layer augmented the antioxidant and antibacterial properties of the produced membranes.

In the third study presented in this thesis (chapter 5), a 3D_SAC was produced by combining the electrospinning and the 3D printing techniques. The obtained data show that the top layer was able to avoid the *S. aureus* and *P. aeruginosa*' infiltration and exhibit mechanical properties similar to that of the native human skin. On the other side, the CS_SA 3D printed bottom hydrogel layer presented a suitable porosity and wettability, as well as biological properties that support the fibroblasts' adhesion, migration and proliferation. Further, the antimicrobial properties of CS were highlighted by the inhibition of the *S. aureus and P. aeruginosa* growth.

Overall, the results obtained in these experimental works demonstrated that the produced asymmetric electrospun membranes exhibit properties close to those considered ideal for a wound dressing – as summarized in Table 6.1. Further, the versality of electrospinning technique allowed the production of the asymmetric membranes, through the combination of different natural/synthetic polymers, incorporation of biomolecules within nanofibers, that mimic the epidermis and dermis properties. Moreover, the combination of electrospinning with 3D printing techniques opens numerous possibilities for the development of personalized asymmetric skin substitutes for wound healing applications.

Table 6.1. Comparison between the properties of the different electrospun asymmetric wound dressings developed during this PhD thesis and the values considered ideal for the wound dressings.

Parameters		Desired values	PCL/ CS_AV_PEO	SF_PCL/ SF_HA_THY	3D_SAC
Thickness (mm)	Top layer	0.5-1.5	Not evaluated (n.e.)	0.05-1.5	0.55 ± 0.16
	Bottom layer	0.6-3	n.e.	1.5-4	1.59 ± 0.19
Porosity (%)	Top layer	60-90%	55 ± 5	64. 28 ± 2. 59	56.66 ± 2.47
	Bottom layer		97.8 ± 4.5	85. 24 ± 2. 47	99.08 ± 2.55
WVTR (mL/m²/day)		2000-2500	1252.35 ± 21.22	2070.62 ± 102.52	1737.85± 92.12
Water contact angle (°)	Top layer	>90°	126.2 ± 1.21	103.10 ± 6.57	61.27 ± 4.15
	Bottom layer	<90°	69.06 ± 3.78	38.77 ± 5.32	23.75 ± 2.46
Young modulus (MPa)		4.6-20	27.14 ± 3.56	14.70 ± 4.42	27.92 ± 8.09
					0.05 ± 0.01
Tensile strength (MPa)		5-30	15.31 ± 2.57	7.59 ± 1.26	34.92 ± 7.39
					0.16 ± 0.05
Elongation at break (%)		35-115	20.98 ± 0.39	57.3 9 ± 13. 78	155.37 ± 5.71
					n.e.
Antimicrobial activity	Top layer	Avoid the bacterial infiltration	Bacterial infiltration was inhibited, revealing a similar capacity to that displayed by the filter paper		
	Bottom layer	Inhibit the microorganism growth	Antibacterial efficiency of 99.99% (*S. aureus*) and 99.97% (*E. coli*).	Antibacterial efficiency of 87.42% (*S. aureus*) and 58.43% (*P. aeruginosa*).	Antibacterial efficiency of 90.91% (*S. aureus*) and 66.85% (*P. aeruginosa*).

6.2 Future Perspectives

To enhance the performance of the produced asymmetric wound dressings and to further improve the patients' quality of life, different approaches should be investigated in the future (as illustrated in Figure 6.1). In the following topics are presented the future assays/approaches that can be considered:

1. <u>In vivo validation of the asymmetric wound dressings</u>

The *in vivo* evaluation of the asymmetric wound dressings will be crucial to fully disclose their potential for treating a skin injury. Indeed, these assays will provide insights into the wound dressings' ability to protect the wound site, promote the wound closure and new tissue formation. Furthermore, these assays also enable the assessment of the membranes' systemic histocompatibility, thereby paving the way for their possible translation into clinical assays.

2. Incorporation of other biomolecules into the nanofibers

The incorporation of other biological molecules (*e.g.*, GFs, vitamins, anti-inflammatory drugs, and cells) into the wound dressings can be pursued to further improve their biological performance. As previously described, the skin regeneration process is comprised of different phases (hemostasis, inflammation, proliferation, remodelling), which involve the interaction between cells, GFs and cytokines. Taking this into account, the controlled and targeted release of these biomolecules at the wound site can be explored to regulate the healing, control the inflammation as well as promote the angiogenesis, collagen deposition, cell migration, differentiation, and proliferation.

3. Incorporation of sensors into the electrospun membranes

Recently, researchers identified the importance of incorporating sensors into electrospun membranes for diagnostic or theragnostic purposes. In fact, biosensor-integrated electrospun membranes should be able to detect low levels of bacterial contamination, and consequently emit a signal alerting for the risk of infection. On the other side, this smart sensor can be engineered to trigger the sustained release of drugs from the membranes to maintain the optimal healing conditions. At the same time, the sensor should provide to the doctor/patient an overview of the different parameters indicative of the wound status, such as pH, temperature, moisture, and exudates production.

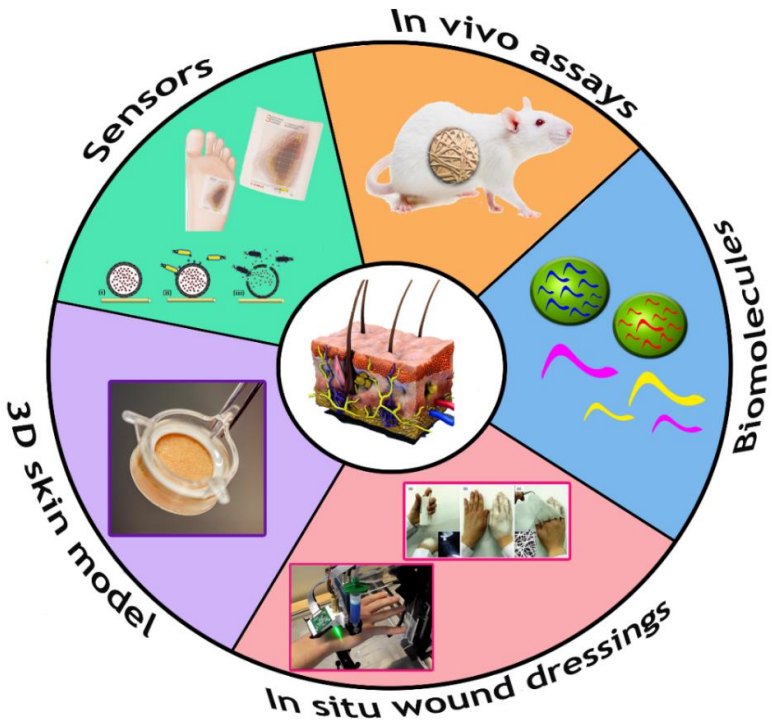

Figure 6.1. Illustrative representation of the possible future perspectives for the development of electrospun membranes.

4. In situ forming wound dressings

In near future, the use of *in situ* forming wound dressings can be a promising approach for wound management. The advancement of innovative fabrication techniques such as *in situ* electrospinning and 3D printing along with the emergence of the new functional biomaterials can provide the necessary toolkit for the production of skin substitutes that are tailored to the patients wound requirements.

5. Study of the 3D_SAC potential to be used as in vitro skin model

These asymmetric wound dressings, in particular 3D_SAC, can be investigated and optimized for the production of *in vitro* 3D skin models. In fact, the production of human skin models (*in vitro* human full-thickness skin models that mimic the skin physiological functions), may be an alternative to animal experimentation, thereby complying to the demands of the regulatory authorities, animal welfare organizations, consumers and scientists. Furthermore, these may also provide a platform for improving and extend our knowledge about the biological processes occurring in the skin. Therefore, there is here a great opportunity for discovering new skin equivalents to be used in the field of drugs/cosmetics development.